UNIVERSITÉ DE SHERBROOKE

Faculté de génie

Département de génie civil et de génie du bâtiment

Étude de la propagation des fumées lors d'un incendie de façade double peau (FDP) photovoltaïques intégrés au bâtiment (PVIB) sur la base des essais à l'hélium à petite échelle et de simulations

Study of smoke spread during building integrated photovoltaic (BIPV) double skin façade (DSF) fire based on small-scale helium tests and simulations

Thèse de doctorat

Spécialité : Génie civil

Monireh Aram

Sherbrooke (Québec) Canada

December 2022

MEMBRES DU JURY

Prof. Dahai Qi

Directeur

Dr. Yoon Ko

Co-Directeur

Prof. Jay Lacey

Rapporteur

Prof. Ali Hakkaki-Fard

Évaluateur

Dr. Yi Wang

Évaluateur

ABSTRACT

Reducing energy consumption and electricity demand in buildings by using advanced clean and energy-efficient technologies such as building attached photovoltaics (BAPVs) and building integrated photovoltaics (BIPVs) systems have been widely applied in new and existing constructions. Meanwhile, they can cause a new critical challenge, i.e., fire safety. Plumes from the PV panel fires could spread into the buildings through the windows and ventilation openings. This creates toxic conditions for people in and around the buildings, leading to inhalation injuries from the toxic chemicals released by solar panels and their batteries. The risk of fire can be elevated by affecting the propagation of fire inside and outside the building. Furthermore, interferes with the smoke and venting system, firefighting operation, and electrical shock dangers. Most of the studies on PV panels are to find the cause of failure, improve the cell efficiency, cost reduction, and extract maximum power, while there is the need to study the system for smoke propagation as well. Applying BIPV on the building causes major changes in the traditional method of using structural components. These changes may include changes in the material, standard distances, gaps, and duties of elements each of which can bring new issues. In this research, a case of BIPV application on the building double skin façade is studied.to observe the physics of smoke spread from ignited BIPV on the façade to the indoor environment. Therefore, a small-scale model is designed using a helium surrogate based on the helium-smoke plume similarity and Froud modeling. The validity of the CFD model is observed and the mentioned scaling method is verified by comparing the similarity of simulation results between the small-scale with helium, small-scale with fire, and full-scale with fire cases. Moreover, from the parametric experimental study, it has been seen that regardless of the fire location the greatest risk is for the top floor. According to the helium concentration results (both transient and steady-state), central floors can be the safest places for receiving smoke from the plenum. The profile of velocity is independent of the HRR magnitude. However, the fire risk can dramatically increase with the higher HRRs.

Keywords: helium smoke similarity, BIPV DSF fire, smoke spread, CFD simulations, PIV, helium experiment, FDS, Scale method

Résumé

La réduction de la consommation d'énergie et de la demande d'électricité dans les bâtiments en utilisant des technologies avancées propres et économes en énergie telles que les systèmes photovoltaïques attachés au bâtiment (BAPV) et les systèmes photovoltaïques intégrés au bâtiment (BIPV) a été largement appliquée dans les constructions nouvelles et existantes. Pendant ce temps, ils peuvent poser un nouveau défi critique, à savoir la sécurité incendie. Les panaches des feux de panneaux photovoltaïques pourraient se propager dans les bâtiments par les fenêtres et les ouvertures de ventilation. Cela crée des conditions toxiques pour les personnes à l'intérieur et autour des bâtiments, entraînant des blessures par inhalation des produits chimiques toxiques libérés par les panneaux solaires et leurs batteries. Le risque d'incendie peut être accru en affectant la propagation du feu à l'intérieur et à l'extérieur du bâtiment. En outre, interfère avec le système de fumée et d'évacuation, les opérations de lutte contre l'incendie et les risques de choc électrique. La plupart des études sur les panneaux photovoltaïques visent à trouver la cause de la défaillance, à améliorer l'efficacité des cellules, à réduire les coûts et à extraire une puissance maximale, tandis qu'il est également nécessaire d'étudier le système de propagation de la fumée. L'application du BIPV sur le bâtiment entraîne des changements majeurs dans la méthode traditionnelle d'utilisation des composants structurels. Ces changements peuvent inclure des changements dans le matériau, les distances standard, les lacunes et les fonctions des éléments, chacun pouvant apporter de nouveaux problèmes. Dans cette recherche, un cas d'application de BIPV sur la façade à double peau d'un bâtiment est étudié. Par conséquent, un modèle à petite échelle est conçu à l'aide d'un substitut d'hélium basé sur la similarité du panache de fumée d'hélium et la modélisation de Froud. La validité du modèle CFD est observée et la méthode de mise à l'échelle mentionnée est vérifiée en comparant la similitude des résultats de simulation entre les cas à petite échelle avec hélium, à petite échelle avec incendie et à grande échelle avec incendie. De plus, à partir de l'étude expérimentale paramétrique, il a été constaté que, quel que soit l'emplacement de l'incendie, le plus grand risque se situe au dernier étage. Selon les résultats de concentration d'hélium (à la fois transitoires et en régime permanent), les planchers centraux peuvent être les endroits les plus sûrs pour recevoir la fumée du plénum. Le profil de vitesse est indépendant de l'amplitude du

HRR. Cependant, le risque d'incendie peut augmenter considérablement avec les HRR plus élevés.

ACKNOWLEDGEMENT

I would like to express deepest appreciation and thanks to my supervisor, Prof. Dahai Qi, for his great advice and supervision. His valuable and constructive suggestions as a research supervisor, understanding and consideration as the second family, that any international student lacks in Canada, made the journey way easier.

I would also like to express sincere gratitude and appreciation to my co-supervisor, Dr. Yoon Ko, who helped me to improve my logical thinking, problem-solving and communication skills.

Working with her brought me lots of chances, collaborations, and experiences.

I wish to thank the examining committee jury members, Prof. Lacey, Prof. Hakkaki-Fard, and Dr. Wang, for their time in reviewing my work.

I gratefully acknowledge, Dr. Huizhong Lu, from Compute Canada – Mammoth-Mp2b - Université de Sherbrooke. Dr. Lu helped me install and code the FDS software and complete every Mp2 cluster simulation.

I also gratefully acknowledge Mr. Frédéric Turcotte from Department of Civil and Building Engineering, Université de Sherbrooke. Assembling the model and conducting experiment was impossible without his skills and expertise.

I wish to thank my friends and colleagues, Dr. Haohan Sha, Dr. Xin Zhang, and Mr. Ibrahim Abdelhady. They helped me to conduct the experiments, build the simulation model, review my paper and thesis, and gather the references.

Finally, I need to engrave it here as an everlasting reminder that this PhD journey means a lot to me. Therefore, I would like to send great appreciations to my parents, sisters, and brother. Without their support it was impossible to see the light at the end of the dark tunnel.

TABLE OF CONTENTS

LIST OF FIGURES

LIST OF TABLES

NOMENCLATURE

B	Buoyancy flux (m^4/s^3)
BIPV	Building integrated photovoltaics
CFD	Computational fluid dynamics
C_p	Specific heat capacity of the air (J/(kg·K))
FDS	Fire dynamics simulator
FOV	Field of view
Fr	Froude number
FSF	Full-scale with fire
g	Acceleration due to Earth's gravity (m/s^2)
GHG	Greenhouse gas
h	Room vertical wall height (m)
HRR	Heat release rate (kW)
HRRPUA	Heat release rate per area (kW/m^2)
l	Geometry length (m)
L	Characteristic linear dimension (m)
LES	Large eddy simulation
NIST	National Institute of Standards and Technology
NRMSE	Normalized root mean squared error
PET	Polyethylene terephthalate
PIV	Particle image velocimetry
PV	Photovoltaic
Q	Heat release rate (kW)

$\hat{Q}$	heat release rate per area (kW/m^2)
q	Volumetric flow rate (m^3/s)
RANS	Reynolds-Averaged Navier-Stokes
Ri	Richardson number
SSF	Small-scale with fire
SSH	Small-scale with helium surrogate
T	Temperature (K)
t	Time (s)
T*	Dimensionless temperature and volumetric fraction
u	Velocity (m/s)
u*	Dimensionless velocity

Greek symbols

β	Thermal expansion coefficient (1/K)
θ	Roof angle (°)
ρ	Density (kg/m^3)
τ	Times
χ	Volumetric fraction (mol/mol)

Subscripts

a	Ambient air
c	Convective
helium	Helium
mix	Mixture between air and helium

smoke	Fire smoke
s	Sub-Scale model
f	Full-Scale model

PREFACE

This is a traditional thesis composed of the Introduction, Methodology, Results and Discussion, and Conclusions. Chapters 1 and 2 present the introduction and the comprehensive state-of-the-art review. Chapter 3 illustrates the methodology including theory, experiment properties, and CFD simulations. Then Chapters 4-6 show the results of the discussion in different scenarios. For the reader to better understand the thesis, the summary and thesis organization are illustrated in Section 1.2. The nomenclature, References, and Appendix are illustrated at the end of the thesis.

Chapter 1 Introduction

1.1.Background

In a global effort to minimize the negative impact of buildings on the environment through conservation of energy and resources, governments are working to develop and adopt increasingly stringent green building regulations and policies. Under this background, the advanced clean and energy efficient technologies are driving changes in building design, which include new building new building thermal envelope systems; high insulation materials; green roof/wall; high performance glazing systems; photovoltaic panels; and renewable energy generation and storage systems. While the energy efficiency of these green building features has been extensively studied the unintended consequence of the use of these new technologies have not been thoroughly explored. Recent fire accidents and studies demonstrated that many of the energy efficient technologies and green building features pose unintended fire hazards which could be hardly mitigated by the capability of conventional fire protection systems. New renewable energy systems including photovoltaic systems and new energy generating/storage systems also have become worldwide fire safety concerns and firefighting challenges. The importance of the safety issue introduced by this new technology brought the International Energy Agency group to allocate one of their tasks to contribute its development. The IEA (International Energy Agency) Photovoltaic Power System Programme (PVPS) is one of the Technology Collaboration Programme established within the IEA. IEA-PVPS Task 15 titled as ¨ Enabling Framework for the development of BIPV¨, Subtask E as ¨pre-normative international research on BIPV (Building Integrated Photovoltaic) characterisation methods¨ and Activity E3 ¨Fire Safety¨ directly points to the fire safety of BIPV modules and installations.

The PV system can be installed as BAPV (Building Attached Photo Voltaic) or BIPV . Each of the named technologies have their specific fire safety issues, yet the fire safety issues for BIPV would be of more complexity and need further study. BIPVs are involved in the building behaviour more than the BAPVs, since they have functionality as building elements too. As BIPVs can be set to the building façade, glazing, roof they would bring the building to a worse condition in case of a fire. As an example, in buildings with BIPV DSF, the smoke generated from the BIPV panels, or any other part of the building can be trapped into one area or be

transferred to the indoor area through the openings. In case of BIPV double skin façade (DSF), a fire could start from the BIPV DSF, and the smoke and toxic gases could get trapped in the vertical void of the façade, result in higher temperatures and easily migrate to the indoor space, edendangering the occupants' lives and causing property damage. Moreover, employing BIPV on DSF provides less access to the fire source in the case of initiation of fire on the PV modules. However, there are no fire protection codes and standards addressing the fire safety of BIPV DSF to avoid these possibilities of fire and smoke danger. Also, there is no requirement for smoke and fire control of BIPV DSF based on experience and research.

There are multiple elements engaged when studying the BIPV DSF fire safety such as the location of installation, type of the employed PV modules, influence of the wind, specification of the installation and so on. To proof the influence of each of these factors on the smoke behavior of the BIPV system there should be experiments and simulations conducted. With the output of the small-scale tests on the samples, it is possible to obtain the reaction to fire parameters and to hire correct data in the simulation process. The background research shows that the small-scale reaction to fire tests on the PV panels are studied several times while there is not enough consideration of generated smoke and the applied system on a real building. As discussed, to obtain effective and applicable fire and smoke protection for BIPV a challenge must be tackled that is the lack of data which could be used in developing design guidelines for smoke spread while considering the fire cases in the BIPV system.

1.2.Summary and thesis organization

According to the mentioned fire risk of the BIPV systems, to overcome the issue, in this research, a case of BIPV application on the building façade is studied. This research aims to firstly, develop a novel method to use small scale helium test to replace full size model with fire; and secondly, investigate the mechanism of BIPV double skin façade (DSF) fire induced smoke movement. The proposed methodology includes theory development, helium surrogation experiment and computer simulations using FDS.

Overall order of the current research is as follows:

Chapter 1 is a brief introduction on the overall research topic, followed by **Chapter 2** that demonstrates the available literature on photovoltaic fires comprehensively and identifies the associated research gap briefly. The connections are depicted in Figure 1.

Based on the available literature and the objectives which are included in the first two chapters, **Chapter 3** defines the proposed methodology. In brief, the similarity theory between helium and fire smoke tests is mentioned, and Froude modeling as the scaling method is then coupled with the similarity theory between helium and fire smoke. Therefore, a new scaling method is developed to study smoke propagation on the BIPV DSF fire to the indoor environment. This section also includes all the information associated to the experimental, analytical and CFD simulation properties. In the end of the chapter, the grid independent study conducted for the CFD simulations is included.

Chapter 4 follows the methodology section and employs the similarity method between helium and fire smoke. Accordingly, the BIPV DSF fire experiment is designed and conducted. Then the experimental measurements are used to validate the CFD simulation results for scenarios with real fire and helium surrogate. The simulations are done using Fire Dynamic Simulator (FDS). In conclusion, the theory of helium similarity is verified by comparing the simulation results between helium surrogate and fire smoke.

Chapter 5 is prepared to use the scale method which is mentioned in the proposed methodology (Chapter 3). This verification is done by comparing the temperature and dimensionless velocity between small-scale and full-scale case study, with the scale of 1/30.

Following Chapter 4 and 5, the theory of helium and smoke similarity and the scaling method are justified. Consequently, **Chapter 6** is a parametric study to inspect the mechanism of smoke transfer from an ignited BIPV DSF through the openings to the indoor environment. The various parameters include three different locations of fire on the façade and three different heat release rates.

The main body of the research are placed in Chapter 4 to 6 and **Chapter 7** collects the results and conclusions of the study and points out the limitations and future works.

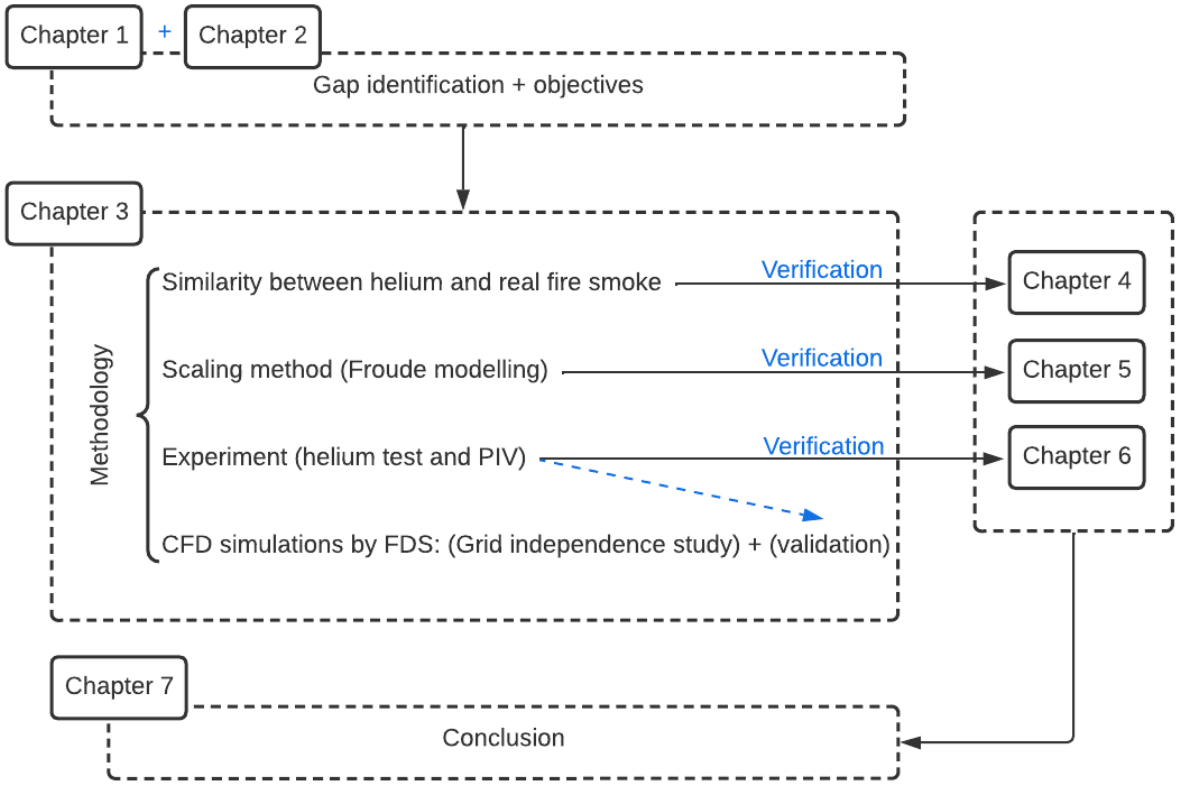

Figure 1. Structure of the thesis

Chapter 2 Comprehensive state-of-the-art review

Chapter 2 completes the preliminary information provided in Chapter 1 by a comprehensive review on the PV systems, the reported incidents, the associated fire risks, mitigation strategies as well as reviewing the available literature on the current experimental methods to study the BIPV fire products such as smoke (section 2.2 to 2.5). Consequently, the research gaps are identified (section 2.8) and based on these gaps the main objectives of the study are defined (section 2.9)

2.1. Introduction

Considering that the buildings sector accounts for a notable amount of energy use and accordingly greenhouse gas (GHG) emissions [1], reducing energy consumption and electricity demand in buildings using advanced clean and energy efficient technologies is essential for achieving worldwide commitment. To make buildings more energy efficient, advanced clean and energy efficient technologies, especially PV systems, have become widely applied in new and existing buildings and communities, which, meanwhile, brings a new and intractable challenge to fire smoke protection.

It was reported that by August 2019, seven of 240 Walmart stores, which had solar panels installed on the roofs, had solar roof fires [2]. It is important, therefore, to conduct a systematic review of PV fires and their causes, PV fire characteristics and mitigation strategies and current codes and standards. This helps to identify research gaps in understanding the fire risks of PV systems and contribute to the wide and safe application of PV systems in buildings thereby reducing GHG.

There are two principle categories for PV systems: Building-Attached PV (BAPV) systems and Building-Integrated PV (BIPV) systems [3]. BAPV systems are mounted on the surface of finished roofs or walls without playing any structural role in the building. In contrast, BIPV systems are installed as roofing panels, façade claddings and glass curtainwalls so they have a direct effect on a part of the structure's function by taking the place of the conventional building components such as the roof or façade. Both BAPV and BIPV systems cause fire safety

challenges for buildings. While fires could start from faults in a PV cell, the risk of fire can be elevated by the fire spreading over the PV panels and eventually inside the building. The fumes from PV fires could enter the buildings through windows and roof openings (e.g., chimneys and ventilation openings) and create toxic conditions for people in and around the buildings, leading to smoke inhalation injuries since solar panels and batteries contain toxic chemicals. Therefore, current building fire protection systems (e.g., smoke detection and smoke control systems) need to be reviewed for any additional requirements for PV fires. Also, new requirements for fire suppression and firefighting need to be developed since PV fires could create hazardous reactions in the presence of water (applied by building sprinkler systems or firefighters).

Studies on the safety of PV panels are only at the stage of reviewing the performance failures and faults to improve PV cell efficiency and are not at the stage of reviewing the impact on the overall building fire safety. It should be noted that fault occurrences can drastically endanger the reliability and safety of the system and the whole building. For instance, any electrical fault in the DC section of a PV system has a disastrous effect on the energy yield, which is unpredictable most of the time and sometimes proves to be the cause of a burn-down of the whole system even if the system is believed to be fully equipped with protection devices [4].

Due to the lack of understanding and systematic research on the fire risk of PV systems, specially BIPVs (case of direct safety threat to the occupants), are of particular concern. The current building codes and standards also do not provide comprehensive provisions for various applications of PV systems. The prerequisite of reaching the full provision is further research on PV fire and its impact on the overall building fire safety while the current studies are at the stage of looking into the performance failures and faults of PV cells rather than the PV building systems. The objective of the present study, therefore, is to conduct a systematic review of the current literature to find research gaps and develop research plans for codes and standard development to help fire-safe adaptation of PV system into buildings.

The available reviews on the PV systems are limited to the aspects of the PV cells. For instance, there are reviews on the fault diagnosis and the fault protection challenges [5]. Moreover, there are reviews which outlines various commercially available PVs [6], comprehensive review of the applications in terms of energy generation amount, nominal power, efficiency, type and

performance assessment approaches [7]. More generally, some design, operation and maintenance reviews can be found [8].

This study outlines the challenges associated with the possible fire risk in photovoltaics. Considering life safety associated with fire risk of PV, this study reviews different scientific and technical data related to the fire safety of PV panel systems in buildings rather than other PV applications, such as on vehicles and free-standing solar structure. Thus, real building fires that occurred in the PV systems are reviewed for their causes and damage in Section 2. Various faults in the PV system, which can be a potential fire risk, are summarized in Section 3. Section 4 discusses current studies on the fire characteristics of an ignited PV panel in various situations. Section 5 introduces the endeavors to lessen the systems' aftereffects by applying mitigation strategies. In this way, the insufficiencies and gaps are proposed for future investigations.

In this systematic review, there was a process of definition, classification and narrowing down to the desired refinement level which make it different from the traditional narrative review [9]. The review process can be divided to three main stages. At the first stage by reviewing 15 articles, the definition and main classification of the available had been revealed. Firstly, a limited number were those with a focus on photovoltaics fire behavior. The second group goes to those discussing the available imperfections, errors from the electrical point of view. The last group generally discussed the available rules regulation and test methods on the PV panels. The number of referenced articles in each group increased in the second stage by searching the related keywords. This literature can be accessed in each stage by the following main keywords: 1) PV module, fire reaction, PV panel fires, reaction to fire, fire behavior, fire experiments, cone calorimeter, heat flux; 2) PV safety issues, reliability, PV electrical faults; 3) PV fire mitigation, fire codes, fire test, PV backsheet, PV test protocol. The articles have been collected from internationally recognized journals, conference proceedings, study, and test reports via search engines such as Google Scholar, ScienceDirect and SpringerLink. The last stage was to conclude to show the unstudied region or the parts which needs further research. Figure 2 shows the overview of these three main stages and the measures taken in each stage.

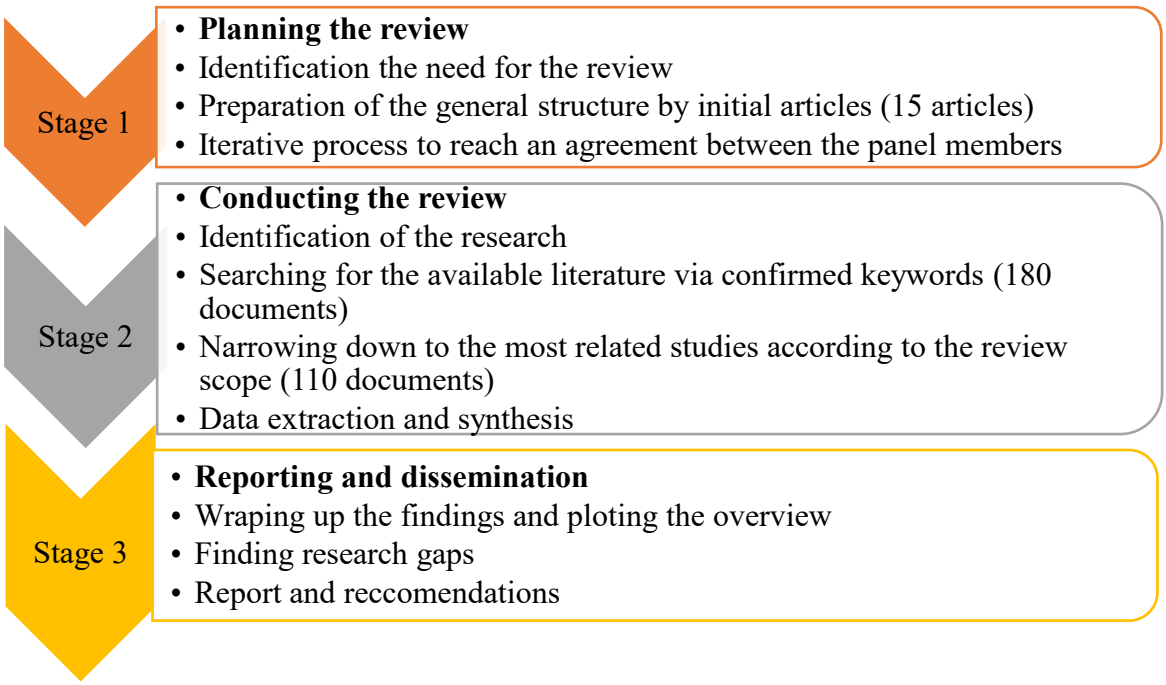

Figure 2. Stages of the systematic review

2.2. Real cases of fire incidents in the PV panel systems

The survey study conducted by the Italian National Firefighters Brigade [10], reports 1600 fire incidents out of a total of nearly 590,000 installed and operating PV plants in Italy. Grant [11] also provide a report on some serious PV fires in buildings, such as an April 2009 fire in Bakersfield, Calif., a May 2013 fire in LaFarge, Wis., and a September 2013 fire in Delanco, NJ [10].

According to comprehensive research conducted in Germany for the 2-year period from 2011-2013, 430 cases of fire or heat damage were reported among 1.3 million PV systems. Half of the cases were caused by PV panel systems, and the other half were started from an external source. It is reported that approximately a third of the fires caused by the PV panel systems were due to PV component defects. The rest of the cases were equally caused by planning errors and installation errors [12]. Laukamp et al. also reviewed 180 cases of fire damage and overheating and 220 cases of PV systems damaged from an external fire source [14].

A representative selection of PV fire incidents is presented in Table 1. These fire incidents reflect a diverse set of causes and damages [15], which will be categorized and analyzed in Section 2.3. It should be noted that some of the cases presented in Table 1 do not have enough information about the extent of damage, and more importantly, the real causes of the fire incidents are not identified, only their probable causes.

Table 1. Documented examples of fire incidents involving PV systems

Location	Condition	Damage	Reason
March 2009, Simi valley CA [15]	Residential, PV integrated on roof	Not available	Residential fire started in a shingle module of an integrated roof PV system
June 2009 Germany, Bursdadt [15]	Warehouse	Not available	Fire occurred at the PV module within the array
Bakersfield, CA, US 2009 [16]	Large retail store, 380 kW array on roof	Fire didn't penetrate metal roof decking	The rooftop system was the cause of the fire
Mount Holly, North Carolina, US 2011 [16]	Drywall manufacturer, PV on roof	Not available	Ground fault related
Goch, Germany 2012 [16]	Warehouse, PV on roof	3995 m^2 roof area involved	Associated with a defect in the PV system
Delanco, NJ, US 2013 [16]	Warehouse, 1.6 MW on roof	A 30,000 m^2 structure was destroyed	Initiated in the cold storage facility
La Farge WI, US 2013 [16]	Office, 70 kW on roof	A wing of the 4,000 m^2 building was destroyed	A fire in the building caused the rooftop PV system to energize the entire metallic roof during the fire
Norderney, Germany 2013 [16]	Factory, PV on roof	Damage of a few million euros	Victim (from the building to the roof)

Florence Township, NJ, US 2013 [16]	Retail store distribution warehouse, PV on roof	Building and contents were destroyed (28000 m^2 roof area)	Initiated on the roof!!
Walldorf, 2014 [16]	Warehouse, PV on flat roof	Damage of a few thousand euros	Fire initiated from the roof owing to a technical defect
Sagamihara, Japan 2014 (NEWS)	A wooden two-story one-year old house	Half burned	A fire broke out around the roof-integrated solar panel
Saitama, Japan 2017 (NEWS)	ASKUL warehouse, PV on roof	More than 45000 m^2 was involved	The fire broke out on the first floor where cardboard boxes were stored.
Ohio, Maryland, CA, US 2012-2018 [16]	Walmart stores	Not available	A defect in the solar panel system
Redland, CA, US 2018 [16]	Amazon's warehouse	Not available	Malfunction in the solar panel array
Tesla solar panels in Walmart stores, US 2019 [2]	Seven of 240 stores in which solar panels were installed on roofs caught fire.	Resulting in multiply fires across the US	Systematic negligence in operating, installing and maintaining the solar system by the producer company
Ichihara, Japan 2019 (NEWS)	Mega power station on Yamakura Dam, 50000 sheets	No injuries	Typhoon impact

2.3. Faults in PV panel

PV panel systems, like other power generating systems, can fail due to different faults. These failures can cause a fire in PV modules, which can spread and become a hazard. Based on the review of the current literature about PV systems and related fire incidents in Section 2.2, a major classification for fire scenarios in PV panels consists of an "original fire scenario" and a "victim fire scenario". This is directly pointed by Mazziotti et al. [17] that the fire risk in PV must be noticed both as a cause or as a victim. Moreover, a general classification of faults is provided by Pillai and Rajasekar [5], including the same idea as Mazziotti. Considering the

primary categories, each of them can be sub-divided into physical, environmental, electrical, natural, and manmade classes according to the root cause of the initiation.

An overview of the various kinds of faults discussed in this paper is presented in the tree diagram of Figure 3.

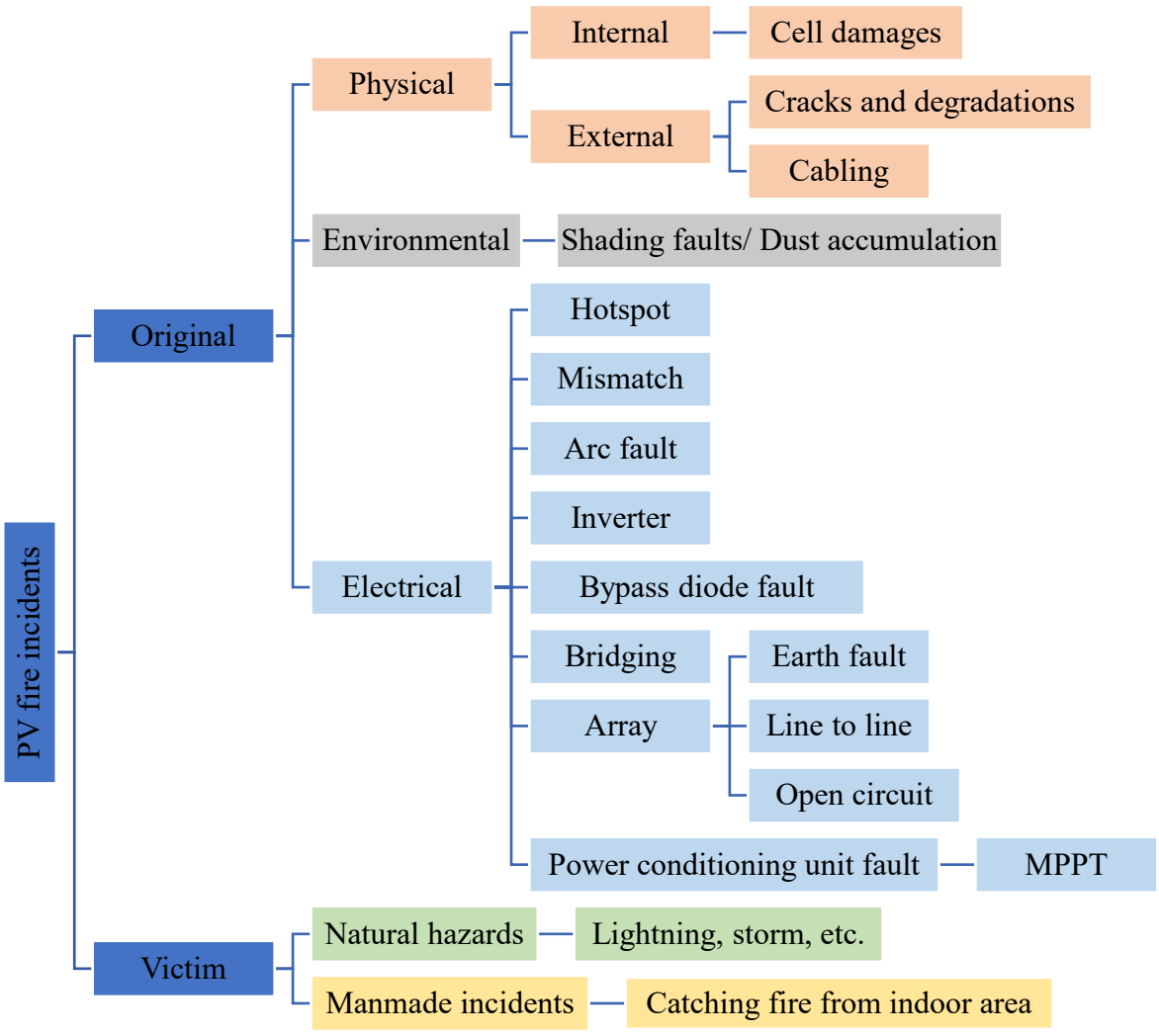

Figure 3. Classification of PV fire incidents based on the faults

The tree diagram shows a major classification of faults and failures in PV panel systems that are believed to lead to potential fires. The major classification is based on the origin of a fire. If a fire starts from a problem in a PV system itself, then it goes under the label of 'original' fire; otherwise, it is a 'victim' fire. The original fire is sub-classified into physical, environmental, and electrical categories. The physical category consists of internal and external problems related to the location of a problem. The environmental category includes the cases in which a PV panel causes a fire due to some environmental impacts such as shading faults or dust accumulation on the panel surface. The electrical category has the most varied types of failures. The various original fire cases are discussed according to three categories to understand how PV systems can initiate a fire.

2.3.1. Original fire scenarios

The original fire scenario includes the incidents that are initiated within the PV system by its components. There are several reviews on failures in PV panel systems [5], maintenance [8] and cooling strategies [18], which give great insight on the potential kinds and extent of fire risks. In this section, various types of failures, including physical (cell damage, crack, degradation), environmental (dust and shading), and electrical (hotspot, mismatch, arcing, ground, line-line), are discussed with a focus on their consequent fire hazards.

2.3.1.1. Physical category

Physical faults internal to PV cells, such as cracked cells, broken solder joints and shorts between a cell string and the metal substrate, are reported to cause fires within various types of PV systems. The internal and external physical faults can cause overheating produced by poor connections (i.e. a mechanically loosened connection results in insufficient electrical resistance). In this way, a PV system has the potential to initiate a progressive failure that could cause a glowing connection at a much too high and undesired temperature [19]. Therefore, poor connection among PV modules, PV arrays and inverters, which are connected in a series, causes fires to break out. A good example of this is presented in Cancelliere's study [10], which depicts an ignited PV power switchboard due to poor physical connection.

2.3.1.2. Environmental category

Shading is a fault occurring when PV panels are partially covered usually by natural reasons, such as accumulated dust [20], tree shading, passing clouds, building shades or any other objects, which can significantly affect the system performance. The effects are classified into three main groups: (a) a reduction in the energy input to the cells; (b) an increase in energy losses in the shaded cells; (c) reduction in illumination with reverse bias in the cell (because of the improper illumination distribution over the surface of the PV panels) [21]. Among the above-discussed cases, the worst scenario happens when the whole surface (or a considerable portion) is shaded by any of these external objects. This directly results in a localized hotspot due to the current flows through small areas, which are large enough to produce a high and undesired temperature [22].

There is some evidence which shows that the non-uniformities including partial shading on the module surfaces cause localized overheating and heat stress, resulting in fires [23]. This failure is a safety gap, which is not studied enough, considering that aging modules show more non-uniformities. This draws attention to the importance of a module usage period. Since not all the causes of shading are controllable or reduced (e.g. by periodical and planed PV maintenance to avoid dust accumulation), more research attention needs to be directed at the fire safety aspect of PV faults.

2.3.1.3. Electrical

It is stated that PV arrays have unique fault scenarios, which differ from the traditional power sources. Concerning the installation location, faults for the PV system can be categorized into three main groups:

- Faults in the arrays;

  Firth et al. [24] used a category including four different faults in the array to construct a simple empirical performance model. Forman [25] introduced five principal causes of failure in the array. Meyer and Van Dyk [26] considered degradation of PV module performance parameters in several modes located in the PV array. Nguyen and Lehman [28] considered faults in the PV array and its performance under changing illumination conditions. Patel and Agarwal [29] focused on the MPPT scheme operating under

partially shaded conditions. Spertino and Akilimali [30]focused on two typical faults in the large PV arrays (mismatch and reverse current). [31] conducted research on fault detection in array fields by employing PV circuit simulation. [32] studied faults in PV array during the night to day switches. [33] analyzed faults in the PV array under low irradiance conditions and reverse connections. Zhao and Lehman [34] discussed line-line faults related challenges in the PV arrays. Moreover, Zhao et al. [35] introduced challenges to overcurrent protection devices in PV array.

- Disorder in the power conditioning unit

  Chan et al. [36] presented the reliability estimation of the power stages in three grid-connected PVs. [37] demonstrated an integrated method for reliability assessment of converters in the PV system. [38] discussed distributed MPPT to solve the effect of module mismatching. Ji et al. [39] studied a real MPPT method to compensate mismatching caused by partial shading. [40] introduced a novel variable step size incremental-resistance MPPT algorithm for improving the speed and the accuracy. [41] also developed a method to improve PV inverter reliability.

- Abnormality on the utility grid

  [42] conducted the first systematic study of the performances of inverters connected to the same electrical power system in PVs. Petrone et al. [43] provided an overview of the problem related to the PV power processing system. [44] studied an islanding detection method to mitigate islanding (a serious safety risk) of PV.

This section is to briefly mention each fault and the related literature. Most of the common electrical faults are in the first category including instance hotspot, mismatch, line-line, open circuit, and ground which will be discussed further in sections 3.1.3.1 to 3.1.3.5. Other electrical faults including MPPT, Battery Bank, AC and DC side belong to the power conditioning unit and utility grid. The latter two groups are less probable to happen and are briefly introduced in section 3.1.3.6.

Hotspot

A “hotspot” is caused by many original or victim faults, which occur on a PV module. In this case a solar cell or a group of solar cells is forced into reverse bias and must dissipate power

that can result in abnormally high cell temperatures in a restricted area on the surface [22]. This localized hot area has the potential to and is energized enough to start a fire, for example on the backsheet. A hotspot is the most important electrical cause of ignition as noted by the UL research project [45] and [10]. [46] also introduced “hot spot” as a fire originating within a solar power system as a point of ignition. This fault is formed under other fault conditions such as partial shading, imperfect material production, flaws or damages to the PV cells themselves.

Mismatch

The term, mismatch, describes the difference in performance between individual solar panels in an array. This difference can be due to shading in a restricted area on the surface or the degradation of some cells or cell misalignment. The panels are connected to each other. When one of them underperforms, a reverse current may occur in a module which is responsible for a specific fire ignition process named ‘mismatch’ [10]. Qiu et al. [47] studied mismatch in thin film PV modules. Moreover, the above case may result in power losses and hotspots [48]. By providing a hotspot, a restricted localized high temperature can be formed, which is high enough to produce the energy required for igniting the PV panel. Moreover, a comprehensive study of the mismatch fault is provided by other researchers but not as a cause of a fire; Grunow et al. [49] studied hotspot risk due to cell permanent mismatching in silicon cell modules. Hammond et al. [50] studied mismatch fault formed by soiling of PV module under various irradiance intensity during the day. Heidari et al. [52] presented the impact of snow and ground interference on mismatch fault. Nguyen [53] also used a MATLAB model to study the partial shading effect on creating a mismatch.

Arcing

An electrical arc is known for its bright light emission in both the visible and ultraviolet ranges. In addition to eye damage caused by this light it is distinguished by extreme temperatures even higher than 10000 K; thus, the potential resulting fire can easily spread to the other components and even cross the array restriction. Arcing, therefore, is the biggest threat from faults within the PV panel with its resulting temperature being high enough to ignite the area. The preliminary classification of this type of fault is series arcs (due to a bad connection or a break in wiring), parallel (line to neutral) arcs (resulting from a failure of insulation between positive and negative terminals of an array or sub-array) and line to ground arcs.

A parallel arc is a kind of short circuit that generally occurs at a high-level. Short circuits can cause an electrical shock if the frame is not properly grounded. In the case of parallel arcs, the entire system voltage is available for ignition and producing the electric arc; even smaller currents are enough to produce a stable electric arc. Fortunately, parallel arcs do not occur frequently because of the double insulation of the cables in the PV system. Of the three groups classified above, series arcs are the most likely to occur since there are countless serial connections in an array and thermal cycling and aging in the system cause poor connections over time [54]. If one of the connections in the serially connected points deteriorates or fails during the operation period, an elevated transition resistance will be produced, which causes the surface to become overheated from the current flow. When the heat generated distributes, it can result in melting and diffusion of the other contact materials to the point that the connection is fully ruined. In this situation, it is probable that an electric arc forms over the air gap; this arc is initially very small. Series arcs are within the limited current level in comparison to the parallel electric arcs, since a fraction of the voltage drops via the inverter.

Another important point is that the destruction increases when a series arc develops into a parallel arc. In this case, the Lorentz force gives the parallel electric arc the slope it needs to move from the PV module and direct the fire hazard to the inverter [12]. Last but not least, a persistent DC electrical arc is one of the major causes of fire ignition in a PV power plant [10]. There are many studies on the arc fault protection strategies such as the study conducted by Xia et al. [55] on the arc fault detection for household photovoltaic systems. Separated from the other probable failures, any form of arcing can rapidly ignite a disastrous fire, which can potentially cross the PV system restriction and spread to other sections. This is a subject of discussion in several research articles; Bower et al. [56] studied the creation of arc fault detector and mentioned its importance in fire prevention. Johnson et al. conducted several studies, including dynamic equivalent PV circuit model for arc fault, differentiating series and parallel arc faults, and thermal finite element model of arc faults [57]–[60]. Moreover, Johnson and Kang [61] presented an arc fault detector algorithm to improve the fire safety of PV system.

Ground

Because of the electrical conductivity nature of the PV panel system, there is always a possibility of electric shock. This can be prevented by connecting the noncurrent carrying parts to the earth

using Earth Ground Conductors (EGC). The random connection between these EGC and Current Carrying Conductors (CCC) in a PV array produces rapid and persistent current flow to the ground [62]. Moreover, analysis of grounded and ungrounded PV systems is provided in [63]. This term is named ‘ground fault’. As claimed by Zhao and JR [64], a ground fault is the most common fault in PV panel systems and is capable of producing large fault currents easily increasing the risk of fire hazards. There is a wide range of causes of this fault in the PV panel system, which are well discussed in the following pieces of research; Forman [25] evaluates grounding effect on the performance of terrestrial PV modules. Zhao [65] also discussed grounding in a section of his master thesis. A typical ground fault is introduced by Zhao and JR [64] in a PV array under and its protection method. Some of the causes are improper insulation of cables (chewed cable by animals); incidental short circuits between the regular conductor and ground; ground faults within the PV module.

Line-line

Line-line faults happen when there is unexpected short-circuiting between two nodes in the PV array with different potentials. These kinds of faults do not happen as frequently as some other faults such as ground faults or hotspots in the PV systems and are more difficult to detect and remove with the current protection systems. The line-line fault is sometimes interpreted as a short-circuit fault in a grounded system or a double ground fault in an ungrounded system [66]. It is assumed that there is no ground involvement in this kind of fault detection; otherwise, it will be within the ground fault classification [65]. Zhao et al. [35] introduced the potential fire risk of line-line fault and the challenges of protection.

Other probable faults in a PV system

There are some other types of electrical faults, and knowing the overall descriptions may give the reader key insight on evaluating fire hazards; Zhao et al. [67] discussed several typical faults that may occur in the PV array. Alam et al. [68] reviewed PV faults comprehensively and introduced other kind of faults as catastrophic faults and reviewed types, detection and mitigation techniques. Jain et al. [69] studied converter input, converter component and sensor faults. Low irradiance and reverse connection in a string of PV module is investigated by Zhao et al. [33]. Briefly, these residual undiscussed faults are categorized as follows:

a) MPPT (maximum power point tracker) and inverter faults, which usually happen due to a shortcoming in the converter and switch. Wang et al. [70] studied imperfections in MPPT charge controlers under partially shaded condition;

b) Bypass faults that may occur after short circuits due to large reverse current flow during faults;

c) Open-circuit faults that may happen after line-line failure [71];

d) Faults in blocking diodes that are due to the reverse current flow;

e) Battery bank failure, which can be an output of abnormal charging conditions;

f) Connection errors that are usually results of wrong or reverse connection of panels;

g) Bridging faults, which are due to inappropriate connections between two points of different potential in a string of modules or cabling. This fault can be explored in the following articles; Akram and Lotfifard [71] studied connections on panels and loose cables in a PV string causing bridging and cabling faults. Davarifar et al. [72] discussed bridging as a typical fault in the DC side of the PV system. Hua and Ku [74] presented a novel stand alone PV lighting system with MPPT implementation. Schimpf and Narum [75] focused on wire damage's effect on creating arc fault in the DC side of PV.

Most of the faults mentioned in Categories a to g above occur less frequently than the others, such as MPPT, bypass, open circuit, etc., and have less influence on PV panel performance and probable fire risks. Furthermore, as can be seen, the rare cases usually occur as aftereffects of other more frequent and hazardous faults. The nature of the electrical faults is closely related to each other and some of them are specific version of the others. The intention of this review is to separate the faults and to fit them in the best possible classification. So that in a glance, the most important errors which can lead to a disaster will be noticed. A detailed discussion of each of these faults is beyond the focus of the interests of this paper and needs technical and precise investigation.

2.3.2.Victim fire scenarios

The other major classification is of victim cases in which PV systems are ignited by an external fire source. Manmade incidents include a fire scenario in which a fire is already initiated in other

spaces and later spreads to the PV array area [76]. For example, a fire started in a room on the top floor can grow large and the flames coming out through the window can ignite the roof and roof-mounted PV systems.

PV fires can initiate due to natural hazards such as lightning, typhoons, wildfires and heatwaves. Wildfires and heatwaves are related to the issue of "Climate Change". While many efforts are being made to find mitigation methodologies, these disasters are expected to become frequent and extreme. In particular, a heatwave degrades the safety level of PV systems because it increases ambient temperatures and compromises the operating equipment. The elevated temperature can accelerate the contact degradation of PV cells. A real case is presented in [12], where a fire breaks out in the engineering room of a PV system because of an under-estimation of summer heat stress on the equipment.

Although some studies discuss the probable effects that climate change can have on energy consumption or equipment performance, the potential hazards of the impact of this phenomenon on PV panel fire safety have not been studied. For instance, when electrically charged, the temperature of a PV module (in watt-peak) is reported to be beyond the standard test condition (i.e. 25 °C). In some cases, the ambient temperature reached 40 °C; the solar cell of an average solar installation with proper ventilation can easily reach 65 °C or more [77]. Considering the possibility of being overheated, not only must the performance of the energy production be considered but also the imposed heat stress on the connections and inverters and other parts of the array Therefore, heatwaves, wildfires and unusual temporary hot climate situations can easily increase the temperature of the parts of the panel surfaces, which are already at a thermally excited state. In this way, an unpredictable area of the PV module may have the potential to ignite and start a fire.

2.4. Fire characteristics

Once ignited by an external fire source or a system fault, PV panels burn since they are combustible. PV panels are usually layered and made of silicon as semiconductors and other layers such as PET (polyethylene-vinyl acetate), TPT (tedlar-polyester-tedlar), EVA (ethylene-vinyl acetate) and some cover layers etc. Each of these materials contributes to the fire characteristics and smoke/toxic gas emissions, affecting people and the environment. A

schematic of various impacts associated with a PV fire on the immediate environment is illustrated in Figure 4. The main aspects of fire production are:

a) Flame: the extent of the flame propagation depends on the thermal properties of the burning PV and environmental conditions such as air temperature and wind affecting the burning.
b) Emissions: this varies with the PV type and burning rate. For instance, the composition of gas effluents (CO, CO_2 and toxic gases) is completely different for the PV type and materials used for backsheets or cover layers.
c) Fire residues and debris: the amount and the toxicity of the fire residues is different for each of the burnt specimens. Therefore, extensive and comprehensive investigations and fire tests are required.
d) The interaction of water from the suppression system and the combustion residues: This is a critical point to be considered while it seems that there have not been enough studies conducted on the effectiveness of the use of water for putting out PV fires.
e) Smoke and its distribution: One of the major and most visible and sensible outcomes of a fire incident is smoke. In some stages of ignition, there is no visible flame, but smoke is produced. This can lead to the degradation of air quality when there is poor ventilation. Therefore, without proper ventilation, the condition may become untenable for humans.
f) Soil toxicity: This is to some extent associated with the mixture of water and residues; the toxicants of which can contaminate the soil. However, it is challenging to detoxify the soil and ground water.

As the central theme is the evaluation of fire incidents on a PV panel system, one aspect of the investigations should focus on toxicity and gas emissions. Another important aspect is flame propagation over PV panels. Parameters such as the temperature and heat release rate over time are discussed in this section. PV fire suppression, firefighting and the toxicity of fire residues are not studied or identified for future research needs. Moreover, no study has been conducted on the smoke flow distribution entering the indoor spaces. Smoke transfer is possible via the shafts and roof ducts or by the breakage of the BIPVs. This section discusses the parameters used in the literature to measure fire size and its potential to degrade the safety level of the PV panel system.

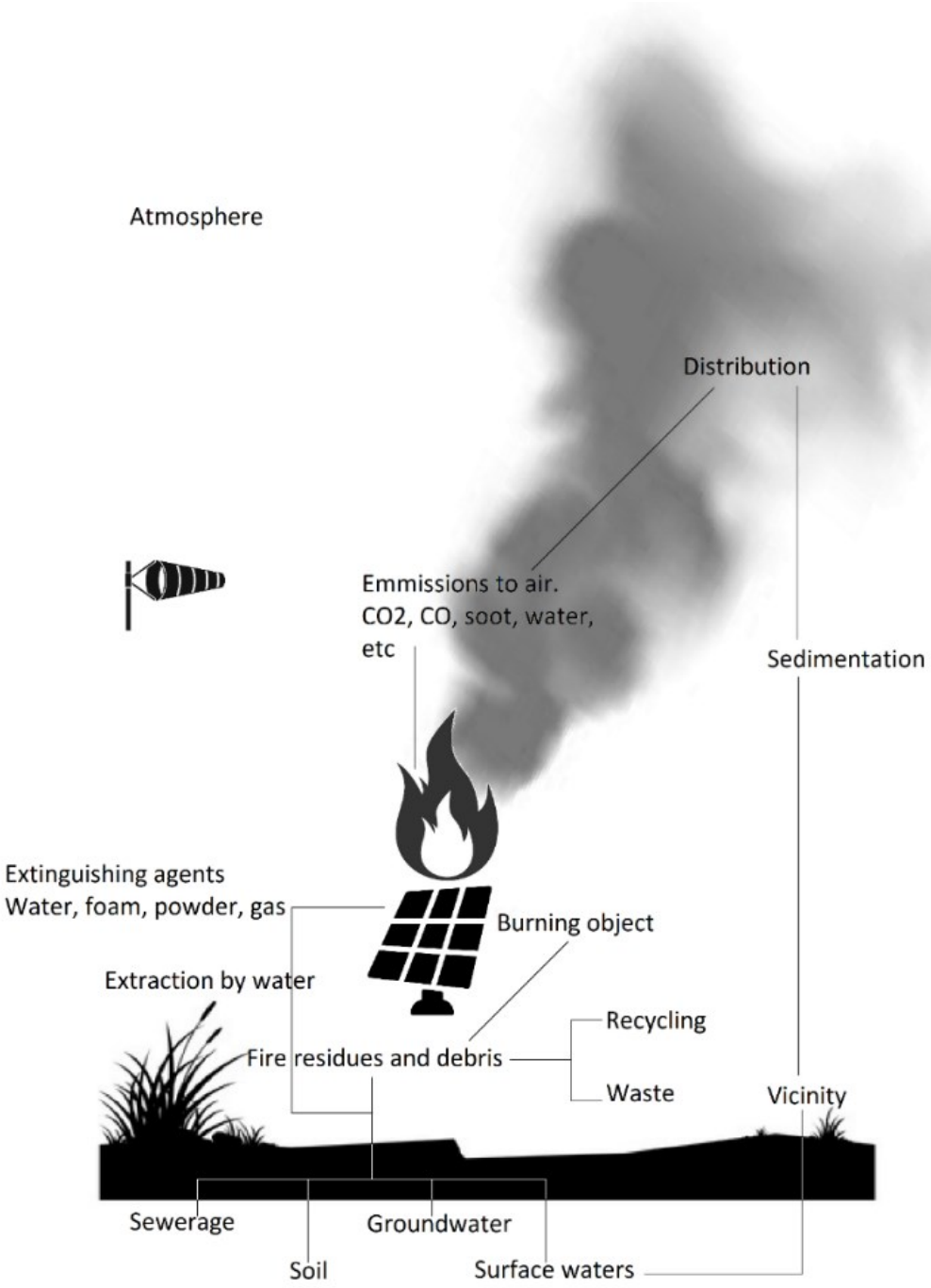

Figure 4. Illustration of environmental aspects associated with a fire event of PV

2.4.1.Testing apparatus

To study the reaction to fire, the Cone Calorimeter (CC) is one of the most acceptable fire testing bench scale methods, in which a sample is exposed to a uniform heat flux from the conical heater

as if it is exposed to a real fire. It is found that the results of the tests in the cone calorimeter correlate well with those measured from large-scale fire experiments [78]. Thus, they can be used to predict and evaluate the combustibility and the reaction to fire characteristics of PV panels. Details about the standard test method for the CC are discussed in [79]. CC test results of some PV types are published as follows: Chow et al. [81] used the CC test to evaluate fire behaviour of two commonly used PV brands and Ju et al. [82] used the same approach to test the combustibility of flexible PVs. Ju et al. [83] performed a CC test to simulate the face/back of polycrystalline silicon PV exposed to external heat. Ju et al. [84] also used the CC test to observe two widely used photovoltaic (PV) panels' (with different coverings) behaviour under various incident heat fluxes. Last but not least, Yin et al. [86] used the CC test to study the combustion behaviour of the CIGS thin film module. Almost all the experiments on the PV panels, tested sample PV panels (sample size 10 by 10 cm) in the horizontal direction in the CC. It was debated by Tsai [87] that orientation affects test results for assessing the fire hazard of materials and he concluded that vertical orientation is recommended for evaluating material fire performance. Hence, more varied orientations and angles to the exposed heat must be considered while trying to evaluate the fire characteristics of PV panels since they can be used for facade and roofing.

2.4.2.Parameters

Ju et al. [82] indicated that flashover room fires affect the installed PV in the vicinity. Therefore, ignition of the panels under high heat fluxes is foreseeable. The radiation from the plume coming out from the window of the flashover room fire affects the module. Thus, exploring the connections between the heat flux and fire characteristics of the PV panel is of high importance.

The most important and applicable parameters, which are used to define the reaction to fire characteristic of an ignition process, are ignition time, ignition temperature, heat release rate (HRR) and mass loss rate (MLR). The details about these parameters are introduced as follows:

4.2.1. Ignition time

A key parameter for characterizing the thermal decomposition behavior of materials, is ignition time (IT), which describes fire resistance. The higher the IT, the longer it takes to ignite a material. This term is defined as the time interval from the initial exposure to irradiation to the

moment a flame visibly arises on the material surface [88]. In general, different heat flux levels are imposed on the specimen surface to measure their effect on fire behavior. Babrauskas [89] recommends a heat flux level of 25-50 kW/m^2 as the appropriate level for most purposes. However, for PV panels, relatively higher heat fluxes are required to obtain the complete burning characteristics. It is indicated in [80] that the glass cover of PV panels insulates the combustible layer when the heat fluxes are lower than 70 kW/m^2. The heat fluxes ranged from 18 to 45 kW/m^2 in [90], and a higher level reaching 70 kW/m^2 was used in [82], [84]. The studies show that an increase in heat flux results in a sharp decrease in IT. Evaluations of ignition time versus heat flux are well discussed in [84], [90]. The rapid decrease in the IT of two samples with increasing heat fluxes was explored in [82]. Tsai [87] considered the orientation of cone calorimeter on the results of burning polymethylmethacrylate to assess the fire risk.

IT can also be checked theoretically by equation (2-1) for a thermally thick condition [91], [92]:

$$t_{ig} = \frac{\pi}{4} k\rho c \left(\frac{T_{ig}-T_\infty}{\dot{q_e''}}\right)^2 \quad (2\text{-}1)$$

where t_{ig} represents ignition time k, ρ and c are thermal conductivity, density and specific heat, T_{ig} is the ignition temperature, T_∞ is the ambient temperature and $\dot{q_e''}$ is the incident heat flux. Some studies try to calculate the IT by estimating the heat observed ($\dot{q}''$) based on critical heat flux (CHF). CHF is defined as the minimum value of heat flux for which the composite inflammation is perceived, and below this value of heat flux no flame forms [88]. The approach is only valid for thermally thick materials since the correlation is different for other types. Therefore, prior to defining the evaluation method, the thermal behavior of the selected sample must be studied to determine whether it is thermally thin or thick. For the thermally thick or thin verification, the following two methods may be applied:

1) Plot t_{ig}^{-1} and $t_{ig}^{-0.5}$ versus external heat fluxes and see if the curve of t_{ig}^{-1} as a function of the external heat flux is nonlinear while $t_{ig}^{-0.5}$ vs external heat fluxes can be replaced with a straight line within an acceptable fitting degree. This approach verifies that the sample behaves as a thermally thick material. It also indicates that a thermally thick sample has a temperature gradient while a thermally thin sample has a uniform inside temperature (as

Figure 5 depicts the evaluation for a PV sample). The curve of the t_{ig}^{-1} as function of the external heat flux was produced to see if the trend is linear or nonlinear.

2) Some tests can be conducted to look for the probable temperature gradient inside a test sample, using two thermocouples mounted on the exposure and the rear surface of the sample in different coordinates. By exposing a heat flux, the maximum temperature difference inside the sample can be observed. If there is a gradient, it can be concluded that the specimen is thermally thick. This is the method employed by Yang et al. [90] in studying the flammability of PV modules (
3) Figure 6. Thermocouple setup in reference [90]

Two thermocouples were employed on the exposure surface and the rear surface to measure the temperature profiles.

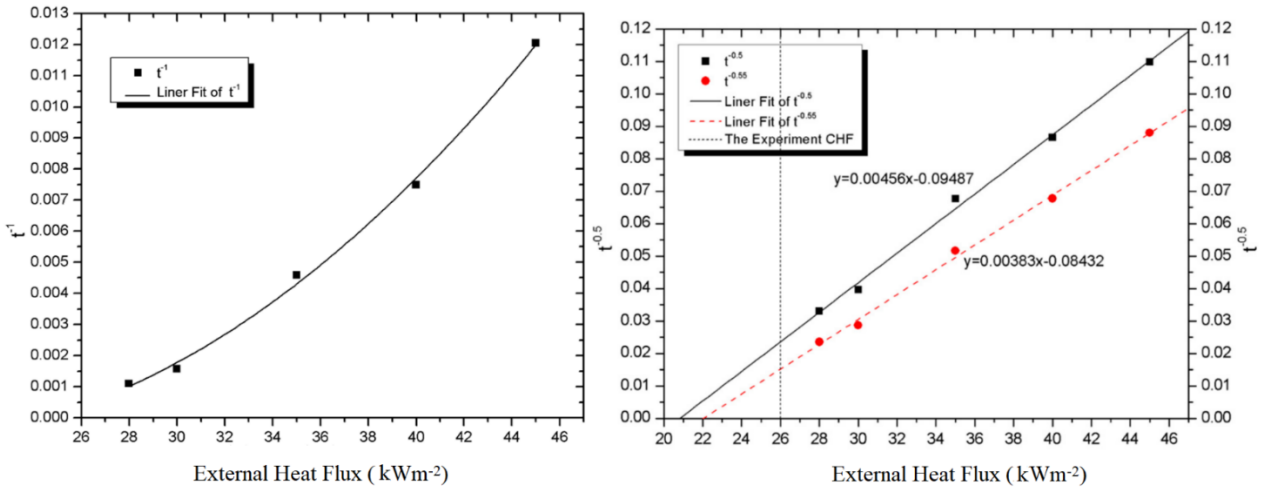

Figure 5. Ignition times plotted assuming a thermally thin condition (on left) and a thermally thick condition (on right) (Source:[90])

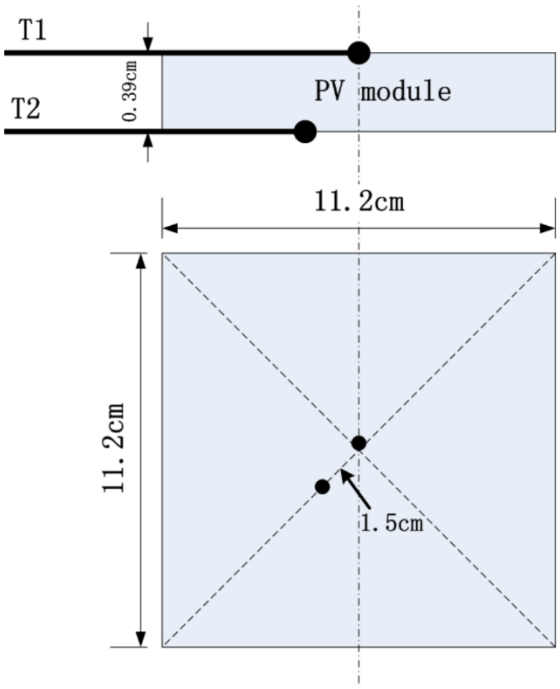

Figure 6. Thermocouple setup in reference [90]

Ju et al. [84] calculated the ignition time of two different PV samples with various heat flux exposures. The only difference between the two samples was the material used in the covering layer. The overall measurements showed a reduction of the ignition time from 641s to 51s at a heat flux of 30 kW/m^2 when the covering layer changed from glass to PET (polyethylene-vinyl acetate). observed the ignition time of two commonly used polycrystalline silicon PV modules; one made of silicate and the other mainly made of epoxy resin, which is claimed to have fire retardants. A difference of 14 s was observed in the ignition times of the two samples while they were exposed to the 70 kW/m^2 heat flux. Similarly for tracking the ignition time, chose small typical polycrystalline silicon PV modules. The parameter had a continuous reduction from 913 to 83 while the heat flux increased from 28 to 45 kW/m^2. The same approach was used in [82] to observe the variation of ignition time under different heat fluxes for FPV (flexible photovoltaic) samples. In addition, Yin et al. [86] reported a decrease in time to ignition from 128s to 38s when the heat flux increased from 25 to 45 kW/m^2.

It is shown that by increasing the exposed heat flux, the ignition time of PV samples rapidly decreases, which gives a great insight to the fire resistance of PV panels and indicates how

quickly heat transfers through different layers from the exposed surface to combustible layers in different selected samples.

4.2.2. Surface temperature

When a sample is subjected to a heat flux, the surface temperature tends to increase gradually. By measuring surface temperatures at the exposed and unexposed sides of a PV panel, the ignition temperature is determined by applying the equation (2-2) [82]:

$$\dot{q}''_{min} = h_c\left(T_{ig} - T_\infty\right) + \sigma\left(T_{ig}^4 - T_\infty^4\right) \quad (2\text{-}2)$$

where $\dot{q}''_{min}$ is the experimental critical heat flux, h_c is the convective heat transfer coefficient and σ is the Stephan-Boltzmann constant. To get a valid ignition surface temperature, the experiments require observations using camera records.

There are not many studies on the surface temperature of ignited PV panels. Yang et al. [90] showed the temperature profile of the two thermocouples installed under the external heat flux of 25 kW/m^2. A maximum difference of 100 degrees was observed between the exposed and unexposed sides of a sample. The same method was applied in [85] to measure the temperatures on the exposed and unexposed surfaces over time. With the temperature measurements obtained, Ju et al. (2018) [82]calculated the ignition time for two different samples. The ignition time was determined to be about 670K for both FPV and PET+TPT (PET: polyethylene terephthalate and TPT: tedlar-polyester-tedlar). Moreover, the temperature difference was observed to increase for both samples with increasing heat fluxes.

4.2.3. Heat Release Rate and Heat of Combustion

Heat release rate (HRR) describes the size of a fire and is the most important parameter in a fire hazard analysis. HRR is the rate at which heat is produced through combustion reactions. In addition, it provides the basis for hazard calculations for fire intensity and fire spread [93] and Kodur and Harmathy [92] named HRR as the most important parameter for fire extent description as well. Furthermore, the maximum HRR (i.e. the peak value of an HRR curve) [79] and the duration of the curve are also used in design calculations of fire protection systems.

The HRR is calculated by using the oxygen consumption calorimetry [84]. Figure 7 illustrates HRRs versus time for different heat fluxes exposed to a tested PV sample Ju et al. [84] showed

that the peak HRR increases, and the duration of heat released (the width of the curve) greatly decreases with an increase in the irradiance level, from which it can be determined that increasing heat fluxes accelerate the combustion/decomposition process. In addition, the fire growth rate index (FIGRA) is used for a better understanding of the ignition process.

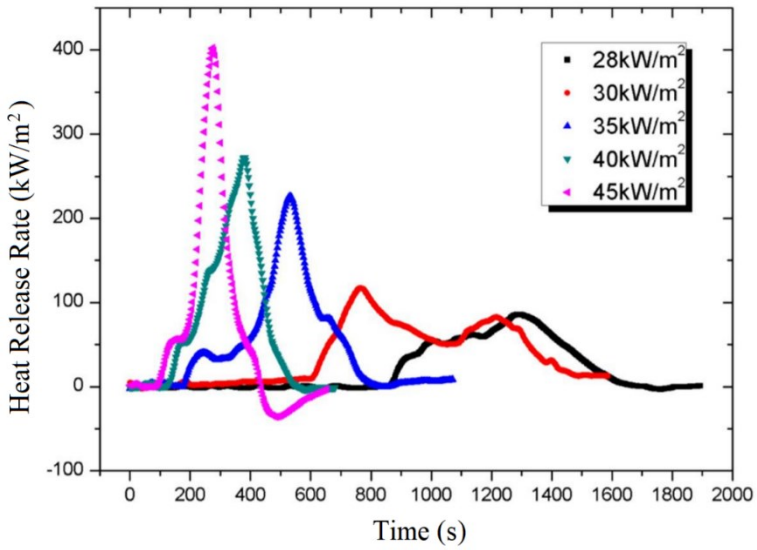

Figure 7. Heat release rate of PV module as a function of time (Source: [90])

Besides the heat release rate analysis, some of the studies (later discussed) investigated the thermal decomposition and burning behavior of samples using thermo-gravimetry analysis (TGA). This approach can be used to determine the fire behavior of each layer of a sample PV module. Thus, it is possible to find the main component responsible for the burning. To illustrate, Ju et al. [82] conducted a comparison between FPV and PET (polyethylene-vinyl acetate) +TPT (tedlar-polyester-tedlar) using thermo-gravimetry differential scanning calorimetry (TG-DSC). Chow et al. [81] studied a silicate product with polyurethane adhesive and an epoxy resin. The tests demonstrated various thermal behaviors of different samples by the TGA approach.

The HRRs of various types of PV samples are published. Ju et al. [84] reported that the measured HRR increases to a first peak and then goes to a second peak. The second peaks are higher than the first ones, so the second peak is considered as the peak HRR. The range of HRR variations under the heat fluxes of 70 to 18 kW/m^2 and 70 to 26 kW/m^2 respectively for the samples A and

B are reported to be 951 to 380 kW/m^2 and 500 to 130 kW/m^2. Ju et al. [82] observed only one peak HRR. The values of peak HRR continuously reduced from 700 to 390 kW/m^2 while the external heat flux decreased from 70 to 20 kW/m^2. The same process was tracked in [80], [85], [90] to measure the HRR values for various external heat fluxes.

Equally important is the heat of combustion that is another fire characteristic of materials. The effective heat of combustion (EHC) is a parameter that corresponds to the heat released from the combustion of a unit mass of a material, which can be measured by dividing the HRR value by the MLR.

EHC was explored by Ju et al. [82] for two different samples of FPV and PET (polyethylene-vinyl acetate) +TPT (tedlar-polyester-tedlar). The average EHC was measured 20±0.2 MJ/kg for both samples. Likewise, Chow et al. [81] computed the EHC values for two types of samples under various heat fluxes (EHC varies from 31.2 to 27.4 MJ/kg for the heat fluxes between 70 to 20 kW/m^2 in sample A while the value remains around 14.4 MJ/kg under all heat fluxes for sample B).

4.2.4. Mass Loss Rate

Mass loss rate is an indicator of how much pyrolysis, volatilization and burning occurs in the sample during the test under constant heat flux. This term is closely related to the HRR and yields of combustion products (e.g. CO and soot) [94]. The mass and mass loss rate evolution as a function of time for different heat fluxes for the typical polycrystalline silicon PV module is presented in Figure 8.

The theoretical method to calculate the MLR is by the following equation:

$$MLR = \frac{m_t - m_{t-\Delta t}}{\Delta t} \quad (2\text{-}3)$$

where m_t shows the mass of the sample in the time of t and Δt is the time difference.

An equation is introduced to quantitatively relate the MLR and heat flux [91], [95]:

$$MLR = \left(\frac{1}{L}\right)\dot{q}_e'' + \frac{(\dot{q}_{fl}'' - \varepsilon\sigma T_v^4)}{L} \quad (2\text{-}4)$$

where L (kJ g^{-1}) denotes the gasification heat of the sample, $\dot{q}_{fl}''$ (kW/m^2) denotes the flame heat flux, T_v (K) is the vaporization temperature and $\dot{q}_e''$ is the incident heat flux.

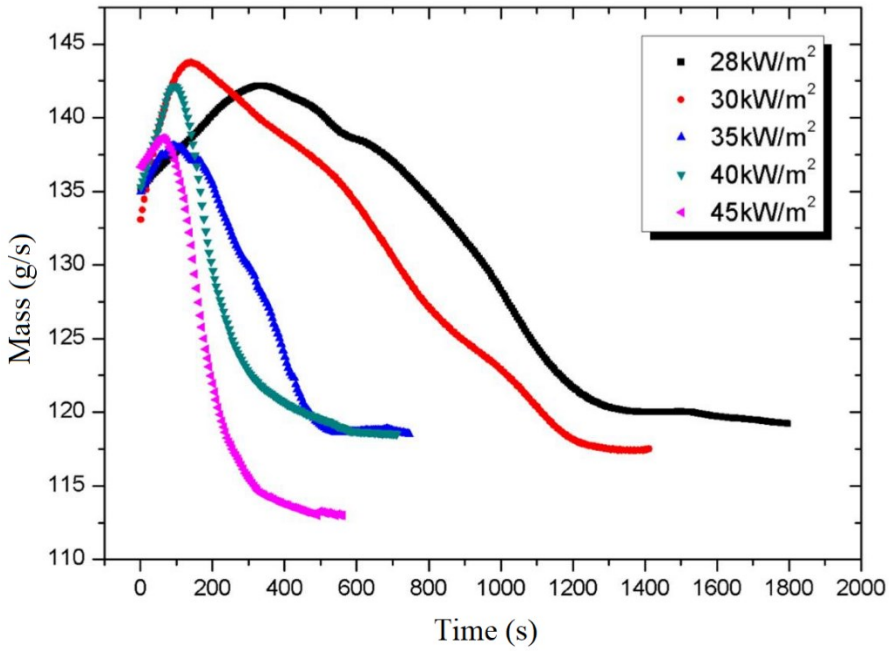

Figure 8. Mass versus experimental time (source: [90])

Figure 8 clearly shows that the photovoltaic module loses its resistance more with the higher heat flux exposed to the sample. The mass loss rate is a variable, dependent on time and the heat flux during the tests. For instance Ju et al. [82] presented MLR evolution varying with test time for the FPV samples. In the MLR measurements, one peak was found and there was no indication of steady pyrolysis. In addition, the presented measurements from PV samples show three different decomposition stages, regardless of the heat fluxes:

- Stage 1: latency period (from the starting moment to the ignition time)
- Stage 2: the ignition of the sample and rapid rise of the MLR after ignition to the peak value.
- Stage 3: the MLR reduces and the remaining sample in the test apparatus will be consumed.

The studies report the mass loss rate as the peak or average value for different heat fluxes. In [80], [85], [90] the MLR changes as a function of HRR were demonstrated. Ju et al. [83] also presented curves of the transient evolution of mass loss rates, where mass loss rate peak amplitude increases, the related peak width decreases with an increase in the irradiance level.

The test is done in two conditions of face up and back up positioning. The values obtained indicate that back-up orientation burns more severely, with a shorter burning time and higher mass loss rate. That is because of the fire protection provided by the glass cover on the face of panel.

2.4.3.Gas analysis

While discussing the safety issues and health threat of a building fire incident, the first and foremost threat is the smoke generated [96]. However, in many countries, smoke toxicity standards are not set in building fire safety codes, rules and regulations [97], which means the importance of smoke toxicity is underestimated. The threshold concentration for life safety is defined for CO (i.e., 1000 ppm), which is a common toxic gas produced from most organic materials. The thresholds for other toxic gases, however, have not been defined due to a lack of effort to determine their thresholds since they are not currently included in the codes [98]. The generation of toxic combustion products depends mainly on the chemical composition of a fuel, yet it is also related to many other factors such as the burning procedure [99], the structure and texture of the materials, and the environment [100].

Experiments using the cone calorimeter can be used as a starting point for investigating smoke toxicity as stated by Babrauskas in a series of research on the toxic hazard of different materials' fire [101]–[104]. Many PV fire behavior studies conduct tests using the cone calorimeter with a section allocated for gas analysis for CO and CO_2 concentrations. The gas production for lower levels of heat flux is lower than that for the higher heat flux levels. The plots of CO and CO_2 concentrations versus time for different heat flux levels as seen in [90] have the same curve shape as the heat release rate for a specific heat flux.

Moreover, to elaborate the toxicity level relative to the impact on life safety, a method named FED (fractional effective exposure dose) is used. FED is the ratio of the concentration of a toxic gas to its LC50 value, and LC50 is the lethal concentration that kills 50% of tested animals. While LC50 does not deviate, the concentration of a toxic gas is affected by the burning conditions. For this reason, Han and Chow [105] suggest that FED can be underestimated when using a gas concentration measured from a cone calorimeter since a concentration from the actual burning of a material under ventilated conditions can yield a larger value.

The values for FED are calculated with CO and CO_2 concentrations, which are also used for gas analysis in the photovoltaic studies. With the measured peak values of the CO and CO_2 concentrations, FED is calculated as below in [85]:

$$\mathrm{FED} = \frac{\mathrm{pk[CO]}}{\mathrm{LC_{50,CO}}} + \frac{\mathrm{pk[CO_2]}}{\mathrm{LC_{50,CO_2}}} \tag{2-5}$$

In the formula, $pk[CO]$ and $pk[CO_2]$ denote the measured peak values of CO and CO_2 in ppm, respectively. The measured value of FED reported in [85] ranges from 0.064 to 0.082 for an external heat flux of 25 to 45 kW/m^2 respectively. When the FED is equal to 1, the toxicity of the gas mixture would be enough to be defined as lethal to 50% of exposed animals. Liao et al. [106] measure FED with different gases and FEC (Fractional Effective Concentration) for the irritant gases as well. The maximum FED reach about 0.325 at 40 kW/m^2 and the peak FEC is 0.35 for 40 kW/m^2 external heat radiation.

2.4.4.Section summary

There are few studies on PV panel fire safety. Most of them use the same approach as the cone calorimeter fire test and measure the temperature by thermocouple on the face or rear surface of the samples. Another method that is applied is TGA which provides a qualitative evaluation of the fire behavior. The problem with the discussion of fire parameters (e.g., ignition time, ignition temperature, heat release rate etc.) is that the variety of samples considered for the experiments is limited. A couple of studies include a gas analysis section, which mainly discusses the CO and CO_2 concentration yielded by burning PV. Other types of gases generated have not been considered yet. In studies on the behavior of PV samples, there is still inadequate consideration of environmental factors e.g., wind effect, orientation of the samples and applied PV on the structures.

2.5. Mitigation strategies

There are suggested strategies, which are believed to limit flame propagation over and around PV panels. This section summarizes the effectiveness of the suggested strategies.

2.5.1.Backsheet

The main components of photovoltaic modules are anti-reflecting coating glass, solar cells, Ethylene-Vinyl Acetate (EVA) sheets and backing material. Among these main layers, the backsheet plays a significant role in safety, productivity and reliability of the module from environmental impacts [107]. As PV modules are usually installed on the rooftop or integrated into buildings, the backsheets are generally designed to resist the impacts of different climatic conditions and external heat, stress and fire. Recent studies on the flammability of different backsheet materials have produced data regarding which materials are suitable with respect to installation locations, probable risks and climatic conditions.

To evaluate and compare reaction-to-fire performances, Nair and Kulkarni [108] chose some common types of commercially available backsheet materials like FEVE (fluoroethylene vinyl ether), PVDF (polyvinylidene fluoride), PET (polyethylene-vinyl acetate) and PVF (polyvinyl fluoride). The arrangements of the layers for the backsheet tests were as follows:

- Backsheet number 1: in three layers and 300 μm thickness as PVDF/PET/PVDF
- Backsheet number 2: in two layers and 275 μm thickness as FEVE/PET
- Backsheet number 3: in three layers and 325 μm thickness as PVF/PET/PVF

In this study a test method was introduced to evaluate the flammability of backsheet materials since there are no fire standards for PV module backsheets nor any fire-flammability regulations for them. Based on the results, in decreasing order of effectiveness, Nair and Kulkarni recommended the third, second and first specimens. The thickness of the third backsheet was determined to be the main reason for its better fire resistance. Moreover, another study [109] tested the flammability and reaction-to-fire of different backsheet materials. Cancelliere and Liciotti [109] chose 4 different types of backsheet materials as follows:

- Backsheet number 1: PET (polyethylene-vinyl acetate)/PET/Primer with a total thickness of 295 μm
- Backsheet number 2: PET/Aluminium/PET/Primer with a total thickness of 370 μm
- Backsheet number 3: Fluoro-Coating/PET/EVA (ethylene-vinyl acetate) with a total thickness of 250 μm

- Backsheet number 4: Outside coating/PET/Inside coating (mono layer) with a total thickness of 315 μm

The experiments [109] claim that the fourth backsheet has a better reaction-to-fire classification ranking than backsheets number one to three. This classification is based on the flame propagation speed and damaged zone.

Due to the electronic nature of PV modules, they have the possibility of electrical faults as discussed earlier in section 3.1. Since the PV modules are electrically conductive, the types of noncombustible materials that can be applied as backsheet are limited. As an example, in [109], aluminium-based backsheet is rated as first class regarding fire resistance; however, it is not the preferred choice since aluminium foil conducts electricity and is not suitable with respect to the electrical behavior of the PV module. Designating an appropriate material as the backsheet for a PV panel is challenging. Hence, multiple factors must be considered regarding the efficiency of backsheet material. Despite this, each of the studies considers a single design element such as the thickness of the backsheet or the number of layers. According to the studies, the fire performance criteria is accurately defined.

2.5.2.Screen

Screen is a mesh or net type surface mounted directly to the leading edge of the PV module to block potential flame from entering the rear surface of rack-mounted PV modules on the roof. The impact of screen on the classification of fire ratings is evaluated by three types of fire tests introduced by UL 790 (Tests for Fire Resistance of Roof Covering Materials).

Backstrom and Tabaddor [110] conducted experiments which evaluated two metallic screens. One was an expanded metal with diagonal openings measuring approximately 0.5-inch or 0.25-inch. The second screen was a typical insect screen material with 18 openings per inch. Furthermore, 24- and 36-inch setbacks with small-opening screens were investigated, and neither demonstrated compliance with the Class A requirements. Experiments that incorporated PV modules with a screen on a noncombustible roof indicated that a 36-inch setback was required to prevent the ignition source flames from extending to the underside of the module. In the case of PV modules with a small-opening screen installed with a 24-inch setback on a Class C roof/noncombustible module, fire spread more than 6½ ft. (Class A criteria) at 4 min and 36 sec and reached the end of the 8-ft. deck at 4 min and 39 sec. An increase in the setback to 26

inches, slightly improved the performance; however, flames reached 2½ ft. at 6 min and 9 sec. The small-opening screen does not meet the Class A fire performance criteria. This strategy is found to be helpful for rooftop installations and ground-mounted solar systems. However, the main challenge is figuring out how to apply a similar mitigation method to integrated PV systems such as building façades. Thus, further study on the use of screens is required to be applicable to various PV module configurations.

2.6. DSF fire

Sometimes new building features and green technologies are combined to reach a higher level of efficiency. As an example,BIPV merged with double skin façade is considered in designing a new building façade and retrofitting an existing building façade since this architectural feature helps taking the control of seasonal heating and cooling with the high efficiency. The architectural feature of BIPV DSF could causefire problems since the current building codes do not clearly provide the design requirements for fire safety. In different countries the reguations set requirements for vertical separation to control the fire and smoke spread risk of BIPV windows and openings. As Yang et al. [111] mentioned the specification of this control strategy for Australia (two openings should be separated for the vertical distances less than 450 mm) as well as USA (as a radius of 1525 m). Moreover Yang et al. also stated that the Chinese code obligates employing vertical separations for the vertical distance between openings is less than 1.2 m. As can be seen there are different distance requirements for vertical separation. According to what is mentioned the acceptance of BIPV systems including facades and other openings in a building system specifies the overall design of the building system. Beside the fact that the BIPV DSF can be the origin of a fire, in the case of indoor fire, the whole building including the exterior façade (BIPV DSF) would be exposed to the fire risk when the internal glass panel of DSF is broken. Consequently, smoke or even flame might spread horizontally and vertically to the other levels through the air cavity in the plenum space of the DSF when there is no fire/smoke separation between floors in the plenum. The available literature for DSFs used scenarios of indoor fire and the way that indoor smoke is transferred to the cavity (plenum) via the openings. Therefore, the width of cavity and the plume shape is taken into the consideration [112]–[115]. The reverse way of smoke propagation from the BIPV double skin

façade to indoors is untouched, while plenum becomes one of the ideal means to propagate smoke and flame from the fire level to the other stories [116].

Since using new technologies may bring more fire risk, a smoke management system is necessary to be designed, which is a set of measures to suppress, control and exhaust fire smoke in a building, and has an essential contribution in protection and safety system [117]. All these measures are applied by designing appropriate evacuation accesses and exits, exhaustion shafts, secure spaces for occupants, through which the spread of fire and fire smoke will be bounded. According to the vital role of these systems, they are required to go through special commissioning methods' validations [118]. Any proposed mitigation methods are firstly simulated, using various available pieces of software. Then the results are required to be validated by experimental tests. In designing small to full-size fire experiments, the major concern is providing efficient fire/smoke source. There are studies employing various methods including cold smoke, hot gas, etc. to visualize the smoke flow pattern, while each method has several limitations.

2.7. Helium test to investigate fire smoke propagation

The cold smoke test is a conventional demonstration method in which unheated theatrical smoke shows the flow pattern. Although this method reveals the flow path, it cannot represent all the characteristics of real fire smoke [118]. The limitation of this method was the reason for moving toward using the hot smoke test. Hot smoke test (HST) has been used for several tunnels by CISRO (Commonwealth Scientific and Industrial Research Organization). HST can describe the fire characteristic in a test, but the concern of smoke temperature and its potential damages persist. This method contains a small clean fire pool (liquid) such as methylated spirit which forms buoyant plume. A tracer catches the flow pattern which is made by presence of artificial smoke. Therefore, the spots of smoke plume and layers can be distinguished. Australian Standard, Smoke management systems- Hot smoke test AS 4391-1999 presents an edition of standardized hot smoke test [119]. US Federal Aviation Administration (FAA) regulated a test procedure which mixes helium and air with equal volumes for smoke detection systems in aircraft cabins. The helium-air and artificial smoke mixture was done in a helium smoke generator (introduced by the FAA test procedure). This method of making buoyant plume later

was employed in testing tunnel ventilations. Vauquelin et al. [120][121][122] discussed the scaling law and centering on buoyancy flux in laboratory scale of plumes of tunnel fires.

As Zhao and Wang [123] brought up the matter that the helium mix had been used mostly for testing environments such as aircraft and tunnels, when the test model is a building the whole story changes. Obviously in tunnels the plume tends to move horizontally, however, multiple zones with various sizes in buildings (considering the complex ventilation systems) make the buildings different from tunnels and aircraft cabins which contain only horizontal spaces. The vertical structural components in a building such as facades, indoor atriums, voids, stairways provide greater possibility of upward smoke movement. Later, Zhao and Wang [124] found that defining the required supply rate of helium-air mixture based on the tunnel ceiling height smoke temperature [120] is not realistic for buildings' atriums. For the vertical building spaces over 20-m height, the entrained air must be considered since they are much greater than the corresponding entrained air in mid-height of tunnels (which are neglected in the HST method). As a result, using pure helium instead of helium-air mixture is introduced to obtain certain plume flow.

2.8. Summary of research gap

Due to the global interest in GHG reduction the use of green technologies is getting more attention. Therefore, the associated risks including fire safety of the edge technologies such as PV increase. Thus, it becomes more important to find better ways to design and install PV systems properly on the building envelope. There are many real fire examples in large scale on the installed PV system on building envelopes which shows that there must be more and urgent attention to the mentioned problem. The following research gaps have been identified in the background study:

a) A reliable but safe, practical, and economical method to conduct the fire smoke propagation tests for a validated study on BIPV DSF.

b) A detailed study on the BIPV DSF fire safety considering several parameters to investigate the smoke transfer from façade to the indoor environment.

2.9. Thesis objectives

According to the identified research gaps mentioned in section 2.8, the following items are the main objectives of the current study:

• To develop a theory of helium and real fire smoke similarity for BIPV DSF fires. This theory will be employed in the helium experiment and associated CFD model. The theory of helium similarity can be verified by comparing validated CFD simulation results between cases with a helium surrogate and fire smoke. This fills in the research gap (a).

• To verify the proposed scaling method by defining three different simulation case (small-scale with helium, small-scale with fire and Full-scale with fire) and comparing the results of the simulation among these cases, which fills in the research gap (a).

• To study the influence of various parameters on the pattern of smoke spread from façade to the indoor environment by a parametric experimental study. These parameters are the location of the fire on the façade and the magnitude of fire (heat release rate). This is a step to fill in the third research gap (b).

Chapter 3 Methodology

3.1. Similarity theory and method of using helium as a surrogate of fire smoke in wind tunnel tests

Based on the ideal plum theory (Figure 9), the volume flow rate from a helium release source can be calculated by the constant bouyancy flux to investigate its similarity to the fire smoke plume. In an ideal plume, across any section, the smoke temperature and the helium density is constant. Therfore the bouyancy flux remains consistent along the height of the plume. Due to the mixture with the ambient air, the further the helium plume or smoke plume moving upward from the source some characteristics change along the height. To elaborate, smoke temperature drops from the initial fire temperature as well as the helium plume volmetric fraction (which becomes less than 1 mol/mol). Thus, to discuss the similarity relationship between these two plumes the following parameters must be considered; (a) convective heat release rate and volume flow rate of the helium, (b) buyancy flux of the real fire and helium, and (c) smoke temperature and helium volumetric fraction.

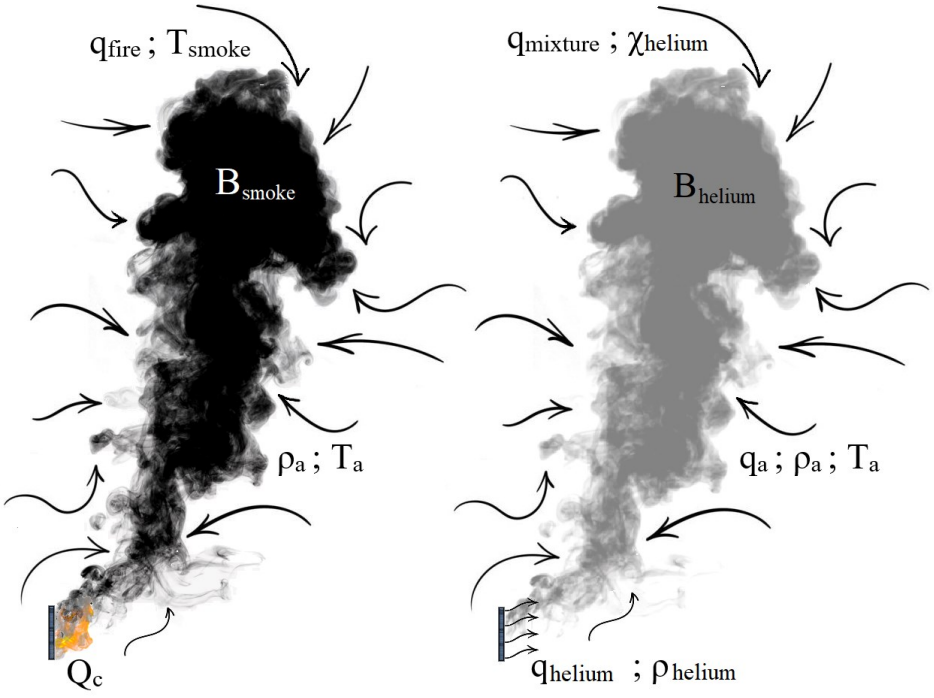

Figure 9. Ideal plumes in fire and helium smoke tests[118][118][118][118][118]

HRR is the term to show the magnitude of energy release by a fire source. The HRR forms by two main groups of convective and radiative heat release rates. The convective HRR (Q_c, kW) which is considered to be generally 70% of the total HRR, is the convection heat transfer of the fire source and can be calculated as follows:

$$Q_c = \rho_{smoke} C_p q_{smoke} (T_{smoke} - T_a) \tag{3-1}$$

Taking into consideration that, ρ_{smoke} is the smoke density in kg/m^3, C_p is the specific heat capacity in kJ/ (kg·K), q_{smoke} is the volume flow rate of the fire smoke plume in m^3/s, and T_{smoke} and T_a are the smoke and the ambient air temperatures in K.

The buoyancy flux of a real fire (B_{smoke}, m^4/s^3) can be obtained by the following equation:

$$B_{smoke} = g q_{smoke} \left(\frac{\rho_a - \rho_{smoke}}{\rho_a} \right) \tag{3-2}$$

where g stands for the acceleration of gravity in m/s^2 and ρ_a is the ambient air density in kg/m^3.

As mentioned, the buoyancy flux is constant at all heights of the ideal plume, the flux of helium (B_{helium}, m^4/s^3) is:

$$B_{helium} = g q_{helium} \left(\frac{\rho_a - \rho_{helium}}{\rho_a} \right) \tag{3-3}$$

In which, q_{helium} is the volume flow rate of the helium plume in m^3/s and ρ_{helium} is the helium density in kg/m^3.

Then based on the assumption that the smoke is an ideal gas, combining the convective HRR and buoyancy flux of a real fire (equations (3-1) and (3-2)) results in:

$$Q_c = \left(\frac{\rho_a C_p T_a}{g} \right) B_{smoke} \tag{3-4}$$

With the same ideal plume between the fire smoke test and the helium smoke test, equations (3-2) and (3-3) are equal and it results in:

$$q_{smoke} = q_{helium} \tag{3-5}$$

On the other hand, by combining the equations (3-2) to (3-5), the volume flow rate of helium, can be calculated:

$$q_{helium} = \frac{Q_c}{C_p T_a(\rho_a - \rho_{helium})} \tag{3-6}$$

The smoke spread from an ignited PV system on the building envelope is driven by the buoyancy which directly depends on the smoke temperature (in K) and velocity (in m/s). Richardson number (Ri) defines the ratio of the buoyancy term and flow shear term. Therefore, this dimensionless number can be selected to investigate the similarity between the dimensionless temperature of the smoke plume and the dimensionless volumetric fraction of the helium plume. For the fire smoke test, Ri can be expressed as:

$$\text{Ri} = \frac{g\beta(T_{smoke} - T_a)L_{smoke}}{u^2} = \frac{g(T_{smoke} - T_a)L_{smoke}}{u^2 T_a} \tag{3-7}$$

Considering that $\beta = \frac{1}{T_a}$ is the volumetric expansion coefficient in 1/K. (3-8)

As shown in the ideal helium plume in Figure 9, the helium is mixed with the ambient air. Consequently, the density and the volume flow rate of the mixture can be obtained by the following equations:

$$\rho_{mix} = \chi_a \rho_a + \chi_{helium}\rho_{helium} \tag{3-9}$$

$$q_{mix} = q_a + q_{helium} \tag{3-10}$$

$$\chi_a = 1 - \chi_{helium} \tag{3-11}$$

q_{mix} is the volume flow rate of the mixture of air and helium in m^3/s, and χ is the volumetric fraction in mol/mol.

For the helium test, *Ri* can be expressed as Eq. (3-12), which is obtained from the Boussinesq approximation [112].

$$Ri = \frac{g(\rho_a - \rho_{mix})L_{helium}}{u^2 \rho_a} \tag{3-12}$$

In the helium test and fire smoke test, the characteristic lengths are kept the same:

$$L_{helium} = L_{smoke} \tag{3-13}$$

To reserve the velocity, *u*, the same between the helium and real fire smoke in equation (3-7), (3-12) and (3-14) must be satisfied.

$$\frac{T_{smoke} - T_a}{T_a} = \frac{\rho_a - \rho_{mix}}{\rho_a} \tag{3-14}$$

Therefore, by combining equations (3-9), (3-11), and (3-14), the connection between smoke temperature and helium volumetric fraction can be expressed as the dimensionless temperature:

$$T^* = \left(\frac{T_{smoke} - T_a}{T_a}\right) = \chi_{helium}\left(\frac{\rho_a - \rho_{helium}}{\rho_a}\right) \tag{3-15}$$

As a conclusion to the developed theory for the similarity between the helium plume and real fire smoke, the helium surrogate method is used to design the experiment based on the main applicable equations as mentioned in Table 2.

Table 2. Helium surrogate similarity

For the helium test setup	Geometry: $l_{helium}=l_{smoke}$
	Volume flow rate of helium: $q_{helium} = \frac{Q_c}{C_p T_a(\rho_a - \rho_{helium})}$
Expected results	Dimensionless temperature: $\frac{T_{smoke}-T_a}{T_a} = \chi_{helium}\left(\frac{\rho_a - \rho_{helium}}{\rho_a}\right)$
	Velocity: $u_{smoke} = u_{helium}$

3.2. Scale method of smoke spread during solar roof fires for wind tunnel helium tests

Froude modeling is known to be the most common modeling approach used for fire smoke control studies [123]. This method is introduced by NFPA 92 [125] to study smoke movement in large spaces. Therefore, in this study, a real size building was scaled down 1 to 30 using Froude modeling. Among all the scaling relations for Froude modeling, in this study, the following equations are utilized to scale down the time, temperature, heat release rate (HRR) and mass flow rate (MFR):

For time scaling:

$$t_s = t_f \sqrt{\frac{l_s}{l_f}} \tag{3-16}$$

For smoke temperature scaling:

$$T_s = T_f \tag{3-17}$$

For HRR scaling:

$$\dot{Q}_s = \dot{Q}_f \left(\frac{l_s}{l_f}\right)^{5/2} \tag{3-18}$$

For MFR scaling:

$$\dot{m}_s = \dot{m}_f \left(\frac{l_s}{l_f}\right)^{5/2} \tag{3-19}$$

where t is time in s, l is length in m, T is temperature in K, Q is HRR in kW, m is mass flow rate, considering that subscript s and f stand for sub-scale and full-scale respectively.

According to the equations (3-16) to (3-19), the similarity between the small-scale and full-scale cases with fire source are assessed.

Moreover, the similarity between the small-scale simulation cases with fire and helium is studied through the following equations [118], [124], [126]:

$$q_{helium} = \frac{Q_c}{C_p T_a (\rho_a - \rho_{helium})} \tag{3-20}$$

where, C_p is the specific heat capacity in kJ/ (kg·K), ρ is density in kg/m^3 considering that the subscripts a and $helium$ are for the ambient air and helium.

Equally important, for the comparison of the cases in different scales, corrected time, temperature, and helium concentration are introduced as equations (3-21) and (3-22). By the volumetric fraction (χ_{helium}) of helium based on the Boussinesq approximation the temperature of smoke is calculated [126].

$$t^* = \frac{t_s}{\sqrt{L_s}} = \frac{t_f}{\sqrt{L_f}} \tag{3-21}$$

$$T^* = \left(\frac{T_{smoke} - T_a}{T_a}\right) = \chi_{helium} \left(\frac{\rho_a - \rho_{helium}}{\rho_a}\right) \tag{3-22}$$

Additionally, the velocity and time are as follows:

$$u_{helium} = u_{smoke} \tag{3-23}$$

$$t_{helium} = t_{smoke} \tag{3-24}$$

In conclusion, according to the Froude modeling and similarity method between helium and fire smoke, the scaling method (1/30) of the helium surrogate for the real fire smoke is summarized in Table 3. The setup properties are defined by geometry, time, and volume flow rate of helium and respectively HRR in fire smoke test.

Table 3. Scaling method summary

Setup conditions of wind tunnel helium tests	Geometry: $l_{s,helium} = l_{s,smoke} = \frac{l_{f,smk}}{30}$
	Time: $t^* = \frac{t_{s,helium}}{\sqrt{L_s}} = \frac{t_{s,smoke}}{\sqrt{L_s}} = \frac{t_{f,smoke}}{\sqrt{L_f}}$
	Volume flow rate of helium: $q_{s,helium} = \frac{Q_{c,s,smoke}}{C_p T_a(\rho_a - \rho_{helium})} = \frac{Q_{c,f,smoke}(\frac{L_s}{L_f})^{\frac{5}{2}}}{C_p T_a(\rho_a - \rho_{helium})}$
Predicted results	Velocity: $u^* = \frac{u_{f,smoke}}{u_{f,smoke,w}} = \frac{u_{s,smoke}}{u_{s,smoke,w}} = \frac{u_{s,helium}}{u_{s,helium,w}}$
	Dimensionless Temperature: $\frac{T_{f,smoke} - T_a}{T_a} = \frac{T_{s,smoke} - T_a}{T_a} = \chi_{s,helium}\left(\frac{\rho_a - \rho_{helium}}{\rho_a}\right)$

3.3. Experiment

3.3.1. Helium test setup

The building called "TELUS William Farrell" a 7-story (above the ground) high-rise office building in Vancouver, is selected in this research as the case study (Figure 10). The gross floor area of the building is approximately 12193 m^2. The usable floor area is around 11430 m^2. Specifically, from the 2nd floor the spaces are defined as offices. The last story is allocated for conference and executive. The building is using principles similar to double-glazed storm windows. The new glazed façade is laid over the old façade. The created one meter-plenum is ventilated with fans powered by the BIPV modules incorporated to the building façade. In the winter when the dampers are closed the plenum acts as an insulator to provide the controlled ventilation.

Figure 10. TELUS section view and the space use [127]

For this study the simplified model of the TELUS building is considered. The geometry of the model is simplified as one internal zone, a universal double skin façade connected to each floor via windows. Figure 11 provides more description of the model including the length, width, height of each floor, the number of floors, openings on each floor. For each floor there are thirteen windows (1 m by 1.8 m) in a row on the inner face of the DSF. Moreover on the back of the building on each floor there is a single opening (1 m by 1.8 m) in the middle of each wall.

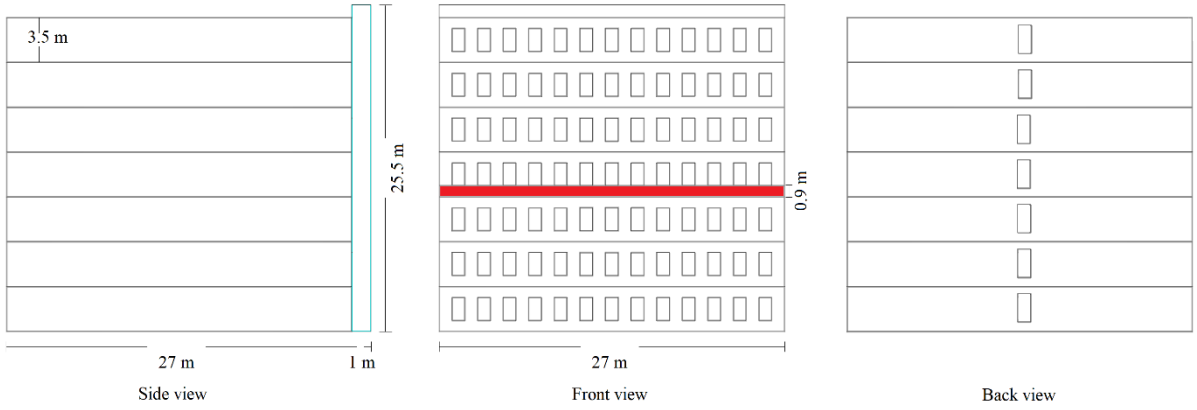

Figure 11. Schematic side, front and back view of the case study building

A series of sub-scale helium tests was conducted on a model made of poly carbonate transparent sheets with 1.27 and 0.63 cm thickness, 0.9 m width. The length and height are the downscaled (devided by 30) measures of the schematic shown in Figure 121. In these tests it is tried to

recreate the FDS simulation condition (such as laminar helium release). Therefore, pure helium was released in a box through which a flow meter controlled the desired release intensity in LPM (liter per minute). As can be seen in Figure 12, a honeycomb is mounted on the release box to make the helium inflow to the model uniform and laminar. It also depicts the location of helium diffusion on the façade the same as simulation design. Therefore, the helium is diffused from the release box covering the whole width of the floor. Intelligent XEN-5320 sensors were employed for the helium concentration measurements in percentage (%) and have 0.01% accuracy under the ambient condition (23°C, 101 kPa and 50% relative humidity). On certain points on each floor and the façade of the model integrated gas sensors are mounted. These sensors are connected to each other in series (Figure 13). This series is blocked on the top end and connected to the read-out computer software on the other end. The helium release rate is 180 LPM, calculated based on the medium PV fire HRR measured by Ju et al (319kW/m^2) [84]. Moreover, the following equation is employed to calculate the helium mass flux:

$$\dot{m}_{he}\ (kg/(\mathrm{m}^2.\mathrm{s})) = \frac{Q_{he} \times \rho_{he}\ (\mathrm{kg}/m^3)}{\mathrm{A}\ (m^2)} \qquad (3\text{-}25)$$

where $\dot{m}_{he}$ is the helium mass flux and A is the helium release area.

Ultimately, for employing in the experiment by using the mass flux, helium release area and helium density the HRR can be converted to the helium flow rate in litre per minute (LPM).

Several fire location on the façade (bottom, middle and top floor) and HRRs (85 kW/m^2, 191 kW/m^2, 319 kW/m^2) are considered.

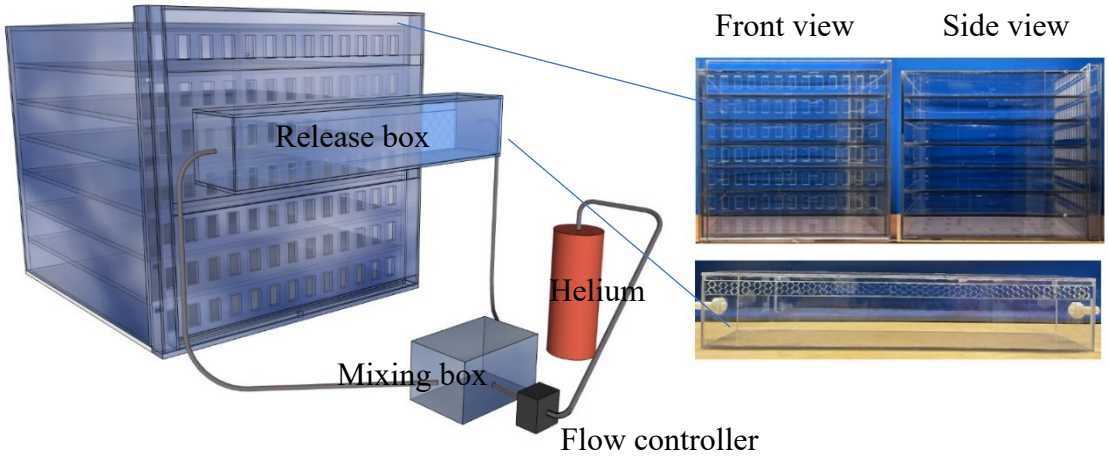

Figure 12. Helium test set-up

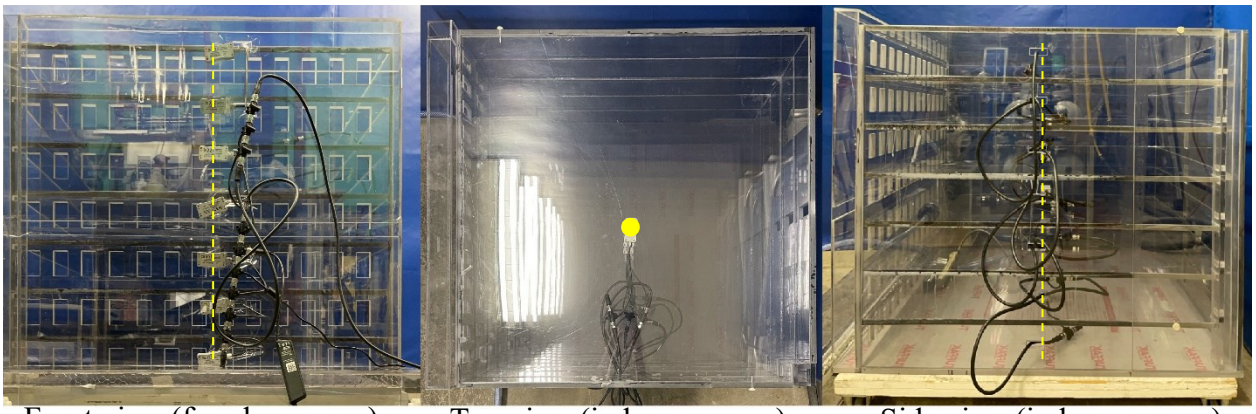

Front view (façade sensors) Top view (indoor sensors) Side view (indoor sensors)

Figure 13. Sensor installation pattern on the model

3.3.2. PIV test setup

After a series of helium concentration measurements, the second phase of experiments were carried out. For this phase, the helium sensors were removed, and the sensors' insert slots on the model body were completely sealed to prevent any undesired infiltration. A new setup was performed as shown in Figure 14 to measure the flow velocity for the required field of views. The helium release box and the rest of previous setup remained unchanged but the Particle image velocimetry (PIV) devices including the CCD (charge-coupled device) camera, light sheet optic were added to the small-scale model in specific configuration. These two parts are then connected to a pulse control unit which transfers the data to the microprocessor and read-out unit. The new setup catches the indoor helium flow velocity in a certain plane.

Double frame measurements with 2 × 200 mJ/pulse at 532 nm and 15 Hz maximum pulse rate are recorded by performing YAG (Yttrium Aluminium Garnet) dual cavity pulsed laser. The CCD camera has a resolution of 2752 × 2200 pixels (6M) and a maximum of 25 frames/s. Mineral oil droplet was the tracer particle source which released to the helium release box by an aerosol generator. It is tried to make a uniform concentration of particles on the zones included in the camera's field of view, which led to more reliable and solid results. Adjustable Timing Unit (PTU-X) made it possible to control the intervals, exposure time, and laser delay. A 20-ns resolution is provided on the timing unit, and a jitter smaller than 50 psec. The FOV (as

demonstrated in Figure 14) includes the side view of the plenum and the entrance part of the indoor zone for each floor. A dual plan calibration target is used (58 mm × 58 mm) and was placed in the model between the floor to ceiling gap to calibrate the FOV on the laser sheet. The laser light sheet in the FOV is generally adjusted between 1 to 3 mm [128] to avoid too thin or too thick planes. Crossing this thickness worsens the quality measurements in the 2D plane. The PIV technical settings are provided in Table 4. PIV technical settings

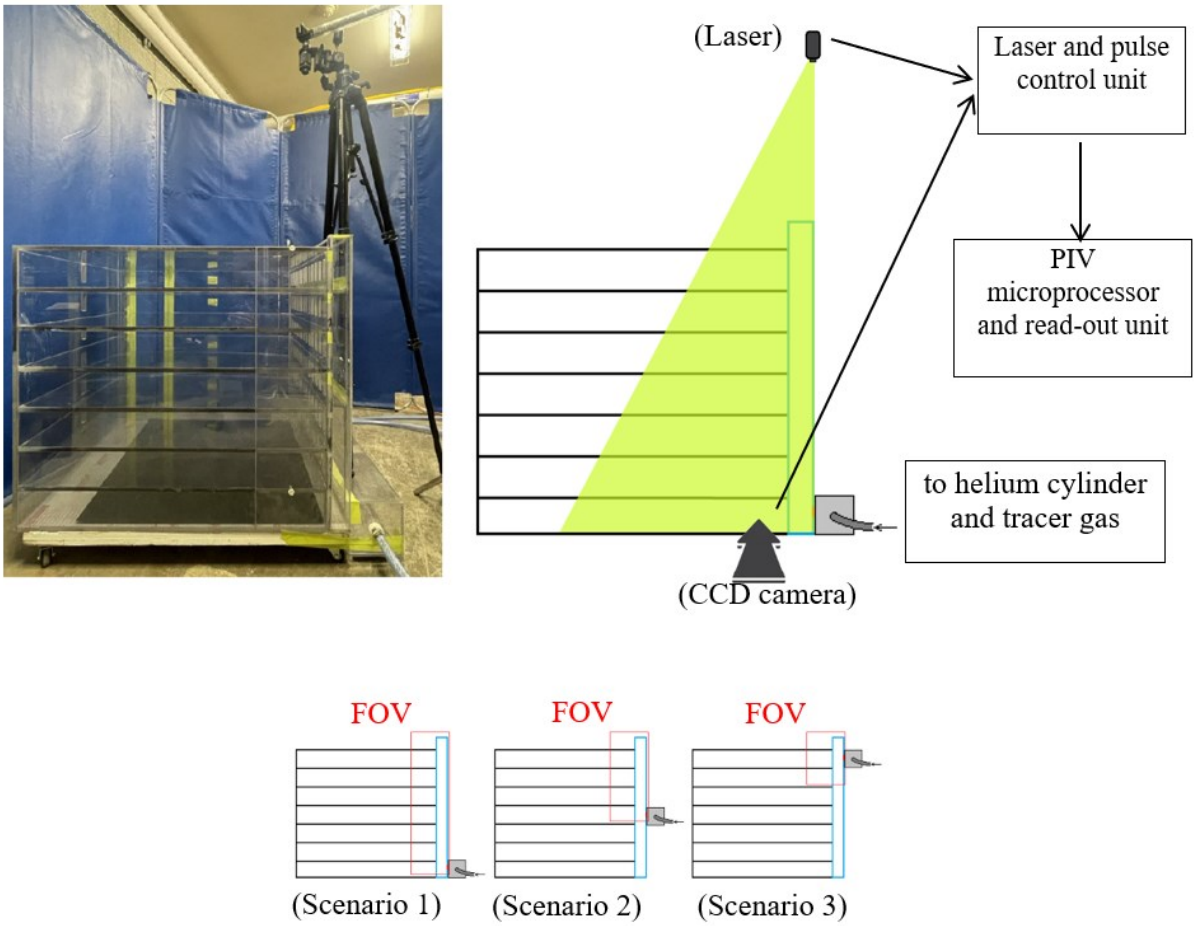

Figure 14. PIV setup and different locations of helium release on BIPV DSF and PIV FOVs

As shown in Figure 14, there are three sizes of FOV for different scenarios. Scenario 1 and 2 have bigger FOVs in comparison to the viewing area of the camera which is 465 mm × 510 mm. In order to capture the whole defined FOV the camera was mounted on a pole which was screwed to the floor on the side of the building (Figure 15). Then for Scenario 1 the camera was moved on three different heights without any horizontal movements and any rotations.

Therefore the test was repeated for three times while the only changing parameter was the camera height. In the same way, for Scenario 2, the camera was moved to two different heights to capture the whole FOV.

Figure 15. Stand for the CCD camera

Table 4. PIV technical settings

Parameters	Value
Field of view (FOV)	465 mm × 510 mm
Time interval	1000 μs
Number of captured pictures	100
Measured time	8 s
Sampling frequency	12.5 Hz

Camera resolution	2752 × 2200 pixel (6M)
Interframe time	150 ns
Pixel depth	8/12 bit
Exposure time	100 µs
Camera lens	60 mm focal length, F/2.8
Laser energy	2 × 200 mJ/pulse at 532 nm

3.3.3. Uncertainty analysis for experiments

For the helium test the uncertainty analysis is done for the sensor located to the indoor zone on 7th floor. The analysis is considered for a period of 100 seconds for the mentioned sensor by repeating the same test (Figure 16).

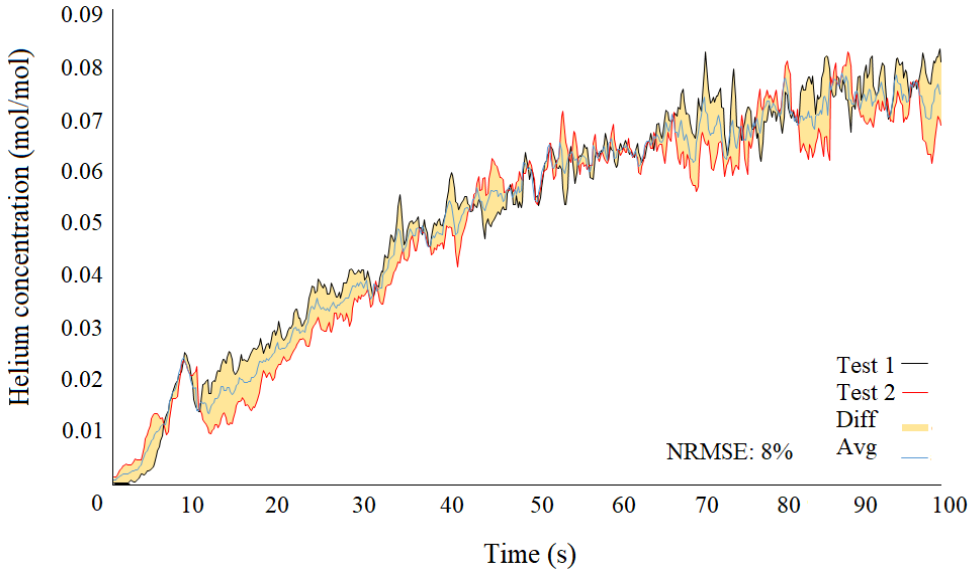

Figure 16. Uncertainty analysis for helium sensors

Moreover, the helium concentration comparisons between the different iterations are quantified using the coefficient of variation- root mean squared error (NRMSE) based on the reference [129]. This equation performs as an indication of the difference.

$$NRMSE = \frac{1}{\theta_{max}-\theta_{min}}\sqrt{\frac{\sum_{j=1}^{n}(\theta_{1,t}-\theta_{2,t})^2}{n}} \quad (3\text{-}26)$$

where n is the quantity of the observation for a variable, θ demonstrates a series of variables and t is the time.

As explained in the section of PIV experiment, to capture the whole height of the plenum for all the cases with fire on the bottom of the plenum the camera had to be relocated three times. When the camera is located on the top, the velocities are captured for the top two floors (7th and 6th). Then again when the camera was moved from top to the middle position from the bottom half height of the 6th floor down to top half height of 3rd floor is captured. The same happened when the camera was moved to bottom position which means that from 3rd floor to the 1st floor is captured. Therefore, in only one case of PIV test there were too many points having overlapping results, which are shown as the zones in yellow color in the Figure 17:

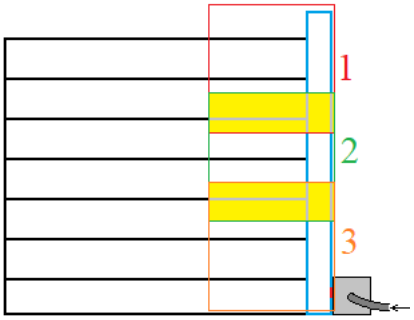

Figure 17. Overlaps in FOVs in PIV images

The same happens for all the cases with fire position on the mid-height as well. Following the research method of the related building-fire studies, this is not separately mentioned. This explanation is added to the manuscript.

3.3.4. Summary of various parameters and test order

Table 6 summarizes the overall test plan in which various parameters are applied. To illustrate, each of the cases with the specific location of fire (bottom, top or middle height) is tested with

three different flow rates for helium release for the concentration measurements. Moreover, PIV test is carried out for each test and helium release rate to measure the indoor air flow velocity.

Table 5. Summary of the test plan

Try	Fire location	Full-scale HRR (kW/m^2)	He/PIV	Conduction time (hr)	He (LPM)
1	Fire (helium release) on the bottom	319	He	1	180
2		319	PIV	0.5	180
3		191	He	1	72
4		191	PIV	0.5	72
5		85	He	1	51.84
6		85	PIV	0.5	51.84
7	Fire (helium release) in the middle	319	He	1	180
8		319	PIV	0.5	180
9		191	He	1	72
10		191	PIV	0.5	72
11		85	He	1	51.84
12		85	PIV	0.5	51.84
13	Fire (helium release) on the top	319	He	1	180
14		319	PIV	0.5	180
15		191	He	1	72
16		191	PIV	0.5	72
17		85	He	1	51.84
18		85	PIV	0.5	51.84

3.4. CFD simulations

3.4.1. CFD setup

The 7-story (above the ground) building was renovated by adding BIPV and glazing skin over the pre-existing brick wall, and the double skins made a 1-m plenum void in between [130]. The new BIPV skin is to provide the required electricity for the building ventilation system. The simplified geometry of the mentioned building is considered while the fire initiates on the exterior façade of BIPV skin. The interior windows are assumed open and exterior windows are closed. The damper on the top of he plenum which exeeds the height of the ceiling of the 7th floor, is considered open. However, the plenum is closed on the buttom and the two sides. As shown in Figure 11, the fire was simulated over an area; 27 m (W) and 0.9 m (H) on the PV glazing façade, with HRR of 319 kW/m^2, as reported in [84]. Fire dynamic simulator (FDS) is employed as the computational fluid dynamic (CFD) tool of large eddy simulation (LES) model. FDS is the product of collaboration led by the National Institute of Standards and Technology (NIST) that provides detailed information on the smoke and heat transfer [131]. Furthermore, the accuracy of FDS has been validated by Hadjisophocleous and Jia [132] and it is made to study the smoke spread and more generally fire behavior in building and urban scale [133], [134]. The governing equations in FDS are suitable for low Mach number fluid flows also referred to as‘‘weakly compressible’’ or ‘‘thermally expandable’’ to express that the divergence of gas mixture is supported only by heat or a change in the mixture composition [135]. Moreover, the sub-grid scale models of Deardorff (default), Dynamic Smagorinsky, and Vreman are embded in the FDS code to tackle the problem with grid resolution and capture the fluid characteristic at all relevant scales [135]. FDS provides both Direct Numerical Simulation (DNS) and three modes of Large Eddy Simulation (LES). In this study, due to computing power limitation Very Large Eddy Simulation (VLES) is applied to simulate the fire scenarios. Deardorff turbulence model is used (which is set as the default) and the Near wall turbulence model is Van Driest.

In this study, the simulation cases are conducted in Mammoth-Mp2b cluster of Calcul Québec which is located at the Université de Sherbrooke. The cluster provide 2×24 cores of CPU node to run a simulation in multithreaded environment. The cases with coarse mesh (one set of 24 cores of CPU nodes), moderate mesh (2 sets of 24 cores of CPU nodes), and refined mesh (4

sets of 24 cores of CPU nodes) simulations took 2 days, 7 and 12 days. The three groups of cases are used for the grid independence study. Then the other cases are generated with moderate mesh. The mesh size is selected based on the smallest dimension of the model which is the thickness of PV panel installed on the façade and the mesh size is refined in the critical spaces which is the plenum, interior windows and the PV panel installed on the façade.The initial time step can be specified by dividing the size of a mesh cell by the characteristic velocity of the flow which is normally set automatically by FDS. During the calculation the time step is adjusted so that the Couran-Friedrichs-Lewy (CFL) condition is satisfied. Further details of the approaches used within FDS for solving the NAS equations and discretisation schemes used, are set as default which are presented in [136].

In the designed model the building walls and roofs are set as adiabatic. For the BIPV façade, reaction and material parameters are chosen as poly methyl methacrylate (PMMA), widely used for PV panel structure, based on FDS Material Data References. The mentioned set up definitions are kept identical for all simulations. The total mesh number and the rest of simulation properties can be found in Table 6. The simulation time is defined as 1000 s which is significant time for occupants escape and enough to reach a quasi-steady state.

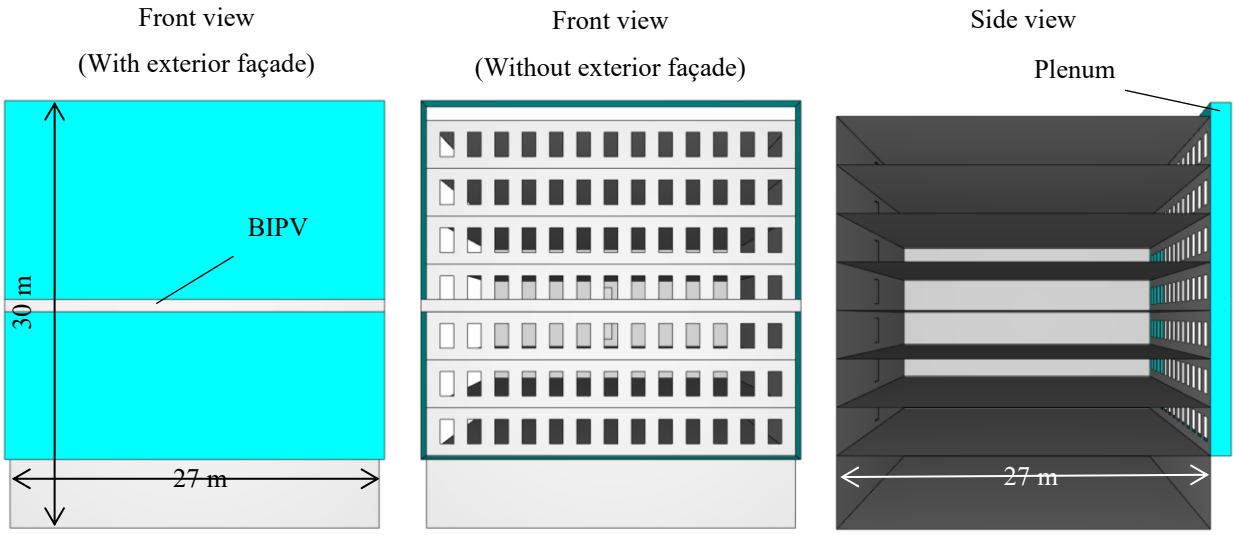

Figure 18. Case study building

3.4.2. Grid independence study

In this study, there are three different groups of cases named as full-scale with fire (FSF), small-scale with fire (SSF) and small scale with helium surrogate (SSH). Therefore, for the grid independence analysis both full-scale and sub-scale cases are considered. To check the grid sensitivity of the simulation model, the method used in several building-fire studies is followed. As what is done by Miao and Chow (2018) [114] to investigate the window plume from a room fire to the DSF by employing the same CFD tool (FDS). Grid independence study was conducted by defining three different grid sizes including refined, moderate, and coarse [137]. The refined cell size is 0.005 m for the small-scale case and 0.15 for the full-scale case. The moderate/coarse mesh sizes are 0.01 m/0.02 m for the small-scale and 0.3 m/0.6 m for the full-scale case respectively. Consequently, the number of created grids is 9,355,192, 1,679,832 and 855,778 for fine, moderate and coarse mesh.

Firstly, the group of the temperatures are observed at the thermocouples located in the same location in each case with the certain mesh size. For the small-scale case the thermocouple is considered in the middle of the plenum on 6th floor and the ignition source is in the middle of the height (on the façade, on 4th floor) (Figure 19). Also for the full-scale case the thermocouple is located in the middle of the plenum on first floor when the ignition source is also on the bottom of the façade (on the façade, on 1st floor) (Figure 20). Moreover, the temperature comparisons between the cases with different grid sizes are quantified using NRMSE based on the reference [129].

Figure 19 and Figure 20 depict temperature measured by the thermocouple in the same location for three mesh sizes (coarse, moderate, and fine).

Table 6. CFD simulation settings

		FSF	SSF	SSH
Building	Initial indoor temperature	20 °C		
	HRR/ Helium mass flux	319 kW/m^2 [84]	58.33 kW/m^2	0.0208 kg/(m^2.s)

	PV size on the façade	27 m (L) × 0.9 m (H)	0.9 m (L) × 0.03 m (H)	
	Domain size	27.5 m (L) × 49 m (W) × 41 m (H)	0.9 m (L) × 1.58 m (W) × 1.4 m (H)	
CFD model	Turbulence model	VLES		
	Energy release per unit mass oxygen	1.314×10^4 kJ/kg		
	Simple chemistry model	1.0 (Carbon), 1.6 (Hydrogen),0.4 (Oxygen)		
Gridding	Moderate gird number	1,679,832		
	Moderate cell size	0.3 m	0.01 m	0.01 m
	Refined cell number	9,355,192		
	Refined cell size	0.15m	0.005m	0.005m
	Coarse cell number	855,778		
	Coarse cell size	0.6 m	0.02m	0.02m

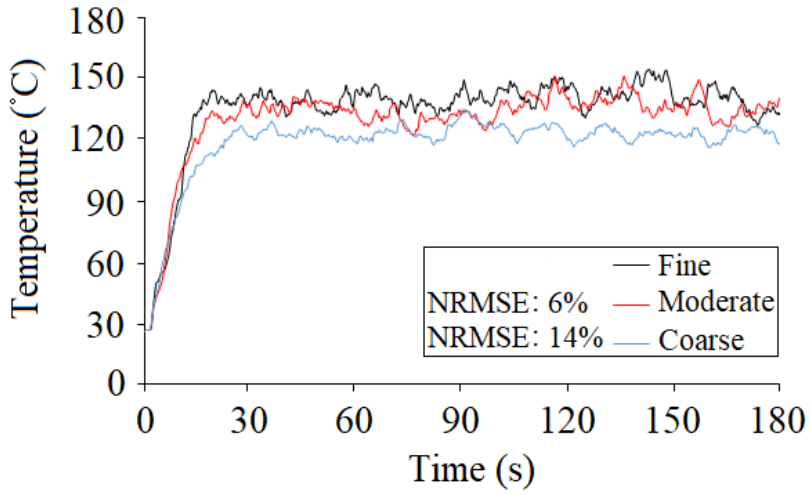

Figure 19. Grid independence study for the temperatures in small-scale case study

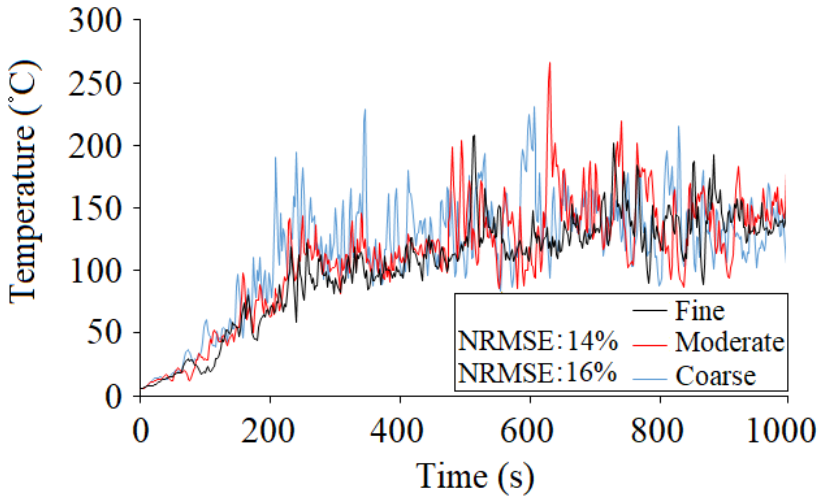

Figure 20. Grid independence study for the temperatures in full-scale case study

The temperature comparison shows closer results between the fine and moderate mesh size. At the same time, the NRMSE for fine/coarse is greater than the same factor for fine/moderate. Results between fine and moderate cases have maximum 14% difference. Therefore, it illustrates that there is no obvious improvement between moderate and fine mesh size. In other words, LES simulation results are independent of both moderate and fine grid resolutions.

Chapter 4 Helium and fire smoke similarity analysis to study smoke spread from ignited BIPV on a DSF

Contributions:

This study employs the governing theory of helium similarity in a series of experimental test. The helium test method is used as a real fire smoke surrogate to study smoke spread from BIPV DSF fire to the indoor environment. The helium tests are conducted on a small-scale model accompanied with PIV to measure the helium volumetric fraction and flow velocity in the case study. The CFD models are designed and then validated by the associated experimental measurements. Therefore, the theory and method of helium similarity are justified.

4.1. Introduction

According to the research gap a), Chapter 4 inspects a new approach (Section 3.1) to use helium as a surrogate of real fire smoke. Therefore, a buoyancy plume of BIPV DSF fire is simulated in a small-scale case study test. The smoke transfer from DSF to the indoor environment is investigated. Firstly, the similarity theory and method were developed to surrogate a helium plume for a real fire plume (Section 3.1). This method connects the mass flow rate of helium release with the heat release rate (HRR) of the real BIPV fire. Moreover, the dimensionless helium volumetric fraction measured in the helium test with the dimensionless temperature measured in the fire smoke test are correlated. Secondly, small-scale helium tests (accompanied with PIV) are conducted in which the helium volumetric fraction and air velocity were measured. Thirdly, numerical models were developed in the Fire Dynamics Simulator (FDS), and later validated by comparing with the results of the helium test. Then, the validated FDS models were applied to simulate PV fire smoke propagation. Finally, the accuracy and efficiency of the method is evaluated by comparing the results between the helium test and fire smoke test.

The procedure schematically shown in Figure 21 is followed to achieve the research objectives. The validation is included in section 4.2.1 and 4.2.2 and the discussion on the obtained results are presented in section 4.2.3 and 4.2.4.

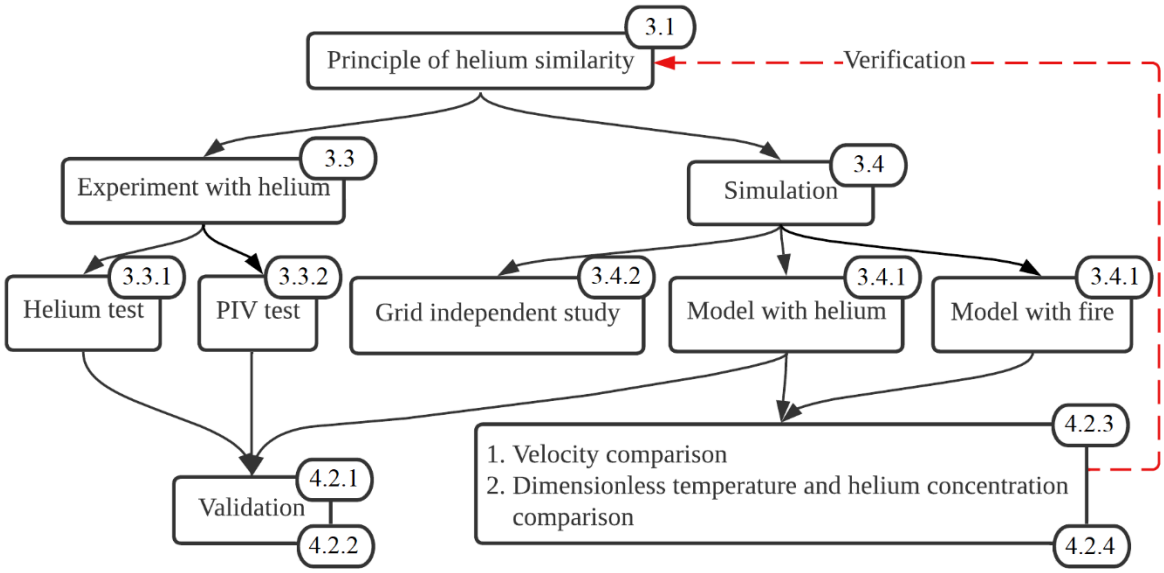

Figure 21. Schematic of the study

4.2. Results and discussion

4.2.1. Validation of indoor helium concentration

To validate the FDS model, according to the experiment description, firstly the measured indoor helium concentrations are compared to the associated simulation results (CFD simulation SSH) for the case that contains the fire on the bottom of the plenum (first floor). In the experiments, these concentrations are measured by the sensors which are mounted on the positions depicted in Figure 13 on each floor. The same position is used for the virtual gas volume fraction devices in the simulations. Figure 22 demonstrates the comparison between these two groups of data for the transient state (from the beginning to the end of simulation/experiment time). As if the case study building has seven floors, the comparisons are presented in two separate groups, associated to the plenum and indoor for each floor. In all the following charts, the vertical axis shows the volume fraction of helium concentration in mol/mol, and the horizontal axis represents the time in seconds.

In general, aside from the good agreement between the simulation results and experiment, the helium concentrations are notably fluctuating more in the plenum than indoors, which is due to the narrower flow pass in the plenum than indoors. As moving along with the height, the helium

concentration drops to less than half in the plenum, while indoor concentration becomes maximum on the 7th floor.

4.2.2. Validation of indoor helium flow velocity

The PIV results for plenum zone and indoor air flow are presented in Figure 23. In these tests and simulations which are used to validate the CFD model, the helium mass flux is 180 LPM. Measured velocities in the test show good agreement with the simulated velocities. The error bars are used in this figure to keep the influence of intense velocity turbulences down. These bars present the derivation between maximum or minimum and averaged values [138].

The general trend shows that the air velocity is remaining in a constant range along with the height in plenum averaged at 0.3 m/s (Figure 23. (a)). However indoor velocities change from zero (beside the boundary layer of floors and ceilings) to its certain maximum along with the height of each storey (Figure 23. (b)). The smallest air velocity on 7th floor is considerable which probably is the reason for higher indoor helium concentration on that floor.

As can be seen in Figure 23, NRMSEs between experiment and simulation velocities are averaged around 23 (indoor) and 24 % (plenum); therefore, it can be considered an acceptable error of less than 30% [138]. The biggest differences between the simulation and experimental results can be seen in the middle of the floor height on the first three floors (floor 1 to 3). The fluctuations in PIV result is caused by the existence of low velocity shear flows which can not be captured and calculated by simulations. Moreover there are bidirectional stream near the entrance of each flow which will be extensively discussed in Chapter 6.

Moreover, Figure 24 depicts the velocity distribution in vectors both for PIV and FDS results. Greater velocities in higher altitudes of the plenum and smaller indoor velocities within lower floors are notable. In the FDS simulations the ambient temperature is set to 20°C with no outdoor wind flow and fixed pressure. In the real situation of the experimental lab, there may exist some disturbed flow around the building model and the overall outdoor flow is impossible to be fixed pressure and zero velocity. Therefore, the small differences of the ambient condition can result in some changes. As can be seen a small vortex right on the top of the plenum is found in FDS result while in the PIV test result there is a flow from right to the left-hand side in that certain location.

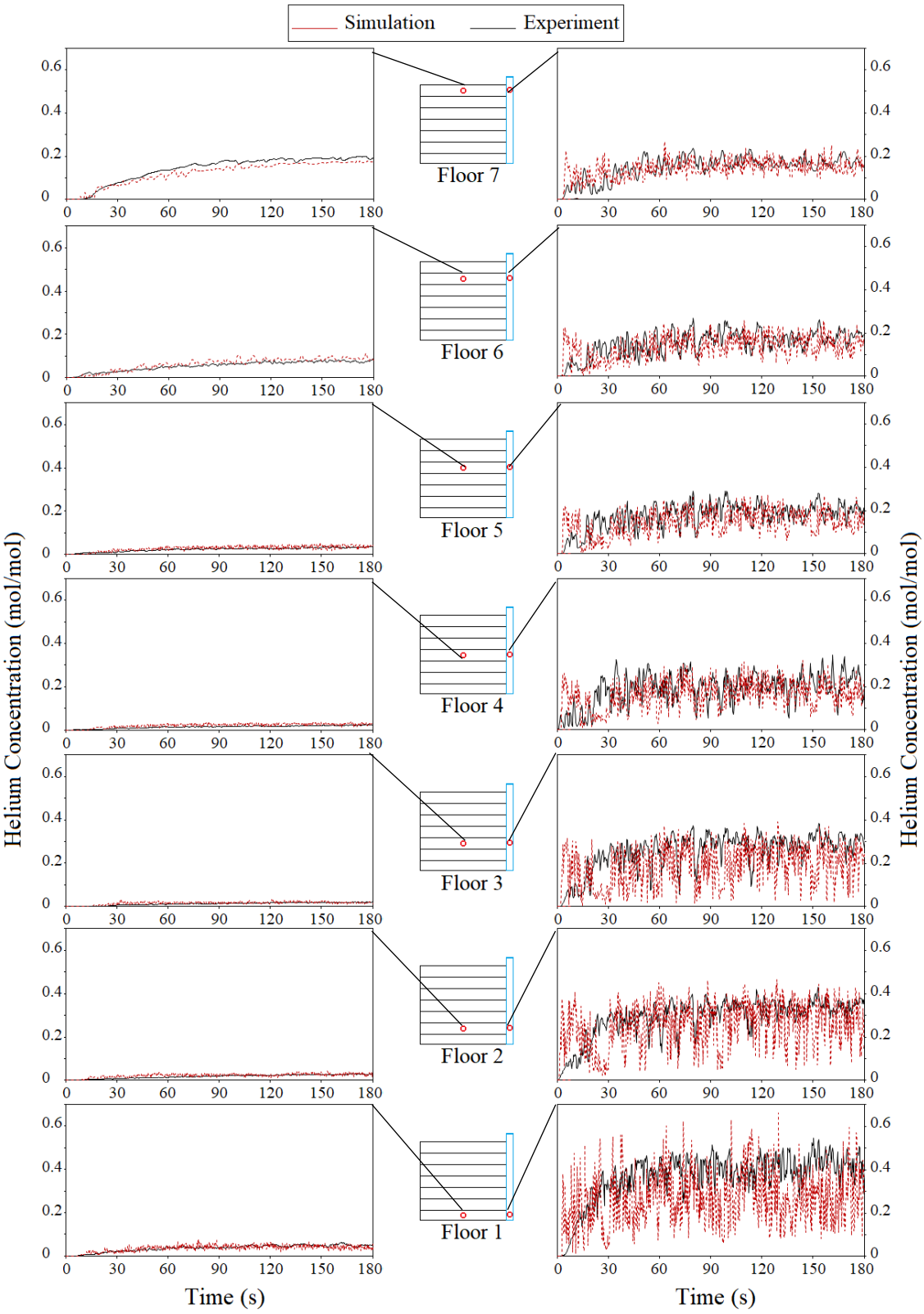

Figure 22. Transient Helium concentration comparison in Experiment and simulation

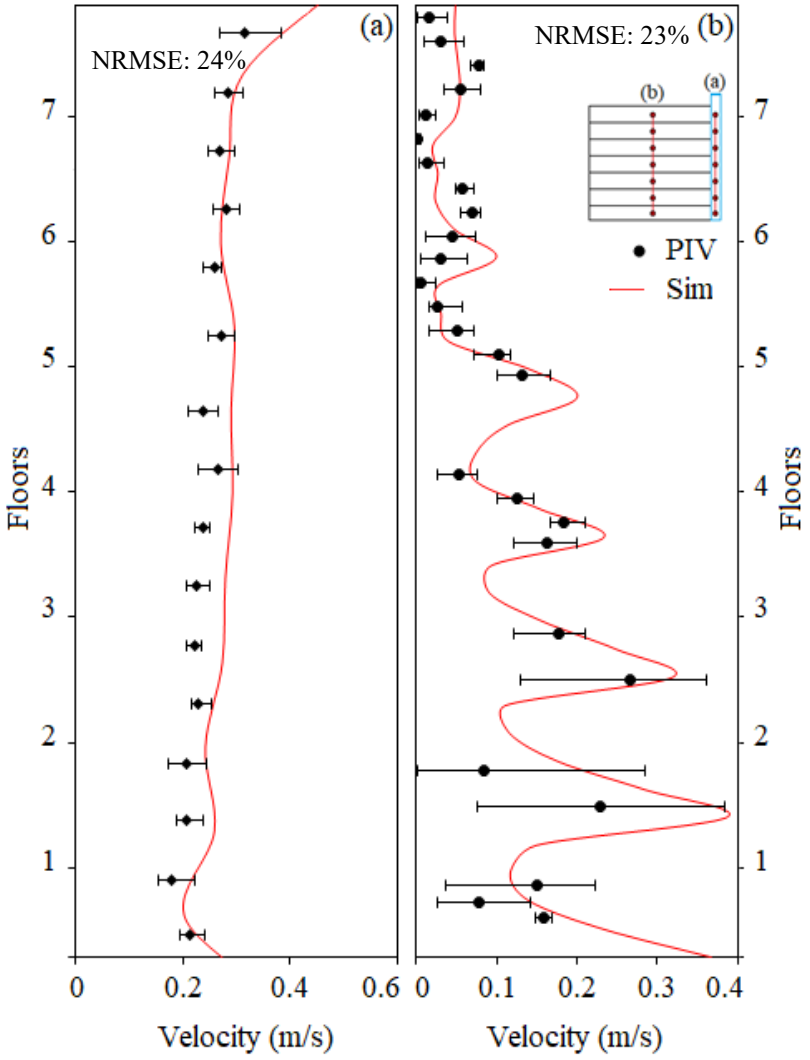

Figure 23. Steady state velocity comparison in Experiment and simulation

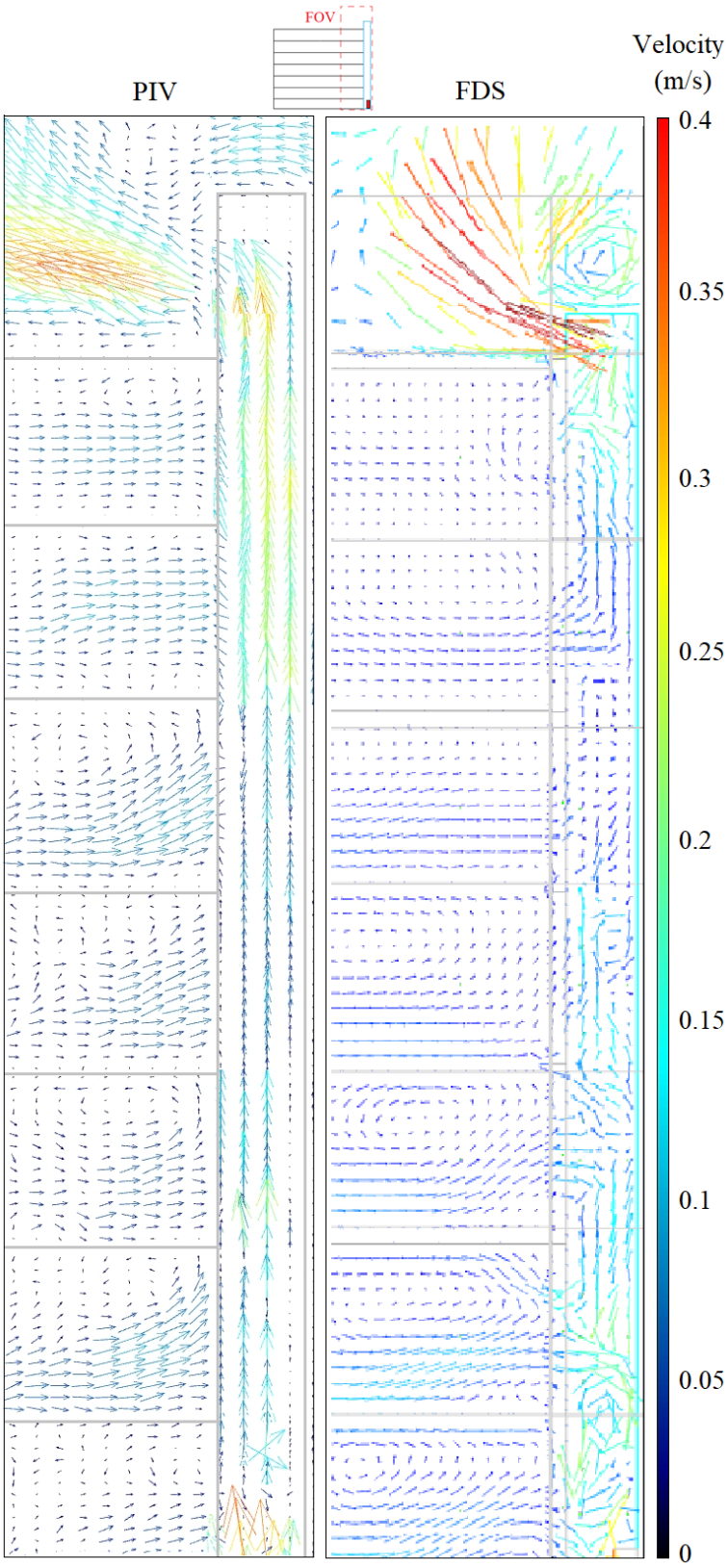

Figure 24. Velocity vector in PIV and FDS

4.2.3. Dimensionless temperature/concentration and velocity comparison

Initially the idea of using helium instead of real fire is validated by the experiments. Based on the findings of Chapter 3 and validation of the FDS simulations, more comparisons between the simulation cases with helium and real fire can be argued.

Figure 25, (a) and (c) show the comparison between the dimensionless temperatures and dimensionless helium concentrations along the height in the steady state. Likewise, the same analogy is done for the velocities along the height on different floors in Figure 25, (b) and (d). The location of the fire/helium release is on the bottom of the plenum (on the façade, 1st floor) with the intensity of 58.33 kW/m^2 for fire or 180 LPM helium release. The NRMSEs are calculated individually for both plenum and indoor environment. The NRMSEs (ranging 1.6 to 11%) show very small differences between the simulation results for the cases with real fire and helium. According to the curves, despite the location of the fire/helium is on the bottom of the building façade, lower flow velocities (in the worst case around 0.1 m/s) and higher helium concentrations or air temperatures happen on the top floors (floor 6 and 7). This makes it crucial to pay extra attention to the escape routes for the top floors' occupants while designing evacuation or suppression systems.

4.2.4. Distribution comparison of dimensionless velocity and temperature

With regard to the fact that up to this point, all the comparisons are related to some specific pointwise measurements, by and large Figure 26 and Figure 27 try to explore the overall flow pattern. The snapshots set is made in Figure 26 to shows how the smoke/helium flow is transported from plenum to the indoors via open windows (in terms of the dimensionless temperature and helium concentration). For SSH (small scale model with helium), as the temperature is constant during the simulation, helium concentration will be representative instead. These shots are taken from the beginning stage (18 seconds) to the moment that all the floors are involved (162 s). The obvious filling sequence between the SSH and SSF (small scale model with fire) cases supports the idea that these two groups are substitutable. In the same way, in Figure 27, a group of snap shots are set side by side to compare the velocity distribution from the beginning of the process to its end. On each time section these two groups follow almost the same pattern with high extent of agreement.

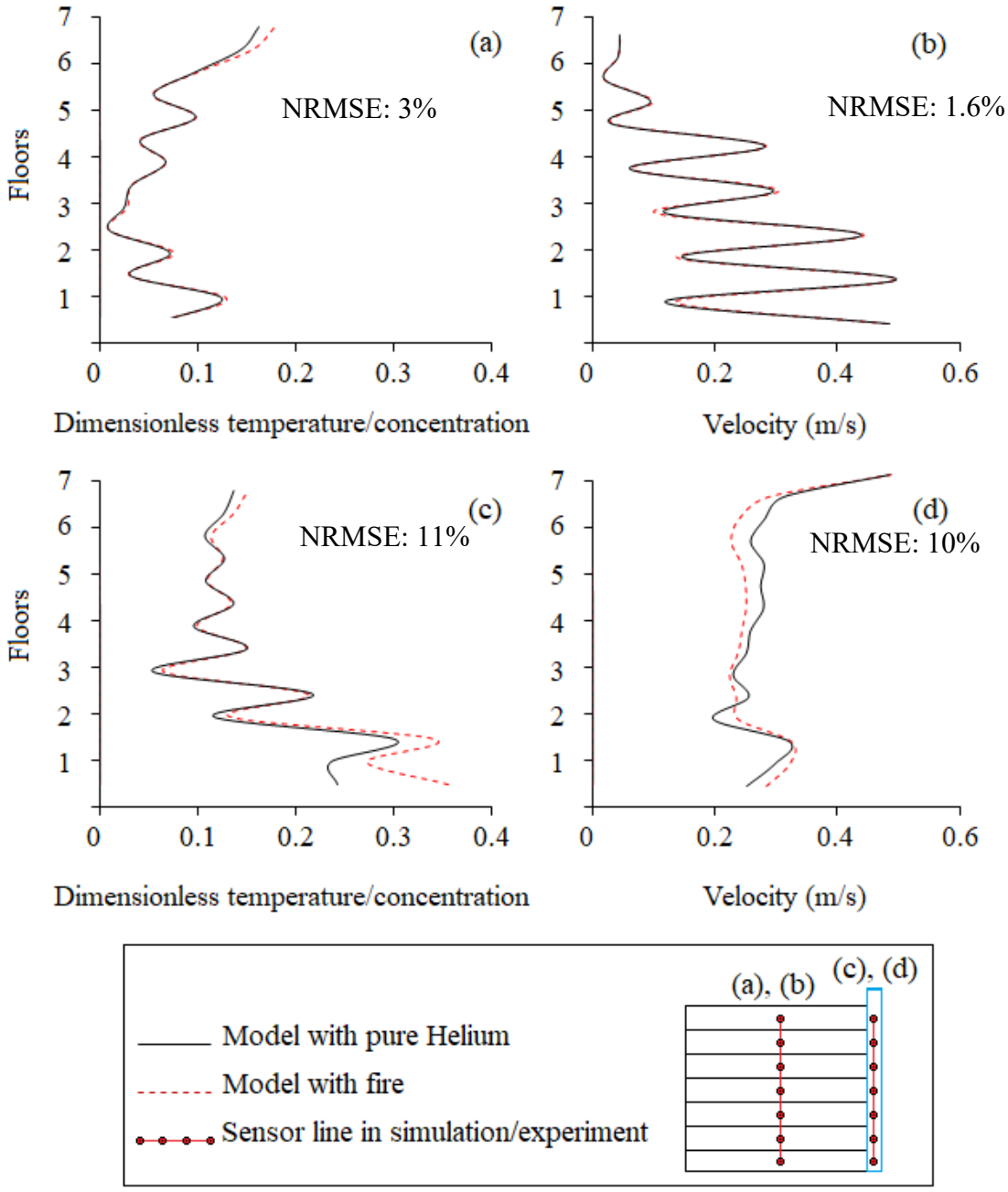

Figure 25. Dimensionless temperature/concentration and velocity comparison

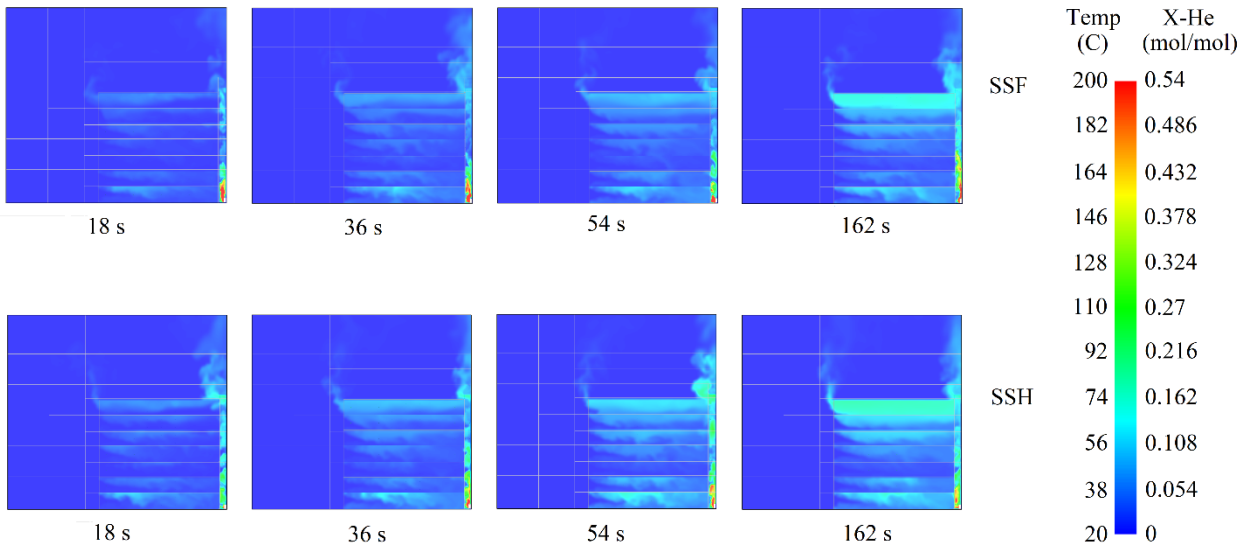

Figure 26. Dimensionless temperature and helium concentration pattern for SSF and SSH

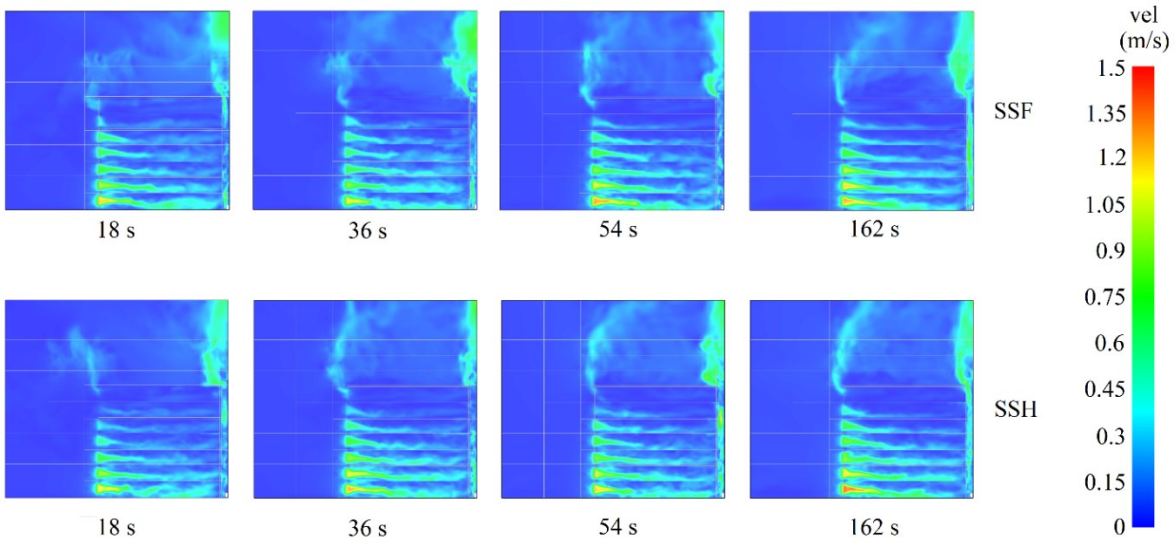

Figure 27. Velocity distribution pattern for SSF and SSH

4.3. Summary

As discussed, using helium in small-scale fire experiments has many advantages in comparison to real fire, hot gas, i.e., obtaining identical plume flow. In order to use helium instead of real fire, the similarity of the principal characteristics of their flows has to be proven, i.e., an acceptable level of agreement should be achieved to support the idea of replacement. In this study, helium is employed to simulate smoke generation from a BIPV double skin façade fire in a high-rise small-scale building. The smoke transfer from the ignited BIPV through the plenum to the indoors was observed. For this purpose:

- The validity of SSH is observed through two separate sets of experiments in terms of helium concentration and air velocity (PIV). The transient helium concentrations were compared to the associated simulation results for two points on each floor, one in the plenum and the other indoor (in total 14 points). Moreover, the steady-state flow velocity profiles were examined on two separate lines, similarly one line along the height of plenum void and another line for indoor. Then the validation of the helium simulation results was confirmed since the coefficients of variation did not show significant deviation from the experimental measurements.
- After the validation, further discussion was presented to verify the similarity between the FDS models with helium and real fire. The dimensionless temperatures and dimensionless helium concentrations are compared for the steady state in both plenum and indoor. Complementary to this, the steady-state flow velocities were observed along the height in SSH and SSF cases (both for the plenum and indoor). The NRMSEs of these comparisons ranged between 1.6 to 11% which means the associated curves fit perfectly on each other. This compatibility was later supported by the identical snapshots of air flow filling the floors one after another for the two SSH and SSF cases.
- Looking at the simulation results supported by the experimental measurements, it is obvious that in case of fires on a BIPV double skin façade, the top floors on a high-rise building are more exposed to the risk (regardless that the fire location is on the bottom of the façade).

Chapter 5 Scaling of smoke spread from BIPV DSF fire using helium surrogate

Contributions:

To study the smoke transfer from ignited BIPV DSF to the indoor environment, in this chapter the scaling method for a small-scale helium experiment is developed and validated. The scale method is proposed based on the similarity analysis between helium and fire smoke (Chapter 4) and Froude modeling (section 3.2).

5.1. Introduction

As shown in Figure 28, firstly full-scale model with fire source is downscaled using Froude modeling which is discussed in section 3.2. Moreover, section 5.2.1 contains the validation of the simulation results between SSF and SSH. Equally important, the similarity assessments between each two pair of SSF, SSH and FSF simulations are presented in section 5.2.2 comprehensively, in terms of dimensionless temperature or helium concentration and mass flow rates.

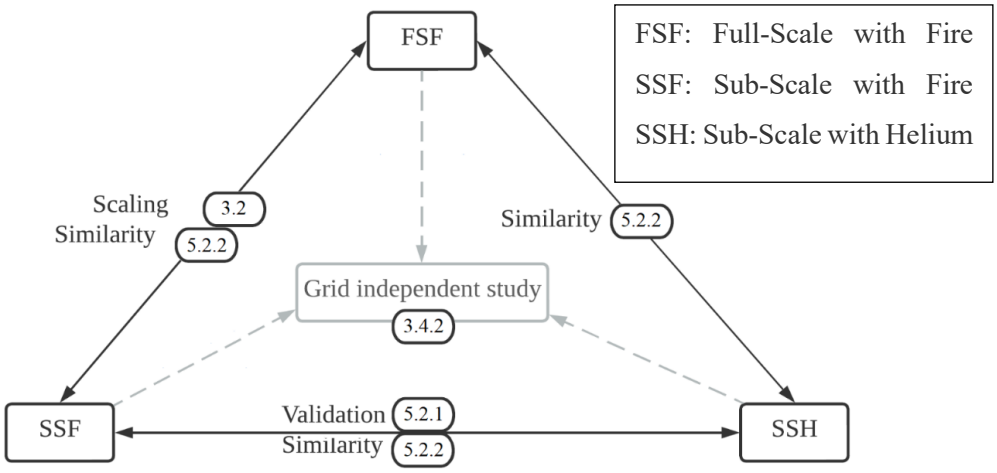

Figure 28. Schematic of proposed methodology

5.2. Results and discussion

5.2.1. Validation of simulation model

As presented in Figure 29, the transient simulation results are compared to the test measurements once in the plenum and once for the indoors separately for each floor above the helium release height (4^{th} floor). Due to the fact that the released helium intends to move upward, the floors below 4^{th} floor do not receive any inlet helium flow through the interior façade openings. To verify this fact, the indoor helium concentration was measured for the lower floors as well as the plenum. The read data showed no significant change in the helium concentration level over the whole test time in floors one to three.

In the following figure, the vertical axis is the volume fraction of the helium concentration in mol/mol and the horizontal axis shows the simulation/experiment time in seconds. The acceptable agreements between the simulation results and experimental measurements are notable. There are more fluctuations in the plenum helium concentration compared to the indoors since the vertical void is way tighter, and the boundary layer becomes narrower respectively which forms more turbulent flow along the stream.

After validation of the helium concentrations, PIV results are presented in Figure 30. As mentioned in section 3.3.2, the FOV includes the plenum and part of the indoor zone from the side view for the floors above the helium release location (4^{th} floor). The error bars are employed in the comparison to minimize the effect of intense velocity turbulences. These error bars present the difference between maximum or minimum and averaged values [138]. As predicted by the simulation results, the velocity measurements by PIV show greater values in the plenum which grow slightly along the height. For indoor flow, the overall velocity is smaller while it even reaches to zero getting close to the floors or ceiling of every story. Calculated NRMSEs show acceptable error of less than 30%.

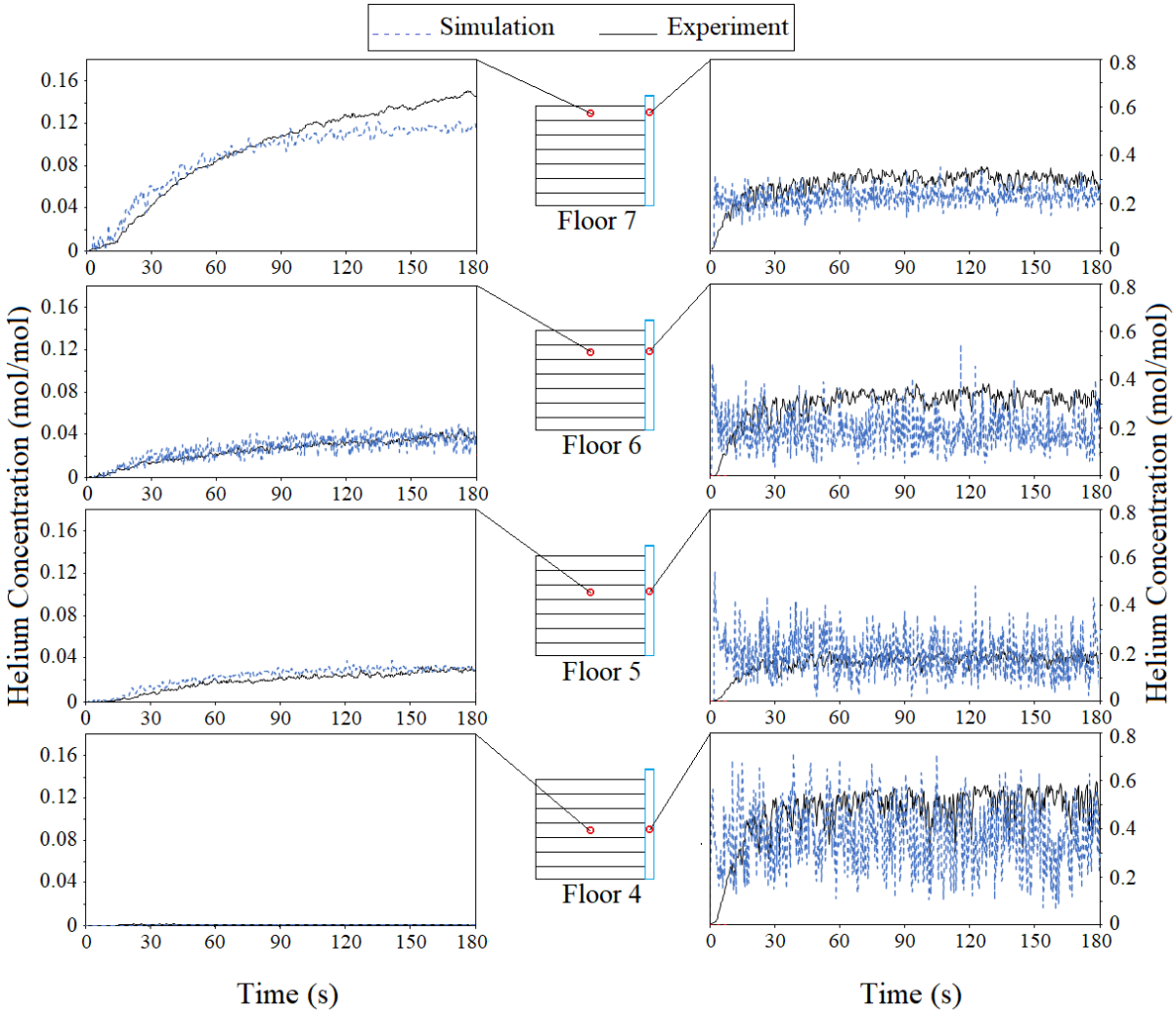

Figure 29. Transient helium concentration comparison in experiment and simulation

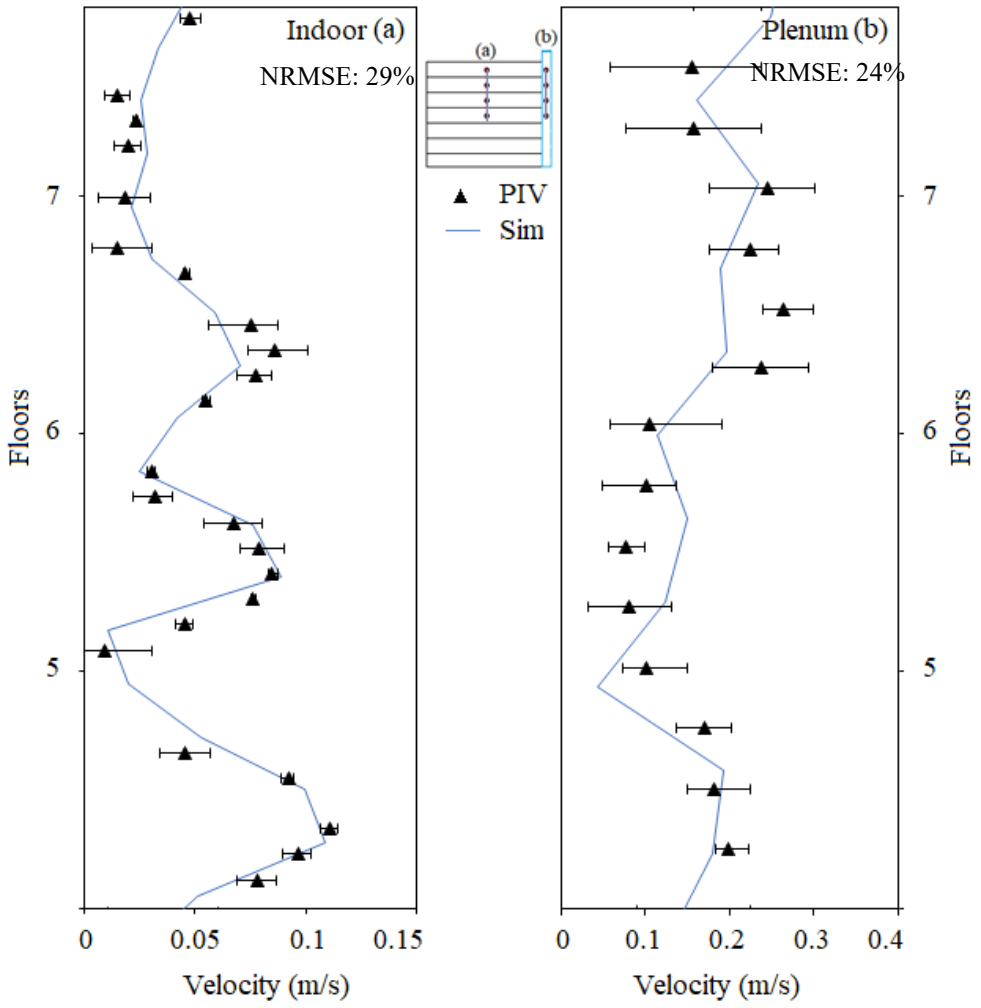

Figure 30. Steady state velocity comparison in the experiment and simulation

5.2.2. Similarity assessment

As shown in section 5.2.1 there is enough evidence that the FDS model is validated and trustable. Considering that, the similarity assessment is done between different groups of the simulation results as: a) Indoor dimensionless temperature/helium concentration between SSH and SSF, SSH and FSF, and FSF and SSF as well as plenum; b) mass flow rate comparison between SSH and SSF, SSH and FSF, and FSF and SSF.

5.2.2.1 Similarity between dimensionless temperature and helium concentration

In this section, temperature comparison results are demonstrated for the plenum and indoors. The results are available for each floor separately. However, the floors below the helium release or fire floor are ignored due to being affectless. To observe the comparison between the temperatures and helium concentrations, the related dimensionless values are calculated. Figure 31 and Figure 32 represent this comparison for SSH and SSF over the simulation time (200 s), SSH and FSF, and SSF and FSF for plenum and indoors respectively. For the last two comparisons, the corrected time has been used since the cases are in different scales (the simulation time differs). Moreover, according to the scaling relations for Froude modeling, real size temperatures can directly be compared to the temperatures of downscaled model. Therefore, for comparing FSF and SSF, the direct temperature observation is demonstrated. For a correct comparison between the temperature in FSF and SSH (as the source of the buoyant flow and the scales are different), firstly the temperatures are scaled down. Then dimensionless downscaled temperatures are compared to the dimensionless helium concentrations over the corrected time.

According to Figure 31, for all three groups of comparisons, the curves show acceptable agreements. Despite the highest temperatures and helium concentrations can be found on the 4^{th} floor, the general trend does not change severely along the height. Therefore, the curves for the 7^{th} floor plenum are almost in the same magnitude as the 4^{th} floor. This is in contrast to the comparison of the indoor results. As presented in Figure 32, the indoor temperature/ helium concentrations on the fire floor are way smaller than the top floor which means the occupants on the top floor are exposed to the smoke risk more than the rest of the building occupants. It is apparent that the similarity between the different simulation cases in the indoors is still notable as in the plenum.

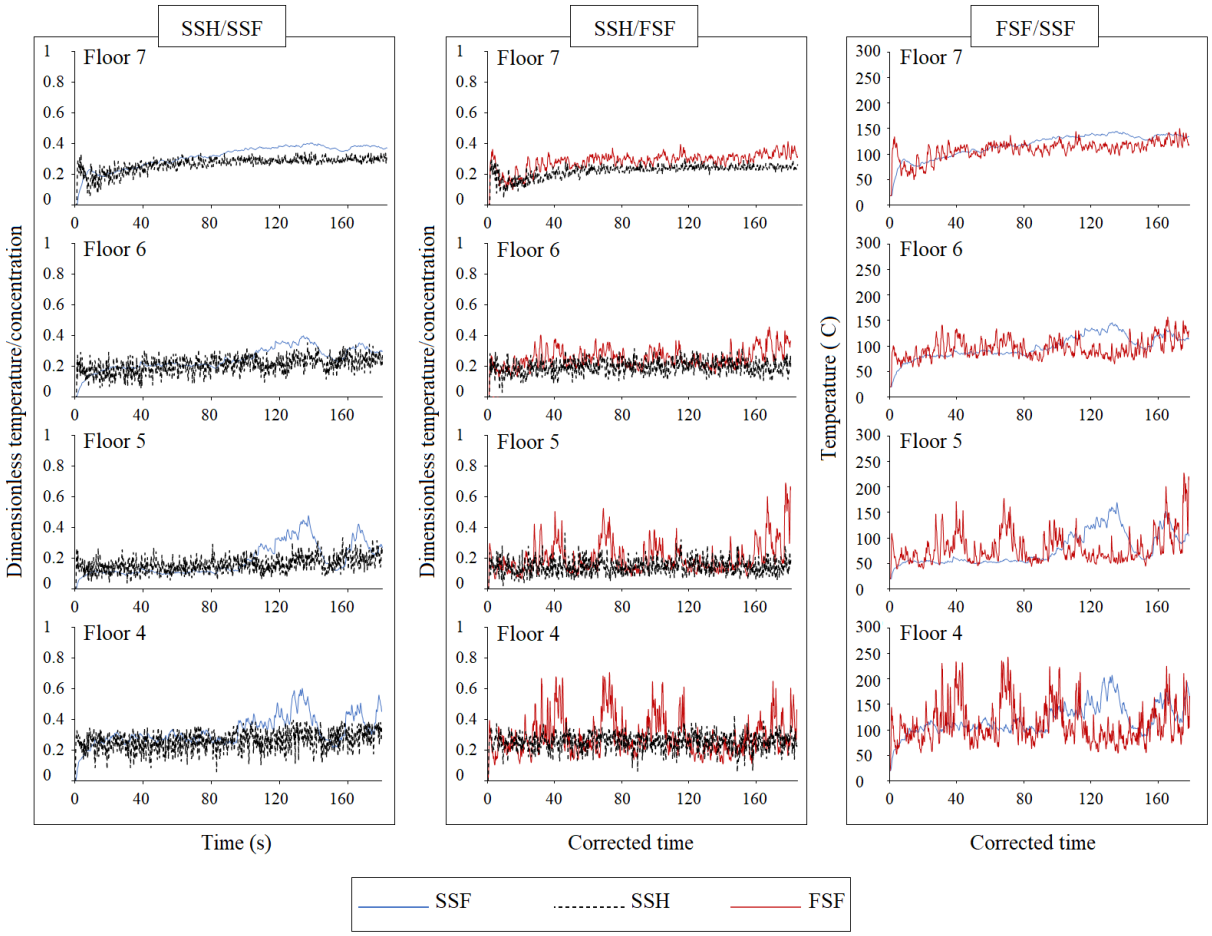

Figure 31. Plenum temperature/helium concentration comparison between SSH and SSF, SSH and FSF, and FSF and SSF

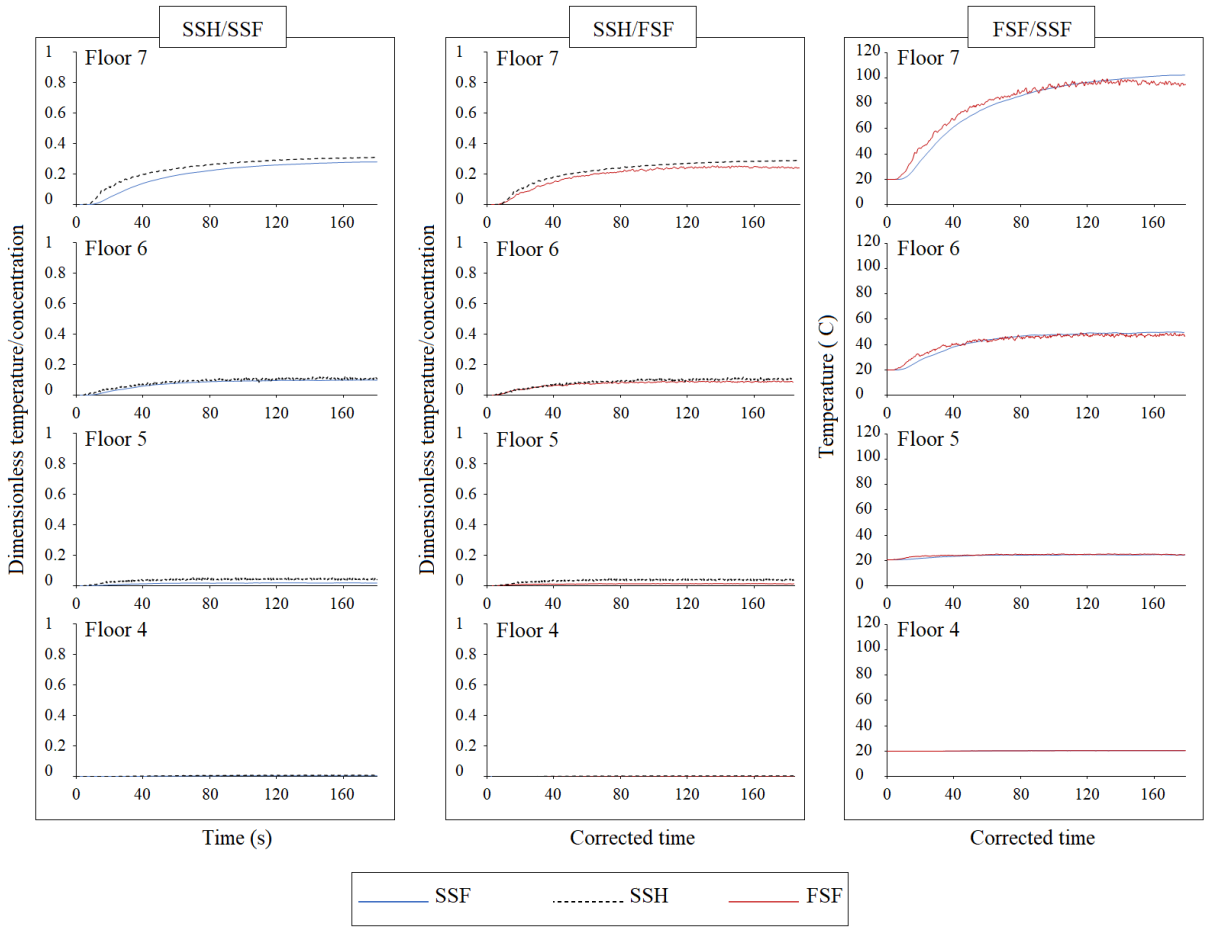

Figure 32. Indoor temperature/helium concentration comparison between SSH and SSF, SSH and FSF, and FSF and SSF

5.2.2.2. Mass flow rate comparison in the entrance

The mass flow rates are obtained for the interior middle window on each floor of each simulated case. As discussed for the temperature/ helium concentrations, the extent of agreement between simulation results are presented in Figure 33. The results are respectively for comparison between the SSH and SSF, SSH and FSF, and finally for the SSF and FSF. To compare mass flow rate of the small-scale cases with the full-scale one, the scaled time is employed (equation 3-16). The figure shows the overall mass flow rate for both directions through the middle window of each floor above fire/helium release floor. As will be discussed in detail in chapter 6, since there are bi directional flows close to the opening on each floor, the negative quantities

stand for the flow going from indoors to the plenum and positive flow means the stream is from plenum to the indoors. Therefore, on 7th floor the MFR is close to zero which means that the positive flow is dominant. Moreover, in 4th floor negative flow is dominant which is the reason of finding the overall MFR curve below zero.

5.2.2.3. Snap shots of the temperature/helium concentration and velocity distribution

Figure 34 includes snapshots of the temperature in various time sections, ranging from transient phase (up to 250 s for FSF, 40 s for SSF and SSH) to steady state. The location of fire/helium release is in the middle of the height (on the façade, 4th floor). The snapshots represent the whole simulation domain which includes the building, above and the zone adjacent to the opening on the back wall of the building.For SSH, as the temperature is constant during the simulation, helium concentration will be representative instead. As can be seen the overall patterns are different during the transient time. However, when they reach the steady state, temperature/concentration distributions follow almost the same pattern. Similarly, the velocity in the same time sections in all three cases are demonstrated in Figure 35. Despite the fact that the snapshots are not related to some specific pointwise measurements, by and large, they are informative for considering the overall flow pattern characteristics.

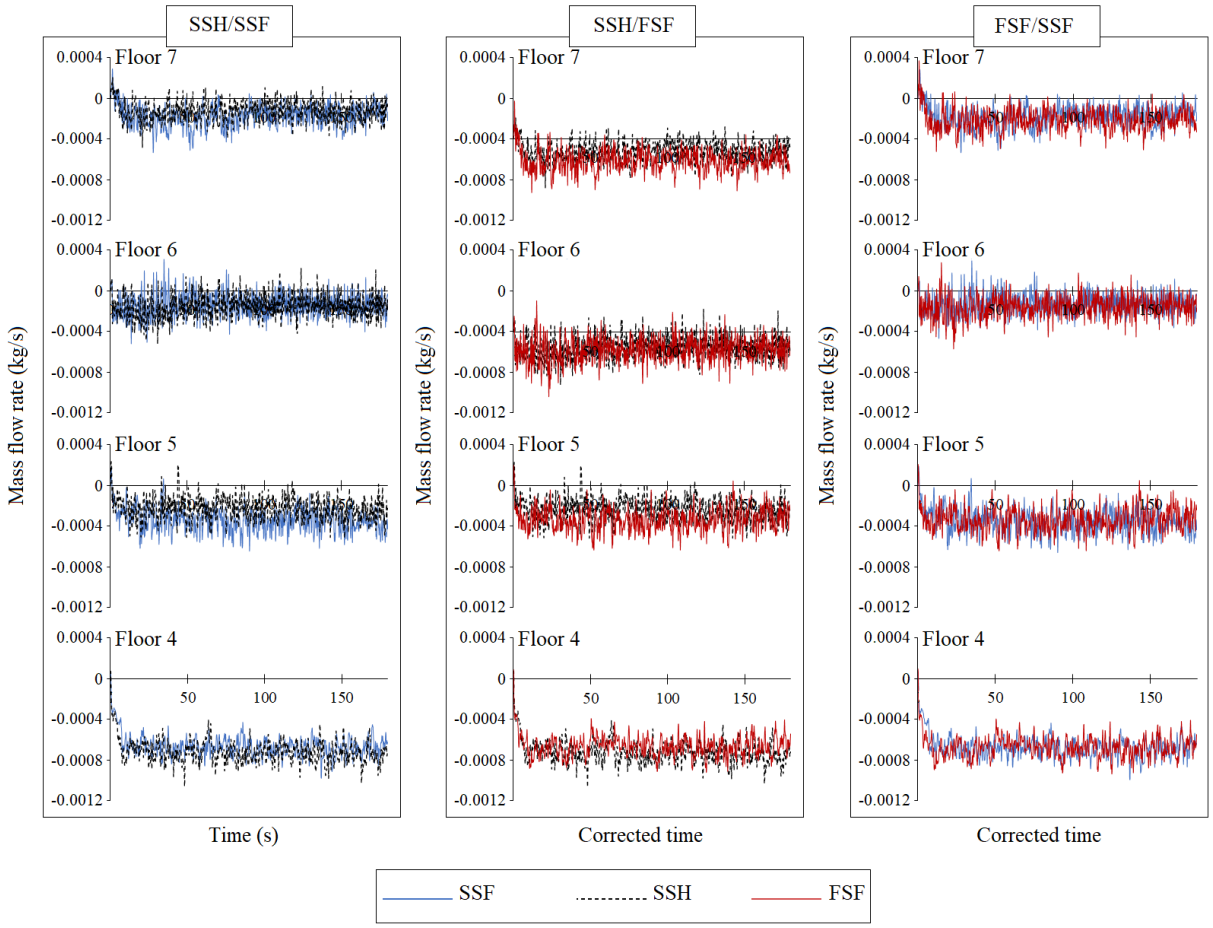

Figure 33. Mass flow rate comparison between SSH and SSF, SSH and FSF, and FSF and SSF

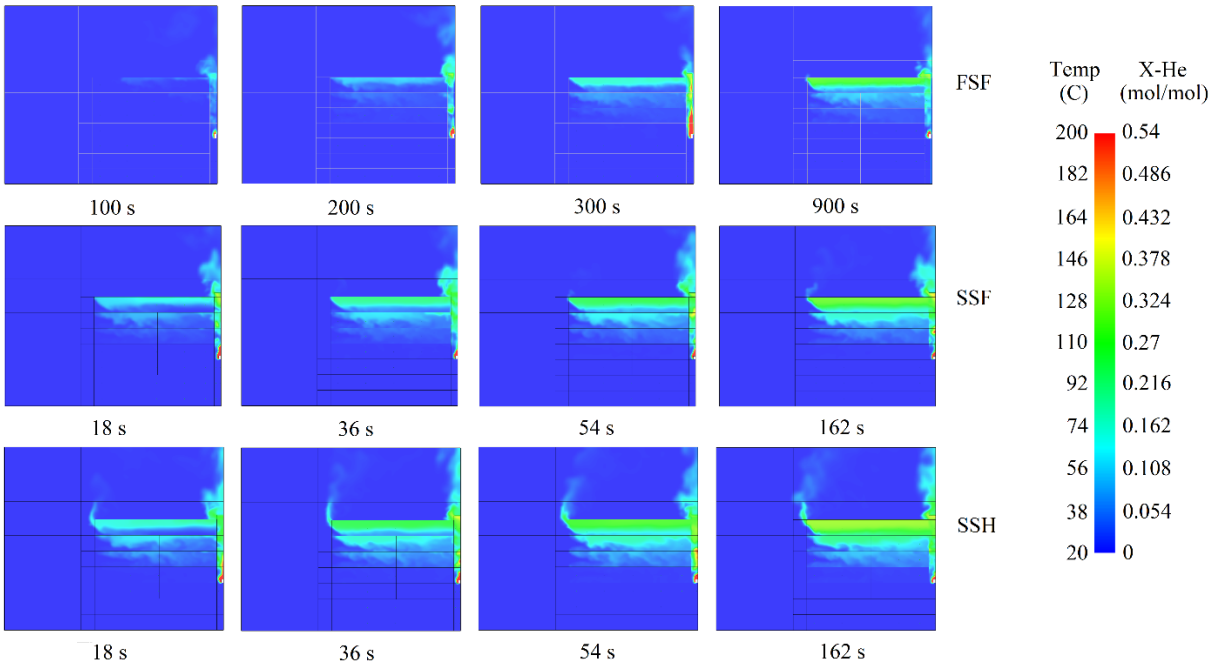

Figure 34. Temperature distribution in different time sections for three cases

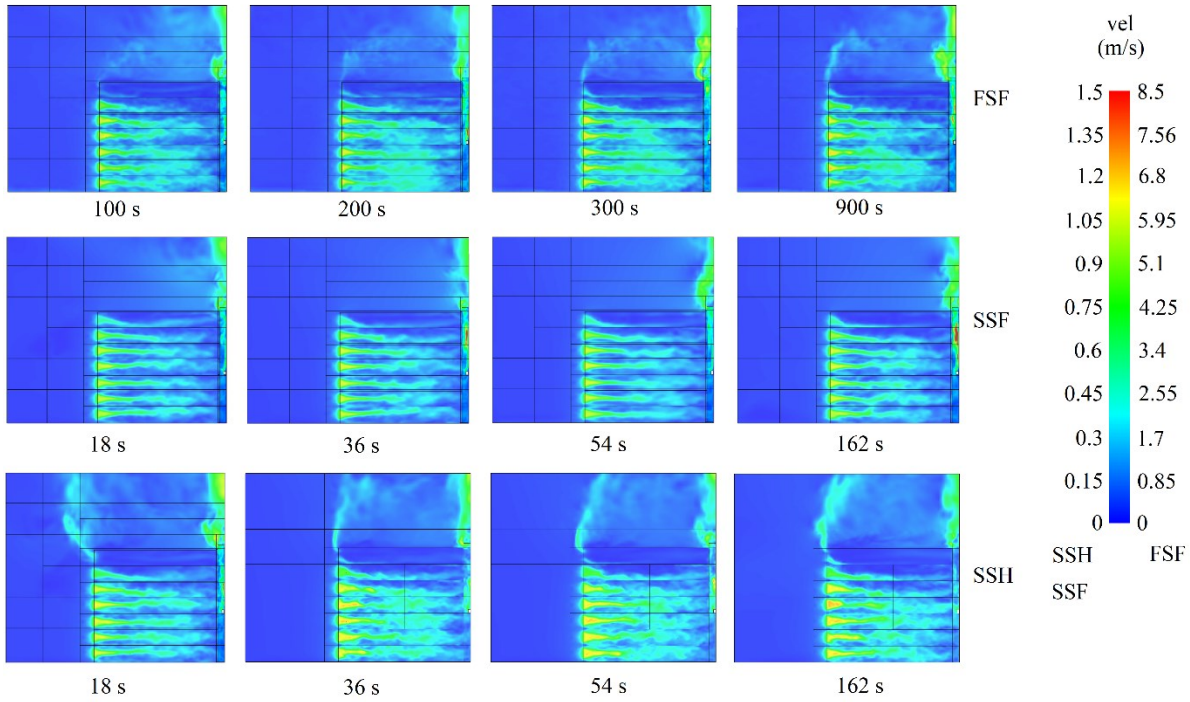

Figure 35. Velocity distribution in different time sections for three cases

5.3. Summary

This study tries to find out that how the smoke from the fire initiated on the BIPV DSF may infiltrate to the building through the interior openings. For this reason, a 7-storey building is selected as a case study. Each floor is connected to the other floors via a BIPV DSF. For a thorough observation, three cases of full-scale building with fire, small-scale building with fire and small-scale building with helium is considered. The two small-scale models, one with fire (using Froude modeling) and the other with helium (using Froude modeling and similarity between hot smoke and helium) are defined. Then, a small-scale experimental model with helium is made to be tested in the laboratory. To prove the credibility of using helium instead of real fire, three series of simulation results (FSF, SSF and SSH) are compared to each other in terms of temperature/helium concentration and velocity. Considering this the following conclusions are made:

- Firstly, the FDS simulation results for the SSH is validated by the experimental measurements. The transient helium concentrations are well matched with the simulation results while the steady state velocities are in the acceptable level of agreement with the PIV results (NRMSEs are less than 30% for indoor and plenum).
- Secondly, the extent of agreement between FSF and SSF, FSF and SSH, and SSF and SSH is observed in terms of dimensionless temperatures/helium concentrations, and MFRs. The similarities between the mentioned curves are notable in both internal and plenum zones. Moreover, the identical distribution pattern in the sectional snapshots supports the latter conclusion. Therefore, these observations contribute to the traditional use of real fire in small-scale fire experiments and suggests using pure helium instead, to reach the same required flow characteristics.
- More importantly, it is proved that the fire risk associated with the BIPV façade can threaten the safety of the occupants. The smoke propagation from the façade's vertical void to different floors supports this idea.

Chapter 6 Parametric experimental investigation on the effect of location and magnitude of BIPV façade fire on the smoke spread

Contributions:

Chapter 6 presents a parametric study on the effect of location and magnitude of BIPV façade fire on smoke spread. The phenomenon of smoke movement was observed. Based on the phenomenon, suggestions and relevant measures of fire smoke protection can be discussed and proposed.. The results demonstrate that adjacent to the opening on each floor bi-directional streams are noted right next to the entrance. The magnitude of this circular flow depends on the inlet velocity from the plenum and the proportion of inlet (from plenum to indoors) and outlet (from indoors to plenum) flows of the adjacent window as well as the velocity of the flow in each direction. Among all three cases of fire location (on the bottom, mid-height and top), the highest risk of involvement happens when the fire is on the bottom. Regardless of the fire location the greatest risk is observed at the top floor. Moreover, according to the helium concentration results central floors can be the safest places regarding receiving smoke from plenum in the studied fire scenarios.

6.1. Introduction

To fill in research gap discussed in Section 2.8 about the experimental investigation on the BIPV DSF fire, this study conducts experiments using helium and PIV in parallel. The introduced scaling method is employed (see Section 3.2). The impact of location of the fire on the facade, and heat release rates (HRR) on smoke spread from BIPV double skin facade fire is observed. Several fire location on the facade (bottom, middle and top floor) and HRRs (85 kW/m^2 , 191 kW/m^2 , 319 kW/m^2) are considered as demonstrated in Figure 36.

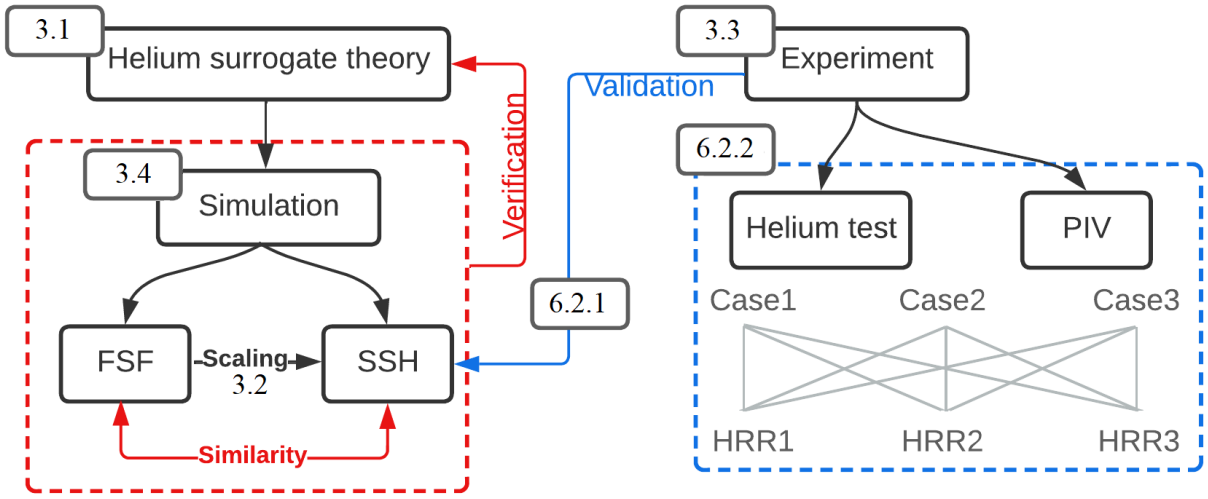

Figure 36. Methodology schematic

6.2. Results and discussions

6.2.1. Compatibility and validation between small-scale helium experiment, small-scale helium, and full-scale real fire FDS model

The two FDS models (full-scale model with fire and small-scale with helium) are compared to the small-scale helium experiment. In all three cases, the fire/helium release location is on the middle height of the building which is 4th floor. Therefore, Figure 37 shows the dimensionless plenum temperature (for full-scale FDS model with fire) and the dimensionless concentration (for the simulation and experimental models with helium) above the fire/helium location. The considered fire intensiy for FSF is 319 kW/m2 which is equivalent to 58.33 kW/m2 for SSF and 0.0208 kg/(m2.s) for SSH.

Dimensionless helium concentration and real fire smoke temperatures are used based on the principal of smoke-helium similarity discussed in section 3.1. Moreover, for the horizontal axis the scaled time is applied since the simulation/test duration was different between full-scale and small-scale cases.

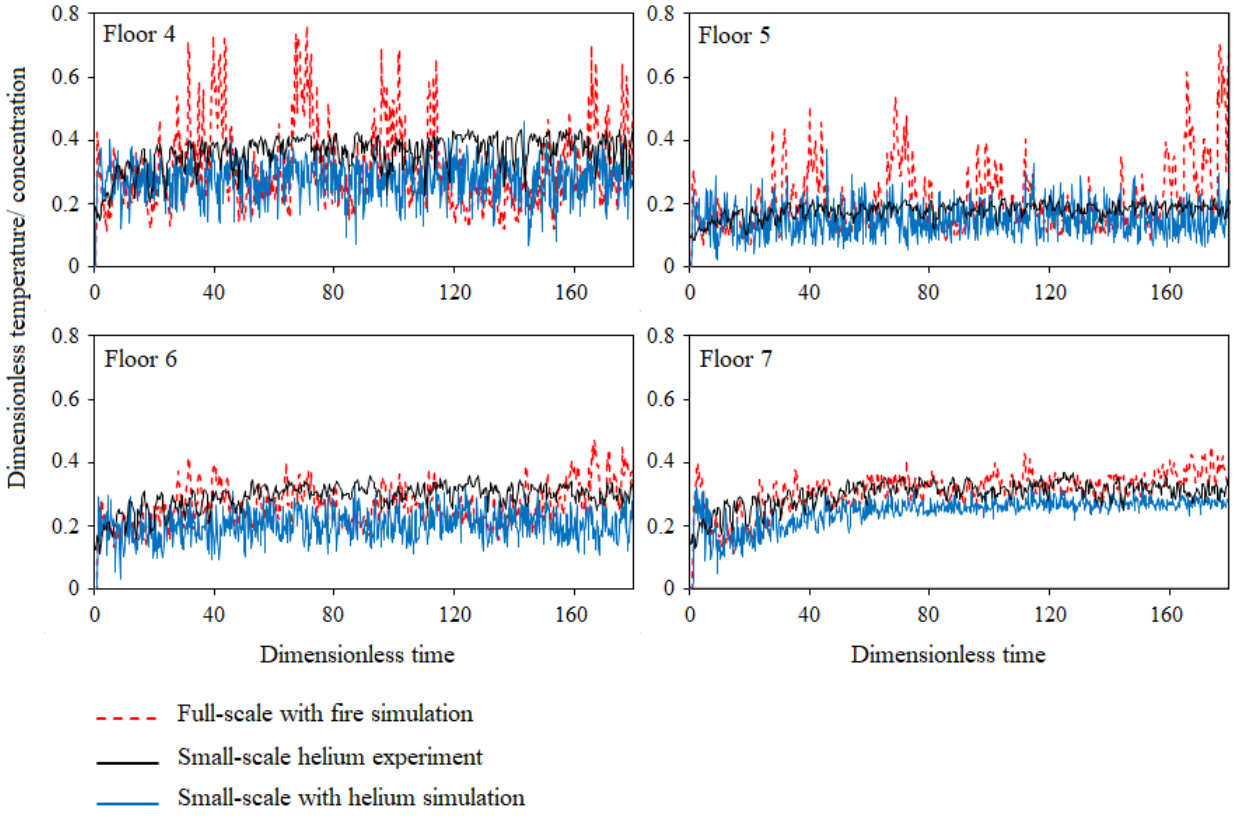

Figure 37. Comparison of transient dimensionless plenum temperature/concentration between FSF simulation, SSH simulation and SSH experiment

As can be seen there is a good agreement between the transient simulation results and at the same time with experimental measurements.

6.2.2. Different fire locations and heat release rates

Figure 38, Figure 39 and Figure 40 present the transient helium concentration for three different heat release rates and three different fire locations. It must be considered that wherever different heat release rates (HRR) are called hereafter, it means the converted helium flow rate (LPM) corresponding to the HRR is used in the experiment (e.g., HRR1 (319 kW) stands for 180 LPM). The transient helium concentration curves show that the flow reaches the steady state after 40 seconds to a constant mean value. It must be mentioned that for Figure 39 and Figure 40, helium

concentrations were measured zero for the floors below a fire floor. Thus, Figure 39 includes floors 4 to 7 and Figure 40 is only for the top floor.

It is clearly distinguishable that the number of floors involved in the smoke spread varies based on the location of the fire. To elaborate, when the fire is on the bottom (Figure 38), in addition to the vertical void on façade (plenum space), all the stories receive smoke while for the case with fire on top only one storey is involved. When the fire is on the bottom, the indoor helium concentration increases 4 times (from less than 0.05 to 0.2 mol/mol) from floor 1 to floor 7. Therefore, in great heat release rates it may be a serious risk to the occupants on the top floor in high-rise buildings in particular with a high HRR of a fire on the BIPV DSF. On the other hand, there is a 2.5-times concentration drop in plenum between floor 1 and floor 7. The same rise and fall of helium concentration can be seen when the fire is initiated on the mid-height.

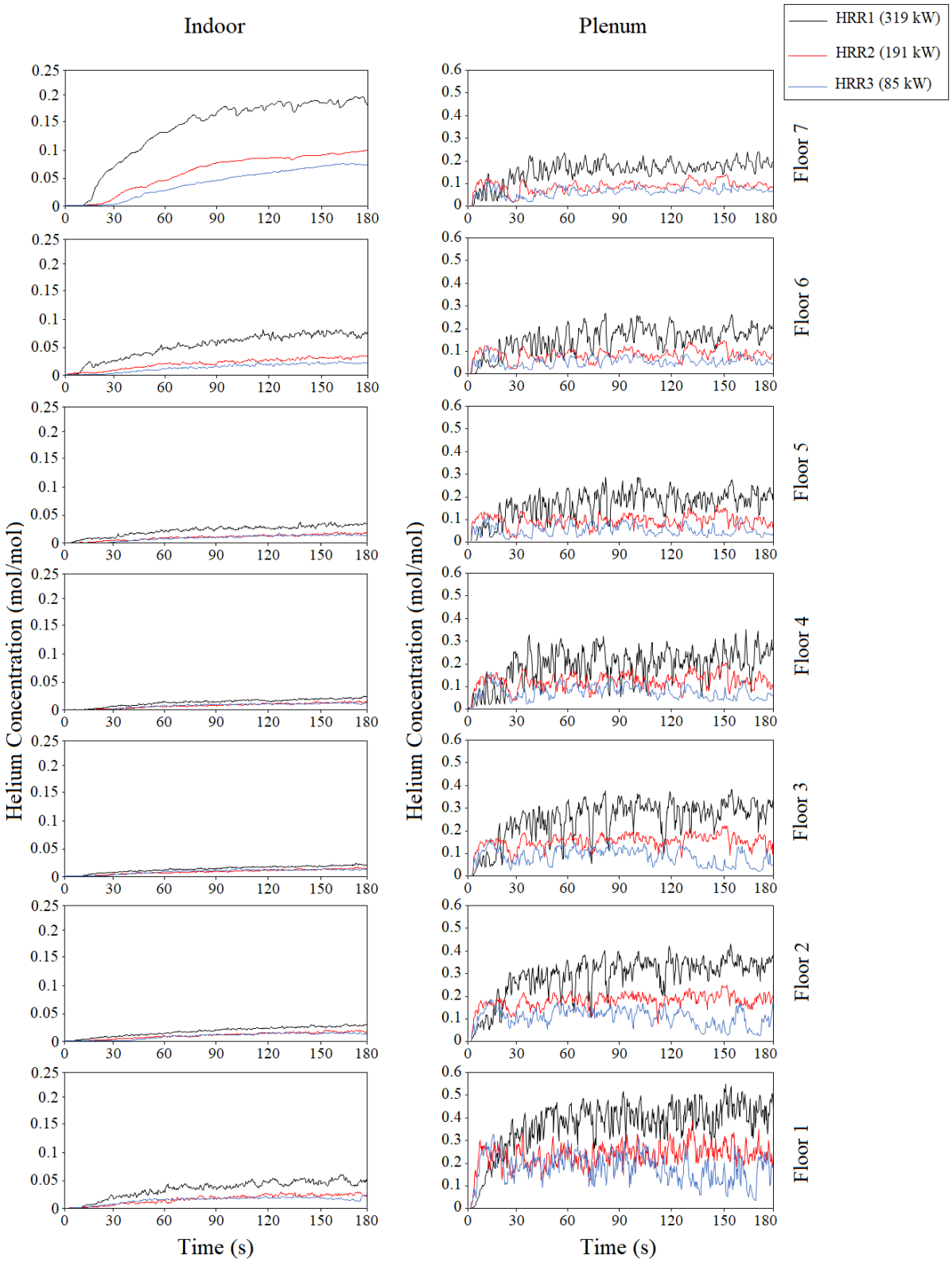

Figure 38. Helium measurements for scenario 1 (fire on the bottom) with different HRRs

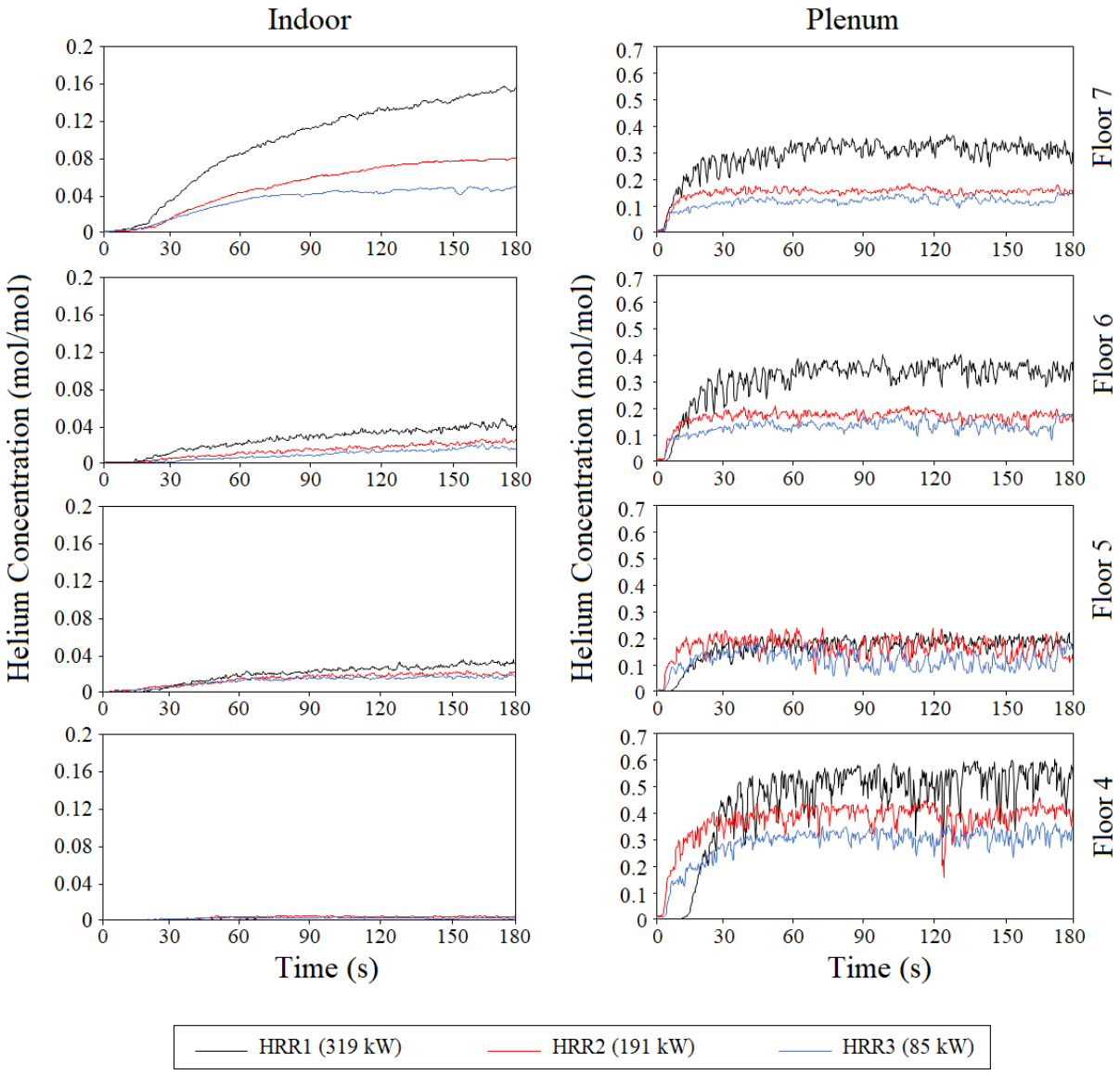

Figure 39. Helium measurements for scenario 2 (fire on the mid-height) with different HRRs

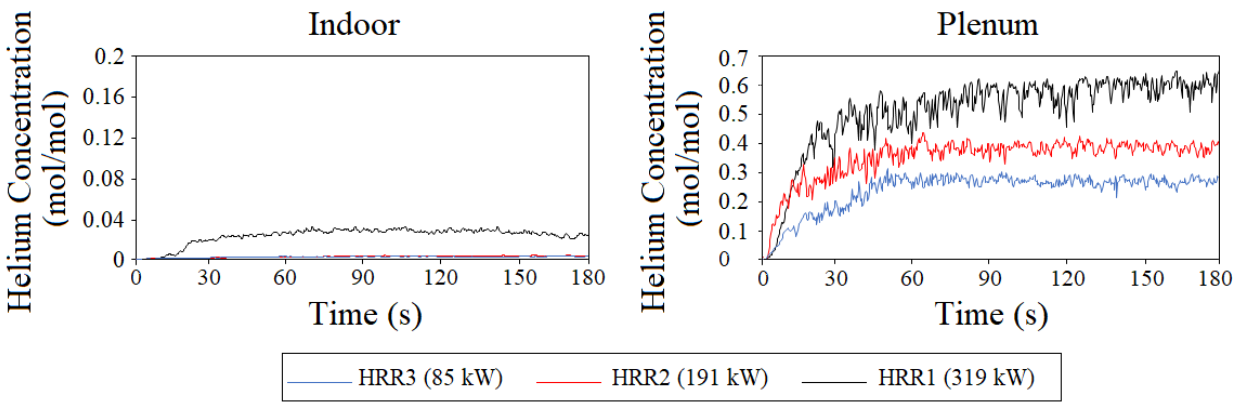

Figure 40. Helium measurements for scenario 3 (fire on the top) with different HRRs

Steady-state helium concentrations and flow velocities for various fire locations and HRRs are respectively provided in Figure 41 and Figure 42. The concentration measurements are done for each floor along a vertical line, once for the plenum and once for the indoor zone. Figure 41 proves that the risk of involvements in the smoke spread increases for more floors when the fire happens on the bottom. It shows that the neutral plane is located somewhere around 4th floor. So below this floor, flow generally tends from indoor zone to the plenum while over it the high pressure flow in the plenum travels to the internal zone. Moreover, the drastic rise of helium concentration on the top floor verifies the safety danger for the occupants on that floor. On the other hand, the measured concentration is great around the fire zone specially in the plenum. Therefore, for designing the critical locations of control center or the major connections such as battery bank, inverter etc. the accessibility in case of incident must be considered. More specifically in semitransparent PV systems (STPV), there is higher possibility of distributing the installation of the solar panels on a larger surface such as whole façade or the whole roof top.

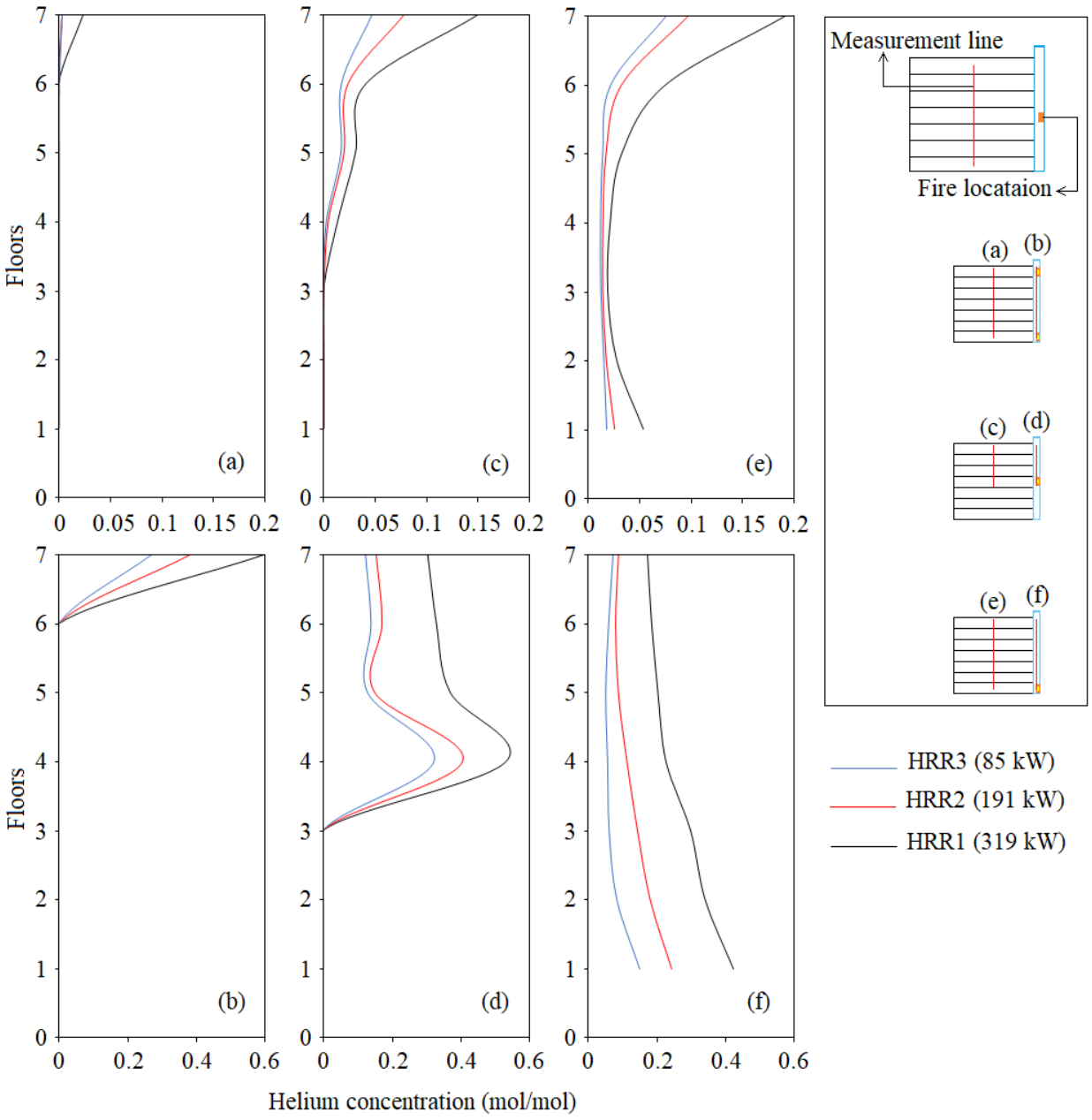

Figure 41. Steady-state results for three fire locations/HRRs

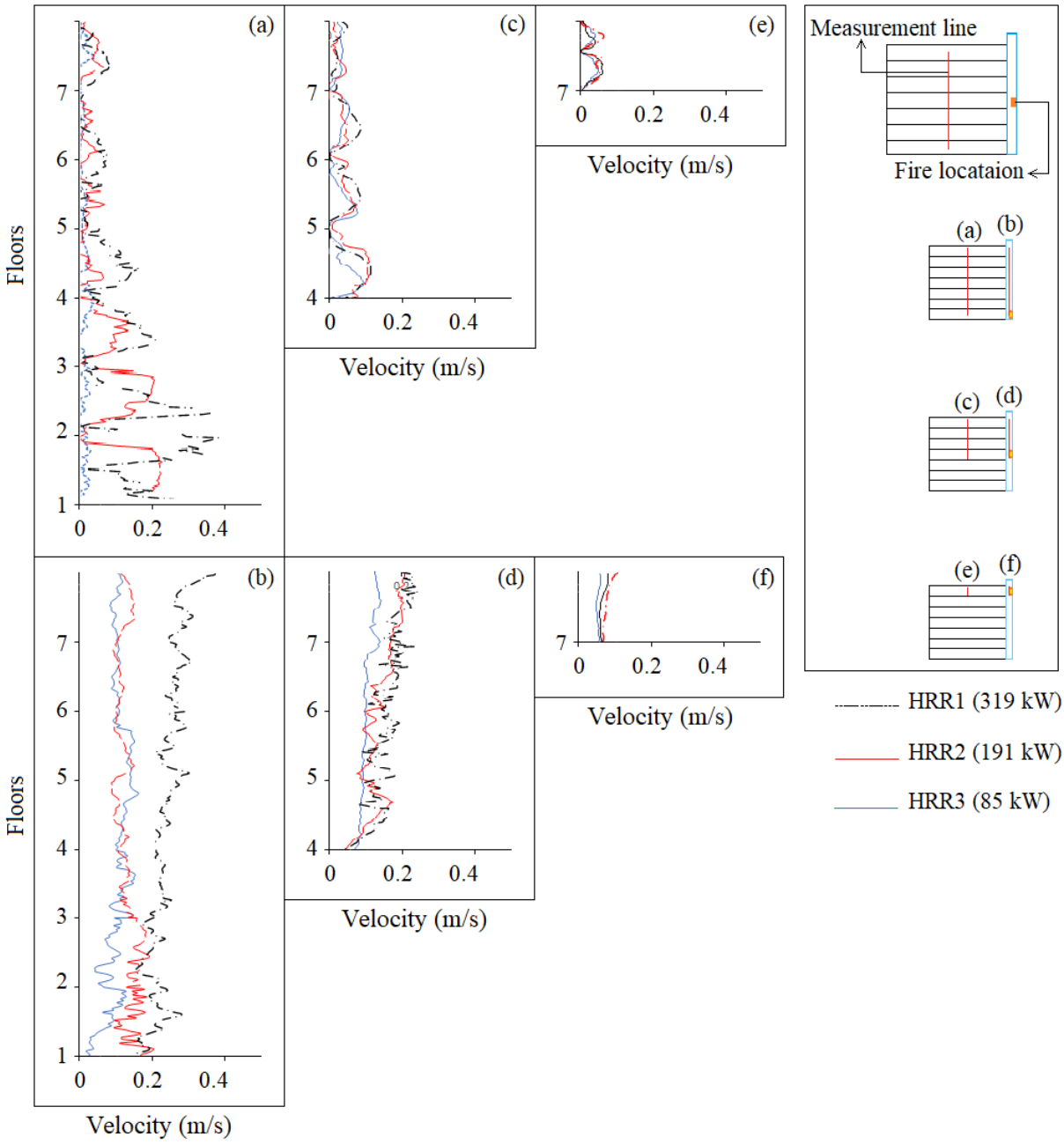

Figure 42. PIV results for three fire locations/HRRs

Since the flow propagation from the plenum to the internal zone is complex, Figure 43 to Figure 45 investigate the flow pattern by velocity vectors for the 9 scenarios with different locations of fire and HRRs. It shows bi-directional flow adjacent to the opening on each floor which makes a circular stream. While the flow tends to enter the plenum via the window, the upward higher

speed plenum flow pushes it back to the internal zone. The formation of eddy differs from floor to floor and depending on fire location and HRR.

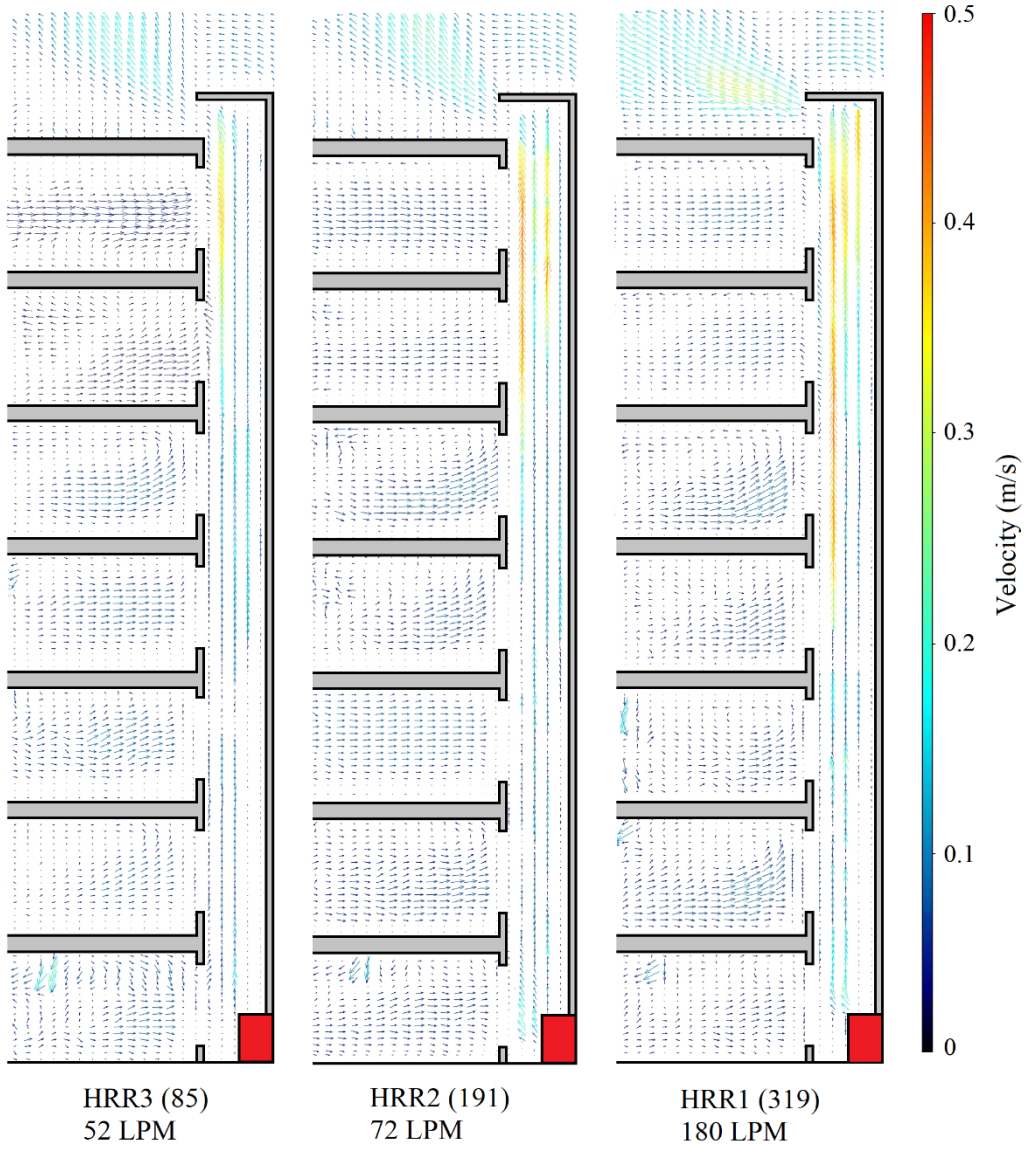

Figure 43. Velocity vector for scenario 1 (fire on the bottom) with three different HRRs

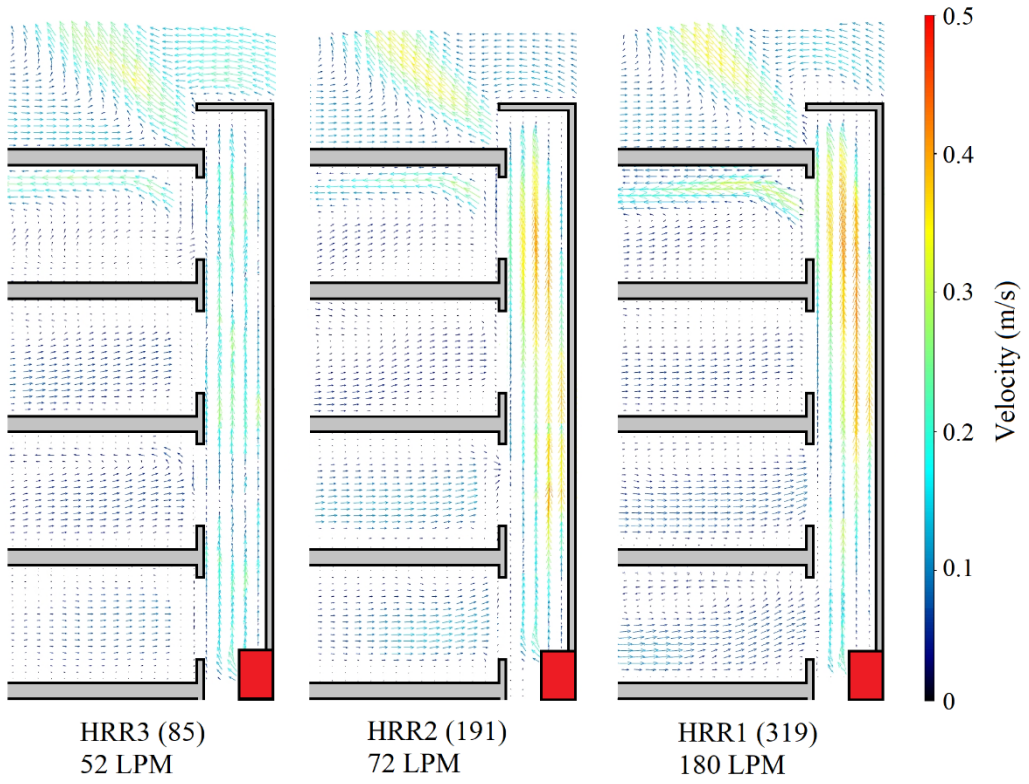

Figure 44. Velocity vector for scenario 2 (fire on the mid-height) with three different HRRs

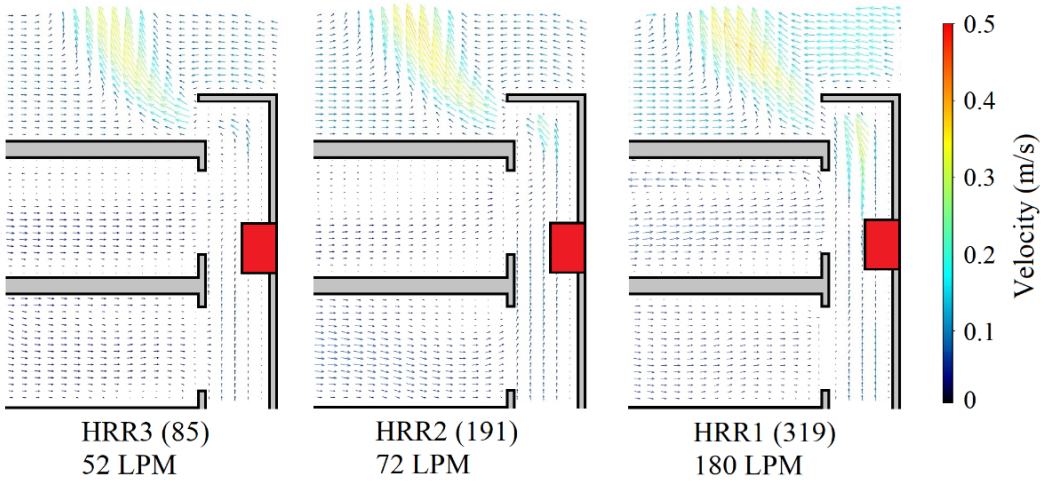

Figure 45. Velocity vector for scenario 3 (fire on the top) with three different HRRs

To explore in more details, Figure 46 provides the flow pattern and the quantity of the associated helium concentrations and velocities for the top, bottom and mid-floor as samples for the case

where the fire is placed on the bottom. The circular stream directly depends on the magnitude of inlet (from plenum to indoors) and outlet (from indoors to plenum) flows of the adjacent window as well as the velocity of the flow in each direction. To elaborate for the first-floor, although the portion of outlet (from indoor to the plenum) is bigger than the inlet, the high velocity of the helium source/plume makes the floor more risky than middle floor (4^{th} floor). Looking into the top floor, the trend is reverse, through which the intake is much bigger and consequently a high helium concentration is observed for the indoor zone but with low velocity. On 4^{th} floor the lowest helium concentration can be seen in the internal zone, since the biggest outlet is formed near the opening. Therefore, the high speed of the upward flow in the plenum tends less to push the flow in, and more amount of helium discharges to the plenum.

Floor	Helium concentration (mol/mol)	Velocity (m/s)	Velocity vector profile
7	0.192	0.08	
4	0.021	0.17	
1	0.028	0.2	

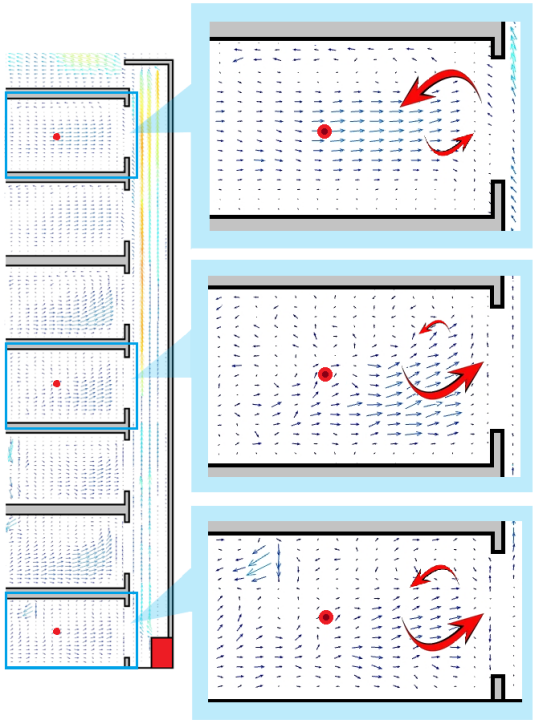

Helium sensor in helium test

Schematic portion of helium flow in the demonstrated direction

Figure 46. Comparing the indoor helium concentration, velocity and flow pattern in floors 1, 4 and 7, when the fire floor is on the bottom

6.3. Summary

Due to the wide application of PV systems and lack of investigation on the BIPV (specifically on the façade), there is high demand of studying scenarios through which the fire behavior and smoke propagation are extensively investigated. Hence in the current research, an experimental study is carried out to verify the smoke propagation from ignited BIPV DSF. The experiment is made of a series of tests on the case study with varying location of the ignition on the façade and heat release rates. The following conclusions have been made:

- The general stream in the vertical cavity of plenum is upward because of the buoyancy. However, adjacent to the opening on each floor bi-directional streams are noted right next to the entrance. The magnitude of this circular flow depends on the inlet velocity from the plenum and the proportion between the outlet and inlet flows.
- It has been seen that among all three cases of fire location (on the bottom, mid-height and top), the highest risk of involvement of smoke spread happens when the fire is on bottom. Regardless of the fire location the greatest risk is for the top floor. Moreover, according to the helium concentration results (both transient and steady state) central floors can be the safest places regarding receiving smoke from plenum, in the studied fire scenarios.
- The profile of velocity is independent of the HRR magnitude. However, the fire risk can dramatically increase with the higher HRRs.

Overall, studying the smoke propagation and fire behavior helps the decision makers to define the best method for the smoke control system design, the suppression system or evacuation. As an example, for the worst case of fire that involves all the floors (fire on the bottom), the middle floors receive the least smoke. Furthermore, the control center, energy storage such as converter and the battery bank locations must be considered as far as possible to the places with the highest risk. Therefore, the accessibility to those would be easier in the case of fire, and the risk of subsequent hazards, such as explosion decreases.

Chapter 7 Conclusion and future work

7.1. Conclusion

According to the available reports and studies on PV systems, they can be count as one of the origins of fire incident on building envelope such as roof, cladding or façade due to numerous reasons which are extensively discussed in chapter 2. Specially when they are embded in the structure of the building as BIPVs and bring more changes, further investigation is required to provide the safe adoption (in terms of fire risk). More specifically there has been less attention to the BIPV facades in comparison to roof applications. Unfortunately the current research and regulations don't cover the available gaps. Therefore, after defining the available gaps in the recent research on the BIPVs, it is mentioned that the main intact area is the associated fire risks including the smoke propagation to the indoor environment. This study conducts a multi phase research on a case study with BIPV DSF. The main PV fire size is considered as 319 kW/m^2 from available literature. The following tasks have been done in brief:

In the first phase, a similarity theory between helium and real fire smoke has been developed to use a helium surrogate instead of the real fire in the experiments. This similarity theory suggests the comparison of the dimensionless temperature in real fire test to the dimensionless helium concentration in a test with helium surrogate for a certain point, while it proves that the flow velocity is conserved. In the second phase, based on the mentioned theory and a scaling method (called Froude modelling) a small-scale experimental test has been designed and conducted for the verification and validation. Moreover, another phase includes the CFD model of the case study by using FDS tool for three groups of simulations; named FSF (full-scale with fire), SSF (small-scale with fire) and SSH (small-scale with helium surrogate). The comparison between the simulation cases will contribute to the validation and verification of the proposed similarity and scaling theory. The following main conclusions are obtained:

- The validity of CFD models is observed through two separate sets of experiments in terms of helium concentration and air velocity (PIV). The transient helium concentrations were compared to the associated simulation results for two points on each floor, one in the plenum and the other indoor (in total 14 points). The PIV results show acceptable compatibly to the associated FDS simulations (NRMSE smaller than 30 %). Moreover, the steady-state flow

velocities were examined on two separate lines, similarly one line along the height of plenum void and another line for indoor. The coefficients of variation of these comparisons ranged between 1.6 to 11% which means the associated curves fit perfectly on each other. This compatibility was later supported by the identical snapshots of air flow filling the floors one after another. This agreement is also explained by the great fit between the transient helium concentration measurements and the simulation results on each floor presented in sections 4.2.1, 4.2.2 and 5.2.1 as well as the flow pattern snap shots).

- On the other hand, the proposed scaling method (Froude modelling) is confirmed by the similarity assessments presented in section 5.2.2. Considering three groups of simulations (SSH, SSF and FSF), the comparison between the associated simulation results for the transient mass flow rates and dimensionless helium concentrations shows small deviations (section 4.2.3, 4.2.4 and 5.2.2). This is also confirmed by the flow pattern snapshots.

Up to this point the validity of the proposed helium similarity theory and the scaling method is confirmed. Thus, the results of the experimental parametric study on the BIPV DSF can be trusted instead of performing the experiments with the real fire. The considered scenarios include three locations of helium release and three different HRRs (which is converted to the corresponding helium flow rate in LPM) for each location of helium release. The following main conclusions are obtained from the conducted parametric study:

- The general stream in the vertical cavity of plenum is upward because of the buoyancy. However, adjacent to the opening on each floor bi-directional streams are noted right next to the entrance. The magnitude of this circular flow depends on the inlet velocity from the plenum and the proportion between the outlet and inlet flow momentums.
- It has been seen that among all three cases of fire location (on the bottom, mid-height and top), the highest risk happens when the fire is on bottom since more floors get involved. Regardless of the fire location the greatest risk is at the top floor. Moreover, according to the helium concentration results (both transient and steady-state) central floors can be the safest places regarding receiving smoke from plenum in the scenarios considered in this study.
- The profile of velocity is independent of the HRR magnitude. However, the fire risk can dramatically increase with the higher HRRs.

Overall, studying the smoke propagation and fire behavior helps the decision makers to define the best method for the smoke control system, suppression system or evacuation. As an example, for the worst case of fire that involves all the floors (fire on the bottom), the middle floors receive the least smoke. Furthermore, the control center, energy storage such as converter and the battery bank locations must be considered as far as possible to the places with the highest risk. Therefore, they would be more accessible in the case of fire, and the risk of subsequent hazards, such as explosion, decreases.

Conclusion (en français)

Après avoir défini les lacunes disponibles dans les recherches récentes sur le photovoltaïque intégré au bâtiment, il est mentionné que la principale zone intacte est celle des risques d'incendie associés, y compris la propagation de la fumée vers l'environnement intérieur. Par conséquent, cette étude mène une recherche en plusieurs phases sur une étude de cas avec BIPV DSF. Les tâches suivantes ont été réalisées en bref :

Dans la première phase, une théorie de similarité entre l'hélium et la vraie fumée de feu a été développée pour utiliser un substitut d'hélium au lieu du vrai feu dans les expériences. Cette théorie suggère la comparaison de la température sans dimension dans un essai au feu réel à la concentration d'hélium sans dimension dans un essai avec substitut d'hélium pour un certain point, tout en prouvant que la vitesse d'écoulement est conservée. Dans la deuxième phase, sur la base de la théorie mentionnée et d'une méthode de mise à l'échelle (appelée modélisation de Froude), un test expérimental à petite échelle a été conçu et réalisé pour la vérification et la validation. De plus, une autre phase comprend le modèle CFD de l'étude de cas en utilisant l'outil FDS pour trois groupes de simulations ; nommé FSF (pleine échelle avec feu), SSF (petite échelle avec feu) et SSH (petite échelle avec substitut d'hélium). La comparaison entre les cas de simulation contribuera à la validation et à la vérification de la théorie de similarité et d'échelle proposée. Les principales conclusions suivantes sont obtenues :

- La validité des modèles CFD est observée à travers deux ensembles distincts d'expériences en termes de concentration d'hélium et de vitesse de l'air (PIV). Les concentrations transitoires d'hélium ont été comparées aux résultats de simulation

associés pour deux points à chaque étage, l'un dans le plénum et l'autre à l'intérieur (au total 14 points). Les résultats PIV montrent une compatibilité acceptable avec les simulations FDS associées (NRMSE inférieur à 30 %). De plus, les vitesses d'écoulement à l'état d'équilibre ont été examinées sur deux lignes distinctes, de la même manière une ligne le long de la hauteur du vide du plénum et une autre ligne pour l'intérieur. Les coefficients de variation de ces comparaisons variaient entre 1,6 et 11 %, ce qui signifie que les courbes associées s'emboîtent parfaitement. Cette compatibilité a ensuite été soutenue par les instantanés identiques du flux d'air remplissant les étages les uns après les autres. Cette concordance s'explique également par la grande adéquation entre les mesures transitoires de concentration d'hélium et les résultats de simulation à chaque étage présenté dans les sections 4.2.1, 4.2.2 et 5.2.1 ainsi que les instantanés du schéma d'écoulement).

- En revanche, la méthode de mise à l'échelle proposée (modélisation de Froude) est confirmée par les évaluations de similarité présentées à la section 5.2.2. En considérant trois groupes de simulations (SSH, SSF et FSF), la comparaison entre les résultats de simulation associés pour les débits massiques transitoires et les concentrations d'hélium sans dimension montre de faibles écarts (section 4.2.3, 4.2.4 et 5.2.2). Ceci est également confirmé par les instantanés du modèle de flux.

Jusqu'à présent, la validité de la théorie de similarité de l'hélium proposée et de la méthode de mise à l'échelle est confirmée. Ainsi, on peut se fier aux résultats de l'étude paramétrique expérimentale sur le BIPV DSF au lieu de réaliser les expériences avec le feu réel. Les principales conclusions suivantes sont tirées de l'étude paramétrique menée :

- Le flux général dans la cavité verticale du plénum est ascendant en raison de l'effet de cheminée. Cependant, à côté de l'ouverture à chaque étage, des flux bidirectionnels sont notés juste à côté de l'entrée. La grandeur de ce flux circulaire dépend de la vitesse d'entrée du plénum et de la proportion entre la sortie et l'entrée.
- On a vu que parmi les trois cas de localisation d'incendie (en bas, à mi-hauteur et en haut), le risque le plus élevé d'implication se produit lorsque l'incendie est en bas. Quel que soit l'emplacement de l'incendie, le plus grand risque concerne le dernier étage. De plus, selon les résultats de concentration d'hélium (à la fois transitoires et en régime

permanent), les planchers centraux peuvent être les endroits les plus sûrs en ce qui concerne la réception de la fumée du plénum.

- Le profil de vitesse est indépendant de l'amplitude HRR. Cependant, le risque d'incendie peut augmenter considérablement avec les HRR plus élevés.

Globalement, l'étude de la propagation des fumées et du comportement du feu aide les décideurs à définir la meilleure méthode d'extinction ou d'évacuation. A titre d'exemple, pour le pire cas d'incendie qui concerne tous les étages (feu du bas), les étages intermédiaires reçoivent le moins de fumée. De plus, le centre de contrôle, le stockage d'énergie tel que le convertisseur et les emplacements du parc de batteries doivent être considérés autant que possible aux endroits les plus à risque. Ainsi, ils seraient plus accessibles en cas d'incendie et le risque d'explosion diminuerait.

7.2. Limitations and future work

- In this research, for the FDS simulations the simplified constant heat release rate on a surface is employed to define the fire surface on the complex geometry of the BIPV DSF. Therefore, from the beginning of the simulation to the end the HRR remains constant while it can be more realistic to have the heat release rate increases over time with increasing fire area. Moreover, the reaction material is defined as simple chemistry. However, there is the possibility to define the fire surface by introducing the material combustion and considering the related pyrolysis and mass loss rate of actual PV materials. Thus, it is suggested to obtain the internal reaction to fire parameters and pyrolysis, using cone calorimeter test and thermogravimetry analysis (TGA), and the combustion properties of the PV materials could be included in the FDS library to further study the BIPV fire risk in various application scenarios. Also, to analyse in detail the smoke hazards posed to occupants, it is suggested to obtain the combustion chemical effluent data from BIPV materials and use the data in smoke spread simulations in a building.
- In this study the external wind effect is not considered on the internal smoke spread. Therefore, for further consideration, it will be a good idea to add the wind effect and

verify the similarity and scaling method. However, it should be mentioned that to pose the wind effect on the building façade, the model needs to be placed in a wind tunnel which brings more limitations in size and scale. Therefore, the scaling method must be verified to make sure that it still works for smaller models.

- It is well-understood and commonly accepted that one can use the density difference in helium mixture to reproduce the buoyance effect in fire plume. However, it is truer in the open plume condition where there is no significant convection heat loss to boundaries (the only heat loss is by radiation). In DSF construction, the fire plume loses significant amount of energy to cold walls, and therefore reduce the overall buoyancy force, on the other hand, the wall will not change the helium concentration/density and buoyancy. This can result in over estimation of temperatures [139].
- In this series of simulations and experiments, all the internal windows are considered open (to pose the greatest risk to involve every floor connected to the double skin façade). However, to further investigate the mechanism of smoke spread from an ignited BIPV DSF to the indoor environment, it will be informative to consider various scenarios with open/closed internal windows.
- Complementary to this, the experimental scenarios can be varied considering other parameters such as opening size, more fire locations and heat release rates. Despite the governing equations on the helium and smoke similarity is justified in this study, it is essential to reassure that the current theoretical analysis works efficiently for various designs and various locations of fire initiations.

Limites et travaux futurs

- Dans cette recherche, pour les simulations FDS, le taux de dégagement de chaleur constant simplifié sur une surface est utilisé pour définir la surface du feu sur la géométrie complexe du BIPV DSF. Par conséquent, du début à la fin de la simulation, le HRR reste constant alors qu'il peut être plus réaliste d'augmenter le taux de dégagement de chaleur tandis que l'amplitude change avec le temps avec l'augmentation de la zone d'incendie. De plus, le matériau de réaction est défini comme une chimie simple. Cependant, il est possible de définir la surface du feu en introduisant la combustion du matériau et en tenant compte de la pyrolyse associée et du taux de perte

de masse des matériaux PV réels. Ainsi, il est suggéré d'obtenir pour étudier plus avant le risque d'incendie BIPV, il peut être défini comme le nouveau matériau brûlant dans la bibliothèque FDS en obtenant la réaction interne aux paramètres d'incendie et la pyrolyse, en utilisant le test au calorimètre à cône et l'analyse thermogravimétrique (TGA), et les propriétés de combustion des matériaux PV pourraient être incluses dans la bibliothèque FDS pour étudier plus avant le risque d'incendie BIPV dans divers scénarios d'application. De plus, pour analyser en détail les risques de fumée posés aux occupants, il est suggéré d'obtenir les données d'effluents chimiques de combustion des matériaux BIPV et d'utiliser les données dans des simulations de propagation de fumée dans un bâtiment.

- Dans cette étude, l'effet du vent extérieur n'est pas pris en compte sur la propagation de la fumée intérieure. Par conséquent, pour un examen plus approfondi, ce sera une bonne idée d'ajouter l'effet du vent et de vérifier la similarité et la méthode de mise à l'échelle. Cependant, il convient de mentionner que pour poser l'effet du vent sur la façade du bâtiment, le modèle doit être placé dans une soufflerie, ce qui apporte plus de limitations en taille et en échelle. Par conséquent, la méthode de mise à l'échelle doit être vérifiée pour s'assurer qu'elle fonctionne toujours pour les modèles plus petits.
- Il est bien compris et communément admis que l'on peut utiliser la différence de densité dans le mélange d'hélium pour reproduire l'effet de flottabilité dans un panache de feu. Cependant, c'est plus vrai dans la condition de panache ouvert où il n'y a pas de perte de chaleur par convection significative vers les parois (la seule perte de chaleur est par rayonnement). Dans la construction DSF, le panache de feu perd une quantité importante d'énergie au profit des murs froids, et réduit donc la force de flottabilité globale, d'autre part, le mur ne changera pas la concentration/densité d'hélium et la flottabilité. Cela peut entraîner une surestimation des températures [139].
- Dans cette série de simulations et d'expérimentations, toutes les fenêtres intérieures sont considérées ouvertes (pour présenter le plus grand risque d'impliquer tous les étages reliés à la façade double peau). Cependant, pour étudier plus avant le mécanisme de propagation de la fumée d'un DSF BIPV enflammé à l'environnement intérieur, il sera instructif d'envisager divers scénarios avec des fenêtres internes ouvertes/fermées.

- En complément de cela, les scénarios expérimentaux peuvent être variés en tenant compte d'autres paramètres tels que la taille de l'ouverture, plus d'emplacements d'incendie et les taux de dégagement de chaleur. Bien que les équations déterminantes sur l'hélium et la similarité des fumées soient justifiées dans cette étude, il est essentiel de s'assurer que l'analyse théorique actuelle fonctionne efficacement pour différentes conceptions et différents emplacements d'initiation d'incendie.

References

[1] United Nations, Adoption of the Paris agreement - Paris agreement, Paris, 2015. https://www.mendeley.com/catalogue/26b9823e-9e2e-3e85-bc9f-3758f4d89690/?utm_source=desktop&utm_medium=1.19.4&utm_campaign=open_catalog&userDocumentId=%7Bdcdb99c4-a918-391e-8d82-eaa94b011cc2%7D (accessed July 21, 2020).

[2] Government of Canada, Pan-Canadian framework on clean growth and climate change, 2016. https://www.canada.ca/content/dam/themes/environment/documents/weather1/20170113-1-en.pdf (accessed January 15, 2020).

[3] H. Shin, T.H. Kim, H. Kim, S. Lee, W. Kim, Environmental shutdown of coal-fired generators for greenhouse gas reduction: A case study of South Korea, Appl Energy. 252 (2019). https://doi.org/10.1016/j.apenergy.2019.113453.

[4] P. Fragkos, K. Fragkiadakis, L. Paroussos, R. Pierfederici, S.S. Vishwanathan, A.C. Köberle, G. Iyer, C.M. He, K. Oshiro, Coupling national and global models to explore policy impacts of NDCs, Energy Policy. 118 (2018) 462–473. https://doi.org/10.1016/j.enpol.2018.04.002.

[5] Z. Zhang, Decoupling China's carbon emissions increase from economic growth: An economic analysis and policy implications, World Dev. 28 (2000) 739–752. https://doi.org/10.1016/S0305-750X(99)00154-0.

[6] P.A. Owusu, S. Asumadu-Sarkodie, A review of renewable energy sources, sustainability issues and climate change mitigation, Cogent Eng. 3 (2016) 1167990. https://doi.org/10.1080/23311916.2016.1167990.

[7] R. Alley, T. Berntsen, N.L. Bindoff, Z. Chen, A. Chidthaisong, P. Friedlingstein, J. Gregory, G. Hegerl, M. Heimann, B. Hewitson, B. Hoskins, F. Joos, J. Jouzel, V. Kattsov, U. Lohmann, M. Manning, T. Matsuno, M. Molina, N. Nicholls, J. Overpeck, D. Qin, G. Raga, V. Ramaswamy, J. Ren, M. Rusticucci, S. Solomon, R. Somerville, T.F. Stocker, P. Stott, R.J. Stouffer, P. Whetton, R.A. Wood, D. Wratt, J. Arblaster, G. Brasseur, J.H. Christensen, K. Denman, D.W. Fahey, P. Forster, E. Jansen, P.D. Jones, R. Knutti, H. le Treut, P. Lemke, G. Meehl, P. Mote, D. Randall, D.A. Stone, K.E. Trenberth, J. Willebrand, F. Zwiers, Climate change 2007: the

physical science basis. Working group I to the fourth assessment report of the IPCC, 2007. https://previa.uclm.es/area/amf/antoine/energias/Ipcc_anotado.pdf (accessed August 23, 2020).

[8] O. Saadatian, L.C. Haw, K. Sopian, M.Y. Sulaiman, Review of windcatcher technologies, Renewable and Sustainable Energy Reviews. 16 (2012) 1477–1495. https://doi.org/10.1016/J.RSER.2011.11.037.

[9] IEA PVPS, Snapshot of global PV markets 2020, task 1 strategic PV analysis and outreach, 2020. www.iea-pvps.org (accessed July 21, 2020).

[10] Arnulf Jäger-Waldau, Jose Donoso, Izumi Kaizuka, Gaëtan Masson, Elina Bosch, Snapshot of global PV markets 2022, (2022) 1–23. https://iea-pvps.org/snapshot-reports/snapshot-2022/ (accessed June 19, 2022).

[11] IEA PVPS, Snapshot of global PV markets 2021, Www.Iea-Pvps.Org. (2021) 1–16. https://iea-pvps.org/wp-content/uploads/2021/04/IEA_PVPS_Snapshot_2021-V3.pdf (accessed June 19, 2022).

[12] N.M. Haegel, R. Margolis, T. Buonassisi, D. Feldman, A. Froitzheim, R. Garabedian, M. Green, S. Glunz, H.M. Henning, B. Holder, I. Kaizuka, B. Kroposki, K. Matsubara, S. Niki, K. Sakurai, R.A. Schindler, W. Tumas, E.R. Weber, G. Wilson, M. Woodhouse, S. Kurtz, Terawatt-scale photovoltaics: Trajectories and challenges, Science (1979). 356 (2017) 141–143. https://doi.org/10.1126/SCIENCE.AAL1288/SUPPL_FILE/AAL1288_HAEGEL_SM.REVISION2.PDF.

[13] C. Zou, B. Xiong, H. Xue, D. Zheng, Z. Ge, Y. Wang, L. Jiang, S. Pan, S. Wu, The role of new energy in carbon neutral, Petroleum Exploration and Development. 48 (2021) 480–491. https://doi.org/10.1016/S1876-3804(21)60039-3.

[14] St.J. Jeff, Walmart reaches settlement with Tesla in lawsuit over solar panel fires, (2019). https://www.greentechmedia.com/articles/read/walmart-settlement-with-tesla-on-solar-panel-fire (accessed August 23, 2020).

[15] Lora Kolodny, Tesla solar panels caught fire at Amazon warehouse in 2018, CNBC. (2018). https://www.cnbc.com/2019/08/23/tesla-solar-panels-caught-fire-at-amazon-warehouse-in-2018-report.html (accessed September 5, 2022).

[16] Annie Palmer, Lora Kolodny, Amazon took solar rooftops offline last year after fires, explosions, CNBC. (2022). https://www.cnbc.com/2022/09/01/amazon-took-solar-rooftops-offline-last-year-after-fires-explosions.html (accessed September 20, 2022).

[17] E&T editorial staff, Amazon switched off its solar rooftops after fires, Engineering and Technology. (2022). https://eandt.theiet.org/content/articles/2022/09/amazon-switched-off-its-solar-rooftops-after-fires-report-says/ (accessed October 15, 2022).

[18] Maggie Harrison, Amazon secretly shut down all its solar rooftops after they started catching fire, Earth and Energy. (2022). https://futurism.com/the-byte/amazon-shut-down-solar-rooftops-fire (accessed October 15, 2022).

[19] Keith Griffith, Walmart sues Tesla after solar panels burst into flames on top of SEVEN stores | Daily Mail Online, Reuters. (2019). https://www.dailymail.co.uk/news/article-7379707/Walmart-sues-Tesla-solar-panels-burst-flames-eight-stores.html (accessed September 20, 2022).

[20] Emiliano Bellini, Japan's largest floating PV plant catches fire after Typhoon Faxai impact – pv magazine International, (2019). https://www.pv-magazine.com/2019/09/09/japans-largest-floating-pv-plant-catches-fire-after-typhoon-faxai-impact/ (accessed September 20, 2022).

[21] W.V. H. Laukamp, G. Bopp, R. Grab, C. Wittwer, H. Häberlin, B. v. Heeckeren, S. Phillip, F. Reil, H. Schmidt, A. Sepanski, H. Thiem, PV fire hazard - analysis and assessment of fire incidents, in: 28th European Photovoltaic Solar Energy Conference and Exhibition, Paris, France, 2013: pp. 4304–4311. https://doi.org/10.4229/28thEUPVSEC2013-5BV.7.71.

[22] N.A.F. Mohd Nizam Ong, M.A. Sadiq, M.S. Md Said, G. Jomaas, M.Z. Mohd Tohir, J.S. Kristensen, Fault tree analysis of fires on rooftops with photovoltaic systems, Journal of Building Engineering. 46 (2022) 103752. https://doi.org/10.1016/J.JOBE.2021.103752.

[23] Emiliano Bellini, Japan: Floating PV plant catches fire after typhoon, PV Magazine. (2019). https://www.windaction.org/posts/52975 (accessed September 20, 2022).

[24] G. Kinsey, G. Heath, A. Wade, P. Sinha, K. Komoto, Photovoltaics and firefighters' operations: best practices in selected countries, (2017).

[25] R. Birt, Solar panel and ESS fire attack: 6 steps firefighters can employ for safe fireground operations, (2021). https://www.firerescue1.com/electric-fire/articles/6-steps-to-safe-effective-solar-panel-ess-fire-attack-JtqmGDpotCQQrBfP/ (accessed September 20, 2022).

[26] PVSTOP, User manual: PVstop for first responders, electrical technicians PV system owners, PV system operators, (2020).

[27] Jeff Fecteau, Photovoltaic (PV) and fire fighter safety, Underwriters Laboratories. (2017). https://www.lafpa.net/PV%20Firefighter%20Safety.pdf (accessed October 15, 2022).

[28] M. Piantedosi, T. Granato, N. Hausman, Solar photovoltaic (PV) fire safety training, SunShot. (n.d.). www.cesa.org (accessed October 15, 2022).

[29] The Ontario fire service health and safety advisory committee, Guidance for improving health and safety in the fire service, 2011.

[30] P. Sinha, R. Balas, L. Krueger, Fate and transport evaluation of potential leaching and fire risks from CdTe PV, in: Conference Record of the IEEE Photovoltaic Specialists Conference, 2011: pp. 002025–002030. https://doi.org/10.1109/PVSC.2011.6186351.

[31] C.L. Chow, S.S. Han, Studying fire behaviour of photovoltaic panels with a cone calorimeter, in: Fire and Materials 2015 - 14th International Conference and Exhibition, Proceedings, Interscience Communications Ltd, 2015: pp. 53–63.

[32] B. Liao, L. Yang, X. Ju, Y. Peng, Y. Gao, Experimental study on burning and toxicity hazards of a PET laminated photovoltaic panel, Solar Energy Materials and Solar Cells. 206 (2020) 110295. https://doi.org/10.1016/j.solmat.2019.110295.

[33] P.D. Moskowitz, V.M. Fthenakis, Toxic materials released from photovoltaic modules during fires: Health risks, Solar Cells. 29 (1990) 63–71. https://doi.org/10.1016/0379-6787(90)90015-W.

[34] P.D. Moskowitz, V.M. Fthenakis, L.D. Hamilton, J.C. Lee, Public health issues in photovoltaic energy systems: an overview of concerns, Solar Cells. 19 (1987) 287–299. https://doi.org/10.1016/0379-6787(87)90084-6.

[35] J. Camarota, Investigating fires in solar photovoltaic systems, Firehouse. (2016). https://www.firehouse.com/prevention-investigation/article/12216062/fire-investigation-solar-photovoltaic-system-investigation-techniques (accessed June 22, 2020).

[36] S. Pester, Fire and solar PV systems-investigations & evidence, 2017. https://assets.publishing.service.gov.uk/government/uploads/system/uploads/attachment_data/file/630639/fire-solar-pv-systems-investigations-evidence.pdf (accessed January 15, 2020).

[37] C.L. Chow, S.S. Han, X.M. Ni, A study on fire behaviour of combustible components of two commonly used photovoltaic panels, Fire Mater. 41 (2017) 65–83. https://doi.org/10.1002/fam.2366.

[38] M. Aram, X. Zhang, D. Qi, Y. Ko, A state-of-the-art review of fire safety of photovoltaic systems in buildings, J Clean Prod. 308 (2021) 127239. https://doi.org/10.1016/j.jclepro.2021.127239.

[39] D. Clare, Walmart sues Tesla after it says solar panels caught fire on store roofs | CNN Business, CNN Business. (2019). https://www.cnn.com/2019/08/20/energy/walmart-tesla-solar-panels-suit (accessed October 21, 2022).

[40] R. Osborn, A little taste of the big stuff going on in this editor's life, The Journal of Light Construction. (2019). https://www.jlconline.com/how-to/electrical/solar-panel-fire_o (accessed July 21, 2020).

[41] D. Hull, B. Echhouse, More Tesla solar-panel fire incidents emerge in wake of Walmart suit, Renewable Energy World. (2019). https://www.renewableenergyworld.com/2019/08/29/more-tesla-solarpanel-fire-incidents-emerge-in-wake-of-walmart-suit/#gref (accessed July 22, 2020).

[42] Ted Daniel, Solar panels are good for the environment and your wallet, but are they safe, Boston 25 News. (2019). https://www.boston25news.com/news/solar-panels-are-good-for-the-environment-and-your-wallet-but-are-they-safe-/1010015229/ (accessed August 18, 2022).

[43] S. Dubai, PV on buildings and fire safety: recommendation for DRRG solar PV systems, 2015. https://www.dewa.gov.ae/images/smartinitiatives/PV_on_Buildings.pdf (accessed July 21, 2020).

[44] International Code Council, International Fire Code, 2012.

[45] B.E. Mateusz Zimny, Numerical modeling of scaled down fire experiments, (2020).

[46] M. Zimny, Physical modeling of a fire with the use of the Froude number, Budownictwo i Architektura. 18 (2019) 71–80. https://doi.org/10.24358/Bud-Arch_19_181_07.

[47] O. Vauquelin, G. Michaux, C. Lucchesi, Scaling laws for a buoyant release used to simulate fire-induced smoke in laboratory experiments, Fire Saf J. 44 (2009) 665–667. https://doi.org/10.1016/J.FIRESAF.2008.11.001.

[48] J. Lassus, L. Courty, J.P. Garo, E. Studer, P. Jourda, P. Aine, Ventilation effects in confined and mechanically ventilated fires, International Journal of Thermal Sciences. 75 (2014) 87–94. https://doi.org/10.1016/J.IJTHERMALSCI.2013.07.015.

[49] N. Tilley, P. Rauwoens, D. Fauconnier, B. Merci, On the extrapolation of CFD results for smoke and heat control in reduced-scale set-ups to full scale: Atrium configuration, Fire Saf J. 59 (2013) 160–165. https://doi.org/10.1016/J.FIRESAF.2013.04.001.

[50] P.Y. Cui, J.H. Zhang, Y.P. Wu, Y. Zhang, J.Z. Zhou, Y. Luo, Y.D. Huang, Wind-tunnel measurements and LES simulations of air pollutant dispersion caused by fire-induced buoyancy plume inside two parallel street canyons, Process Safety and Environmental Protection. 140 (2020) 151–169. https://doi.org/10.1016/J.PSEP.2020.04.047.

[51] C.H. Su, S.C. Wang, Y.H. Chen, C.Y. Wu, Measurement of smoke generation rate using a full-scale hot smoke test for building smoke exhaust systems, Https://Doi.Org/10.1080/14733315.2020.1853881. 21 (2020) 105–121. https://doi.org/10.1080/14733315.2020.1853881.

[52] C.H. Su, S.C. Wang, S.W. Chien, Y.H. Chen, Performance verification and enhancement of mechanical smoke exhaust system in full-scale hot smoke test for a large space, Indoor and Built Environment. 30 (2021) 129–144. https://doi.org/10.1177/1420326X19890903/ASSET/IMAGES/LARGE/10.1177_1420326X19890903-FIG2.JPEG.

[53] A. Jiao, W. Lin, B. Cai, H. Wang, J. Chen, M. Zhang, J. Xiao, Q. Liu, F. Wang, C. Fan, Full-scale experimental study on thermal smoke movement characteristics in an indoor pedestrian street, Case Studies in Thermal Engineering. 34 (2022) 102029. https://doi.org/10.1016/J.CSITE.2022.102029.

[54] M. de Paepe, J.G. Pieters, W.M. Cornelis, D. Gabriels, B. Merci, P. Demeyer, Airflow measurements in and around scale model cattle barns in a wind tunnel: Effect of ventilation opening height, Biosyst Eng. 113 (2012) 22–32. https://doi.org/10.1016/j.biosystemseng.2012.06.003.

[55] R. Wadhwani, C. Sullivan, A. Wickramasinghe, M. Kyng, N. Khan, K. Moinuddin, A review of firebrand studies on generation and transport, Fire Saf J. (2022) 103674. https://doi.org/10.1016/J.FIRESAF.2022.103674.

[56] G. di Cristina, M.R. Gallagher, N.S. Skowronski, A. Simeoni, A. Rangwala, S. kyun Im, Design and implementation of a portable, large-scale wind tunnel for wildfire research, Fire Saf J. 131 (2022) 103607. https://doi.org/10.1016/J.FIRESAF.2022.103607.

[57] S. Suzuki, S.L. Manzello, Investigating the effect of structure to structure separation distance on firebrand accumulation, Front Mech Eng. 0 (2021) 112. https://doi.org/10.3389/FMECH.2020.628510.

[58] S.L. Manzello, S. Suzuki, The combustion of Noble-Fir trees in the presence of an applied wind field, NIST: Fire Research. (2021).

[59] X. Ju, K. Shiino, T. Matsuoka, T. Yamazaki, Y. Nakamura, Scale model experiments of fire whirls over the non-fuel zone around an L-shaped fire source, Combust Flame. 238 (2022) 111930. https://doi.org/10.1016/J.COMBUSTFLAME.2021.111930.

[60] O. Vauquelin, Experimental simulations of fire-induced smoke control in tunnels using an “air-helium reduced scale model”: Principle, limitations, results and future, Tunnelling and Underground Space Technology. 23 (2008) 171–178. https://doi.org/10.1016/j.tust.2007.04.003.

[61] T. Driant, L. Remaki, S. Moreau, A. Desrochers, H. Fellouah, Aerodynamic study of a tricycle wheel subsystem for drag reduction, American Society of Mechanical Engineers, Fluids Engineering Division (Publication) FEDSM. 1 (2013) 247–252. https://doi.org/10.1115/FEDSM2012-72123.

[62] M. Dghim, K. ben Miloud, M. Ferchichi, H. Fellouah, Meandering of a wing-tip vortex in a grid-generated turbulent flow, Physics of Fluids. 33 (2021) 115131. https://doi.org/10.1063/5.0057083.

[63] T. Driant, Réduction de la traînée aérodynamique d'un tricycle de type roadster, Université de Sherbrooke, 2012. https://doi.org/http://hdl.handle.net/11143/6070.

[64] B.M. Cetegen, T.A. Ahmed, Experiments on the periodic instability of buoyant plumes and pool fires, Combust Flame. 93 (1993) 157–184. https://doi.org/10.1016/0010-2180(93)90090-P.

[65] L. Wang, G. Zhao, Numerical study on smoke movement driven by pure helium in atria, Fire Saf J. 61 (2013) 45–53. https://doi.org/10.1016/j.firesaf.2013.07.006.

[66] G. Zhao, Study of Fire Smoke Filling in Buildings by Helium Smoke Tests, Concordia University, 2012. https://core.ac.uk/download/pdf/11081133.pdf (accessed November 18, 2018).

[67] G. Zhao, L. Wang, Using helium smoke as a surrogate of fire smoke for the study of atrium smoke filling, Original Article Journal of Fire Sciences. 32 (2014) 431–447. https://doi.org/10.1177/0734904114529403.

[68] B. van H. Annett Sepanski, Florian Reil, Willi Vaaßen, Dr. Eckart Janknecht, Uwe Hupach, Dr. Nicolas Bogdanski, Assessing fire risks in photovoltaic systems and developing safety concepts for risk minimization, 2018. www.energy.gov (accessed January 15, 2020).

[69] M.R. Ramali, N.A.F. Mohd Nizam Ong, M.S. Md Said, H. Mohamed Yusoff, M.R. Baharudin, A.F. Tharima, F.W. Akashah, M.Z. Mohd Tohir, A review on safety practices for firefighters during photovoltaic (PV) fire, Fire Technol. (2022) 1–24. https://doi.org/10.1007/S10694-022-01269-4/TABLES/7.

[70] M.D. Vaverková, J. Winkler, D. Uldrijan, P. Ogrodnik, T. Vespalcová, J. Aleksiejuk-Gawron, D. Adamcová, E. Koda, Fire hazard associated with different types of photovoltaic power plants: Effect of vegetation management, Renewable and Sustainable Energy Reviews. 162 (2022) 112491. https://doi.org/10.1016/J.RSER.2022.112491.

[71] S. Srivastava, C.S. Malvi, Solar photovoltaic system and its fire safety in Indian scenario, (2022) 441–455. https://doi.org/10.1007/978-981-19-2572-6_33.

[72] X. Ju, X. Zhou, K. Zhao, Y. Hu, T. Mu, Y. Ni, L. Yang, Experimental study on burning behaviors of photovoltaic panels with different coverings using a cone calorimeter, Journal of Renewable and Sustainable Energy. 9 (2017). https://doi.org/10.1063/1.4990830.

[73] X. Ju, X. Zhou, K. Zhao, F. Peng, L. Yang, Experimental study on fire behaviors of flexible photovoltaic panels using a cone calorimeter, J Fire Sci. 36 (2018) 63–77. https://doi.org/10.1177/0734904117740855.

[74] J.S. Kristensen, G. Jomaas, Experimental study of the fire behaviour on flat roof constructions with multiple photovoltaic (PV) panels, Fire Technol. 54 (2018) 1807–1828. https://doi.org/10.1007/s10694-018-0772-5.

[75] Y. Ko, M. Aram, X. Zhang, D. Qi, Fire safety of building integrated photovoltaic systems: Critical review for codes and standards, Indoor and Built Environment. 0 (2022) 1–19. https://doi.org/10.1177/1420326x211073130.

[76] G. Zhao, M. Li, L. Jian, Z. He, J. Shuang, S. Yuping, Q. Zhang, L. Zhongxian, Analysis of fire risk associated with photovoltaic power generation system, Advances in Civil Engineering. 2018 (2018). https://doi.org/10.1155/2018/2623741.

[77] D. Qi, L. (Leon) Wang, J. Ji, M. Li, Dimensionless analytical solutions for steady-state fire smoke spread through high-rise shaft, Fire Saf J. 93 (2017) 12–20. https://doi.org/10.1016/J.FIRESAF.2017.07.002.

[78] D. Qi, L. Wang, R. Zmeureanu, An analytical model of heat and mass transfer through non-adiabatic high-rise shafts during fires, Int J Heat Mass Transf. 72 (2014) 585–594. https://doi.org/10.1016/J.IJHEATMASSTRANSFER.2014.01.042.

[79] D. Qi, Analytical modeling of fire smoke spread in high-rise buildings, Concordia University, 2016. https://spectrum.library.concordia.ca/981726/ (accessed September 20, 2018).

[80] J.M. Lirola, E. Castañeda, B. Lauret, M. Khayet, A review on experimental research using scale models for buildings: Application and methodologies, Energy Build. 142 (2017) 72–110. https://doi.org/10.1016/j.enbuild.2017.02.060.

[81] G. Astarita, Dimensional analysis, scaling, and orders of magnitude, Chem Eng Sci. 52 (1997) 4681–4698. https://doi.org/10.1016/S0009-2509(97)85420-6.

[82] W.H. Snyder, Similarity criteria for the application of fluid models to the study of air pollution meteorology, Boundary Layer Meteorol. 3 (1972) 113–134. https://doi.org/10.1007/BF00769111.

[83] D. Bolster, R.E. Hershberger, R.J. Donnelly, Dynamic similarity, the dimensionless science, Phys Today. 64 (2011) 42. https://doi.org/10.1063/PT.3.1258.

[84] Z.C. Liu, R.J. Adrian, T.J. Hanratty, Reynolds number similarity of orthogonal decomposition of the outer layer of turbulent wall flow, Physics of Fluids. 6 (1994) 2815–2819. https://doi.org/10.1063/1.868169.

[85] S. Yao, D. Zhang, F. Lu, Dimensionless number for dynamic response analysis of box-shaped structures under internal blast loading, Int J Impact Eng. 98 (2016) 13–18. https://doi.org/10.1016/j.ijimpeng.2016.07.005.

[86] J.K.E. Ortega, Dimensionless numbers for plant biology, Trends Plant Sci. 23 (2018) 6–9. https://doi.org/10.1016/j.tplants.2017.09.020.

[87] Grigorii Isaakovic Barenblatt, Scaling, self-similarity, and intermediate asymptotics: dimensional analysis, 2002. https://books.google.ca/books?hl=en&lr=&id=r-Az53e-MTYC&oi=fnd&pg=PR11&dq=traditional+dimensionless+number+similarity&ots=kyrkp8Z4Cm&sig=Ocft9uu9QZ3U9SUdN8FoYUO1Nmc#v=onepage&q=traditional dimensionless number similarity&f=false (accessed August 23, 2020).

[88] P.Y. Cui, Z. Li, W.Q. Tao, Wind-tunnel measurements for thermal effects on the air flow and pollutant dispersion through different scale urban areas, Build Environ. 97 (2016) 137–151. https://doi.org/10.1016/j.buildenv.2015.12.010.

[89] T. Minehiro, K. Fujita, N. Kawabata, M. Hasegawa, F. Tanaka, Backlayering distance of thermal fumes in tunnel fire experiments using a large-scale model, Journal of Fluid Science and Technology. 7 (2012). https://doi.org/10.1299/jfst.7.389.

[90] H.X. Chen, N.A. Liu, W.K. Chow, Wind tunnel tests on compartment fires with crossflow ventilation, Journal of Wind Engineering and Industrial Aerodynamics. 99 (2011) 1025–1035. https://doi.org/10.1016/j.jweia.2011.07.006.

[91] D. Arini, F. Pancawardani, M.A. Santoso, B. Sugiarto, Y.S. Nugroho, Froude modelling of fire phenomena: observation of fire-induced smoke movement in basement structure for firefighting purpose, Procedia Eng. 170 (2017) 182–188. https://doi.org/10.1016/J.PROENG.2017.03.042.

[92] W. Węgrzyński, P. Antosiewicz, T. Burdzy, M. Zimny, A. Krasuski, Smoke obscuration measurements in reduced-scale fire modelling based on Froude number similarity, Sensors (Switzerland). 19 (2019). https://doi.org/10.3390/s19163628.

[93] W. Chen, J. Liu, F. Li, X. Cao, J. Li, X. Zhu, Q. Chen, Ventilation similarity of an aircraft cabin mockup with a real MD-82 commercial airliner, Build Environ. 111 (2017) 80–90. https://doi.org/10.1016/j.buildenv.2016.10.017.

[94] K. Uehara, S. Murakami, S. Oikawa, S. Wakamatsu, Wind tunnel experiments on how thermal stratification affects flow in and above urban street canyons, Atmos Environ. 34 (2000) 1553–1562. https://doi.org/10.1016/S1352-2310(99)00410-0.

[95] E.L. Maylor, Airplane tests of enhanced emergency smoke venting, 1989. https://apps.dtic.mil/dtic/tr/fulltext/u2/a209188.pdf (accessed July 22, 2020).

[96] T.I. Eklund, Generation of a buoyant plume FAA technical center Atlantic city international airport of artificial smoke for airplane, 1990. https://apps.dtic.mil/dtic/tr/fulltext/u2/a229343.pdf (accessed July 22, 2020).

[97] M.R. Phipps, Y. Jaluria, T. Eklund, Helium-based simulation of smoke spread due to fire in enclosed spaces, Combustion Science and Technology. 128 (1997) 49–72. https://doi.org/10.1080/00102209708935704.

[98] Advisory Circulars, Smoke detection, penetration, and evacuation tests and related flight manual emergency procedures, 1994. https://www.faa.gov/documentLibrary/media/Advisory_Circular/AC_25-9A.pdf (accessed July 22, 2020).

[99] R. Roby, C. Douglas, Use of buoyant gases for the simulation of real fire sources, 2010.

[100] O. Vauquelin, O. Mégret, Smoke extraction experiments in case of fire in a tunnel, Fire Saf J. 37 (2002) 525–533. https://doi.org/10.1016/S0379-7112(02)00014-0.

[101] L. Jiang, M. Creyssels, A. Mos, P. Salizzoni, Critical velocity in ventilated tunnels in the case of fire plumes and densimetric plumes, Fire Saf J. 101 (2018) 53–62. https://doi.org/10.1016/j.firesaf.2018.09.001.

[102] W.K. Chow, S.S. Li, Y. Gao, C.L. Chow, Numerical studies on atrium smoke movement and control with validation by field tests, Build Environ. 44 (2009) 1150–1155. https://doi.org/10.1016/j.buildenv.2008.08.008.

[103] F. Toja-Silva, T. Kono, C. Peralta, O. Lopez-Garcia, J. Chen, A review of computational fluid dynamics (CFD) simulations of the wind flow around buildings for urban wind energy exploitation, Journal of Wind Engineering and Industrial Aerodynamics. 180 (2018) 66–87. https://doi.org/10.1016/j.jweia.2018.07.010.

[104] S. Hussain, P.H. Oosthuizen, Validation of numerical modeling of conditions in an atrium space with a hybrid ventilation system, Build Environ. 52 (2012) 152–161. https://doi.org/10.1016/J.BUILDENV.2011.12.016.

[105] P. Smardz, Validation of Fire Dynamics Simulator (FDS) for forced and natural convection flows, University of Ulster, 2006.

[106] K. Hanjalic, Will RANS survive LES? A view of perspectives, in: Journal of Fluids Engineering, Transactions of the ASME, American Society of Mechanical Engineers Digital Collection, 2005: pp. 831–839. https://doi.org/10.1115/1.2037084.

[107] W. Binbin, Comparative research on FLUENT and FDS's numerical simulation of smoke spread in subway platform fire, Procedia Eng. 26 (2011) 1065–1075. https://doi.org/10.1016/j.proeng.2011.11.2275.

[108] N. Luo, A. Li, R. Gao, Z. Tian, W. Zhang, S. Mei, L. Feng, P. Ma, An experiment and simulation of smoke confinement and exhaust efficiency utilizing a modified Opposite Double-Jet Air Curtain, Saf Sci. 55 (2013) 17–25. https://doi.org/10.1016/j.ssci.2012.12.002.

[109] M. Zimny, P. Antosiewicz, G. Krajewski, T. Burdzy, A. Krasuski, W. Węgrzyński, Several problems with Froude-number based scale modeling of fires in small compartments, Energies (Basel). 12 (2019) 3625. https://doi.org/10.3390/en12193625.

[110] S. Brohez, I. Caravita, Fire induced pressure in airtight houses: Experiments and FDS validation, Fire Saf J. 114 (2020) 103008. https://doi.org/10.1016/j.firesaf.2020.103008.

[111] J. Alos-Moya, I. Paya-Zaforteza, A. Hospitaler, E. Loma-Ossorio, Valencia bridge fire tests: Validation of simplified and advanced numerical approaches to model bridge fire scenarios,

Advances in Engineering Software. 128 (2019) 55–68. https://doi.org/10.1016/J.ADVENGSOFT.2018.11.003.

[112] A. Acred, G.R. Hunt, A simplified mathematical approach for modelling stack ventilation in multi-compartment buildings, Build Environ. 71 (2014) 121–130. https://doi.org/10.1016/j.buildenv.2013.09.004.

[113] T. Driant, H. Fellouah, S. Moreau, A. Desrochers, L. Remaki, Numerical simulation and wind tunnel measurements on a tricycle wheel sub-system, International Journal of Engineering Systems Modelling and Simulation. 5 (2013) 159–167. https://doi.org/10.1504/IJESMS.2013.052376.

[114] Z. Zhao, F. Tang, Q. Wang, Z. Qin, Experimental study on the characteristics of fire smoke longitudinal crossflow in adjacent tunnels, Tunnelling and Underground Space Technology. 114 (2021) 103992. https://doi.org/10.1016/J.TUST.2021.103992.

[115] H.W. Tieleman, Wind tunnel simulation of wind loading on low-rise structures: a review, Journal of Wind Engineering and Industrial Aerodynamics. 91 (2003) 1627–1649. https://doi.org/10.1016/J.JWEIA.2003.09.021.

[116] F. Ren, L. Hu, X. Sun, K. Hu, An experimental study on vertical temperature profile of facade fire plume ejected from compartment with an opening subjected to external wind normal to facade, International Journal of Thermal Sciences. 130 (2018) 94–99. https://doi.org/10.1016/J.IJTHERMALSCI.2018.04.008.

[117] M. Noguchi, A. Athienitis, J. Ayoub, B. Berneche, Net zero energy homes of the future: A case study of the ÉcoTerra house in Canada, in: Renewable Energy Congress, Glasgow, Scotland, 2008. https://www.nrcan.gc.ca/sites/www.nrcan.gc.ca/files/canmetenergy/files/pubs/2008-112_OP-J_411-PVTZEH_EcoTerra.pdf.

[118] J. Patel, What is the size of a solar panel & weight of a solar panel, (2020). https://letsavelectricity.com/what-is-the-size-of-a-solar-panel-weight-of-a-solar-panel/ (accessed March 10, 2022).

[119] ECCC, Environment and climate change Canada historical climate Data (1981-2010), (2022). https://climate.weather.gc.ca/index_e.html (accessed July 6, 2022).

[120] C. Zhang, S. Yang, C. Shu, L. (Leon) Wang, T. Stathopoulos, Wind pressure coefficients for buildings with air curtains, Journal of Wind Engineering and Industrial Aerodynamics. 205 (2020) 104265. https://doi.org/10.1016/J.JWEIA.2020.104265.

[121] X. Ju, X. Zhou, F. Peng, Z. Wu, D. Lai, Y. Hu, L. Yang, Correlation analysis of heat flux and fire behaviour and hazards of polycrystalline silicon photovoltaic panels, IOP Conf Ser Mater Sci Eng. 201 (2017). https://doi.org/10.1088/1757-899X/201/1/012036.

[122] S.A. Hasnain, M.S. Nasif, W. Pao, R. Al-Waked, Numerical investigation of smoke contamination in atrium upper balconies at different down stand depths Article History, Build Simul. 10 (2017) 365–381. https://doi.org/10.1007/s12273-016-0333-0.

[123] N. Cai, W.-K. Chow, Numerical studies on heat release rate in a room fire burning wood and liquid fuel Article History, Build Simul. 7 (2014) 511–524. https://doi.org/10.1007/s12273-014-0177-4.

[124] Emma, How to calculate stairs - our easy 101 guide, (2016). https://www.firstinarchitecture.co.uk/how-to-calculate-stairs/ (accessed March 10, 2022).

[125] C.H. Hu, F. Wang, Using a CFD approach for the study of street-level winds in a built-up area, Build Environ. 40 (2005) 617–631. https://doi.org/10.1016/j.buildenv.2004.08.016.

[126] X. Zhang, M. Aram, D. Qi, L.L. Wang, Numerical simulations of smoke spread during solar roof fires, Build Simul. (2021) 1–10. https://doi.org/10.1007/S12273-021-0819-2.

[127] B.P.P. Barbosa, N. de C.L. Brum, Validation and assessment of the CFD-0 module of CONTAM software for airborne contaminant transport simulation in laboratory and hospital applications, Build Environ. 142 (2018) 139–152. https://doi.org/10.1016/j.buildenv.2018.06.013.

[128] R. Wei, S. Huang, R. Sun, X. Liu, Y. He, R. Yuen, J. Wang, Characteristics of steady burning over inclined polymethyl methacrylate surface in different pressure environments, J Therm Anal Calorim. 140 (2020) 637–644. https://doi.org/10.1007/s10973-019-08889-z.

[129] H. Sha, D. Qi, Investigation of mechanical ventilation for cooling in high-rise buildings, Energy Build. 228 (2020) 110440. https://doi.org/10.1016/J.ENBUILD.2020.110440.

[130] C. Shu, L. Wang, M. Mortezazadeh, Dimensional analysis of Reynolds independence and regional critical Reynolds numbers for urban aerodynamics, (2020). https://doi.org/10.1016/j.jweia.2020.104232.

[131] Y. Tominaga, S. ichi Akabayashi, T. Kitahara, Y. Arinami, Air flow around isolated gable-roof buildings with different roof pitches: Wind tunnel experiments and CFD simulations, Build Environ. 84 (2015) 204–213. https://doi.org/10.1016/j.buildenv.2014.11.012.

[132] U. Laboratories, New demonstration video shows you only have 3 minutes to escape a home fire, (2020). https://ul.org/new-demonstration-video-shows-you-only-have-three-minutes-escape-home-fire (accessed September 5, 2022).

[133] L.H. Hu, R. Huo, D. Yang, Large eddy simulation of fire-induced buoyancy driven plume dispersion in an urban street canyon under perpendicular wind flow, J Hazard Mater. 166 (2009) 394–406. https://doi.org/10.1016/j.jhazmat.2008.11.105.

[134] C.H. Liu, M.C. Barth, D.Y.C. Leung, Large-eddy simulation of flow and pollutant transport in street canyons of different building-height-to-street-width ratios, Journal of Applied Meteorology. 43 (2004) 1410–1424. https://doi.org/10.1175/JAM2143.1.

[135] Y.W. Zhang, Z.L. Gu, Y. Cheng, S.C. Lee, Effect of real-time boundary wind conditions on the air flow and pollutant dispersion in an urban street canyon-Large eddy simulations, Atmos Environ. 45 (2011) 3352–3359. https://doi.org/10.1016/j.atmosenv.2011.03.055.

[136] D.J. Wessel, D. E.Claridge, F.H. Kohloss, B.A. Rock, T.D. Underwood, M.W. Woodford, ASHRAE HVAC fundamentals handbook, ASHRAE, 2001. https://sovathrothsama.files.wordpress.com/2016/03/ashrae-hvac-2001-fundamentals-handbook.pdf (accessed July 5, 2020).

[137] A. Roy, A. Ghosh, S. Bhandari, S. Sundaram, T.K. Mallick, Realization of poly(methyl methacrylate)-encapsulated solution-processed carbon-based solar cells: an emerging candidate for buildings' comfort, Ind Eng Chem Res. 59 (2020) 11063–11071. https://doi.org/10.1021/acs.iecr.9b06902.

[138] M. Taguchi, A. Suzuki, N. Ueoka, T. Oku, Effects of poly(methyl methacrylate) addition to perovskite photovoltaic devices, 2067 (2019) 20018. https://doi.org/10.1063/1.5089451.

[139] Rinne Tuomo, Hietaniemi Jukka, Hostikka Simo, Experimental validation of the FDS simulations of smoke and toxic gas concentrations, VTT Technical Research Centre of Finland, 2007. http://www.vtt.fi/publications/index.jsp (accessed May 28, 2021).

[140] Hurley MJ, SFPE handbook of fire protection engineering, 3rd edition, Springer, 2015. https://books.google.ca/books?hl=en&lr=&id=xP2zCgAAQBAJ&oi=fnd&pg=PR2&dq=SFPE+3rd+edition&ots=10YlA0KDUt&sig=5YM1FwcoFvEOD2lBgBQwTR9O-BA#v=onepage&q=SFPE 3rd edition&f=false (accessed April 12, 2021).

[141] Y. Takano, P. Moonen, On the influence of roof shape on flow and dispersion in an urban street canyon, Journal of Wind Engineering and Industrial Aerodynamics. 123 (2013) 107–120. https://doi.org/10.1016/j.jweia.2013.10.006.

[142] M. Tsuchiya, S. Murakami, A. Mochida, K. Kondo, Y. Ishida, Development of a new k-ε model for flow and pressure fields around bluff body, Journal of Wind Engineering and Industrial Aerodynamics. 67–68 (1997) 169–182. https://doi.org/10.1016/S0167-6105(97)00071-8.

[143] M.Z. Jacobson, V. Jadhav, World estimates of PV optimal tilt angles and ratios of sunlight incident upon tilted and tracked PV panels relative to horizontal panels, (2018). https://doi.org/10.1016/j.solener.2018.04.030.

Appendix A (FDS input code for case 2 with helium in small-scale)

SSH319case1stat.fds

Generated by PyroSim - Version 2021.2.0512

12-Aug-2022 12:29:48 PM

```
&HEAD CHID='SSH319case1stat'/
&TIME T_END=180.0/
&DUMP DT_RESTART=300.0, DT_SL3D=0.25/
&RADI RADIATION=.FALSE./

&MESH ID='Meshnew-a-a-a', IJK=86,12,24, XB=0.24,0.67,-1.86,-1.8,0.6,0.72/
&MESH ID='Meshnew-a-a-b', IJK=90,12,24, XB=0.67,1.12,-1.86,-1.8,0.6,0.72/
&MESH ID='Meshnew-a-b-a', IJK=86,12,24, XB=0.24,0.67,-1.86,-1.8,0.72,0.84/
&MESH ID='Meshnew-a-b-b', IJK=90,12,24, XB=0.67,1.12,-1.86,-1.8,0.72,0.84/
&MESH ID='Meshnew-a-c-a', IJK=86,12,20, XB=0.24,0.67,-1.86,-1.8,0.84,0.94/
&MESH ID='Meshnew-a-c-b', IJK=90,12,20, XB=0.67,1.12,-1.86,-1.8,0.84,0.94/
&MESH ID='Meshnew-a-d-a', IJK=86,12,24, XB=0.24,0.67,-1.86,-1.8,0.94,1.06/
&MESH ID='Meshnew-a-d-b', IJK=90,12,24, XB=0.67,1.12,-1.86,-1.8,0.94,1.06/
&MESH ID='Meshnew-a-e-a', IJK=86,12,20, XB=0.24,0.67,-1.86,-1.8,1.06,1.16/
&MESH ID='Meshnew-a-e-b', IJK=90,12,20, XB=0.67,1.12,-1.86,-1.8,1.06,1.16/
&MESH ID='Meshnew-a-f-a', IJK=86,12,24, XB=0.24,0.67,-1.86,-1.8,1.16,1.28/
&MESH ID='Meshnew-a-f-b', IJK=90,12,24, XB=0.67,1.12,-1.86,-1.8,1.16,1.28/
&MESH ID='Meshnew-a-g-a', IJK=86,12,24, XB=0.24,0.67,-1.86,-1.8,1.28,1.4/
&MESH ID='Meshnew-a-g-b', IJK=90,12,24, XB=0.67,1.12,-1.86,-1.8,1.28,1.4/
&MESH ID='Meshnew-a-h', IJK=176,12,20, XB=0.24,1.12,-1.86,-1.8,1.4,1.5/
&MESH ID='Meshnew-a-i-a', IJK=45,96,12, XB=0.24,0.69,-1.8,-0.84,0.6,0.72/
&MESH ID='Meshnew-a-i-b', IJK=43,96,12, XB=0.69,1.12,-1.8,-0.84,0.6,0.72/
&MESH ID='Meshnew-a-j-a', IJK=45,96,12, XB=0.24,0.69,-1.8,-0.84,0.72,0.84/
&MESH ID='Meshnew-a-j-b', IJK=43,96,12, XB=0.69,1.12,-1.8,-0.84,0.72,0.84/
&MESH ID='Meshnew-a-k-a', IJK=45,96,10, XB=0.24,0.69,-1.8,-0.84,0.84,0.94/
&MESH ID='Meshnew-a-k-b', IJK=43,96,10, XB=0.69,1.12,-1.8,-0.84,0.84,0.94/
&MESH ID='Meshnew-a-l-a', IJK=45,96,12, XB=0.24,0.69,-1.8,-0.84,0.94,1.06/
&MESH ID='Meshnew-a-l-b', IJK=43,96,12, XB=0.69,1.12,-1.8,-0.84,0.94,1.06/
```

```
&MESH ID='Meshnew-a-m-a', IJK=45,96,10, XB=0.24,0.69,-1.8,-0.84,1.06,1.16/
&MESH ID='Meshnew-a-m-b', IJK=43,96,10, XB=0.69,1.12,-1.8,-0.84,1.06,1.16/
&MESH ID='Meshnew-a-n-a', IJK=45,96,12, XB=0.24,0.69,-1.8,-0.84,1.16,1.28/
&MESH ID='Meshnew-a-n-b', IJK=43,96,12, XB=0.69,1.12,-1.8,-0.84,1.16,1.28/
&MESH ID='Meshnew-a-o-a', IJK=45,96,12, XB=0.24,0.69,-1.8,-0.84,1.28,1.4/
&MESH ID='Meshnew-a-o-b', IJK=43,96,12, XB=0.69,1.12,-1.8,-0.84,1.28,1.4/
&MESH ID='Meshnew-a-p-a', IJK=45,96,10, XB=0.24,0.69,-1.8,-0.84,1.4,1.5/
&MESH ID='Meshnew-a-p-b', IJK=43,96,10, XB=0.69,1.12,-1.8,-0.84,1.4,1.5/
&MESH ID='Meshnew-b-a-a', IJK=44,102,11, XB=0.24,0.68,-1.86,-0.84,1.5,1.61/
&MESH ID='Meshnew-b-a-b', IJK=44,102,11, XB=0.24,0.68,-1.86,-0.84,1.61,1.72/
&MESH ID='Meshnew-b-b-a', IJK=44,102,11, XB=0.68,1.12,-1.86,-0.84,1.5,1.61/
&MESH ID='Meshnew-b-b-b', IJK=44,102,11, XB=0.68,1.12,-1.86,-0.84,1.61,1.72/
&MESH ID='Meshnew-c-a', IJK=23,51,14, XB=0.24,0.7,-1.86,-0.84,1.72,2.0/
&MESH ID='Meshnew-c-b', IJK=21,51,14, XB=0.7,1.12,-1.86,-0.84,1.72,2.0/
&MESH ID='Meshnew-d-a-a', IJK=88,26,24, XB=0.24,1.12,-0.84,-0.58,0.6,0.84/
&MESH ID='Meshnew-d-a-b', IJK=88,26,22, XB=0.24,1.12,-0.84,-0.58,0.84,1.06/
&MESH ID='Meshnew-d-b-a', IJK=88,26,22, XB=0.24,1.12,-0.84,-0.58,1.06,1.28/
&MESH ID='Meshnew-d-b-b', IJK=88,26,22, XB=0.24,1.12,-0.84,-0.58,1.28,1.5/
&MESH ID='Meshnew-e', IJK=88,26,22, XB=0.24,1.12,-0.84,-0.58,1.5,1.72/
&MESH ID='Meshnew-f', IJK=44,13,14, XB=0.24,1.12,-0.84,-0.58,1.72,2.0/
&MESH ID='Meshnew-g-a-a', IJK=44,15,12, XB=0.24,1.12,-0.58,-0.28,0.6,0.84/
&MESH ID='Meshnew-g-a-b', IJK=44,15,11, XB=0.24,1.12,-0.58,-0.28,0.84,1.06/
&MESH ID='Meshnew-g-b', IJK=44,15,22, XB=0.24,1.12,-0.58,-0.28,1.06,1.5/
&MESH ID='Meshnew-h-merged-a', IJK=44,15,11, XB=0.24,1.12,-0.58,-0.28,1.5,1.72/
&MESH ID='Meshnew-h-merged-b', IJK=44,15,14, XB=0.24,1.12,-0.58,-0.28,1.72,2.0/

&SPEC ID='HELIUM'/

&REAC ID='PMMA',
    FYI='SFPE Handbook, 3rd Edition',
    FUEL='REAC_FUEL',
    C=1.0,
    H=1.6,
    O=0.4,
    CO_YIELD=0.01,
    SOOT_YIELD=0.022,
    RADIATIVE_FRACTION=0.35/
```

&DEVC ID='GAS-L1-L1', QUANTITY='VOLUME FRACTION', SPEC_ID='HELIUM', XYZ=0.353096,-1.742573,0.657301/

&DEVC ID='GAS-L2-L1', QUANTITY='VOLUME FRACTION', SPEC_ID='HELIUM', XYZ=0.353096,-1.742573,0.770001/

&DEVC ID='GAS-L3-L1', QUANTITY='VOLUME FRACTION', SPEC_ID='HELIUM', XYZ=0.353096,-1.742573,0.882701/

&DEVC ID='GAS-L4-L1', QUANTITY='VOLUME FRACTION', SPEC_ID='HELIUM', XYZ=0.353096,-1.742573,0.995401/

&DEVC ID='GAS-L5-L1', QUANTITY='VOLUME FRACTION', SPEC_ID='HELIUM', XYZ=0.353096,-1.742573,1.108101/

&DEVC ID='GAS-L6-L1', QUANTITY='VOLUME FRACTION', SPEC_ID='HELIUM', XYZ=0.353096,-1.742573,1.220801/

&DEVC ID='GAS-L7-L1', QUANTITY='VOLUME FRACTION', SPEC_ID='HELIUM', XYZ=0.353096,-1.742573,1.333501/

&DEVC ID='GAS-L1-L2', QUANTITY='VOLUME FRACTION', SPEC_ID='HELIUM', XYZ=0.353096,-1.592573,0.657301/

&DEVC ID='GAS-L2-L2', QUANTITY='VOLUME FRACTION', SPEC_ID='HELIUM', XYZ=0.353096,-1.592573,0.770001/

&DEVC ID='GAS-L3-L2', QUANTITY='VOLUME FRACTION', SPEC_ID='HELIUM', XYZ=0.353096,-1.592573,0.882701/

&DEVC ID='GAS-L4-L2', QUANTITY='VOLUME FRACTION', SPEC_ID='HELIUM', XYZ=0.353096,-1.592573,0.995401/

&DEVC ID='GAS-L5-L2', QUANTITY='VOLUME FRACTION', SPEC_ID='HELIUM', XYZ=0.353096,-1.592573,1.108101/

&DEVC ID='GAS-L6-L2', QUANTITY='VOLUME FRACTION', SPEC_ID='HELIUM', XYZ=0.353096,-1.592573,1.220801/

&DEVC ID='GAS-L7-L2', QUANTITY='VOLUME FRACTION', SPEC_ID='HELIUM', XYZ=0.353096,-1.592573,1.333501/

&DEVC ID='GAS-L1-L3', QUANTITY='VOLUME FRACTION', SPEC_ID='HELIUM', XYZ=0.353096,-1.392573,0.657301/

&DEVC ID='GAS-L2-L3', QUANTITY='VOLUME FRACTION', SPEC_ID='HELIUM', XYZ=0.353096,-1.392573,0.770001/

&DEVC ID='GAS-L3-L3', QUANTITY='VOLUME FRACTION', SPEC_ID='HELIUM', XYZ=0.353096,-1.392573,0.882701/

&DEVC ID='GAS-L4-L3', QUANTITY='VOLUME FRACTION', SPEC_ID='HELIUM', XYZ=0.353096,-1.392573,0.995401/

&DEVC ID='GAS-L5-L3', QUANTITY='VOLUME FRACTION', SPEC_ID='HELIUM', XYZ=0.353096,-1.392573,1.108101/

&DEVC ID='GAS-L6-L3', QUANTITY='VOLUME FRACTION', SPEC_ID='HELIUM', XYZ=0.353096,-1.392573,1.220801/

&DEVC ID='GAS-L7-L3', QUANTITY='VOLUME FRACTION', SPEC_ID='HELIUM', XYZ=0.353096,-1.392573,1.333501/

&DEVC ID='GAS-L1-L4', QUANTITY='VOLUME FRACTION', SPEC_ID='HELIUM', XYZ=0.353096,-1.192573,0.657301/

&DEVC ID='GAS-L2-L4', QUANTITY='VOLUME FRACTION', SPEC_ID='HELIUM', XYZ=0.353096,-1.192573,0.770001/

&DEVC ID='GAS-L3-L4', QUANTITY='VOLUME FRACTION', SPEC_ID='HELIUM', XYZ=0.353096,-1.192573,0.882701/

&DEVC ID='GAS-L4-L4', QUANTITY='VOLUME FRACTION', SPEC_ID='HELIUM', XYZ=0.353096,-1.192573,0.995401/

&DEVC ID='GAS-L5-L4', QUANTITY='VOLUME FRACTION', SPEC_ID='HELIUM', XYZ=0.353096,-1.192573,1.108101/

&DEVC ID='GAS-L6-L4', QUANTITY='VOLUME FRACTION', SPEC_ID='HELIUM', XYZ=0.353096,-1.192573,1.220801/

&DEVC ID='GAS-L7-L4', QUANTITY='VOLUME FRACTION', SPEC_ID='HELIUM', XYZ=0.353096,-1.192573,1.333501/

&DEVC ID='GAS-L1-L5', QUANTITY='VOLUME FRACTION', SPEC_ID='HELIUM', XYZ=0.353096,-0.992573,0.657301/

&DEVC ID='GAS-L2-L5', QUANTITY='VOLUME FRACTION', SPEC_ID='HELIUM', XYZ=0.353096,-0.992573,0.770001/

&DEVC ID='GAS-L3-L5', QUANTITY='VOLUME FRACTION', SPEC_ID='HELIUM', XYZ=0.353096,-0.992573,0.882701/

&DEVC ID='GAS-L4-L5', QUANTITY='VOLUME FRACTION', SPEC_ID='HELIUM', XYZ=0.353096,-0.992573,0.995401/

&DEVC ID='GAS-L5-L5', QUANTITY='VOLUME FRACTION', SPEC_ID='HELIUM', XYZ=0.353096,-0.992573,1.108101/

&DEVC ID='GAS-L6-L5', QUANTITY='VOLUME FRACTION', SPEC_ID='HELIUM', XYZ=0.353096,-0.992573,1.220801/

&DEVC ID='GAS-L7-L5', QUANTITY='VOLUME FRACTION', SPEC_ID='HELIUM', XYZ=0.353096,-0.992573,1.333501/

&DEVC ID='GAS-L1-M1', QUANTITY='VOLUME FRACTION', SPEC_ID='HELIUM', XYZ=0.673096,-1.742573,0.657301/

&DEVC ID='GAS-L2-M1', QUANTITY='VOLUME FRACTION', SPEC_ID='HELIUM', XYZ=0.673096,-1.742573,0.770001/

&DEVC ID='GAS-L3-M1', QUANTITY='VOLUME FRACTION', SPEC_ID='HELIUM', XYZ=0.673096,-1.742573,0.882701/

&DEVC ID='GAS-L4-M1', QUANTITY='VOLUME FRACTION', SPEC_ID='HELIUM', XYZ=0.673096,-1.742573,0.995401/

&DEVC ID='GAS-L5-M1', QUANTITY='VOLUME FRACTION', SPEC_ID='HELIUM', XYZ=0.673096,-1.742573,1.108101/

&DEVC ID='GAS-L6-M1', QUANTITY='VOLUME FRACTION', SPEC_ID='HELIUM', XYZ=0.673096,-1.742573,1.220801/

&DEVC ID='GAS-L7-M1', QUANTITY='VOLUME FRACTION', SPEC_ID='HELIUM', XYZ=0.673096,-1.742573,1.333501/

&DEVC ID='GAS-L1-M2', QUANTITY='VOLUME FRACTION', SPEC_ID='HELIUM', XYZ=0.673096,-1.592573,0.657301/

&DEVC ID='GAS-L2-M2', QUANTITY='VOLUME FRACTION', SPEC_ID='HELIUM', XYZ=0.673096,-1.592573,0.770001/

&DEVC ID='GAS-L3-M2', QUANTITY='VOLUME FRACTION', SPEC_ID='HELIUM', XYZ=0.673096,-1.592573,0.882701/

&DEVC ID='GAS-L4-M2', QUANTITY='VOLUME FRACTION', SPEC_ID='HELIUM', XYZ=0.673096,-1.592573,0.995401/

&DEVC ID='GAS-L5-M2', QUANTITY='VOLUME FRACTION', SPEC_ID='HELIUM', XYZ=0.673096,-1.592573,1.108101/

&DEVC ID='GAS-L6-M2', QUANTITY='VOLUME FRACTION', SPEC_ID='HELIUM', XYZ=0.673096,-1.592573,1.220801/

&DEVC ID='GAS-L7-M2', QUANTITY='VOLUME FRACTION', SPEC_ID='HELIUM', XYZ=0.673096,-1.592573,1.333501/

&DEVC ID='GAS-L1-M3', QUANTITY='VOLUME FRACTION', SPEC_ID='HELIUM', XYZ=0.673096,-1.392573,0.657301/

&DEVC ID='GAS-L2-M3', QUANTITY='VOLUME FRACTION', SPEC_ID='HELIUM', XYZ=0.673096,-1.392573,0.770001/

&DEVC ID='GAS-L3-M3', QUANTITY='VOLUME FRACTION', SPEC_ID='HELIUM', XYZ=0.673096,-1.392573,0.882701/

&DEVC ID='GAS-L4-M3', QUANTITY='VOLUME FRACTION', SPEC_ID='HELIUM', XYZ=0.673096,-1.392573,0.995401/

&DEVC ID='GAS-L5-M3', QUANTITY='VOLUME FRACTION', SPEC_ID='HELIUM', XYZ=0.673096,-1.392573,1.108101/

&DEVC ID='GAS-L6-M3', QUANTITY='VOLUME FRACTION', SPEC_ID='HELIUM', XYZ=0.673096,-1.392573,1.220801/

&DEVC ID='GAS-L7-M3', QUANTITY='VOLUME FRACTION', SPEC_ID='HELIUM', XYZ=0.673096,-1.392573,1.333501/

&DEVC ID='GAS-L1-M4', QUANTITY='VOLUME FRACTION', SPEC_ID='HELIUM', XYZ=0.673096,-1.192573,0.657301/

&DEVC ID='GAS-L2-M4', QUANTITY='VOLUME FRACTION', SPEC_ID='HELIUM', XYZ=0.673096,-1.192573,0.770001/

&DEVC ID='GAS-L3-M4', QUANTITY='VOLUME FRACTION', SPEC_ID='HELIUM', XYZ=0.673096,-1.192573,0.882701/

&DEVC ID='GAS-L4-M4', QUANTITY='VOLUME FRACTION', SPEC_ID='HELIUM', XYZ=0.673096,-1.192573,0.995401/

&DEVC ID='GAS-L5-M4', QUANTITY='VOLUME FRACTION', SPEC_ID='HELIUM', XYZ=0.673096,-1.192573,1.108101/

&DEVC ID='GAS-L6-M4', QUANTITY='VOLUME FRACTION', SPEC_ID='HELIUM', XYZ=0.673096,-1.192573,1.220801/

&DEVC ID='GAS-L7-M4', QUANTITY='VOLUME FRACTION', SPEC_ID='HELIUM', XYZ=0.673096,-1.192573,1.333501/

&DEVC ID='GAS-L1-M5', QUANTITY='VOLUME FRACTION', SPEC_ID='HELIUM', XYZ=0.673096,-0.992573,0.657301/

&DEVC ID='GAS-L2-M5', QUANTITY='VOLUME FRACTION', SPEC_ID='HELIUM', XYZ=0.673096,-0.992573,0.770001/

&DEVC ID='GAS-L3-M5', QUANTITY='VOLUME FRACTION', SPEC_ID='HELIUM', XYZ=0.673096,-0.992573,0.882701/

&DEVC ID='GAS-L4-M5', QUANTITY='VOLUME FRACTION', SPEC_ID='HELIUM', XYZ=0.673096,-0.992573,0.995401/

&DEVC ID='GAS-L5-M5', QUANTITY='VOLUME FRACTION', SPEC_ID='HELIUM', XYZ=0.673096,-0.992573,1.108101/

&DEVC ID='GAS-L6-M5', QUANTITY='VOLUME FRACTION', SPEC_ID='HELIUM', XYZ=0.673096,-0.992573,1.220801/

&DEVC ID='GAS-L7-M5', QUANTITY='VOLUME FRACTION', SPEC_ID='HELIUM', XYZ=0.673096,-0.992573,1.333501/

&DEVC ID='GAS-L1-R1', QUANTITY='VOLUME FRACTION', SPEC_ID='HELIUM', XYZ=0.993096,-1.742573,0.657301/

&DEVC ID='GAS-L2-R1', QUANTITY='VOLUME FRACTION', SPEC_ID='HELIUM', XYZ=0.993096,-1.742573,0.770001/

&DEVC ID='GAS-L3-R1', QUANTITY='VOLUME FRACTION', SPEC_ID='HELIUM', XYZ=0.993096,-1.742573,0.882701/

&DEVC ID='GAS-L4-R1', QUANTITY='VOLUME FRACTION', SPEC_ID='HELIUM', XYZ=0.993096,-1.742573,0.995401/

&DEVC ID='GAS-L5-R1', QUANTITY='VOLUME FRACTION', SPEC_ID='HELIUM', XYZ=0.993096,-1.742573,1.108101/

&DEVC ID='GAS-L6-R1', QUANTITY='VOLUME FRACTION', SPEC_ID='HELIUM', XYZ=0.993096,-1.742573,1.220801/

&DEVC ID='GAS-L7-R1', QUANTITY='VOLUME FRACTION', SPEC_ID='HELIUM', XYZ=0.993096,-1.742573,1.333501/

&DEVC ID='GAS-L1-R2', QUANTITY='VOLUME FRACTION', SPEC_ID='HELIUM', XYZ=0.993096,-1.592573,0.657301/

&DEVC ID='GAS-L2-R2', QUANTITY='VOLUME FRACTION', SPEC_ID='HELIUM', XYZ=0.993096,-1.592573,0.770001/

&DEVC ID='GAS-L3-R2', QUANTITY='VOLUME FRACTION', SPEC_ID='HELIUM', XYZ=0.993096,-1.592573,0.882701/

&DEVC ID='GAS-L4-R2', QUANTITY='VOLUME FRACTION', SPEC_ID='HELIUM', XYZ=0.993096,-1.592573,0.995401/

&DEVC ID='GAS-L5-R2', QUANTITY='VOLUME FRACTION', SPEC_ID='HELIUM', XYZ=0.993096,-1.592573,1.108101/

&DEVC ID='GAS-L6-R2', QUANTITY='VOLUME FRACTION', SPEC_ID='HELIUM', XYZ=0.993096,-1.592573,1.220801/

&DEVC ID='GAS-L7-R2', QUANTITY='VOLUME FRACTION', SPEC_ID='HELIUM', XYZ=0.993096,-1.592573,1.333501/

&DEVC ID='GAS-L1-R3', QUANTITY='VOLUME FRACTION', SPEC_ID='HELIUM', XYZ=0.993096,-1.392573,0.657301/

&DEVC ID='GAS-L2-R3', QUANTITY='VOLUME FRACTION', SPEC_ID='HELIUM', XYZ=0.993096,-1.392573,0.770001/

&DEVC ID='GAS-L3-R3', QUANTITY='VOLUME FRACTION', SPEC_ID='HELIUM', XYZ=0.993096,-1.392573,0.882701/

&DEVC ID='GAS-L4-R3', QUANTITY='VOLUME FRACTION', SPEC_ID='HELIUM', XYZ=0.993096,-1.392573,0.995401/

&DEVC ID='GAS-L5-R3', QUANTITY='VOLUME FRACTION', SPEC_ID='HELIUM', XYZ=0.993096,-1.392573,1.108101/

&DEVC ID='GAS-L6-R3', QUANTITY='VOLUME FRACTION', SPEC_ID='HELIUM', XYZ=0.993096,-1.392573,1.220801/

&DEVC ID='GAS-L7-R3', QUANTITY='VOLUME FRACTION', SPEC_ID='HELIUM', XYZ=0.993096,-1.392573,1.333501/

&DEVC ID='GAS-L1-R4', QUANTITY='VOLUME FRACTION', SPEC_ID='HELIUM', XYZ=0.993096,-1.192573,0.657301/

&DEVC ID='GAS-L2-R4', QUANTITY='VOLUME FRACTION', SPEC_ID='HELIUM', XYZ=0.993096,-1.192573,0.770001/

&DEVC ID='GAS-L3-R4', QUANTITY='VOLUME FRACTION', SPEC_ID='HELIUM', XYZ=0.993096,-1.192573,0.882701/

&DEVC ID='GAS-L4-R4', QUANTITY='VOLUME FRACTION', SPEC_ID='HELIUM', XYZ=0.993096,-1.192573,0.995401/

&DEVC ID='GAS-L5-R4', QUANTITY='VOLUME FRACTION', SPEC_ID='HELIUM', XYZ=0.993096,-1.192573,1.108101/

&DEVC ID='GAS-L6-R4', QUANTITY='VOLUME FRACTION', SPEC_ID='HELIUM', XYZ=0.993096,-1.192573,1.220801/

&DEVC ID='GAS-L7-R4', QUANTITY='VOLUME FRACTION', SPEC_ID='HELIUM', XYZ=0.993096,-1.192573,1.333501/

&DEVC ID='GAS-L1-R5', QUANTITY='VOLUME FRACTION', SPEC_ID='HELIUM', XYZ=0.993096,-0.992573,0.657301/

&DEVC ID='GAS-L2-R5', QUANTITY='VOLUME FRACTION', SPEC_ID='HELIUM', XYZ=0.993096,-0.992573,0.770001/

&DEVC ID='GAS-L3-R5', QUANTITY='VOLUME FRACTION', SPEC_ID='HELIUM', XYZ=0.993096,-0.992573,0.882701/

&DEVC ID='GAS-L4-R5', QUANTITY='VOLUME FRACTION', SPEC_ID='HELIUM', XYZ=0.993096,-0.992573,0.995401/

&DEVC ID='GAS-L5-R5', QUANTITY='VOLUME FRACTION', SPEC_ID='HELIUM', XYZ=0.993096,-0.992573,1.108101/

&DEVC ID='GAS-L6-R5', QUANTITY='VOLUME FRACTION', SPEC_ID='HELIUM', XYZ=0.993096,-0.992573,1.220801/

&DEVC ID='GAS-L7-R5', QUANTITY='VOLUME FRACTION', SPEC_ID='HELIUM', XYZ=0.993096,-0.992573,1.333501/

&DEVC ID='GAS-L1PL1', QUANTITY='VOLUME FRACTION', SPEC_ID='HELIUM', XYZ=0.353096,-1.818901,0.657301/

&DEVC ID='GAS-L2PL1', QUANTITY='VOLUME FRACTION', SPEC_ID='HELIUM', XYZ=0.353096,-1.818901,0.770001/

&DEVC ID='GAS-L3PL1', QUANTITY='VOLUME FRACTION', SPEC_ID='HELIUM', XYZ=0.353096,-1.818901,0.882701/

&DEVC ID='GAS-L4PL1', QUANTITY='VOLUME FRACTION', SPEC_ID='HELIUM', XYZ=0.353096,-1.818901,0.995401/

&DEVC ID='GAS-L5PL1', QUANTITY='VOLUME FRACTION', SPEC_ID='HELIUM', XYZ=0.353096,-1.818901,1.108101/

&DEVC ID='GAS-L6PL1', QUANTITY='VOLUME FRACTION', SPEC_ID='HELIUM', XYZ=0.353096,-1.818901,1.220801/

&DEVC ID='GAS-L7PL1', QUANTITY='VOLUME FRACTION', SPEC_ID='HELIUM', XYZ=0.353096,-1.818901,1.333501/

&DEVC ID='GAS-L1PL2', QUANTITY='VOLUME FRACTION', SPEC_ID='HELIUM', XYZ=0.353096,-1.848901,0.657301/

&DEVC ID='GAS-L2PL2', QUANTITY='VOLUME FRACTION', SPEC_ID='HELIUM', XYZ=0.353096,-1.848901,0.770001/

&DEVC ID='GAS-L3PL2', QUANTITY='VOLUME FRACTION', SPEC_ID='HELIUM', XYZ=0.353096,-1.848901,0.882701/

&DEVC ID='GAS-L4PL2', QUANTITY='VOLUME FRACTION', SPEC_ID='HELIUM', XYZ=0.353096,-1.848901,0.995401/

&DEVC ID='GAS-L5PL2', QUANTITY='VOLUME FRACTION', SPEC_ID='HELIUM', XYZ=0.353096,-1.848901,1.108101/

&DEVC ID='GAS-L6PL2', QUANTITY='VOLUME FRACTION', SPEC_ID='HELIUM', XYZ=0.353096,-1.848901,1.220801/

&DEVC ID='GAS-L7PL2', QUANTITY='VOLUME FRACTION', SPEC_ID='HELIUM', XYZ=0.353096,-1.848901,1.333501/

&DEVC ID='GAS-L1PM1', QUANTITY='VOLUME FRACTION', SPEC_ID='HELIUM', XYZ=0.673096,-1.818901,0.657301/

&DEVC ID='GAS-L2PM1', QUANTITY='VOLUME FRACTION', SPEC_ID='HELIUM', XYZ=0.673096,-1.818901,0.770001/

&DEVC ID='GAS-L3PM1', QUANTITY='VOLUME FRACTION', SPEC_ID='HELIUM', XYZ=0.673096,-1.818901,0.882701/

&DEVC ID='GAS-L4PM1', QUANTITY='VOLUME FRACTION', SPEC_ID='HELIUM', XYZ=0.673096,-1.818901,0.995401/

&DEVC ID='GAS-L5PM1', QUANTITY='VOLUME FRACTION', SPEC_ID='HELIUM', XYZ=0.673096,-1.818901,1.108101/

&DEVC ID='GAS-L6PM1', QUANTITY='VOLUME FRACTION', SPEC_ID='HELIUM', XYZ=0.673096,-1.818901,1.220801/

&DEVC ID='GAS-L7PM1', QUANTITY='VOLUME FRACTION', SPEC_ID='HELIUM', XYZ=0.673096,-1.818901,1.333501/

&DEVC ID='GAS-L1PM2', QUANTITY='VOLUME FRACTION', SPEC_ID='HELIUM', XYZ=0.673096,-1.848901,0.657301/

&DEVC ID='GAS-L2PM2', QUANTITY='VOLUME FRACTION', SPEC_ID='HELIUM', XYZ=0.673096,-1.848901,0.770001/

&DEVC ID='GAS-L3PM2', QUANTITY='VOLUME FRACTION', SPEC_ID='HELIUM', XYZ=0.673096,-1.848901,0.882701/

&DEVC ID='GAS-L4PM2', QUANTITY='VOLUME FRACTION', SPEC_ID='HELIUM', XYZ=0.673096,-1.848901,0.995401/

&DEVC ID='GAS-L5PM2', QUANTITY='VOLUME FRACTION', SPEC_ID='HELIUM', XYZ=0.673096,-1.848901,1.108101/

&DEVC ID='GAS-L6PM2', QUANTITY='VOLUME FRACTION', SPEC_ID='HELIUM', XYZ=0.673096,-1.848901,1.220801/

&DEVC ID='GAS-L7PM2', QUANTITY='VOLUME FRACTION', SPEC_ID='HELIUM', XYZ=0.673096,-1.848901,1.333501/

&DEVC ID='GAS-L1PR1', QUANTITY='VOLUME FRACTION', SPEC_ID='HELIUM', XYZ=0.993096,-1.818901,0.657301/

&DEVC ID='GAS-L2PR1', QUANTITY='VOLUME FRACTION', SPEC_ID='HELIUM', XYZ=0.993096,-1.818901,0.770001/

&DEVC ID='GAS-L3PR1', QUANTITY='VOLUME FRACTION', SPEC_ID='HELIUM', XYZ=0.993096,-1.818901,0.882701/

&DEVC ID='GAS-L4PR1', QUANTITY='VOLUME FRACTION', SPEC_ID='HELIUM', XYZ=0.993096,-1.818901,0.995401/

&DEVC ID='GAS-L5PR1', QUANTITY='VOLUME FRACTION', SPEC_ID='HELIUM', XYZ=0.993096,-1.818901,1.108101/

&DEVC ID='GAS-L6PR1', QUANTITY='VOLUME FRACTION', SPEC_ID='HELIUM', XYZ=0.993096,-1.818901,1.220801/

&DEVC ID='GAS-L7PR1', QUANTITY='VOLUME FRACTION', SPEC_ID='HELIUM', XYZ=0.993096,-1.818901,1.333501/

&DEVC ID='GAS-L1PR2', QUANTITY='VOLUME FRACTION', SPEC_ID='HELIUM', XYZ=0.993096,-1.848901,0.657301/

&DEVC ID='GAS-L2PR2', QUANTITY='VOLUME FRACTION', SPEC_ID='HELIUM', XYZ=0.993096,-1.848901,0.770001/

&DEVC ID='GAS-L3PR2', QUANTITY='VOLUME FRACTION', SPEC_ID='HELIUM', XYZ=0.993096,-1.848901,0.882701/

&DEVC ID='GAS-L4PR2', QUANTITY='VOLUME FRACTION', SPEC_ID='HELIUM', XYZ=0.993096,-1.848901,0.995401/

&DEVC ID='GAS-L5PR2', QUANTITY='VOLUME FRACTION', SPEC_ID='HELIUM', XYZ=0.993096,-1.848901,1.108101/

&DEVC ID='GAS-L6PR2', QUANTITY='VOLUME FRACTION', SPEC_ID='HELIUM', XYZ=0.993096,-1.848901,1.220801/

&DEVC ID='GAS-L7PR2', QUANTITY='VOLUME FRACTION', SPEC_ID='HELIUM', XYZ=0.993096,-1.848901,1.333501/

&DEVC ID='FLOW01', QUANTITY='MASS FLOW', XB=0.658902,0.691102,-1.807546,-1.807546,0.63235,0.69031/

&DEVC ID='FLOW02', QUANTITY='MASS FLOW', XB=0.658902,0.691102,-1.807546,-1.807546,0.74505,0.80301/

&DEVC ID='FLOW03', QUANTITY='MASS FLOW', XB=0.658902,0.691102,-1.807546,-1.807546,0.85775,0.91571/

&DEVC ID='FLOW04', QUANTITY='MASS FLOW', XB=0.658902,0.691102,-1.807546,-1.807546,0.97045,1.02841/

&DEVC ID='FLOW05', QUANTITY='MASS FLOW', XB=0.658902,0.691102,-1.807546,-1.807546,1.08315,1.14111/

&DEVC ID='FLOW06', QUANTITY='MASS FLOW', XB=0.658902,0.691102,-1.807546,-1.807546,1.19585,1.25381/

```
&DEVC ID='FLOW07', QUANTITY='MASS FLOW', XB=0.658902,0.691102,-1.807546,-1.807546,1.30855,1.36651/
&DEVC ID='heat flow', QUANTITY='HEAT FLOW', XB=0.658902,0.658902,-1.839737,-0.294136,0.60498,2.00568/
&DEVC ID='mass flow', QUANTITY='MASS FLOW', XB=0.658902,0.658902,-1.839737,-0.294137,0.60498,2.00568/
&DEVC ID='volume flow', QUANTITY='VOLUME FLOW', XB=0.658902,0.658902,-1.839737,-0.294137,0.60498,2.00568/
&DEVC ID='heat flow plenum', QUANTITY='HEAT FLOW', XB=0.240302,1.109702,-1.807546,-1.807546,1.39388,1.42608/
&DEVC ID='mass flow plenum', QUANTITY='MASS FLOW', XB=0.240302,1.109702,-1.807546,-1.807546,1.39388,1.42608/
&DEVC ID='volume flow plenum', QUANTITY='VOLUME FLOW', XB=0.240302,1.109702,-1.807546,-1.807546,1.39388,1.42608/

&SURF ID='ADIABATIC',
    COLOR='GRAY 80',
    ADIABATIC=.TRUE./
&SURF ID='fire-helium',
    RGB=255,102,0,
    TMP_FRONT=0.0,
    MASS_FLUX=0.0208,
    SPEC_ID='HELIUM',
    TAU_MF=1.0/

&OBST ID='Obstruction', XB=0.240302,1.109702,-1.855846,-1.839736,0.60498,0.633155, SURF_ID6='ADIABATIC','ADIABATIC','ADIABATIC','fire-helium','ADIABATIC','ADIABATIC'/
&OBST ID='west wall', XB=0.24,0.24,-1.81,-1.8,0.6,0.72, COLOR='INVISIBLE', SURF_ID='ADIABATIC'/
&OBST ID='west wall', XB=0.24,0.24,-1.81,-1.8,0.72,0.84, COLOR='INVISIBLE', SURF_ID='ADIABATIC'/
&OBST ID='west wall', XB=0.24,0.24,-1.81,-1.8,0.84,0.94, COLOR='INVISIBLE', SURF_ID='ADIABATIC'/
&OBST ID='west wall', XB=0.24,0.24,-1.81,-1.8,0.94,1.06, COLOR='INVISIBLE', SURF_ID='ADIABATIC'/
&OBST ID='west wall', XB=0.24,0.24,-1.81,-1.8,1.06,1.16, COLOR='INVISIBLE', SURF_ID='ADIABATIC'/
&OBST ID='west wall', XB=0.24,0.24,-1.81,-1.8,1.16,1.28, COLOR='INVISIBLE', SURF_ID='ADIABATIC'/
&OBST ID='west wall', XB=0.24,0.24,-1.81,-1.8,1.28,1.395, COLOR='INVISIBLE', SURF_ID='ADIABATIC'/
&OBST ID='west wall', XB=0.24,0.24,-1.8,-0.94,0.6,0.72, COLOR='INVISIBLE', SURF_ID='ADIABATIC'/
&OBST ID='west wall', XB=0.24,0.24,-1.8,-0.94,0.72,0.84, COLOR='INVISIBLE', SURF_ID='ADIABATIC'/
&OBST ID='west wall', XB=0.24,0.24,-1.8,-0.94,0.84,0.94, COLOR='INVISIBLE', SURF_ID='ADIABATIC'/
&OBST ID='west wall', XB=0.24,0.24,-1.8,-0.94,0.94,1.06, COLOR='INVISIBLE', SURF_ID='ADIABATIC'/
&OBST ID='west wall', XB=0.24,0.24,-1.8,-0.94,1.06,1.16, COLOR='INVISIBLE', SURF_ID='ADIABATIC'/
&OBST ID='west wall', XB=0.24,0.24,-1.8,-0.94,1.16,1.28, COLOR='INVISIBLE', SURF_ID='ADIABATIC'/
```

&OBST ID='west wall', XB=0.24,0.24,-1.8,-0.94,1.28,1.39, COLOR='INVISIBLE', SURF_ID='ADIABATIC'/

&OBST ID='roof', XB=0.24,0.67,-1.81,-1.8,1.395,1.395, COLOR='GRAY 68', SURF_ID='ADIABATIC'/

&OBST ID='roof', XB=0.67,1.11,-1.81,-1.8,1.395,1.395, COLOR='GRAY 68', SURF_ID='ADIABATIC'/

&OBST ID='roof', XB=0.24,0.69,-1.8,-0.94,1.39,1.39, COLOR='GRAY 68', SURF_ID='ADIABATIC'/

&OBST ID='roof', XB=0.69,1.11,-1.8,-0.94,1.39,1.39, COLOR='GRAY 68', SURF_ID='ADIABATIC'/

&OBST ID='east wall', XB=1.11,1.11,-1.81,-1.8,0.6,0.72, COLOR='INVISIBLE', SURF_ID='ADIABATIC'/

&OBST ID='east wall', XB=1.11,1.11,-1.81,-1.8,0.72,0.84, COLOR='INVISIBLE', SURF_ID='ADIABATIC'/

&OBST ID='east wall', XB=1.11,1.11,-1.81,-1.8,0.84,0.94, COLOR='INVISIBLE', SURF_ID='ADIABATIC'/

&OBST ID='east wall', XB=1.11,1.11,-1.81,-1.8,0.94,1.06, COLOR='INVISIBLE', SURF_ID='ADIABATIC'/

&OBST ID='east wall', XB=1.11,1.11,-1.81,-1.8,1.06,1.16, COLOR='INVISIBLE', SURF_ID='ADIABATIC'/

&OBST ID='east wall', XB=1.11,1.11,-1.81,-1.8,1.16,1.28, COLOR='INVISIBLE', SURF_ID='ADIABATIC'/

&OBST ID='east wall', XB=1.11,1.11,-1.81,-1.8,1.28,1.395, COLOR='INVISIBLE', SURF_ID='ADIABATIC'/

&OBST ID='east wall', XB=1.11,1.11,-1.8,-0.94,0.6,0.72, COLOR='INVISIBLE', SURF_ID='ADIABATIC'/

&OBST ID='east wall', XB=1.11,1.11,-1.8,-0.94,0.72,0.84, COLOR='INVISIBLE', SURF_ID='ADIABATIC'/

&OBST ID='east wall', XB=1.11,1.11,-1.8,-0.94,0.84,0.94, COLOR='INVISIBLE', SURF_ID='ADIABATIC'/

&OBST ID='east wall', XB=1.11,1.11,-1.8,-0.94,0.94,1.06, COLOR='INVISIBLE', SURF_ID='ADIABATIC'/

&OBST ID='east wall', XB=1.11,1.11,-1.8,-0.94,1.06,1.16, COLOR='INVISIBLE', SURF_ID='ADIABATIC'/

&OBST ID='east wall', XB=1.11,1.11,-1.8,-0.94,1.16,1.28, COLOR='INVISIBLE', SURF_ID='ADIABATIC'/

&OBST ID='east wall', XB=1.11,1.11,-1.8,-0.94,1.28,1.39, COLOR='INVISIBLE', SURF_ID='ADIABATIC'/

&OBST ID='floor of conference salon', XB=0.24,0.67,-1.81,-1.8,1.28,1.28, COLOR='GRAY 68', SURF_ID='ADIABATIC'/

&OBST ID='floor of conference salon', XB=0.67,1.11,-1.81,-1.8,1.28,1.28, COLOR='GRAY 68', SURF_ID='ADIABATIC'/

&OBST ID='floor of conference salon', XB=0.24,0.69,-1.8,-0.94,1.28,1.28, COLOR='GRAY 68', SURF_ID='ADIABATIC'/

&OBST ID='floor of conference salon', XB=0.69,1.11,-1.8,-0.94,1.28,1.28, COLOR='GRAY 68', SURF_ID='ADIABATIC'/

&OBST ID='floor of 6th level', XB=0.24,0.67,-1.81,-1.8,1.17,1.17, COLOR='GRAY 68', SURF_ID='ADIABATIC'/

&OBST ID='floor of 6th level', XB=0.67,1.11,-1.81,-1.8,1.17,1.17, COLOR='GRAY 68', SURF_ID='ADIABATIC'/

&OBST ID='floor of 6th level', XB=0.24,0.69,-1.8,-0.94,1.17,1.17, COLOR='GRAY 68', SURF_ID='ADIABATIC'/

&OBST ID='floor of 6th level', XB=0.69,1.11,-1.8,-0.94,1.17,1.17, COLOR='GRAY 68', SURF_ID='ADIABATIC'/

&OBST ID='floor of 5th level', XB=0.24,0.67,-1.81,-1.8,1.055,1.055, COLOR='GRAY 68', SURF_ID='ADIABATIC'/

&OBST ID='floor of 5th level', XB=0.67,1.11,-1.81,-1.8,1.055,1.055, COLOR='GRAY 68', SURF_ID='ADIABATIC'/

&OBST ID='floor of 5th level', XB=0.24,0.69,-1.8,-0.94,1.06,1.06, COLOR='GRAY 68', SURF_ID='ADIABATIC'/

&OBST ID='floor of 5th level', XB=0.69,1.11,-1.8,-0.94,1.06,1.06, COLOR='GRAY 68', SURF_ID='ADIABATIC'/

&OBST ID='floor of 4th level', XB=0.24,0.67,-1.81,-1.8,0.945,0.945, COLOR='GRAY 68', SURF_ID='ADIABATIC'/

&OBST ID='floor of 4th level', XB=0.67,1.11,-1.81,-1.8,0.945,0.945, COLOR='GRAY 68', SURF_ID='ADIABATIC'/

&OBST ID='floor of 4th level', XB=0.24,0.69,-1.8,-0.94,0.94,0.94, COLOR='GRAY 68', SURF_ID='ADIABATIC'/

&OBST ID='floor of 4th level', XB=0.69,1.11,-1.8,-0.94,0.94,0.94, COLOR='GRAY 68', SURF_ID='ADIABATIC'/

&OBST ID='floor of 3rd level', XB=0.24,0.67,-1.81,-1.8,0.83,0.83, COLOR='GRAY 68', SURF_ID='ADIABATIC'/

&OBST ID='floor of 3rd level', XB=0.67,1.11,-1.81,-1.8,0.83,0.83, COLOR='GRAY 68', SURF_ID='ADIABATIC'/

&OBST ID='floor of 3rd level', XB=0.24,0.69,-1.8,-0.94,0.83,0.83, COLOR='GRAY 68', SURF_ID='ADIABATIC'/

&OBST ID='floor of 3rd level', XB=0.69,1.11,-1.8,-0.94,0.83,0.83, COLOR='GRAY 68', SURF_ID='ADIABATIC'/

&OBST ID='floor of 2nd level', XB=0.24,0.67,-1.81,-1.8,0.72,0.72, COLOR='GRAY 68', SURF_ID='ADIABATIC'/

&OBST ID='floor of 2nd level', XB=0.67,1.11,-1.81,-1.8,0.72,0.72, COLOR='GRAY 68', SURF_ID='ADIABATIC'/

&OBST ID='floor of 2nd level', XB=0.24,0.69,-1.8,-0.94,0.72,0.72, COLOR='GRAY 68', SURF_ID='ADIABATIC'/

&OBST ID='floor of 2nd level', XB=0.69,1.11,-1.8,-0.94,0.72,0.72, COLOR='GRAY 68', SURF_ID='ADIABATIC'/

&OBST ID='floor of 1st level', XB=0.24,0.67,-1.81,-1.8,0.605,0.605, COLOR='GRAY 68', SURF_ID='ADIABATIC'/

&OBST ID='floor of 1st level', XB=0.67,1.11,-1.81,-1.8,0.605,0.605, COLOR='GRAY 68', SURF_ID='ADIABATIC'/

&OBST ID='floor of 1st level', XB=0.24,0.69,-1.8,-0.94,0.6,0.6, COLOR='GRAY 68', SURF_ID='ADIABATIC'/

&OBST ID='floor of 1st level', XB=0.69,1.11,-1.8,-0.94,0.6,0.6, COLOR='GRAY 68', SURF_ID='ADIABATIC'/

&OBST ID='plenum west', XB=0.24,0.24,-1.855,-1.81,0.605,0.72, COLOR='INVISIBLE', SURF_ID='ADIABATIC'/

&OBST ID='plenum west', XB=0.24,0.24,-1.855,-1.81,0.72,0.84, COLOR='INVISIBLE', SURF_ID='ADIABATIC'/

&OBST ID='plenum west', XB=0.24,0.24,-1.855,-1.81,0.84,0.94, COLOR='INVISIBLE', SURF_ID='ADIABATIC'/

&OBST ID='plenum west', XB=0.24,0.24,-1.855,-1.81,0.94,1.06, COLOR='INVISIBLE', SURF_ID='ADIABATIC'/

&OBST ID='plenum west', XB=0.24,0.24,-1.855,-1.81,1.06,1.16, COLOR='INVISIBLE', SURF_ID='ADIABATIC'/

&OBST ID='plenum west', XB=0.24,0.24,-1.855,-1.81,1.16,1.28, COLOR='INVISIBLE', SURF_ID='ADIABATIC'/

&OBST ID='plenum west', XB=0.24,0.24,-1.855,-1.81,1.28,1.4, COLOR='INVISIBLE', SURF_ID='ADIABATIC'/

&OBST ID='plenum west', XB=0.24,0.24,-1.855,-1.81,1.4,1.425, COLOR='INVISIBLE', SURF_ID='ADIABATIC'/

&OBST ID='plenum top', XB=0.24,1.11,-1.855,-1.81,1.425,1.425, COLOR='CYAN', SURF_ID='ADIABATIC'/

&OBST ID='plenum east', XB=1.11,1.11,-1.855,-1.81,0.605,0.72, COLOR='CYAN', SURF_ID='ADIABATIC'/

&OBST ID='plenum east', XB=1.11,1.11,-1.855,-1.81,0.72,0.84, COLOR='CYAN', SURF_ID='ADIABATIC'/

&OBST ID='plenum east', XB=1.11,1.11,-1.855,-1.81,0.84,0.94, COLOR='CYAN', SURF_ID='ADIABATIC'/

&OBST ID='plenum east', XB=1.11,1.11,-1.855,-1.81,0.94,1.06, COLOR='CYAN', SURF_ID='ADIABATIC'/

&OBST ID='plenum east', XB=1.11,1.11,-1.855,-1.81,1.06,1.16, COLOR='CYAN', SURF_ID='ADIABATIC'/

&OBST ID='plenum east', XB=1.11,1.11,-1.855,-1.81,1.16,1.28, COLOR='CYAN', SURF_ID='ADIABATIC'/

&OBST ID='plenum east', XB=1.11,1.11,-1.855,-1.81,1.28,1.4, COLOR='CYAN', SURF_ID='ADIABATIC'/

&OBST ID='plenum east', XB=1.11,1.11,-1.855,-1.81,1.4,1.425, COLOR='CYAN', SURF_ID='ADIABATIC'/

&OBST ID='plenum south face', XB=0.24,0.67,-1.855,-1.855,0.605,0.72, COLOR='INVISIBLE', SURF_ID='ADIABATIC'/

&OBST ID='plenum south face', XB=0.67,1.11,-1.855,-1.855,0.605,0.72, COLOR='INVISIBLE', SURF_ID='ADIABATIC'/

&OBST ID='plenum south face', XB=0.24,0.67,-1.855,-1.855,0.72,0.84, COLOR='INVISIBLE', SURF_ID='ADIABATIC'/

&OBST ID='plenum south face', XB=0.67,1.11,-1.855,-1.855,0.72,0.84, COLOR='INVISIBLE', SURF_ID='ADIABATIC'/

&OBST ID='plenum south face', XB=0.24,0.67,-1.855,-1.855,0.84,0.94, COLOR='INVISIBLE', SURF_ID='ADIABATIC'/

&OBST ID='plenum south face', XB=0.67,1.11,-1.855,-1.855,0.84,0.94, COLOR='INVISIBLE', SURF_ID='ADIABATIC'/

&OBST ID='plenum south face', XB=0.24,0.67,-1.855,-1.855,0.94,1.06, COLOR='INVISIBLE', SURF_ID='ADIABATIC'/

&OBST ID='plenum south face', XB=0.67,1.11,-1.855,-1.855,0.94,1.06, COLOR='INVISIBLE', SURF_ID='ADIABATIC'/

&OBST ID='plenum south face', XB=0.24,0.67,-1.855,-1.855,1.06,1.16, COLOR='INVISIBLE', SURF_ID='ADIABATIC'/

&OBST ID='plenum south face', XB=0.67,1.11,-1.855,-1.855,1.06,1.16, COLOR='INVISIBLE', SURF_ID='ADIABATIC'/

&OBST ID='plenum south face', XB=0.24,0.67,-1.855,-1.855,1.16,1.28, COLOR='INVISIBLE', SURF_ID='ADIABATIC'/

&OBST ID='plenum south face', XB=0.67,1.11,-1.855,-1.855,1.16,1.28, COLOR='INVISIBLE', SURF_ID='ADIABATIC'/

&OBST ID='plenum south face', XB=0.24,0.67,-1.855,-1.855,1.28,1.4, COLOR='INVISIBLE', SURF_ID='ADIABATIC'/

&OBST ID='plenum south face', XB=0.67,1.11,-1.855,-1.855,1.28,1.4, COLOR='INVISIBLE', SURF_ID='ADIABATIC'/

&OBST ID='plenum south face', XB=0.24,1.11,-1.855,-1.855,1.4,1.425, COLOR='INVISIBLE', SURF_ID='ADIABATIC'/

&OBST ID='plenum buttom', XB=0.24,0.67,-1.855,-1.81,0.605,0.605, COLOR='CYAN', SURF_ID='ADIABATIC'/

&OBST ID='plenum buttom', XB=0.67,1.11,-1.855,-1.81,0.605,0.605, COLOR='CYAN', SURF_ID='ADIABATIC'/

&OBST ID='AcDbRegion - 11B2', XB=0.24,0.275,-1.81,-1.81,0.6,0.72, COLOR='GRAY 80', SURF_ID='ADIABATIC'/

&OBST ID='AcDbRegion - 11B2', XB=0.275,0.305,-1.81,-1.81,0.6,0.63, COLOR='GRAY 80', SURF_ID='ADIABATIC'/

&OBST ID='AcDbRegion - 11B2', XB=0.275,0.305,-1.81,-1.81,0.69,0.72, COLOR='GRAY 80', SURF_ID='ADIABATIC'/

&OBST ID='AcDbRegion - 11B2', XB=0.305,0.335,-1.81,-1.81,0.6,0.72, COLOR='GRAY 80', SURF_ID='ADIABATIC'/

&OBST ID='AcDbRegion - 11B2', XB=0.335,0.37,-1.81,-1.81,0.6,0.63, COLOR='GRAY 80', SURF_ID='ADIABATIC'/

&OBST ID='AcDbRegion - 11B2', XB=0.335,0.37,-1.81,-1.81,0.69,0.72, COLOR='GRAY 80', SURF_ID='ADIABATIC'/

&OBST ID='AcDbRegion - 11B2', XB=0.37,0.4,-1.81,-1.81,0.6,0.72, COLOR='GRAY 80', SURF_ID='ADIABATIC'/

&OBST ID='AcDbRegion - 11B2', XB=0.4,0.435,-1.81,-1.81,0.6,0.63, COLOR='GRAY 80', SURF_ID='ADIABATIC'/

&OBST ID='AcDbRegion - 11B2', XB=0.4,0.435,-1.81,-1.81,0.69,0.72, COLOR='GRAY 80', SURF_ID='ADIABATIC'/

&OBST ID='AcDbRegion - 11B2', XB=0.435,0.465,-1.81,-1.81,0.6,0.72, COLOR='GRAY 80', SURF_ID='ADIABATIC'/

&OBST ID='AcDbRegion - 11B2', XB=0.465,0.5,-1.81,-1.81,0.6,0.63, COLOR='GRAY 80', SURF_ID='ADIABATIC'/

&OBST ID='AcDbRegion - 11B2', XB=0.465,0.5,-1.81,-1.81,0.69,0.72, COLOR='GRAY 80', SURF_ID='ADIABATIC'/

&OBST ID='AcDbRegion - 11B2', XB=0.5,0.53,-1.81,-1.81,0.6,0.72, COLOR='GRAY 80', SURF_ID='ADIABATIC'/

&OBST ID='AcDbRegion - 11B2', XB=0.53,0.56,-1.81,-1.81,0.6,0.63, COLOR='GRAY 80', SURF_ID='ADIABATIC'/

&OBST ID='AcDbRegion - 11B2', XB=0.53,0.56,-1.81,-1.81,0.69,0.72, COLOR='GRAY 80', SURF_ID='ADIABATIC'/

&OBST ID='AcDbRegion - 11B2', XB=0.56,0.595,-1.81,-1.81,0.6,0.72, COLOR='GRAY 80', SURF_ID='ADIABATIC'/

&OBST ID='AcDbRegion - 11B2', XB=0.595,0.625,-1.81,-1.81,0.6,0.63, COLOR='GRAY 80', SURF_ID='ADIABATIC'/

&OBST ID='AcDbRegion - 11B2', XB=0.595,0.625,-1.81,-1.81,0.69,0.72, COLOR='GRAY 80', SURF_ID='ADIABATIC'/

&OBST ID='AcDbRegion - 11B2', XB=0.625,0.66,-1.81,-1.81,0.6,0.72, COLOR='GRAY 80', SURF_ID='ADIABATIC'/

&OBST ID='AcDbRegion - 11B2', XB=0.66,0.67,-1.81,-1.81,0.6,0.63, COLOR='GRAY 80', SURF_ID='ADIABATIC'/

&OBST ID='AcDbRegion - 11B2', XB=0.66,0.67,-1.81,-1.81,0.69,0.72, COLOR='GRAY 80', SURF_ID='ADIABATIC'/

&OBST ID='AcDbRegion - 11B2', XB=0.67,0.69,-1.81,-1.81,0.6,0.63, COLOR='GRAY 80', SURF_ID='ADIABATIC'/

&OBST ID='AcDbRegion - 11B2', XB=0.67,0.69,-1.81,-1.81,0.69,0.72, COLOR='GRAY 80', SURF_ID='ADIABATIC'/

&OBST ID='AcDbRegion - 11B2', XB=0.69,0.725,-1.81,-1.81,0.6,0.72, COLOR='GRAY 80', SURF_ID='ADIABATIC'/

&OBST ID='AcDbRegion - 11B2', XB=0.725,0.755,-1.81,-1.81,0.6,0.63, COLOR='GRAY 80', SURF_ID='ADIABATIC'/

&OBST ID='AcDbRegion - 11B2', XB=0.725,0.755,-1.81,-1.81,0.69,0.72, COLOR='GRAY 80', SURF_ID='ADIABATIC'/

&OBST ID='AcDbRegion - 11B2', XB=0.755,0.79,-1.81,-1.81,0.6,0.72, COLOR='GRAY 80', SURF_ID='ADIABATIC'/

&OBST ID='AcDbRegion - 11B2', XB=0.79,0.82,-1.81,-1.81,0.6,0.63, COLOR='GRAY 80', SURF_ID='ADIABATIC'/

&OBST ID='AcDbRegion - 11B2', XB=0.79,0.82,-1.81,-1.81,0.69,0.72, COLOR='GRAY 80', SURF_ID='ADIABATIC'/

&OBST ID='AcDbRegion - 11B2', XB=0.82,0.85,-1.81,-1.81,0.6,0.72, COLOR='GRAY 80', SURF_ID='ADIABATIC'/

&OBST ID='AcDbRegion - 11B2', XB=0.85,0.885,-1.81,-1.81,0.6,0.63, COLOR='GRAY 80', SURF_ID='ADIABATIC'/

&OBST ID='AcDbRegion - 11B2', XB=0.85,0.885,-1.81,-1.81,0.69,0.72, COLOR='GRAY 80', SURF_ID='ADIABATIC'/

&OBST ID='AcDbRegion - 11B2', XB=0.885,0.915,-1.81,-1.81,0.6,0.72, COLOR='GRAY 80', SURF_ID='ADIABATIC'/

&OBST ID='AcDbRegion - 11B2', XB=0.915,0.95,-1.81,-1.81,0.6,0.63, COLOR='GRAY 80', SURF_ID='ADIABATIC'/

&OBST ID='AcDbRegion - 11B2', XB=0.915,0.95,-1.81,-1.81,0.69,0.72, COLOR='GRAY 80', SURF_ID='ADIABATIC'/

&OBST ID='AcDbRegion - 11B2', XB=0.95,0.98,-1.81,-1.81,0.6,0.72, COLOR='GRAY 80', SURF_ID='ADIABATIC'/

&OBST ID='AcDbRegion - 11B2', XB=0.98,1.015,-1.81,-1.81,0.6,0.63, COLOR='GRAY 80', SURF_ID='ADIABATIC'/

&OBST ID='AcDbRegion - 11B2', XB=0.98,1.015,-1.81,-1.81,0.69,0.72, COLOR='GRAY 80', SURF_ID='ADIABATIC'/

&OBST ID='AcDbRegion - 11B2', XB=1.015,1.045,-1.81,-1.81,0.6,0.72, COLOR='GRAY 80', SURF_ID='ADIABATIC'/

&OBST ID='AcDbRegion - 11B2', XB=1.045,1.08,-1.81,-1.81,0.6,0.63, COLOR='GRAY 80', SURF_ID='ADIABATIC'/

&OBST ID='AcDbRegion - 11B2', XB=1.045,1.08,-1.81,-1.81,0.69,0.72, COLOR='GRAY 80', SURF_ID='ADIABATIC'/

&OBST ID='AcDbRegion - 11B2', XB=1.08,1.11,-1.81,-1.81,0.6,0.72, COLOR='GRAY 80', SURF_ID='ADIABATIC'/

&OBST ID='AcDbRegion - 11B2', XB=0.24,0.275,-1.81,-1.81,0.72,0.84, COLOR='GRAY 80', SURF_ID='ADIABATIC'/

&OBST ID='AcDbRegion - 11B2', XB=0.275,0.305,-1.81,-1.81,0.72,0.745, COLOR='GRAY 80', SURF_ID='ADIABATIC'/

&OBST ID='AcDbRegion - 11B2', XB=0.275,0.305,-1.81,-1.81,0.805,0.84, COLOR='GRAY 80', SURF_ID='ADIABATIC'/

&OBST ID='AcDbRegion - 11B2', XB=0.305,0.335,-1.81,-1.81,0.72,0.84, COLOR='GRAY 80', SURF_ID='ADIABATIC'/

&OBST ID='AcDbRegion - 11B2', XB=0.335,0.37,-1.81,-1.81,0.72,0.745, COLOR='GRAY 80', SURF_ID='ADIABATIC'/

&OBST ID='AcDbRegion - 11B2', XB=0.335,0.37,-1.81,-1.81,0.805,0.84, COLOR='GRAY 80', SURF_ID='ADIABATIC'/

&OBST ID='AcDbRegion - 11B2', XB=0.37,0.4,-1.81,-1.81,0.72,0.84, COLOR='GRAY 80', SURF_ID='ADIABATIC'/

&OBST ID='AcDbRegion - 11B2', XB=0.4,0.435,-1.81,-1.81,0.72,0.745, COLOR='GRAY 80', SURF_ID='ADIABATIC'/

&OBST ID='AcDbRegion - 11B2', XB=0.4,0.435,-1.81,-1.81,0.805,0.84, COLOR='GRAY 80', SURF_ID='ADIABATIC'/

&OBST ID='AcDbRegion - 11B2', XB=0.435,0.465,-1.81,-1.81,0.72,0.84, COLOR='GRAY 80', SURF_ID='ADIABATIC'/

&OBST ID='AcDbRegion - 11B2', XB=0.465,0.5,-1.81,-1.81,0.72,0.745, COLOR='GRAY 80', SURF_ID='ADIABATIC'/

&OBST ID='AcDbRegion - 11B2', XB=0.465,0.5,-1.81,-1.81,0.805,0.84, COLOR='GRAY 80', SURF_ID='ADIABATIC'/

&OBST ID='AcDbRegion - 11B2', XB=0.5,0.53,-1.81,-1.81,0.72,0.84, COLOR='GRAY 80', SURF_ID='ADIABATIC'/

&OBST ID='AcDbRegion - 11B2', XB=0.53,0.56,-1.81,-1.81,0.72,0.745, COLOR='GRAY 80', SURF_ID='ADIABATIC'/

&OBST ID='AcDbRegion - 11B2', XB=0.53,0.56,-1.81,-1.81,0.805,0.84, COLOR='GRAY 80', SURF_ID='ADIABATIC'/

&OBST ID='AcDbRegion - 11B2', XB=0.56,0.595,-1.81,-1.81,0.72,0.84, COLOR='GRAY 80', SURF_ID='ADIABATIC'/

&OBST ID='AcDbRegion - 11B2', XB=0.595,0.625,-1.81,-1.81,0.72,0.745, COLOR='GRAY 80', SURF_ID='ADIABATIC'/

&OBST ID='AcDbRegion - 11B2', XB=0.595,0.625,-1.81,-1.81,0.805,0.84, COLOR='GRAY 80', SURF_ID='ADIABATIC'/

&OBST ID='AcDbRegion - 11B2', XB=0.625,0.66,-1.81,-1.81,0.72,0.84, COLOR='GRAY 80', SURF_ID='ADIABATIC'/

&OBST ID='AcDbRegion - 11B2', XB=0.66,0.67,-1.81,-1.81,0.72,0.745, COLOR='GRAY 80', SURF_ID='ADIABATIC'/

&OBST ID='AcDbRegion - 11B2', XB=0.66,0.67,-1.81,-1.81,0.805,0.84, COLOR='GRAY 80', SURF_ID='ADIABATIC'/

&OBST ID='AcDbRegion - 11B2', XB=0.67,0.69,-1.81,-1.81,0.72,0.745, COLOR='GRAY 80', SURF_ID='ADIABATIC'/

&OBST ID='AcDbRegion - 11B2', XB=0.67,0.69,-1.81,-1.81,0.805,0.84, COLOR='GRAY 80', SURF_ID='ADIABATIC'/

&OBST ID='AcDbRegion - 11B2', XB=0.69,0.725,-1.81,-1.81,0.72,0.84, COLOR='GRAY 80', SURF_ID='ADIABATIC'/

&OBST ID='AcDbRegion - 11B2', XB=0.725,0.755,-1.81,-1.81,0.72,0.745, COLOR='GRAY 80', SURF_ID='ADIABATIC'/

&OBST ID='AcDbRegion - 11B2', XB=0.725,0.755,-1.81,-1.81,0.805,0.84, COLOR='GRAY 80', SURF_ID='ADIABATIC'/

&OBST ID='AcDbRegion - 11B2', XB=0.755,0.79,-1.81,-1.81,0.72,0.84, COLOR='GRAY 80', SURF_ID='ADIABATIC'/

&OBST ID='AcDbRegion - 11B2', XB=0.79,0.82,-1.81,-1.81,0.72,0.745, COLOR='GRAY 80', SURF_ID='ADIABATIC'/

&OBST ID='AcDbRegion - 11B2', XB=0.79,0.82,-1.81,-1.81,0.805,0.84, COLOR='GRAY 80', SURF_ID='ADIABATIC'/

&OBST ID='AcDbRegion - 11B2', XB=0.82,0.85,-1.81,-1.81,0.72,0.84, COLOR='GRAY 80', SURF_ID='ADIABATIC'/

&OBST ID='AcDbRegion - 11B2', XB=0.85,0.885,-1.81,-1.81,0.72,0.745, COLOR='GRAY 80', SURF_ID='ADIABATIC'/

&OBST ID='AcDbRegion - 11B2', XB=0.85,0.885,-1.81,-1.81,0.805,0.84, COLOR='GRAY 80', SURF_ID='ADIABATIC'/

&OBST ID='AcDbRegion - 11B2', XB=0.885,0.915,-1.81,-1.81,0.72,0.84, COLOR='GRAY 80', SURF_ID='ADIABATIC'/

&OBST ID='AcDbRegion - 11B2', XB=0.915,0.95,-1.81,-1.81,0.72,0.745, COLOR='GRAY 80', SURF_ID='ADIABATIC'/

&OBST ID='AcDbRegion - 11B2', XB=0.915,0.95,-1.81,-1.81,0.805,0.84, COLOR='GRAY 80', SURF_ID='ADIABATIC'/

&OBST ID='AcDbRegion - 11B2', XB=0.95,0.98,-1.81,-1.81,0.72,0.84, COLOR='GRAY 80', SURF_ID='ADIABATIC'/

&OBST ID='AcDbRegion - 11B2', XB=0.98,1.015,-1.81,-1.81,0.72,0.745, COLOR='GRAY 80', SURF_ID='ADIABATIC'/

&OBST ID='AcDbRegion - 11B2', XB=0.98,1.015,-1.81,-1.81,0.805,0.84, COLOR='GRAY 80', SURF_ID='ADIABATIC'/

&OBST ID='AcDbRegion - 11B2', XB=1.015,1.045,-1.81,-1.81,0.72,0.84, COLOR='GRAY 80', SURF_ID='ADIABATIC'/

&OBST ID='AcDbRegion - 11B2', XB=1.045,1.08,-1.81,-1.81,0.72,0.745, COLOR='GRAY 80', SURF_ID='ADIABATIC'/

&OBST ID='AcDbRegion - 11B2', XB=1.045,1.08,-1.81,-1.81,0.805,0.84, COLOR='GRAY 80', SURF_ID='ADIABATIC'/

&OBST ID='AcDbRegion - 11B2', XB=1.08,1.11,-1.81,-1.81,0.72,0.84, COLOR='GRAY 80', SURF_ID='ADIABATIC'/

&OBST ID='AcDbRegion - 11B2', XB=0.24,0.275,-1.81,-1.81,0.84,0.94, COLOR='GRAY 80', SURF_ID='ADIABATIC'/

&OBST ID='AcDbRegion - 11B2', XB=0.275,0.305,-1.81,-1.81,0.84,0.86, COLOR='GRAY 80', SURF_ID='ADIABATIC'/

&OBST ID='AcDbRegion - 11B2', XB=0.275,0.305,-1.81,-1.81,0.915,0.94, COLOR='GRAY 80', SURF_ID='ADIABATIC'/

&OBST ID='AcDbRegion - 11B2', XB=0.305,0.335,-1.81,-1.81,0.84,0.94, COLOR='GRAY 80', SURF_ID='ADIABATIC'/

&OBST ID='AcDbRegion - 11B2', XB=0.335,0.37,-1.81,-1.81,0.84,0.86, COLOR='GRAY 80', SURF_ID='ADIABATIC'/

&OBST ID='AcDbRegion - 11B2', XB=0.335,0.37,-1.81,-1.81,0.915,0.94, COLOR='GRAY 80', SURF_ID='ADIABATIC'/

&OBST ID='AcDbRegion - 11B2', XB=0.37,0.4,-1.81,-1.81,0.84,0.94, COLOR='GRAY 80', SURF_ID='ADIABATIC'/

&OBST ID='AcDbRegion - 11B2', XB=0.4,0.435,-1.81,-1.81,0.84,0.86, COLOR='GRAY 80', SURF_ID='ADIABATIC'/

&OBST ID='AcDbRegion - 11B2', XB=0.4,0.435,-1.81,-1.81,0.915,0.94, COLOR='GRAY 80', SURF_ID='ADIABATIC'/

&OBST ID='AcDbRegion - 11B2', XB=0.435,0.465,-1.81,-1.81,0.84,0.94, COLOR='GRAY 80', SURF_ID='ADIABATIC'/

&OBST ID='AcDbRegion - 11B2', XB=0.465,0.5,-1.81,-1.81,0.84,0.86, COLOR='GRAY 80', SURF_ID='ADIABATIC'/

&OBST ID='AcDbRegion - 11B2', XB=0.465,0.5,-1.81,-1.81,0.915,0.94, COLOR='GRAY 80', SURF_ID='ADIABATIC'/

&OBST ID='AcDbRegion - 11B2', XB=0.5,0.53,-1.81,-1.81,0.84,0.94, COLOR='GRAY 80', SURF_ID='ADIABATIC'/

&OBST ID='AcDbRegion - 11B2', XB=0.53,0.56,-1.81,-1.81,0.84,0.86, COLOR='GRAY 80', SURF_ID='ADIABATIC'/

&OBST ID='AcDbRegion - 11B2', XB=0.53,0.56,-1.81,-1.81,0.915,0.94, COLOR='GRAY 80', SURF_ID='ADIABATIC'/

&OBST ID='AcDbRegion - 11B2', XB=0.56,0.595,-1.81,-1.81,0.84,0.94, COLOR='GRAY 80', SURF_ID='ADIABATIC'/

&OBST ID='AcDbRegion - 11B2', XB=0.595,0.625,-1.81,-1.81,0.84,0.86, COLOR='GRAY 80', SURF_ID='ADIABATIC'/

&OBST ID='AcDbRegion - 11B2', XB=0.595,0.625,-1.81,-1.81,0.915,0.94, COLOR='GRAY 80', SURF_ID='ADIABATIC'/

&OBST ID='AcDbRegion - 11B2', XB=0.625,0.66,-1.81,-1.81,0.84,0.94, COLOR='GRAY 80', SURF_ID='ADIABATIC'/

&OBST ID='AcDbRegion - 11B2', XB=0.66,0.67,-1.81,-1.81,0.84,0.86, COLOR='GRAY 80', SURF_ID='ADIABATIC'/

&OBST ID='AcDbRegion - 11B2', XB=0.66,0.67,-1.81,-1.81,0.915,0.94, COLOR='GRAY 80', SURF_ID='ADIABATIC'/

&OBST ID='AcDbRegion - 11B2', XB=0.67,0.69,-1.81,-1.81,0.84,0.86, COLOR='GRAY 80', SURF_ID='ADIABATIC'/

&OBST ID='AcDbRegion - 11B2', XB=0.67,0.69,-1.81,-1.81,0.915,0.94, COLOR='GRAY 80', SURF_ID='ADIABATIC'/

&OBST ID='AcDbRegion - 11B2', XB=0.69,0.725,-1.81,-1.81,0.84,0.94, COLOR='GRAY 80', SURF_ID='ADIABATIC'/

&OBST ID='AcDbRegion - 11B2', XB=0.725,0.755,-1.81,-1.81,0.84,0.86, COLOR='GRAY 80', SURF_ID='ADIABATIC'/

&OBST ID='AcDbRegion - 11B2', XB=0.725,0.755,-1.81,-1.81,0.915,0.94, COLOR='GRAY 80', SURF_ID='ADIABATIC'/

&OBST ID='AcDbRegion - 11B2', XB=0.755,0.79,-1.81,-1.81,0.84,0.94, COLOR='GRAY 80', SURF_ID='ADIABATIC'/

&OBST ID='AcDbRegion - 11B2', XB=0.79,0.82,-1.81,-1.81,0.84,0.86, COLOR='GRAY 80', SURF_ID='ADIABATIC'/

&OBST ID='AcDbRegion - 11B2', XB=0.79,0.82,-1.81,-1.81,0.915,0.94, COLOR='GRAY 80', SURF_ID='ADIABATIC'/

&OBST ID='AcDbRegion - 11B2', XB=0.82,0.85,-1.81,-1.81,0.84,0.94, COLOR='GRAY 80', SURF_ID='ADIABATIC'/

&OBST ID='AcDbRegion - 11B2', XB=0.85,0.885,-1.81,-1.81,0.84,0.86, COLOR='GRAY 80', SURF_ID='ADIABATIC'/

&OBST ID='AcDbRegion - 11B2', XB=0.85,0.885,-1.81,-1.81,0.915,0.94, COLOR='GRAY 80', SURF_ID='ADIABATIC'/

&OBST ID='AcDbRegion - 11B2', XB=0.885,0.915,-1.81,-1.81,0.84,0.94, COLOR='GRAY 80', SURF_ID='ADIABATIC'/

&OBST ID='AcDbRegion - 11B2', XB=0.915,0.95,-1.81,-1.81,0.84,0.86, COLOR='GRAY 80', SURF_ID='ADIABATIC'/

&OBST ID='AcDbRegion - 11B2', XB=0.915,0.95,-1.81,-1.81,0.915,0.94, COLOR='GRAY 80', SURF_ID='ADIABATIC'/

&OBST ID='AcDbRegion - 11B2', XB=0.95,0.98,-1.81,-1.81,0.84,0.94, COLOR='GRAY 80', SURF_ID='ADIABATIC'/

&OBST ID='AcDbRegion - 11B2', XB=0.98,1.015,-1.81,-1.81,0.84,0.86, COLOR='GRAY 80', SURF_ID='ADIABATIC'/

&OBST ID='AcDbRegion - 11B2', XB=0.98,1.015,-1.81,-1.81,0.915,0.94, COLOR='GRAY 80', SURF_ID='ADIABATIC'/

&OBST ID='AcDbRegion - 11B2', XB=1.015,1.045,-1.81,-1.81,0.84,0.94, COLOR='GRAY 80', SURF_ID='ADIABATIC'/

&OBST ID='AcDbRegion - 11B2', XB=1.045,1.08,-1.81,-1.81,0.84,0.86, COLOR='GRAY 80', SURF_ID='ADIABATIC'/

&OBST ID='AcDbRegion - 11B2', XB=1.045,1.08,-1.81,-1.81,0.915,0.94, COLOR='GRAY 80', SURF_ID='ADIABATIC'/

&OBST ID='AcDbRegion - 11B2', XB=1.08,1.11,-1.81,-1.81,0.84,0.94, COLOR='GRAY 80', SURF_ID='ADIABATIC'/

&OBST ID='AcDbRegion - 11B2', XB=0.24,0.275,-1.81,-1.81,0.94,1.06, COLOR='GRAY 80', SURF_ID='ADIABATIC'/

&OBST ID='AcDbRegion - 11B2', XB=0.275,0.305,-1.81,-1.81,0.94,0.97, COLOR='GRAY 80', SURF_ID='ADIABATIC'/

&OBST ID='AcDbRegion - 11B2', XB=0.275,0.305,-1.81,-1.81,1.03,1.06, COLOR='GRAY 80', SURF_ID='ADIABATIC'/

&OBST ID='AcDbRegion - 11B2', XB=0.305,0.335,-1.81,-1.81,0.94,1.06, COLOR='GRAY 80', SURF_ID='ADIABATIC'/

&OBST ID='AcDbRegion - 11B2', XB=0.335,0.37,-1.81,-1.81,0.94,0.97, COLOR='GRAY 80', SURF_ID='ADIABATIC'/

&OBST ID='AcDbRegion - 11B2', XB=0.335,0.37,-1.81,-1.81,1.03,1.06, COLOR='GRAY 80', SURF_ID='ADIABATIC'/

&OBST ID='AcDbRegion - 11B2', XB=0.37,0.4,-1.81,-1.81,0.94,1.06, COLOR='GRAY 80', SURF_ID='ADIABATIC'/

&OBST ID='AcDbRegion - 11B2', XB=0.4,0.435,-1.81,-1.81,0.94,0.97, COLOR='GRAY 80', SURF_ID='ADIABATIC'/

&OBST ID='AcDbRegion - 11B2', XB=0.4,0.435,-1.81,-1.81,1.03,1.06, COLOR='GRAY 80', SURF_ID='ADIABATIC'/

&OBST ID='AcDbRegion - 11B2', XB=0.435,0.465,-1.81,-1.81,0.94,1.06, COLOR='GRAY 80', SURF_ID='ADIABATIC'/

&OBST ID='AcDbRegion - 11B2', XB=0.465,0.5,-1.81,-1.81,0.94,0.97, COLOR='GRAY 80', SURF_ID='ADIABATIC'/

&OBST ID='AcDbRegion - 11B2', XB=0.465,0.5,-1.81,-1.81,1.03,1.06, COLOR='GRAY 80', SURF_ID='ADIABATIC'/

&OBST ID='AcDbRegion - 11B2', XB=0.5,0.53,-1.81,-1.81,0.94,1.06, COLOR='GRAY 80', SURF_ID='ADIABATIC'/

&OBST ID='AcDbRegion - 11B2', XB=0.53,0.56,-1.81,-1.81,0.94,0.97, COLOR='GRAY 80', SURF_ID='ADIABATIC'/

&OBST ID='AcDbRegion - 11B2', XB=0.53,0.56,-1.81,-1.81,1.03,1.06, COLOR='GRAY 80', SURF_ID='ADIABATIC'/

&OBST ID='AcDbRegion - 11B2', XB=0.56,0.595,-1.81,-1.81,0.94,1.06, COLOR='GRAY 80', SURF_ID='ADIABATIC'/

&OBST ID='AcDbRegion - 11B2', XB=0.595,0.625,-1.81,-1.81,0.94,0.97, COLOR='GRAY 80', SURF_ID='ADIABATIC'/

&OBST ID='AcDbRegion - 11B2', XB=0.595,0.625,-1.81,-1.81,1.03,1.06, COLOR='GRAY 80', SURF_ID='ADIABATIC'/

&OBST ID='AcDbRegion - 11B2', XB=0.625,0.66,-1.81,-1.81,0.94,1.06, COLOR='GRAY 80', SURF_ID='ADIABATIC'/

&OBST ID='AcDbRegion - 11B2', XB=0.66,0.67,-1.81,-1.81,0.94,0.97, COLOR='GRAY 80', SURF_ID='ADIABATIC'/

&OBST ID='AcDbRegion - 11B2', XB=0.66,0.67,-1.81,-1.81,1.03,1.06, COLOR='GRAY 80', SURF_ID='ADIABATIC'/

&OBST ID='AcDbRegion - 11B2', XB=0.67,0.69,-1.81,-1.81,0.94,0.97, COLOR='GRAY 80', SURF_ID='ADIABATIC'/

&OBST ID='AcDbRegion - 11B2', XB=0.67,0.69,-1.81,-1.81,1.03,1.06, COLOR='GRAY 80', SURF_ID='ADIABATIC'/

&OBST ID='AcDbRegion - 11B2', XB=0.69,0.725,-1.81,-1.81,0.94,1.06, COLOR='GRAY 80', SURF_ID='ADIABATIC'/

&OBST ID='AcDbRegion - 11B2', XB=0.725,0.755,-1.81,-1.81,0.94,0.97, COLOR='GRAY 80', SURF_ID='ADIABATIC'/

&OBST ID='AcDbRegion - 11B2', XB=0.725,0.755,-1.81,-1.81,1.03,1.06, COLOR='GRAY 80', SURF_ID='ADIABATIC'/

&OBST ID='AcDbRegion - 11B2', XB=0.755,0.79,-1.81,-1.81,0.94,1.06, COLOR='GRAY 80', SURF_ID='ADIABATIC'/

&OBST ID='AcDbRegion - 11B2', XB=0.79,0.82,-1.81,-1.81,0.94,0.97, COLOR='GRAY 80', SURF_ID='ADIABATIC'/

&OBST ID='AcDbRegion - 11B2', XB=0.79,0.82,-1.81,-1.81,1.03,1.06, COLOR='GRAY 80', SURF_ID='ADIABATIC'/

&OBST ID='AcDbRegion - 11B2', XB=0.82,0.85,-1.81,-1.81,0.94,1.06, COLOR='GRAY 80', SURF_ID='ADIABATIC'/

&OBST ID='AcDbRegion - 11B2', XB=0.85,0.885,-1.81,-1.81,0.94,0.97, COLOR='GRAY 80', SURF_ID='ADIABATIC'/

&OBST ID='AcDbRegion - 11B2', XB=0.85,0.885,-1.81,-1.81,1.03,1.06, COLOR='GRAY 80', SURF_ID='ADIABATIC'/

&OBST ID='AcDbRegion - 11B2', XB=0.885,0.915,-1.81,-1.81,0.94,1.06, COLOR='GRAY 80', SURF_ID='ADIABATIC'/

&OBST ID='AcDbRegion - 11B2', XB=0.915,0.95,-1.81,-1.81,0.94,0.97, COLOR='GRAY 80', SURF_ID='ADIABATIC'/

&OBST ID='AcDbRegion - 11B2', XB=0.915,0.95,-1.81,-1.81,1.03,1.06, COLOR='GRAY 80', SURF_ID='ADIABATIC'/

&OBST ID='AcDbRegion - 11B2', XB=0.95,0.98,-1.81,-1.81,0.94,1.06, COLOR='GRAY 80', SURF_ID='ADIABATIC'/

&OBST ID='AcDbRegion - 11B2', XB=0.98,1.015,-1.81,-1.81,0.94,0.97, COLOR='GRAY 80', SURF_ID='ADIABATIC'/

&OBST ID='AcDbRegion - 11B2', XB=0.98,1.015,-1.81,-1.81,1.03,1.06, COLOR='GRAY 80', SURF_ID='ADIABATIC'/

&OBST ID='AcDbRegion - 11B2', XB=1.015,1.045,-1.81,-1.81,0.94,1.06, COLOR='GRAY 80', SURF_ID='ADIABATIC'/

&OBST ID='AcDbRegion - 11B2', XB=1.045,1.08,-1.81,-1.81,0.94,0.97, COLOR='GRAY 80', SURF_ID='ADIABATIC'/

&OBST ID='AcDbRegion - 11B2', XB=1.045,1.08,-1.81,-1.81,1.03,1.06, COLOR='GRAY 80', SURF_ID='ADIABATIC'/

&OBST ID='AcDbRegion - 11B2', XB=1.08,1.11,-1.81,-1.81,0.94,1.06, COLOR='GRAY 80', SURF_ID='ADIABATIC'/

&OBST ID='AcDbRegion - 11B2', XB=0.24,0.275,-1.81,-1.81,1.06,1.16, COLOR='GRAY 80', SURF_ID='ADIABATIC'/

&OBST ID='AcDbRegion - 11B2', XB=0.275,0.305,-1.81,-1.81,1.06,1.085, COLOR='GRAY 80', SURF_ID='ADIABATIC'/

&OBST ID='AcDbRegion - 11B2', XB=0.275,0.305,-1.81,-1.81,1.14,1.16, COLOR='GRAY 80', SURF_ID='ADIABATIC'/

&OBST ID='AcDbRegion - 11B2', XB=0.305,0.335,-1.81,-1.81,1.06,1.16, COLOR='GRAY 80', SURF_ID='ADIABATIC'/

&OBST ID='AcDbRegion - 11B2', XB=0.335,0.37,-1.81,-1.81,1.06,1.085, COLOR='GRAY 80', SURF_ID='ADIABATIC'/

&OBST ID='AcDbRegion - 11B2', XB=0.335,0.37,-1.81,-1.81,1.14,1.16, COLOR='GRAY 80', SURF_ID='ADIABATIC'/

&OBST ID='AcDbRegion - 11B2', XB=0.37,0.4,-1.81,-1.81,1.06,1.16, COLOR='GRAY 80', SURF_ID='ADIABATIC'/

&OBST ID='AcDbRegion - 11B2', XB=0.4,0.435,-1.81,-1.81,1.06,1.085, COLOR='GRAY 80', SURF_ID='ADIABATIC'/

&OBST ID='AcDbRegion - 11B2', XB=0.4,0.435,-1.81,-1.81,1.14,1.16, COLOR='GRAY 80', SURF_ID='ADIABATIC'/

&OBST ID='AcDbRegion - 11B2', XB=0.435,0.465,-1.81,-1.81,1.06,1.16, COLOR='GRAY 80', SURF_ID='ADIABATIC'/

&OBST ID='AcDbRegion - 11B2', XB=0.465,0.5,-1.81,-1.81,1.06,1.085, COLOR='GRAY 80', SURF_ID='ADIABATIC'/

&OBST ID='AcDbRegion - 11B2', XB=0.465,0.5,-1.81,-1.81,1.14,1.16, COLOR='GRAY 80', SURF_ID='ADIABATIC'/

&OBST ID='AcDbRegion - 11B2', XB=0.5,0.53,-1.81,-1.81,1.06,1.16, COLOR='GRAY 80', SURF_ID='ADIABATIC'/

&OBST ID='AcDbRegion - 11B2', XB=0.53,0.56,-1.81,-1.81,1.06,1.085, COLOR='GRAY 80', SURF_ID='ADIABATIC'/

&OBST ID='AcDbRegion - 11B2', XB=0.53,0.56,-1.81,-1.81,1.14,1.16, COLOR='GRAY 80', SURF_ID='ADIABATIC'/

&OBST ID='AcDbRegion - 11B2', XB=0.56,0.595,-1.81,-1.81,1.06,1.16, COLOR='GRAY 80', SURF_ID='ADIABATIC'/

&OBST ID='AcDbRegion - 11B2', XB=0.595,0.625,-1.81,-1.81,1.06,1.085, COLOR='GRAY 80', SURF_ID='ADIABATIC'/

&OBST ID='AcDbRegion - 11B2', XB=0.595,0.625,-1.81,-1.81,1.14,1.16, COLOR='GRAY 80', SURF_ID='ADIABATIC'/

&OBST ID='AcDbRegion - 11B2', XB=0.625,0.66,-1.81,-1.81,1.06,1.16, COLOR='GRAY 80', SURF_ID='ADIABATIC'/

&OBST ID='AcDbRegion - 11B2', XB=0.66,0.67,-1.81,-1.81,1.06,1.085, COLOR='GRAY 80', SURF_ID='ADIABATIC'/

&OBST ID='AcDbRegion - 11B2', XB=0.66,0.67,-1.81,-1.81,1.14,1.16, COLOR='GRAY 80', SURF_ID='ADIABATIC'/

&OBST ID='AcDbRegion - 11B2', XB=0.67,0.69,-1.81,-1.81,1.06,1.085, COLOR='GRAY 80', SURF_ID='ADIABATIC'/

&OBST ID='AcDbRegion - 11B2', XB=0.67,0.69,-1.81,-1.81,1.14,1.16, COLOR='GRAY 80', SURF_ID='ADIABATIC'/

&OBST ID='AcDbRegion - 11B2', XB=0.69,0.725,-1.81,-1.81,1.06,1.16, COLOR='GRAY 80', SURF_ID='ADIABATIC'/

&OBST ID='AcDbRegion - 11B2', XB=0.725,0.755,-1.81,-1.81,1.06,1.085, COLOR='GRAY 80', SURF_ID='ADIABATIC'/

&OBST ID='AcDbRegion - 11B2', XB=0.725,0.755,-1.81,-1.81,1.14,1.16, COLOR='GRAY 80', SURF_ID='ADIABATIC'/

&OBST ID='AcDbRegion - 11B2', XB=0.755,0.79,-1.81,-1.81,1.06,1.16, COLOR='GRAY 80', SURF_ID='ADIABATIC'/

&OBST ID='AcDbRegion - 11B2', XB=0.79,0.82,-1.81,-1.81,1.06,1.085, COLOR='GRAY 80', SURF_ID='ADIABATIC'/

&OBST ID='AcDbRegion - 11B2', XB=0.79,0.82,-1.81,-1.81,1.14,1.16, COLOR='GRAY 80', SURF_ID='ADIABATIC'/

&OBST ID='AcDbRegion - 11B2', XB=0.82,0.85,-1.81,-1.81,1.06,1.16, COLOR='GRAY 80', SURF_ID='ADIABATIC'/

&OBST ID='AcDbRegion - 11B2', XB=0.85,0.885,-1.81,-1.81,1.06,1.085, COLOR='GRAY 80', SURF_ID='ADIABATIC'/

&OBST ID='AcDbRegion - 11B2', XB=0.85,0.885,-1.81,-1.81,1.14,1.16, COLOR='GRAY 80', SURF_ID='ADIABATIC'/

&OBST ID='AcDbRegion - 11B2', XB=0.885,0.915,-1.81,-1.81,1.06,1.16, COLOR='GRAY 80', SURF_ID='ADIABATIC'/

&OBST ID='AcDbRegion - 11B2', XB=0.915,0.95,-1.81,-1.81,1.06,1.085, COLOR='GRAY 80', SURF_ID='ADIABATIC'/

&OBST ID='AcDbRegion - 11B2', XB=0.915,0.95,-1.81,-1.81,1.14,1.16, COLOR='GRAY 80', SURF_ID='ADIABATIC'/

&OBST ID='AcDbRegion - 11B2', XB=0.95,0.98,-1.81,-1.81,1.06,1.16, COLOR='GRAY 80', SURF_ID='ADIABATIC'/

&OBST ID='AcDbRegion - 11B2', XB=0.98,1.015,-1.81,-1.81,1.06,1.085, COLOR='GRAY 80', SURF_ID='ADIABATIC'/

&OBST ID='AcDbRegion - 11B2', XB=0.98,1.015,-1.81,-1.81,1.14,1.16, COLOR='GRAY 80', SURF_ID='ADIABATIC'/

&OBST ID='AcDbRegion - 11B2', XB=1.015,1.045,-1.81,-1.81,1.06,1.16, COLOR='GRAY 80', SURF_ID='ADIABATIC'/

&OBST ID='AcDbRegion - 11B2', XB=1.045,1.08,-1.81,-1.81,1.06,1.085, COLOR='GRAY 80', SURF_ID='ADIABATIC'/

&OBST ID='AcDbRegion - 11B2', XB=1.045,1.08,-1.81,-1.81,1.14,1.16, COLOR='GRAY 80', SURF_ID='ADIABATIC'/

&OBST ID='AcDbRegion - 11B2', XB=1.08,1.11,-1.81,-1.81,1.06,1.16, COLOR='GRAY 80', SURF_ID='ADIABATIC'/

&OBST ID='AcDbRegion - 11B2', XB=0.24,0.275,-1.81,-1.81,1.16,1.28, COLOR='GRAY 80', SURF_ID='ADIABATIC'/

&OBST ID='AcDbRegion - 11B2', XB=0.275,0.305,-1.81,-1.81,1.16,1.195, COLOR='GRAY 80', SURF_ID='ADIABATIC'/

&OBST ID='AcDbRegion - 11B2', XB=0.275,0.305,-1.81,-1.81,1.255,1.28, COLOR='GRAY 80', SURF_ID='ADIABATIC'/

&OBST ID='AcDbRegion - 11B2', XB=0.305,0.335,-1.81,-1.81,1.16,1.28, COLOR='GRAY 80', SURF_ID='ADIABATIC'/

&OBST ID='AcDbRegion - 11B2', XB=0.335,0.37,-1.81,-1.81,1.16,1.195, COLOR='GRAY 80', SURF_ID='ADIABATIC'/

&OBST ID='AcDbRegion - 11B2', XB=0.335,0.37,-1.81,-1.81,1.255,1.28, COLOR='GRAY 80', SURF_ID='ADIABATIC'/

&OBST ID='AcDbRegion - 11B2', XB=0.37,0.4,-1.81,-1.81,1.16,1.28, COLOR='GRAY 80', SURF_ID='ADIABATIC'/

&OBST ID='AcDbRegion - 11B2', XB=0.4,0.435,-1.81,-1.81,1.16,1.195, COLOR='GRAY 80', SURF_ID='ADIABATIC'/

&OBST ID='AcDbRegion - 11B2', XB=0.4,0.435,-1.81,-1.81,1.255,1.28, COLOR='GRAY 80', SURF_ID='ADIABATIC'/

&OBST ID='AcDbRegion - 11B2', XB=0.435,0.465,-1.81,-1.81,1.16,1.28, COLOR='GRAY 80', SURF_ID='ADIABATIC'/

&OBST ID='AcDbRegion - 11B2', XB=0.465,0.5,-1.81,-1.81,1.16,1.195, COLOR='GRAY 80', SURF_ID='ADIABATIC'/

&OBST ID='AcDbRegion - 11B2', XB=0.465,0.5,-1.81,-1.81,1.255,1.28, COLOR='GRAY 80', SURF_ID='ADIABATIC'/

&OBST ID='AcDbRegion - 11B2', XB=0.5,0.53,-1.81,-1.81,1.16,1.28, COLOR='GRAY 80', SURF_ID='ADIABATIC'/

&OBST ID='AcDbRegion - 11B2', XB=0.53,0.56,-1.81,-1.81,1.16,1.195, COLOR='GRAY 80', SURF_ID='ADIABATIC'/

&OBST ID='AcDbRegion - 11B2', XB=0.53,0.56,-1.81,-1.81,1.255,1.28, COLOR='GRAY 80', SURF_ID='ADIABATIC'/

&OBST ID='AcDbRegion - 11B2', XB=0.56,0.595,-1.81,-1.81,1.16,1.28, COLOR='GRAY 80', SURF_ID='ADIABATIC'/

&OBST ID='AcDbRegion - 11B2', XB=0.595,0.625,-1.81,-1.81,1.16,1.195, COLOR='GRAY 80', SURF_ID='ADIABATIC'/

&OBST ID='AcDbRegion - 11B2', XB=0.595,0.625,-1.81,-1.81,1.255,1.28, COLOR='GRAY 80', SURF_ID='ADIABATIC'/

&OBST ID='AcDbRegion - 11B2', XB=0.625,0.66,-1.81,-1.81,1.16,1.28, COLOR='GRAY 80', SURF_ID='ADIABATIC'/

&OBST ID='AcDbRegion - 11B2', XB=0.66,0.67,-1.81,-1.81,1.16,1.195, COLOR='GRAY 80', SURF_ID='ADIABATIC'/

&OBST ID='AcDbRegion - 11B2', XB=0.66,0.67,-1.81,-1.81,1.255,1.28, COLOR='GRAY 80', SURF_ID='ADIABATIC'/

&OBST ID='AcDbRegion - 11B2', XB=0.67,0.69,-1.81,-1.81,1.16,1.195, COLOR='GRAY 80', SURF_ID='ADIABATIC'/

&OBST ID='AcDbRegion - 11B2', XB=0.67,0.69,-1.81,-1.81,1.255,1.28, COLOR='GRAY 80', SURF_ID='ADIABATIC'/

&OBST ID='AcDbRegion - 11B2', XB=0.69,0.725,-1.81,-1.81,1.16,1.28, COLOR='GRAY 80', SURF_ID='ADIABATIC'/

&OBST ID='AcDbRegion - 11B2', XB=0.725,0.755,-1.81,-1.81,1.16,1.195, COLOR='GRAY 80', SURF_ID='ADIABATIC'/

&OBST ID='AcDbRegion - 11B2', XB=0.725,0.755,-1.81,-1.81,1.255,1.28, COLOR='GRAY 80', SURF_ID='ADIABATIC'/

&OBST ID='AcDbRegion - 11B2', XB=0.755,0.79,-1.81,-1.81,1.16,1.28, COLOR='GRAY 80', SURF_ID='ADIABATIC'/

&OBST ID='AcDbRegion - 11B2', XB=0.79,0.82,-1.81,-1.81,1.16,1.195, COLOR='GRAY 80', SURF_ID='ADIABATIC'/

&OBST ID='AcDbRegion - 11B2', XB=0.79,0.82,-1.81,-1.81,1.255,1.28, COLOR='GRAY 80', SURF_ID='ADIABATIC'/

&OBST ID='AcDbRegion - 11B2', XB=0.82,0.85,-1.81,-1.81,1.16,1.28, COLOR='GRAY 80', SURF_ID='ADIABATIC'/

&OBST ID='AcDbRegion - 11B2', XB=0.85,0.885,-1.81,-1.81,1.16,1.195, COLOR='GRAY 80', SURF_ID='ADIABATIC'/

&OBST ID='AcDbRegion - 11B2', XB=0.85,0.885,-1.81,-1.81,1.255,1.28, COLOR='GRAY 80', SURF_ID='ADIABATIC'/

&OBST ID='AcDbRegion - 11B2', XB=0.885,0.915,-1.81,-1.81,1.16,1.28, COLOR='GRAY 80', SURF_ID='ADIABATIC'/

&OBST ID='AcDbRegion - 11B2', XB=0.915,0.95,-1.81,-1.81,1.16,1.195, COLOR='GRAY 80', SURF_ID='ADIABATIC'/

&OBST ID='AcDbRegion - 11B2', XB=0.915,0.95,-1.81,-1.81,1.255,1.28, COLOR='GRAY 80', SURF_ID='ADIABATIC'/

&OBST ID='AcDbRegion - 11B2', XB=0.95,0.98,-1.81,-1.81,1.16,1.28, COLOR='GRAY 80', SURF_ID='ADIABATIC'/

&OBST ID='AcDbRegion - 11B2', XB=0.98,1.015,-1.81,-1.81,1.16,1.195, COLOR='GRAY 80', SURF_ID='ADIABATIC'/

&OBST ID='AcDbRegion - 11B2', XB=0.98,1.015,-1.81,-1.81,1.255,1.28, COLOR='GRAY 80', SURF_ID='ADIABATIC'/

&OBST ID='AcDbRegion - 11B2', XB=1.015,1.045,-1.81,-1.81,1.16,1.28, COLOR='GRAY 80', SURF_ID='ADIABATIC'/

&OBST ID='AcDbRegion - 11B2', XB=1.045,1.08,-1.81,-1.81,1.16,1.195, COLOR='GRAY 80', SURF_ID='ADIABATIC'/

&OBST ID='AcDbRegion - 11B2', XB=1.045,1.08,-1.81,-1.81,1.255,1.28, COLOR='GRAY 80', SURF_ID='ADIABATIC'/

&OBST ID='AcDbRegion - 11B2', XB=1.08,1.11,-1.81,-1.81,1.16,1.28, COLOR='GRAY 80', SURF_ID='ADIABATIC'/

&OBST ID='AcDbRegion - 11B2', XB=0.24,0.275,-1.81,-1.81,1.28,1.395, COLOR='GRAY 80', SURF_ID='ADIABATIC'/

&OBST ID='AcDbRegion - 11B2', XB=0.275,0.305,-1.81,-1.81,1.28,1.31, COLOR='GRAY 80', SURF_ID='ADIABATIC'/

&OBST ID='AcDbRegion - 11B2', XB=0.275,0.305,-1.81,-1.81,1.365,1.395, COLOR='GRAY 80', SURF_ID='ADIABATIC'/

&OBST ID='AcDbRegion - 11B2', XB=0.305,0.335,-1.81,-1.81,1.28,1.395, COLOR='GRAY 80', SURF_ID='ADIABATIC'/

&OBST ID='AcDbRegion - 11B2', XB=0.335,0.37,-1.81,-1.81,1.28,1.31, COLOR='GRAY 80', SURF_ID='ADIABATIC'/

&OBST ID='AcDbRegion - 11B2', XB=0.335,0.37,-1.81,-1.81,1.365,1.395, COLOR='GRAY 80', SURF_ID='ADIABATIC'/

&OBST ID='AcDbRegion - 11B2', XB=0.37,0.4,-1.81,-1.81,1.28,1.395, COLOR='GRAY 80', SURF_ID='ADIABATIC'/

&OBST ID='AcDbRegion - 11B2', XB=0.4,0.435,-1.81,-1.81,1.28,1.31, COLOR='GRAY 80', SURF_ID='ADIABATIC'/

&OBST ID='AcDbRegion - 11B2', XB=0.4,0.435,-1.81,-1.81,1.365,1.395, COLOR='GRAY 80', SURF_ID='ADIABATIC'/

&OBST ID='AcDbRegion - 11B2', XB=0.435,0.465,-1.81,-1.81,1.28,1.395, COLOR='GRAY 80', SURF_ID='ADIABATIC'/

&OBST ID='AcDbRegion - 11B2', XB=0.465,0.5,-1.81,-1.81,1.28,1.31, COLOR='GRAY 80', SURF_ID='ADIABATIC'/

&OBST ID='AcDbRegion - 11B2', XB=0.465,0.5,-1.81,-1.81,1.365,1.395, COLOR='GRAY 80', SURF_ID='ADIABATIC'/

&OBST ID='AcDbRegion - 11B2', XB=0.5,0.53,-1.81,-1.81,1.28,1.395, COLOR='GRAY 80', SURF_ID='ADIABATIC'/

&OBST ID='AcDbRegion - 11B2', XB=0.53,0.56,-1.81,-1.81,1.28,1.31, COLOR='GRAY 80', SURF_ID='ADIABATIC'/

&OBST ID='AcDbRegion - 11B2', XB=0.53,0.56,-1.81,-1.81,1.365,1.395, COLOR='GRAY 80', SURF_ID='ADIABATIC'/

&OBST ID='AcDbRegion - 11B2', XB=0.56,0.595,-1.81,-1.81,1.28,1.395, COLOR='GRAY 80', SURF_ID='ADIABATIC'/

&OBST ID='AcDbRegion - 11B2', XB=0.595,0.625,-1.81,-1.81,1.28,1.31, COLOR='GRAY 80', SURF_ID='ADIABATIC'/

&OBST ID='AcDbRegion - 11B2', XB=0.595,0.625,-1.81,-1.81,1.365,1.395, COLOR='GRAY 80', SURF_ID='ADIABATIC'/

&OBST ID='AcDbRegion - 11B2', XB=0.625,0.66,-1.81,-1.81,1.28,1.395, COLOR='GRAY 80', SURF_ID='ADIABATIC'/

&OBST ID='AcDbRegion - 11B2', XB=0.66,0.67,-1.81,-1.81,1.28,1.31, COLOR='GRAY 80', SURF_ID='ADIABATIC'/

&OBST ID='AcDbRegion - 11B2', XB=0.66,0.67,-1.81,-1.81,1.365,1.395, COLOR='GRAY 80', SURF_ID='ADIABATIC'/

&OBST ID='AcDbRegion - 11B2', XB=0.67,0.69,-1.81,-1.81,1.28,1.31, COLOR='GRAY 80', SURF_ID='ADIABATIC'/

&OBST ID='AcDbRegion - 11B2', XB=0.67,0.69,-1.81,-1.81,1.365,1.395, COLOR='GRAY 80', SURF_ID='ADIABATIC'/

&OBST ID='AcDbRegion - 11B2', XB=0.69,0.725,-1.81,-1.81,1.28,1.395, COLOR='GRAY 80', SURF_ID='ADIABATIC'/

&OBST ID='AcDbRegion - 11B2', XB=0.725,0.755,-1.81,-1.81,1.28,1.31, COLOR='GRAY 80', SURF_ID='ADIABATIC'/

&OBST ID='AcDbRegion - 11B2', XB=0.725,0.755,-1.81,-1.81,1.365,1.395, COLOR='GRAY 80', SURF_ID='ADIABATIC'/

&OBST ID='AcDbRegion - 11B2', XB=0.755,0.79,-1.81,-1.81,1.28,1.395, COLOR='GRAY 80', SURF_ID='ADIABATIC'/

&OBST ID='AcDbRegion - 11B2', XB=0.79,0.82,-1.81,-1.81,1.28,1.31, COLOR='GRAY 80', SURF_ID='ADIABATIC'/

&OBST ID='AcDbRegion - 11B2', XB=0.79,0.82,-1.81,-1.81,1.365,1.395, COLOR='GRAY 80', SURF_ID='ADIABATIC'/

&OBST ID='AcDbRegion - 11B2', XB=0.82,0.85,-1.81,-1.81,1.28,1.395, COLOR='GRAY 80', SURF_ID='ADIABATIC'/

&OBST ID='AcDbRegion - 11B2', XB=0.85,0.885,-1.81,-1.81,1.28,1.31, COLOR='GRAY 80', SURF_ID='ADIABATIC'/

&OBST ID='AcDbRegion - 11B2', XB=0.85,0.885,-1.81,-1.81,1.365,1.395, COLOR='GRAY 80', SURF_ID='ADIABATIC'/

&OBST ID='AcDbRegion - 11B2', XB=0.885,0.915,-1.81,-1.81,1.28,1.395, COLOR='GRAY 80', SURF_ID='ADIABATIC'/

&OBST ID='AcDbRegion - 11B2', XB=0.915,0.95,-1.81,-1.81,1.28,1.31, COLOR='GRAY 80', SURF_ID='ADIABATIC'/

&OBST ID='AcDbRegion - 11B2', XB=0.915,0.95,-1.81,-1.81,1.365,1.395, COLOR='GRAY 80', SURF_ID='ADIABATIC'/

&OBST ID='AcDbRegion - 11B2', XB=0.95,0.98,-1.81,-1.81,1.28,1.395, COLOR='GRAY 80', SURF_ID='ADIABATIC'/

&OBST ID='AcDbRegion - 11B2', XB=0.98,1.015,-1.81,-1.81,1.28,1.31, COLOR='GRAY 80', SURF_ID='ADIABATIC'/

&OBST ID='AcDbRegion - 11B2', XB=0.98,1.015,-1.81,-1.81,1.365,1.395, COLOR='GRAY 80', SURF_ID='ADIABATIC'/

&OBST ID='AcDbRegion - 11B2', XB=1.015,1.045,-1.81,-1.81,1.28,1.395, COLOR='GRAY 80', SURF_ID='ADIABATIC'/

&OBST ID='AcDbRegion - 11B2', XB=1.045,1.08,-1.81,-1.81,1.28,1.31, COLOR='GRAY 80', SURF_ID='ADIABATIC'/

&OBST ID='AcDbRegion - 11B2', XB=1.045,1.08,-1.81,-1.81,1.365,1.395, COLOR='GRAY 80', SURF_ID='ADIABATIC'/

&OBST ID='AcDbRegion - 11B2', XB=1.08,1.11,-1.81,-1.81,1.28,1.395, COLOR='GRAY 80', SURF_ID='ADIABATIC'/

&OBST ID='north wall', XB=0.24,0.65,-0.94,-0.94,0.6,0.72, COLOR='GRAY 68', SURF_ID='ADIABATIC'/

&OBST ID='north wall', XB=0.65,0.68,-0.94,-0.94,0.6,0.63, COLOR='GRAY 68', SURF_ID='ADIABATIC'/

&OBST ID='north wall', XB=0.65,0.68,-0.94,-0.94,0.7,0.72, COLOR='GRAY 68', SURF_ID='ADIABATIC'/

&OBST ID='north wall', XB=0.68,0.69,-0.94,-0.94,0.6,0.72, COLOR='GRAY 68', SURF_ID='ADIABATIC'/

&OBST ID='north wall', XB=0.69,1.11,-0.94,-0.94,0.6,0.72, COLOR='GRAY 68', SURF_ID='ADIABATIC'/

&OBST ID='north wall', XB=0.24,0.65,-0.94,-0.94,0.72,0.84, COLOR='GRAY 68', SURF_ID='ADIABATIC'/

&OBST ID='north wall', XB=0.65,0.68,-0.94,-0.94,0.72,0.74, COLOR='GRAY 68', SURF_ID='ADIABATIC'/

&OBST ID='north wall', XB=0.65,0.68,-0.94,-0.94,0.81,0.84, COLOR='GRAY 68', SURF_ID='ADIABATIC'/

&OBST ID='north wall', XB=0.68,0.69,-0.94,-0.94,0.72,0.84, COLOR='GRAY 68', SURF_ID='ADIABATIC'/

&OBST ID='north wall', XB=0.69,1.11,-0.94,-0.94,0.72,0.84, COLOR='GRAY 68', SURF_ID='ADIABATIC'/

&OBST ID='north wall', XB=0.24,0.65,-0.94,-0.94,0.84,0.94, COLOR='GRAY 68', SURF_ID='ADIABATIC'/

&OBST ID='north wall', XB=0.65,0.68,-0.94,-0.94,0.84,0.85, COLOR='GRAY 68', SURF_ID='ADIABATIC'/

&OBST ID='north wall', XB=0.65,0.68,-0.94,-0.94,0.92,0.94, COLOR='GRAY 68', SURF_ID='ADIABATIC'/

&OBST ID='north wall', XB=0.68,0.69,-0.94,-0.94,0.84,0.94, COLOR='GRAY 68', SURF_ID='ADIABATIC'/

&OBST ID='north wall', XB=0.69,1.11,-0.94,-0.94,0.84,0.94, COLOR='GRAY 68', SURF_ID='ADIABATIC'/

&OBST ID='north wall', XB=0.24,0.65,-0.94,-0.94,0.94,1.06, COLOR='GRAY 68', SURF_ID='ADIABATIC'/

&OBST ID='north wall', XB=0.65,0.68,-0.94,-0.94,0.94,0.97, COLOR='GRAY 68', SURF_ID='ADIABATIC'/

&OBST ID='north wall', XB=0.65,0.68,-0.94,-0.94,1.04,1.06, COLOR='GRAY 68', SURF_ID='ADIABATIC'/

&OBST ID='north wall', XB=0.68,0.69,-0.94,-0.94,0.94,1.06, COLOR='GRAY 68', SURF_ID='ADIABATIC'/

&OBST ID='north wall', XB=0.69,1.11,-0.94,-0.94,0.94,1.06, COLOR='GRAY 68', SURF_ID='ADIABATIC'/

&OBST ID='north wall', XB=0.24,0.65,-0.94,-0.94,1.06,1.16, COLOR='GRAY 68', SURF_ID='ADIABATIC'/

&OBST ID='north wall', XB=0.65,0.68,-0.94,-0.94,1.06,1.08, COLOR='GRAY 68', SURF_ID='ADIABATIC'/

&OBST ID='north wall', XB=0.65,0.68,-0.94,-0.94,1.15,1.16, COLOR='GRAY 68', SURF_ID='ADIABATIC'/

&OBST ID='north wall', XB=0.68,0.69,-0.94,-0.94,1.06,1.16, COLOR='GRAY 68', SURF_ID='ADIABATIC'/

&OBST ID='north wall', XB=0.69,1.11,-0.94,-0.94,1.06,1.16, COLOR='GRAY 68', SURF_ID='ADIABATIC'/

&OBST ID='north wall', XB=0.24,0.65,-0.94,-0.94,1.16,1.28, COLOR='GRAY 68', SURF_ID='ADIABATIC'/

&OBST ID='north wall', XB=0.65,0.68,-0.94,-0.94,1.16,1.19, COLOR='GRAY 68', SURF_ID='ADIABATIC'/

&OBST ID='north wall', XB=0.65,0.68,-0.94,-0.94,1.26,1.28, COLOR='GRAY 68', SURF_ID='ADIABATIC'/

&OBST ID='north wall', XB=0.68,0.69,-0.94,-0.94,1.16,1.28, COLOR='GRAY 68', SURF_ID='ADIABATIC'/

&OBST ID='north wall', XB=0.69,1.11,-0.94,-0.94,1.16,1.28, COLOR='GRAY 68', SURF_ID='ADIABATIC'/

&OBST ID='north wall', XB=0.24,0.65,-0.94,-0.94,1.28,1.39, COLOR='GRAY 68', SURF_ID='ADIABATIC'/

&OBST ID='north wall', XB=0.65,0.68,-0.94,-0.94,1.28,1.3, COLOR='GRAY 68', SURF_ID='ADIABATIC'/

&OBST ID='north wall', XB=0.65,0.68,-0.94,-0.94,1.37,1.39, COLOR='GRAY 68', SURF_ID='ADIABATIC'/

&OBST ID='north wall', XB=0.68,0.69,-0.94,-0.94,1.28,1.39, COLOR='GRAY 68', SURF_ID='ADIABATIC'/

&OBST ID='north wall', XB=0.69,1.11,-0.94,-0.94,1.28,1.39, COLOR='GRAY 68', SURF_ID='ADIABATIC'/

&VENT ID='Mesh Vent: Meshnew-a-a-a [XMIN]', SURF_ID='ADIABATIC', XB=0.24,0.24,-1.86,-1.8,0.6,0.72/

&VENT ID='Mesh Vent: Meshnew-a-a-a [YMIN]', SURF_ID='ADIABATIC', XB=0.24,0.67,-1.86,-1.86,0.6,0.72/

&VENT ID='Mesh Vent: Meshnew-a-a-a [ZMIN]', SURF_ID='ADIABATIC', XB=0.24,0.67,-1.86,-1.8,0.6,0.6/

&VENT ID='Mesh Vent: Meshnew-a-a-b [XMAX]', SURF_ID='ADIABATIC', XB=1.12,1.12,-1.86,-1.8,0.6,0.72/

&VENT ID='Mesh Vent: Meshnew-a-a-b [YMIN]', SURF_ID='ADIABATIC', XB=0.67,1.12,-1.86,-1.86,0.6,0.72/

&VENT ID='Mesh Vent: Meshnew-a-a-b [ZMIN]', SURF_ID='ADIABATIC', XB=0.67,1.12,-1.86,-1.8,0.6,0.6/

&VENT ID='Mesh Vent: Meshnew-a-b-a [XMIN]', SURF_ID='ADIABATIC', XB=0.24,0.24,-1.86,-1.8,0.72,0.84/

&VENT ID='Mesh Vent: Meshnew-a-b-a [YMIN]', SURF_ID='ADIABATIC', XB=0.24,0.67,-1.86,-1.86,0.72,0.84/

&VENT ID='Mesh Vent: Meshnew-a-b-b [XMAX]', SURF_ID='ADIABATIC', XB=1.12,1.12,-1.86,-1.8,0.72,0.84/

&VENT ID='Mesh Vent: Meshnew-a-b-b [YMIN]', SURF_ID='ADIABATIC', XB=0.67,1.12,-1.86,-1.86,0.72,0.84/

&VENT ID='Mesh Vent: Meshnew-a-c-a [XMIN]', SURF_ID='ADIABATIC', XB=0.24,0.24,-1.86,-1.8,0.84,0.94/

&VENT ID='Mesh Vent: Meshnew-a-c-a [YMIN]', SURF_ID='ADIABATIC', XB=0.24,0.67,-1.86,-1.86,0.84,0.94/

&VENT ID='Mesh Vent: Meshnew-a-c-b [XMAX]', SURF_ID='ADIABATIC', XB=1.12,1.12,-1.86,-1.8,0.84,0.94/

&VENT ID='Mesh Vent: Meshnew-a-c-b [YMIN]', SURF_ID='ADIABATIC', XB=0.67,1.12,-1.86,-1.86,0.84,0.94/

&VENT ID='Mesh Vent: Meshnew-a-d-a [XMIN]', SURF_ID='ADIABATIC', XB=0.24,0.24,-1.86,-1.8,0.94,1.06/

&VENT ID='Mesh Vent: Meshnew-a-d-a [YMIN]', SURF_ID='ADIABATIC', XB=0.24,0.67,-1.86,-1.86,0.94,1.06/

&VENT ID='Mesh Vent: Meshnew-a-d-b [XMAX]', SURF_ID='ADIABATIC', XB=1.12,1.12,-1.86,-1.8,0.94,1.06/

&VENT ID='Mesh Vent: Meshnew-a-d-b [YMIN]', SURF_ID='ADIABATIC', XB=0.67,1.12,-1.86,-1.86,0.94,1.06/

&VENT ID='Mesh Vent: Meshnew-a-e-a [XMIN]', SURF_ID='ADIABATIC', XB=0.24,0.24,-1.86,-1.8,1.06,1.16/

&VENT ID='Mesh Vent: Meshnew-a-e-a [YMIN]', SURF_ID='ADIABATIC', XB=0.24,0.67,-1.86,-1.86,1.06,1.16/

&VENT ID='Mesh Vent: Meshnew-a-e-b [XMAX]', SURF_ID='ADIABATIC', XB=1.12,1.12,-1.86,-1.8,1.06,1.16/

&VENT ID='Mesh Vent: Meshnew-a-e-b [YMIN]', SURF_ID='ADIABATIC', XB=0.67,1.12,-1.86,-1.86,1.06,1.16/

&VENT ID='Mesh Vent: Meshnew-a-f-a [XMIN]', SURF_ID='ADIABATIC', XB=0.24,0.24,-1.86,-1.8,1.16,1.28/

&VENT ID='Mesh Vent: Meshnew-a-f-a [YMIN]', SURF_ID='ADIABATIC', XB=0.24,0.67,-1.86,-1.86,1.16,1.28/

&VENT ID='Mesh Vent: Meshnew-a-f-b [XMAX]', SURF_ID='ADIABATIC', XB=1.12,1.12,-1.86,-1.8,1.16,1.28/

&VENT ID='Mesh Vent: Meshnew-a-f-b [YMIN]', SURF_ID='ADIABATIC', XB=0.67,1.12,-1.86,-1.86,1.16,1.28/

&VENT ID='Mesh Vent: Meshnew-a-g-a [XMIN]', SURF_ID='ADIABATIC', XB=0.24,0.24,-1.86,-1.8,1.28,1.4/

&VENT ID='Mesh Vent: Meshnew-a-g-a [YMIN]', SURF_ID='ADIABATIC', XB=0.24,0.67,-1.86,-1.86,1.28,1.4/

&VENT ID='Mesh Vent: Meshnew-a-g-b [XMAX]', SURF_ID='ADIABATIC', XB=1.12,1.12,-1.86,-1.8,1.28,1.4/

&VENT ID='Mesh Vent: Meshnew-a-g-b [YMIN]', SURF_ID='ADIABATIC', XB=0.67,1.12,-1.86,-1.86,1.28,1.4/

&VENT ID='Mesh Vent: Meshnew-a-h [XMAX]', SURF_ID='ADIABATIC', XB=1.12,1.12,-1.86,-1.8,1.4,1.5/

&VENT ID='Mesh Vent: Meshnew-a-h [XMIN]', SURF_ID='ADIABATIC', XB=0.24,0.24,-1.86,-1.8,1.4,1.5/

&VENT ID='Mesh Vent: Meshnew-a-h [YMIN]', SURF_ID='ADIABATIC', XB=0.24,1.12,-1.86,-1.86,1.4,1.5/

&VENT ID='Mesh Vent: Meshnew-a-i-a [XMIN]', SURF_ID='ADIABATIC', XB=0.24,0.24,-1.8,-0.84,0.6,0.72/

&VENT ID='Mesh Vent: Meshnew-a-i-a [ZMIN]', SURF_ID='ADIABATIC', XB=0.24,0.69,-1.8,-0.84,0.6,0.6/

&VENT ID='Mesh Vent: Meshnew-a-i-b [XMAX]', SURF_ID='ADIABATIC', XB=1.12,1.12,-1.8,-0.84,0.6,0.72/

&VENT ID='Mesh Vent: Meshnew-a-i-b [ZMIN]', SURF_ID='ADIABATIC', XB=0.69,1.12,-1.8,-0.84,0.6,0.6/

&VENT ID='Mesh Vent: Meshnew-a-j-a [XMIN]', SURF_ID='ADIABATIC', XB=0.24,0.24,-1.8,-0.84,0.72,0.84/

&VENT ID='Mesh Vent: Meshnew-a-j-b [XMAX]', SURF_ID='ADIABATIC', XB=1.12,1.12,-1.8,-0.84,0.72,0.84/

&VENT ID='Mesh Vent: Meshnew-a-k-a [XMIN]', SURF_ID='ADIABATIC', XB=0.24,0.24,-1.8,-0.84,0.84,0.94/

&VENT ID='Mesh Vent: Meshnew-a-k-b [XMAX]', SURF_ID='ADIABATIC', XB=1.12,1.12,-1.8,-0.84,0.84,0.94/

&VENT ID='Mesh Vent: Meshnew-a-l-a [XMIN]', SURF_ID='ADIABATIC', XB=0.24,0.24,-1.8,-0.84,0.94,1.06/

&VENT ID='Mesh Vent: Meshnew-a-l-b [XMAX]', SURF_ID='ADIABATIC', XB=1.12,1.12,-1.8,-0.84,0.94,1.06/

&VENT ID='Mesh Vent: Meshnew-a-m-a [XMIN]', SURF_ID='ADIABATIC', XB=0.24,0.24,-1.8,-0.84,1.06,1.16/

&VENT ID='Mesh Vent: Meshnew-a-m-b [XMAX]', SURF_ID='ADIABATIC', XB=1.12,1.12,-1.8,-0.84,1.06,1.16/

&VENT ID='Mesh Vent: Meshnew-a-n-a [XMIN]', SURF_ID='ADIABATIC', XB=0.24,0.24,-1.8,-0.84,1.16,1.28/

&VENT ID='Mesh Vent: Meshnew-a-n-b [XMAX]', SURF_ID='ADIABATIC', XB=1.12,1.12,-1.8,-0.84,1.16,1.28/

&VENT ID='Mesh Vent: Meshnew-a-o-a [XMIN]', SURF_ID='ADIABATIC', XB=0.24,0.24,-1.8,-0.84,1.28,1.4/

&VENT ID='Mesh Vent: Meshnew-a-o-b [XMAX]', SURF_ID='ADIABATIC', XB=1.12,1.12,-1.8,-0.84,1.28,1.4/

&VENT ID='Mesh Vent: Meshnew-a-p-a [XMIN]', SURF_ID='ADIABATIC', XB=0.24,0.24,-1.8,-0.84,1.4,1.5/

&VENT ID='Mesh Vent: Meshnew-a-p-b [XMAX]', SURF_ID='ADIABATIC', XB=1.12,1.12,-1.8,-0.84,1.4,1.5/

&VENT ID='Mesh Vent: Meshnew-b-a-a [XMIN]', SURF_ID='ADIABATIC', XB=0.24,0.24,-1.86,-0.84,1.5,1.61/

&VENT ID='Mesh Vent: Meshnew-b-a-a [YMIN]', SURF_ID='ADIABATIC', XB=0.24,0.68,-1.86,-1.86,1.5,1.61/

&VENT ID='Mesh Vent: Meshnew-b-a-b [XMIN]', SURF_ID='ADIABATIC', XB=0.24,0.24,-1.86,-0.84,1.61,1.72/

&VENT ID='Mesh Vent: Meshnew-b-a-b [YMIN]', SURF_ID='ADIABATIC', XB=0.24,0.68,-1.86,-1.86,1.61,1.72/

&VENT ID='Mesh Vent: Meshnew-b-b-a [XMAX]', SURF_ID='ADIABATIC', XB=1.12,1.12,-1.86,-0.84,1.5,1.61/

&VENT ID='Mesh Vent: Meshnew-b-b-a [YMIN]', SURF_ID='ADIABATIC', XB=0.68,1.12,-1.86,-1.86,1.5,1.61/

&VENT ID='Mesh Vent: Meshnew-b-b-b [XMAX]', SURF_ID='ADIABATIC', XB=1.12,1.12,-1.86,-0.84,1.61,1.72/

&VENT ID='Mesh Vent: Meshnew-b-b-b [YMIN]', SURF_ID='ADIABATIC', XB=0.68,1.12,-1.86,-1.86,1.61,1.72/

&VENT ID='Mesh Vent: Meshnew-c-a [XMIN]', SURF_ID='ADIABATIC', XB=0.24,0.24,-1.86,-0.84,1.72,2.0/

&VENT ID='Mesh Vent: Meshnew-c-a [YMIN]', SURF_ID='ADIABATIC', XB=0.24,0.7,-1.86,-1.86,1.72,2.0/

&VENT ID='Mesh Vent: Meshnew-c-a [ZMAX]', SURF_ID='OPEN', XB=0.24,0.7,-1.86,-0.84,2.0,2.0/

&VENT ID='Mesh Vent: Meshnew-c-b [XMAX]', SURF_ID='ADIABATIC', XB=1.12,1.12,-1.86,-0.84,1.72,2.0/

&VENT ID='Mesh Vent: Meshnew-c-b [YMIN]', SURF_ID='ADIABATIC', XB=0.7,1.12,-1.86,-1.86,1.72,2.0/

&VENT ID='Mesh Vent: Meshnew-c-b [ZMAX]', SURF_ID='OPEN', XB=0.7,1.12,-1.86,-0.84,2.0,2.0/

&VENT ID='Mesh Vent: Meshnew-d-a-a [XMAX]', SURF_ID='ADIABATIC', XB=1.12,1.12,-0.84,-0.58,0.6,0.84/

&VENT ID='Mesh Vent: Meshnew-d-a-a [XMIN]', SURF_ID='ADIABATIC', XB=0.24,0.24,-0.84,-0.58,0.6,0.84/

&VENT ID='Mesh Vent: Meshnew-d-a-a [ZMIN]', SURF_ID='ADIABATIC', XB=0.24,1.12,-0.84,-0.58,0.6,0.6/

&VENT ID='Mesh Vent: Meshnew-d-a-b [XMAX]', SURF_ID='ADIABATIC', XB=1.12,1.12,-0.84,-0.58,0.84,1.06/

&VENT ID='Mesh Vent: Meshnew-d-a-b [XMIN]', SURF_ID='ADIABATIC', XB=0.24,0.24,-0.84,-0.58,0.84,1.06/

&VENT ID='Mesh Vent: Meshnew-d-b-a [XMAX]', SURF_ID='ADIABATIC', XB=1.12,1.12,-0.84,-0.58,1.06,1.28/

&VENT ID='Mesh Vent: Meshnew-d-b-a [XMIN]', SURF_ID='ADIABATIC', XB=0.24,0.24,-0.84,-0.58,1.06,1.28/

&VENT ID='Mesh Vent: Meshnew-d-b-b [XMAX]', SURF_ID='ADIABATIC', XB=1.12,1.12,-0.84,-0.58,1.28,1.5/

&VENT ID='Mesh Vent: Meshnew-d-b-b [XMIN]', SURF_ID='ADIABATIC', XB=0.24,0.24,-0.84,-0.58,1.28,1.5/

&VENT ID='Mesh Vent: Meshnew-e [XMAX]', SURF_ID='ADIABATIC', XB=1.12,1.12,-0.84,-0.58,1.5,1.72/

&VENT ID='Mesh Vent: Meshnew-e [XMIN]', SURF_ID='ADIABATIC', XB=0.24,0.24,-0.84,-0.58,1.5,1.72/

&VENT ID='Mesh Vent: Meshnew-f [XMAX]', SURF_ID='ADIABATIC', XB=1.12,1.12,-0.84,-0.58,1.72,2.0/

&VENT ID='Mesh Vent: Meshnew-f [XMIN]', SURF_ID='ADIABATIC', XB=0.24,0.24,-0.84,-0.58,1.72,2.0/

&VENT ID='Mesh Vent: Meshnew-f [ZMAX]', SURF_ID='OPEN', XB=0.24,1.12,-0.84,-0.58,2.0,2.0/

&VENT ID='Mesh Vent: Meshnew-g-a-a [XMAX]', SURF_ID='ADIABATIC', XB=1.12,1.12,-0.58,-0.28,0.6,0.84/

&VENT ID='Mesh Vent: Meshnew-g-a-a [XMIN]', SURF_ID='ADIABATIC', XB=0.24,0.24,-0.58,-0.28,0.6,0.84/

&VENT ID='Mesh Vent: Meshnew-g-a-a [YMAX]', SURF_ID='OPEN', XB=0.24,1.12,-0.28,-0.28,0.6,0.84/

&VENT ID='Mesh Vent: Meshnew-g-a-a [ZMIN]', SURF_ID='ADIABATIC', XB=0.24,1.12,-0.58,-0.28,0.6,0.6/

&VENT ID='Mesh Vent: Meshnew-g-a-b [XMAX]', SURF_ID='ADIABATIC', XB=1.12,1.12,-0.58,-0.28,0.84,1.06/

&VENT ID='Mesh Vent: Meshnew-g-a-b [XMIN]', SURF_ID='ADIABATIC', XB=0.24,0.24,-0.58,-0.28,0.84,1.06/

&VENT ID='Mesh Vent: Meshnew-g-a-b [YMAX]', SURF_ID='OPEN', XB=0.24,1.12,-0.28,-0.28,0.84,1.06/

&VENT ID='Mesh Vent: Meshnew-g-b [XMAX]', SURF_ID='ADIABATIC', XB=1.12,1.12,-0.58,-0.28,1.06,1.5/

&VENT ID='Mesh Vent: Meshnew-g-b [XMIN]', SURF_ID='ADIABATIC', XB=0.24,0.24,-0.58,-0.28,1.06,1.5/

&VENT ID='Mesh Vent: Meshnew-g-b [YMAX]', SURF_ID='OPEN', XB=0.24,1.12,-0.28,-0.28,1.06,1.5/

&VENT ID='Mesh Vent: Meshnew-h-merged-a [XMAX]', SURF_ID='ADIABATIC', XB=1.12,1.12,-0.58,-0.28,1.5,1.72/

&VENT ID='Mesh Vent: Meshnew-h-merged-a [XMIN]', SURF_ID='ADIABATIC', XB=0.24,0.24,-0.58,-0.28,1.5,1.72/

&VENT ID='Mesh Vent: Meshnew-h-merged-a [YMAX]', SURF_ID='OPEN', XB=0.24,1.12,-0.28,-0.28,1.5,1.72/

&VENT ID='Mesh Vent: Meshnew-h-merged-b [XMAX]', SURF_ID='ADIABATIC', XB=1.12,1.12,-0.58,-0.28,1.72,2.0/

&VENT ID='Mesh Vent: Meshnew-h-merged-b [XMIN]', SURF_ID='ADIABATIC', XB=0.24,0.24,-0.58,-0.28,1.72,2.0/

&VENT ID='Mesh Vent: Meshnew-h-merged-b [YMAX]', SURF_ID='OPEN', XB=0.24,1.12,-0.28,-0.28,1.72,2.0/

&VENT ID='Mesh Vent: Meshnew-h-merged-b [ZMAX]', SURF_ID='OPEN', XB=0.24,1.12,-0.58,-0.28,2.0,2.0/

&SLCF QUANTITY='VELOCITY', VECTOR=.TRUE., PBY=-1.340646/

&SLCF QUANTITY='TEMPERATURE', PBY=-1.340646/

&SLCF QUANTITY='VELOCITY', VECTOR=.TRUE., PBY=-0.954246/

&SLCF QUANTITY='TEMPERATURE', PBY=-0.954246/

&SLCF QUANTITY='VELOCITY', VECTOR=.TRUE., PBY=-1.823646/

&SLCF QUANTITY='TEMPERATURE', PBY=-1.823646/

&SLCF QUANTITY='VELOCITY', VECTOR=.TRUE., PBX=0.658902/

&SLCF QUANTITY='TEMPERATURE', PBX=0.658902/

&SLCF QUANTITY='VOLUME FRACTION', SPEC_ID='HELIUM', VECTOR=.TRUE., PBX=0.658902/

&DEVC ID='Velocity P L_STEADY STATE', QUANTITY='VELOCITY', XB=0.62,0.62,-1.82,-1.82,0.63,1.41, POINTS=15/

&DEVC ID='Velocity In Mid_STEADY STATE', QUANTITY='VELOCITY', XB=0.67,0.67,-1.39,-1.39,0.63,1.36, POINTS=14/

&DEVC ID='Velocity P Mid_STEADY STATE', QUANTITY='VELOCITY', XB=0.67,0.67,-1.82,-1.82,0.63,1.41, POINTS=15/

&DEVC ID='Velocity P R_STEADY STATE', QUANTITY='VELOCITY', XB=0.72,0.72,-1.82,-1.82,0.63,1.41, POINTS=15/

&DEVC ID='Velocity In B_STEADY STATE', QUANTITY='VELOCITY', XB=0.67,0.67,-1.29,-1.29,0.63,1.36, POINTS=14/

&DEVC ID='Velocity In F_STEADY STATE', QUANTITY='VELOCITY', XB=0.67,0.67,-1.49,-1.49,0.63,1.36, POINTS=14/

&DEVC ID='Viscosity P L_STEADY STATE', QUANTITY='VISCOSITY', XB=0.62,0.62,-1.82,-1.82,0.63,1.41, POINTS=15/

&DEVC ID='Viscosity P Mid_STEADY STATE', QUANTITY='VISCOSITY', XB=0.67,0.67,-1.82,-1.82,0.63,1.41, POINTS=15/

&DEVC ID='Viscosity P R_STEADY STATE', QUANTITY='VISCOSITY', XB=0.72,0.72,-1.82,-1.82,0.63,1.41, POINTS=15/

&DEVC ID='Viscosity In F_STEADY STATE', QUANTITY='VISCOSITY', XB=0.67,0.67,-1.49,-1.49,0.63,1.36, POINTS=14/

&DEVC ID='Viscosity In Mid_STEADY STATE', QUANTITY='VISCOSITY', XB=0.67,0.67,-1.39,-1.39,0.63,1.36, POINTS=14/

&DEVC ID='Viscosity In B_STEADY STATE', QUANTITY='VISCOSITY', XB=0.67,0.67,-1.29,-1.29,0.63,1.36, POINTS=14/

&DEVC ID='Density In B_STEADY STATE', QUANTITY='DENSITY', XB=0.67,0.67,-1.29,-1.29,0.63,1.36, POINTS=14/

&DEVC ID='Density In Mid_STEADY STATE', QUANTITY='DENSITY', XB=0.67,0.67,-1.39,-1.39,0.63,1.36, POINTS=14/

&DEVC ID='Density In F_STEADY STATE', QUANTITY='DENSITY', XB=0.67,0.67,-1.49,-1.49,0.63,1.36, POINTS=14/

&DEVC ID='Density P R_STEADY STATE', QUANTITY='DENSITY', XB=0.72,0.72,-1.82,-1.82,0.63,1.41, POINTS=15/

&DEVC ID='Density P Mid_STEADY STATE', QUANTITY='DENSITY', XB=0.67,0.67,-1.82,-1.82,0.63,1.41, POINTS=15/

&DEVC ID='Density P L_STEADY STATE', QUANTITY='DENSITY', XB=0.62,0.62,-1.82,-1.82,0.63,1.41, POINTS=15/

&DEVC ID='Helium In B_STEADY STATE', QUANTITY='VOLUME FRACTION', SPEC_ID='HELIUM', XB=0.67,0.67,-1.39,-1.39,0.63,1.36, POINTS=14/

&DEVC ID='Helium In Mid_STEADY STATE', QUANTITY='VOLUME FRACTION', SPEC_ID='HELIUM', XB=0.67,0.67,-1.29,-1.29,0.63,1.36, POINTS=14/

&DEVC ID='Helium In F_STEADY STATE', QUANTITY='VOLUME FRACTION', SPEC_ID='HELIUM', XB=0.67,0.67,-1.49,-1.49,0.63,1.36, POINTS=14/

&DEVC ID='Helium P R_STEADY STATE', QUANTITY='VOLUME FRACTION', SPEC_ID='HELIUM', XB=0.72,0.72,-1.82,-1.82,0.63,1.41, POINTS=15/

&DEVC ID='Helium P Mid_STEADY STATE', QUANTITY='VOLUME FRACTION', SPEC_ID='HELIUM', XB=0.67,0.67,-1.82,-1.82,0.63,1.41, POINTS=15/

&DEVC ID='Helium P L_STEADY STATE', QUANTITY='VOLUME FRACTION', SPEC_ID='HELIUM', XB=0.62,0.62,-1.82,-1.82,0.63,1.41, POINTS=15/

&TAIL /

Appendix B (FDS input code for case 2 with fire in small-scale)

SSF319case1stat.fds

Generated by PyroSim - Version 2021.2.0512

12-Aug-2022 12:29:11 PM

```
&HEAD CHID='SSF319case1stat'/
&TIME T_END=180.0/
&DUMP DT_RESTART=300.0, DT_SL3D=0.25/
&RADI RADIATION=.FALSE./

&MESH ID='Meshnew-a-a-a', IJK=86,12,24, XB=0.24,0.67,-1.86,-1.8,0.6,0.72/
&MESH ID='Meshnew-a-a-b', IJK=90,12,24, XB=0.67,1.12,-1.86,-1.8,0.6,0.72/
&MESH ID='Meshnew-a-b-a', IJK=86,12,24, XB=0.24,0.67,-1.86,-1.8,0.72,0.84/
&MESH ID='Meshnew-a-b-b', IJK=90,12,24, XB=0.67,1.12,-1.86,-1.8,0.72,0.84/
&MESH ID='Meshnew-a-c-a', IJK=86,12,20, XB=0.24,0.67,-1.86,-1.8,0.84,0.94/
&MESH ID='Meshnew-a-c-b', IJK=90,12,20, XB=0.67,1.12,-1.86,-1.8,0.84,0.94/
&MESH ID='Meshnew-a-d-a', IJK=86,12,24, XB=0.24,0.67,-1.86,-1.8,0.94,1.06/
&MESH ID='Meshnew-a-d-b', IJK=90,12,24, XB=0.67,1.12,-1.86,-1.8,0.94,1.06/
&MESH ID='Meshnew-a-e-a', IJK=86,12,20, XB=0.24,0.67,-1.86,-1.8,1.06,1.16/
&MESH ID='Meshnew-a-e-b', IJK=90,12,20, XB=0.67,1.12,-1.86,-1.8,1.06,1.16/
&MESH ID='Meshnew-a-f-a', IJK=86,12,24, XB=0.24,0.67,-1.86,-1.8,1.16,1.28/
&MESH ID='Meshnew-a-f-b', IJK=90,12,24, XB=0.67,1.12,-1.86,-1.8,1.16,1.28/
&MESH ID='Meshnew-a-g-a', IJK=86,12,24, XB=0.24,0.67,-1.86,-1.8,1.28,1.4/
&MESH ID='Meshnew-a-g-b', IJK=90,12,24, XB=0.67,1.12,-1.86,-1.8,1.28,1.4/
&MESH ID='Meshnew-a-h', IJK=176,12,20, XB=0.24,1.12,-1.86,-1.8,1.4,1.5/
&MESH ID='Meshnew-a-i-a', IJK=45,96,12, XB=0.24,0.69,-1.8,-0.84,0.6,0.72/
&MESH ID='Meshnew-a-i-b', IJK=43,96,12, XB=0.69,1.12,-1.8,-0.84,0.6,0.72/
&MESH ID='Meshnew-a-j-a', IJK=45,96,12, XB=0.24,0.69,-1.8,-0.84,0.72,0.84/
&MESH ID='Meshnew-a-j-b', IJK=43,96,12, XB=0.69,1.12,-1.8,-0.84,0.72,0.84/
&MESH ID='Meshnew-a-k-a', IJK=45,96,10, XB=0.24,0.69,-1.8,-0.84,0.84,0.94/
&MESH ID='Meshnew-a-k-b', IJK=43,96,10, XB=0.69,1.12,-1.8,-0.84,0.84,0.94/
&MESH ID='Meshnew-a-l-a', IJK=45,96,12, XB=0.24,0.69,-1.8,-0.84,0.94,1.06/
&MESH ID='Meshnew-a-l-b', IJK=43,96,12, XB=0.69,1.12,-1.8,-0.84,0.94,1.06/
```

```
&MESH ID='Meshnew-a-m-a', IJK=45,96,10, XB=0.24,0.69,-1.8,-0.84,1.06,1.16/
&MESH ID='Meshnew-a-m-b', IJK=43,96,10, XB=0.69,1.12,-1.8,-0.84,1.06,1.16/
&MESH ID='Meshnew-a-n-a', IJK=45,96,12, XB=0.24,0.69,-1.8,-0.84,1.16,1.28/
&MESH ID='Meshnew-a-n-b', IJK=43,96,12, XB=0.69,1.12,-1.8,-0.84,1.16,1.28/
&MESH ID='Meshnew-a-o-a', IJK=45,96,12, XB=0.24,0.69,-1.8,-0.84,1.28,1.4/
&MESH ID='Meshnew-a-o-b', IJK=43,96,12, XB=0.69,1.12,-1.8,-0.84,1.28,1.4/
&MESH ID='Meshnew-a-p-a', IJK=45,96,10, XB=0.24,0.69,-1.8,-0.84,1.4,1.5/
&MESH ID='Meshnew-a-p-b', IJK=43,96,10, XB=0.69,1.12,-1.8,-0.84,1.4,1.5/
&MESH ID='Meshnew-b-a-a', IJK=44,102,11, XB=0.24,0.68,-1.86,-0.84,1.5,1.61/
&MESH ID='Meshnew-b-a-b', IJK=44,102,11, XB=0.24,0.68,-1.86,-0.84,1.61,1.72/
&MESH ID='Meshnew-b-b-a', IJK=44,102,11, XB=0.68,1.12,-1.86,-0.84,1.5,1.61/
&MESH ID='Meshnew-b-b-b', IJK=44,102,11, XB=0.68,1.12,-1.86,-0.84,1.61,1.72/
&MESH ID='Meshnew-c-a', IJK=23,51,14, XB=0.24,0.7,-1.86,-0.84,1.72,2.0/
&MESH ID='Meshnew-c-b', IJK=21,51,14, XB=0.7,1.12,-1.86,-0.84,1.72,2.0/
&MESH ID='Meshnew-d-a-a', IJK=88,26,24, XB=0.24,1.12,-0.84,-0.58,0.6,0.84/
&MESH ID='Meshnew-d-a-b', IJK=88,26,22, XB=0.24,1.12,-0.84,-0.58,0.84,1.06/
&MESH ID='Meshnew-d-b-a', IJK=88,26,22, XB=0.24,1.12,-0.84,-0.58,1.06,1.28/
&MESH ID='Meshnew-d-b-b', IJK=88,26,22, XB=0.24,1.12,-0.84,-0.58,1.28,1.5/
&MESH ID='Meshnew-e', IJK=88,26,22, XB=0.24,1.12,-0.84,-0.58,1.5,1.72/
&MESH ID='Meshnew-f', IJK=44,13,14, XB=0.24,1.12,-0.84,-0.58,1.72,2.0/
&MESH ID='Meshnew-g-a-a', IJK=44,15,12, XB=0.24,1.12,-0.58,-0.28,0.6,0.84/
&MESH ID='Meshnew-g-a-b', IJK=44,15,11, XB=0.24,1.12,-0.58,-0.28,0.84,1.06/
&MESH ID='Meshnew-g-b', IJK=44,15,22, XB=0.24,1.12,-0.58,-0.28,1.06,1.5/
&MESH ID='Meshnew-h-merged-a', IJK=44,15,11, XB=0.24,1.12,-0.58,-0.28,1.5,1.72/
&MESH ID='Meshnew-h-merged-b', IJK=44,15,14, XB=0.24,1.12,-0.58,-0.28,1.72,2.0/


&REAC ID='PMMA',
    FYI='SFPE Handbook, 3rd Edition',
    FUEL='REAC_FUEL',
    C=1.0,
    H=1.6,
    O=0.4,
    CO_YIELD=0.01,
    SOOT_YIELD=0.022,
    RADIATIVE_FRACTION=0.35/
```

&DEVC ID='TC-L1-M1', QUANTITY='THERMOCOUPLE', XYZ=0.673096,-1.742573,0.657301/
&DEVC ID='TC-L2-M1', QUANTITY='THERMOCOUPLE', XYZ=0.673096,-1.742573,0.770001/
&DEVC ID='TC-L3-M1', QUANTITY='THERMOCOUPLE', XYZ=0.673096,-1.742573,0.882701/
&DEVC ID='TC-L4-M1', QUANTITY='THERMOCOUPLE', XYZ=0.673096,-1.742573,0.995401/
&DEVC ID='TC-L5-M1', QUANTITY='THERMOCOUPLE', XYZ=0.673096,-1.742573,1.108101/
&DEVC ID='TC-L6-M1', QUANTITY='THERMOCOUPLE', XYZ=0.673096,-1.742573,1.214361/
&DEVC ID='TC-L7-M1', QUANTITY='THERMOCOUPLE', XYZ=0.673096,-1.742573,1.336721/
&DEVC ID='TC-L1-M2', QUANTITY='THERMOCOUPLE', XYZ=0.673096,-1.592573,0.657301/
&DEVC ID='TC-L2-M2', QUANTITY='THERMOCOUPLE', XYZ=0.673096,-1.592573,0.770001/
&DEVC ID='TC-L3-M2', QUANTITY='THERMOCOUPLE', XYZ=0.673096,-1.592573,0.882701/
&DEVC ID='TC-L4-M2', QUANTITY='THERMOCOUPLE', XYZ=0.673096,-1.592573,0.995401/
&DEVC ID='TC-L5-M2', QUANTITY='THERMOCOUPLE', XYZ=0.673096,-1.592573,1.108101/
&DEVC ID='TC-L6-M2', QUANTITY='THERMOCOUPLE', XYZ=0.673096,-1.592573,1.214361/
&DEVC ID='TC-L7-M2', QUANTITY='THERMOCOUPLE', XYZ=0.673096,-1.592573,1.336721/
&DEVC ID='TC-L1-M3', QUANTITY='THERMOCOUPLE', XYZ=0.673096,-1.392573,0.657301/
&DEVC ID='TC-L2-M3', QUANTITY='THERMOCOUPLE', XYZ=0.673096,-1.392573,0.770001/
&DEVC ID='TC-L3-M3', QUANTITY='THERMOCOUPLE', XYZ=0.673096,-1.392573,0.882701/
&DEVC ID='TC-L4-M3', QUANTITY='THERMOCOUPLE', XYZ=0.673096,-1.392573,0.995401/
&DEVC ID='TC-L5-M3', QUANTITY='THERMOCOUPLE', XYZ=0.673096,-1.392573,1.108101/
&DEVC ID='TC-L6-M3', QUANTITY='THERMOCOUPLE', XYZ=0.673096,-1.392573,1.214361/
&DEVC ID='TC-L7-M3', QUANTITY='THERMOCOUPLE', XYZ=0.673096,-1.392573,1.336721/
&DEVC ID='TC-L1-M4', QUANTITY='THERMOCOUPLE', XYZ=0.673096,-1.192573,0.657301/
&DEVC ID='TC-L2-M4', QUANTITY='THERMOCOUPLE', XYZ=0.673096,-1.192573,0.770001/
&DEVC ID='TC-L3-M4', QUANTITY='THERMOCOUPLE', XYZ=0.673096,-1.192573,0.882701/
&DEVC ID='TC-L4-M4', QUANTITY='THERMOCOUPLE', XYZ=0.673096,-1.192573,0.995401/
&DEVC ID='TC-L5-M4', QUANTITY='THERMOCOUPLE', XYZ=0.673096,-1.192573,1.108101/
&DEVC ID='TC-L6-M4', QUANTITY='THERMOCOUPLE', XYZ=0.673096,-1.192573,1.214361/
&DEVC ID='TC-L7-M4', QUANTITY='THERMOCOUPLE', XYZ=0.673096,-1.192573,1.336721/
&DEVC ID='TC-L1-M5', QUANTITY='THERMOCOUPLE', XYZ=0.673096,-0.992573,0.657301/
&DEVC ID='TC-L2-M5', QUANTITY='THERMOCOUPLE', XYZ=0.673096,-0.992573,0.770001/
&DEVC ID='TC-L3-M5', QUANTITY='THERMOCOUPLE', XYZ=0.673096,-0.992573,0.882701/
&DEVC ID='TC-L4-M5', QUANTITY='THERMOCOUPLE', XYZ=0.673096,-0.992573,0.995401/
&DEVC ID='TC-L5-M5', QUANTITY='THERMOCOUPLE', XYZ=0.673096,-0.992573,1.108101/
&DEVC ID='TC-L6-M5', QUANTITY='THERMOCOUPLE', XYZ=0.673096,-0.992573,1.214361/
&DEVC ID='TC-L7-M5', QUANTITY='THERMOCOUPLE', XYZ=0.673096,-0.992573,1.336721/
&DEVC ID='TC-L1-L1', QUANTITY='THERMOCOUPLE', XYZ=0.353096,-1.742573,0.657301/
&DEVC ID='TC-L2-L1', QUANTITY='THERMOCOUPLE', XYZ=0.353096,-1.742573,0.770001/

&DEVC ID='TC-L3-L1', QUANTITY='THERMOCOUPLE', XYZ=0.353096,-1.742573,0.882701/
&DEVC ID='TC-L4-L1', QUANTITY='THERMOCOUPLE', XYZ=0.353096,-1.742573,0.995401/
&DEVC ID='TC-L5-L1', QUANTITY='THERMOCOUPLE', XYZ=0.353096,-1.742573,1.108101/
&DEVC ID='TC-L6-L1', QUANTITY='THERMOCOUPLE', XYZ=0.353096,-1.742573,1.214361/
&DEVC ID='TC-L7-L1', QUANTITY='THERMOCOUPLE', XYZ=0.353096,-1.742573,1.336721/
&DEVC ID='TC-L1-L2', QUANTITY='THERMOCOUPLE', XYZ=0.353096,-1.592573,0.657301/
&DEVC ID='TC-L2-L2', QUANTITY='THERMOCOUPLE', XYZ=0.353096,-1.592573,0.770001/
&DEVC ID='TC-L3-L2', QUANTITY='THERMOCOUPLE', XYZ=0.353096,-1.592573,0.882701/
&DEVC ID='TC-L4-L2', QUANTITY='THERMOCOUPLE', XYZ=0.353096,-1.592573,0.995401/
&DEVC ID='TC-L5-L2', QUANTITY='THERMOCOUPLE', XYZ=0.353096,-1.592573,1.108101/
&DEVC ID='TC-L6-L2', QUANTITY='THERMOCOUPLE', XYZ=0.353096,-1.592573,1.214361/
&DEVC ID='TC-L7-L2', QUANTITY='THERMOCOUPLE', XYZ=0.353096,-1.592573,1.336721/
&DEVC ID='TC-L1-L3', QUANTITY='THERMOCOUPLE', XYZ=0.353096,-1.392573,0.657301/
&DEVC ID='TC-L2-L3', QUANTITY='THERMOCOUPLE', XYZ=0.353096,-1.392573,0.770001/
&DEVC ID='TC-L3-L3', QUANTITY='THERMOCOUPLE', XYZ=0.353096,-1.392573,0.882701/
&DEVC ID='TC-L4-L3', QUANTITY='THERMOCOUPLE', XYZ=0.353096,-1.392573,0.995401/
&DEVC ID='TC-L5-L3', QUANTITY='THERMOCOUPLE', XYZ=0.353096,-1.392573,1.108101/
&DEVC ID='TC-L6-L3', QUANTITY='THERMOCOUPLE', XYZ=0.353096,-1.392573,1.214361/
&DEVC ID='TC-L7-L3', QUANTITY='THERMOCOUPLE', XYZ=0.353096,-1.392573,1.336721/
&DEVC ID='TC-L1-L4', QUANTITY='THERMOCOUPLE', XYZ=0.353096,-1.192573,0.657301/
&DEVC ID='TC-L2-L4', QUANTITY='THERMOCOUPLE', XYZ=0.353096,-1.192573,0.770001/
&DEVC ID='TC-L3-L4', QUANTITY='THERMOCOUPLE', XYZ=0.353096,-1.192573,0.882701/
&DEVC ID='TC-L4-L4', QUANTITY='THERMOCOUPLE', XYZ=0.353096,-1.192573,0.995401/
&DEVC ID='TC-L5-L4', QUANTITY='THERMOCOUPLE', XYZ=0.353096,-1.192573,1.108101/
&DEVC ID='TC-L6-L4', QUANTITY='THERMOCOUPLE', XYZ=0.353096,-1.192573,1.214361/
&DEVC ID='TC-L7-L4', QUANTITY='THERMOCOUPLE', XYZ=0.353096,-1.192573,1.336721/
&DEVC ID='TC-L1-L5', QUANTITY='THERMOCOUPLE', XYZ=0.353096,-0.992573,0.657301/
&DEVC ID='TC-L2-L5', QUANTITY='THERMOCOUPLE', XYZ=0.353096,-0.992573,0.770001/
&DEVC ID='TC-L3-L5', QUANTITY='THERMOCOUPLE', XYZ=0.353096,-0.992573,0.882701/
&DEVC ID='TC-L4-L5', QUANTITY='THERMOCOUPLE', XYZ=0.353096,-0.992573,0.995401/
&DEVC ID='TC-L5-L5', QUANTITY='THERMOCOUPLE', XYZ=0.353096,-0.992573,1.108101/
&DEVC ID='TC-L6-L5', QUANTITY='THERMOCOUPLE', XYZ=0.353096,-0.992573,1.214361/
&DEVC ID='TC-L7-L5', QUANTITY='THERMOCOUPLE', XYZ=0.353096,-0.992573,1.336721/
&DEVC ID='TC-L1-R1', QUANTITY='THERMOCOUPLE', XYZ=0.993096,-1.742573,0.657301/
&DEVC ID='TC-L2-R1', QUANTITY='THERMOCOUPLE', XYZ=0.993096,-1.742573,0.770001/
&DEVC ID='TC-L3-R1', QUANTITY='THERMOCOUPLE', XYZ=0.993096,-1.742573,0.882701/
&DEVC ID='TC-L4-R1', QUANTITY='THERMOCOUPLE', XYZ=0.993096,-1.742573,0.995401/

&DEVC ID='TC-L5-R1', QUANTITY='THERMOCOUPLE', XYZ=0.993096,-1.742573,1.108101/
&DEVC ID='TC-L6-R1', QUANTITY='THERMOCOUPLE', XYZ=0.993096,-1.742573,1.214361/
&DEVC ID='TC-L7-R1', QUANTITY='THERMOCOUPLE', XYZ=0.993096,-1.742573,1.336721/
&DEVC ID='TC-L1-R2', QUANTITY='THERMOCOUPLE', XYZ=0.993096,-1.592573,0.657301/
&DEVC ID='TC-L2-R2', QUANTITY='THERMOCOUPLE', XYZ=0.993096,-1.592573,0.770001/
&DEVC ID='TC-L3-R2', QUANTITY='THERMOCOUPLE', XYZ=0.993096,-1.592573,0.882701/
&DEVC ID='TC-L4-R2', QUANTITY='THERMOCOUPLE', XYZ=0.993096,-1.592573,0.995401/
&DEVC ID='TC-L5-R2', QUANTITY='THERMOCOUPLE', XYZ=0.993096,-1.592573,1.108101/
&DEVC ID='TC-L6-R2', QUANTITY='THERMOCOUPLE', XYZ=0.993096,-1.592573,1.214361/
&DEVC ID='TC-L7-R2', QUANTITY='THERMOCOUPLE', XYZ=0.993096,-1.592573,1.336721/
&DEVC ID='TC-L1-R3', QUANTITY='THERMOCOUPLE', XYZ=0.993096,-1.392573,0.657301/
&DEVC ID='TC-L2-R3', QUANTITY='THERMOCOUPLE', XYZ=0.993096,-1.392573,0.770001/
&DEVC ID='TC-L3-R3', QUANTITY='THERMOCOUPLE', XYZ=0.993096,-1.392573,0.882701/
&DEVC ID='TC-L4-R3', QUANTITY='THERMOCOUPLE', XYZ=0.993096,-1.392573,0.995401/
&DEVC ID='TC-L5-R3', QUANTITY='THERMOCOUPLE', XYZ=0.993096,-1.392573,1.108101/
&DEVC ID='TC-L6-R3', QUANTITY='THERMOCOUPLE', XYZ=0.993096,-1.392573,1.214361/
&DEVC ID='TC-L7-R3', QUANTITY='THERMOCOUPLE', XYZ=0.993096,-1.392573,1.336721/
&DEVC ID='TC-L1-R4', QUANTITY='THERMOCOUPLE', XYZ=0.993096,-1.192573,0.657301/
&DEVC ID='TC-L2-R4', QUANTITY='THERMOCOUPLE', XYZ=0.993096,-1.192573,0.770001/
&DEVC ID='TC-L3-R4', QUANTITY='THERMOCOUPLE', XYZ=0.993096,-1.192573,0.882701/
&DEVC ID='TC-L4-R4', QUANTITY='THERMOCOUPLE', XYZ=0.993096,-1.192573,0.995401/
&DEVC ID='TC-L5-R4', QUANTITY='THERMOCOUPLE', XYZ=0.993096,-1.192573,1.108101/
&DEVC ID='TC-L6-R4', QUANTITY='THERMOCOUPLE', XYZ=0.993096,-1.192573,1.214361/
&DEVC ID='TC-L7-R4', QUANTITY='THERMOCOUPLE', XYZ=0.993096,-1.192573,1.336721/
&DEVC ID='TC-L1-R5', QUANTITY='THERMOCOUPLE', XYZ=0.993096,-0.992573,0.657301/
&DEVC ID='TC-L2-R5', QUANTITY='THERMOCOUPLE', XYZ=0.993096,-0.992573,0.770001/
&DEVC ID='TC-L3-R5', QUANTITY='THERMOCOUPLE', XYZ=0.993096,-0.992573,0.882701/
&DEVC ID='TC-L4-R5', QUANTITY='THERMOCOUPLE', XYZ=0.993096,-0.992573,0.995401/
&DEVC ID='TC-L5-R5', QUANTITY='THERMOCOUPLE', XYZ=0.993096,-0.992573,1.108101/
&DEVC ID='TC-L6-R5', QUANTITY='THERMOCOUPLE', XYZ=0.993096,-0.992573,1.214361/
&DEVC ID='TC-L7-R5', QUANTITY='THERMOCOUPLE', XYZ=0.993096,-0.992573,1.336721/
&DEVC ID='TC-L1PM1', QUANTITY='THERMOCOUPLE', XYZ=0.673096,-1.818901,0.657301/
&DEVC ID='TC-L2PM1', QUANTITY='THERMOCOUPLE', XYZ=0.673096,-1.818901,0.770001/
&DEVC ID='TC-L3PM1', QUANTITY='THERMOCOUPLE', XYZ=0.673096,-1.818901,0.882701/
&DEVC ID='TC-L4PM1', QUANTITY='THERMOCOUPLE', XYZ=0.673096,-1.818901,0.995401/
&DEVC ID='TC-L5PM1', QUANTITY='THERMOCOUPLE', XYZ=0.673096,-1.818901,1.108101/
&DEVC ID='TC-L6PM1', QUANTITY='THERMOCOUPLE', XYZ=0.673096,-1.818901,1.220801/

&DEVC ID='TC-L7PM1', QUANTITY='THERMOCOUPLE', XYZ=0.673096,-1.818901,1.333501/
&DEVC ID='TC-L1PM2', QUANTITY='THERMOCOUPLE', XYZ=0.673096,-1.848901,0.657301/
&DEVC ID='TC-L2PM2', QUANTITY='THERMOCOUPLE', XYZ=0.673096,-1.848901,0.770001/
&DEVC ID='TC-L3PM2', QUANTITY='THERMOCOUPLE', XYZ=0.673096,-1.848901,0.882701/
&DEVC ID='TC-L4PM2', QUANTITY='THERMOCOUPLE', XYZ=0.673096,-1.848901,0.995401/
&DEVC ID='TC-L5PM2', QUANTITY='THERMOCOUPLE', XYZ=0.673096,-1.848901,1.108101/
&DEVC ID='TC-L6PM2', QUANTITY='THERMOCOUPLE', XYZ=0.673096,-1.848901,1.220801/
&DEVC ID='TC-L7PM2', QUANTITY='THERMOCOUPLE', XYZ=0.673096,-1.848901,1.333501/
&DEVC ID='TC-L1PL1', QUANTITY='THERMOCOUPLE', XYZ=0.353096,-1.818901,0.657301/
&DEVC ID='TC-L2PL1', QUANTITY='THERMOCOUPLE', XYZ=0.353096,-1.818901,0.770001/
&DEVC ID='TC-L3PL1', QUANTITY='THERMOCOUPLE', XYZ=0.353096,-1.818901,0.882701/
&DEVC ID='TC-L4PL1', QUANTITY='THERMOCOUPLE', XYZ=0.353096,-1.818901,0.995401/
&DEVC ID='TC-L5PL1', QUANTITY='THERMOCOUPLE', XYZ=0.353096,-1.818901,1.108101/
&DEVC ID='TC-L6PL1', QUANTITY='THERMOCOUPLE', XYZ=0.353096,-1.818901,1.220801/
&DEVC ID='TC-L7PL1', QUANTITY='THERMOCOUPLE', XYZ=0.353096,-1.818901,1.333501/
&DEVC ID='TC-L1PL2', QUANTITY='THERMOCOUPLE', XYZ=0.353096,-1.848901,0.657301/
&DEVC ID='TC-L2PL2', QUANTITY='THERMOCOUPLE', XYZ=0.353096,-1.848901,0.770001/
&DEVC ID='TC-L3PL2', QUANTITY='THERMOCOUPLE', XYZ=0.353096,-1.848901,0.882701/
&DEVC ID='TC-L4PL2', QUANTITY='THERMOCOUPLE', XYZ=0.353096,-1.848901,0.995401/
&DEVC ID='TC-L5PL2', QUANTITY='THERMOCOUPLE', XYZ=0.353096,-1.848901,1.108101/
&DEVC ID='TC-L6PL2', QUANTITY='THERMOCOUPLE', XYZ=0.353096,-1.848901,1.220801/
&DEVC ID='TC-L7PL2', QUANTITY='THERMOCOUPLE', XYZ=0.353096,-1.848901,1.333501/
&DEVC ID='TC-L1PR1', QUANTITY='THERMOCOUPLE', XYZ=0.993096,-1.818901,0.657301/
&DEVC ID='TC-L2PR1', QUANTITY='THERMOCOUPLE', XYZ=0.993096,-1.818901,0.770001/
&DEVC ID='TC-L3PR1', QUANTITY='THERMOCOUPLE', XYZ=0.993096,-1.818901,0.882701/
&DEVC ID='TC-L4PR1', QUANTITY='THERMOCOUPLE', XYZ=0.993096,-1.818901,0.995401/
&DEVC ID='TC-L5PR1', QUANTITY='THERMOCOUPLE', XYZ=0.993096,-1.818901,1.108101/
&DEVC ID='TC-L6PR1', QUANTITY='THERMOCOUPLE', XYZ=0.993096,-1.818901,1.220801/
&DEVC ID='TC-L7PR1', QUANTITY='THERMOCOUPLE', XYZ=0.993096,-1.818901,1.333501/
&DEVC ID='TC-L1PR2', QUANTITY='THERMOCOUPLE', XYZ=0.993096,-1.848901,0.657301/
&DEVC ID='TC-L2PR2', QUANTITY='THERMOCOUPLE', XYZ=0.993096,-1.848901,0.770001/
&DEVC ID='TC-L3PR2', QUANTITY='THERMOCOUPLE', XYZ=0.993096,-1.848901,0.882701/
&DEVC ID='TC-L4PR2', QUANTITY='THERMOCOUPLE', XYZ=0.993096,-1.848901,0.995401/
&DEVC ID='TC-L5PR2', QUANTITY='THERMOCOUPLE', XYZ=0.993096,-1.848901,1.108101/
&DEVC ID='TC-L6PR2', QUANTITY='THERMOCOUPLE', XYZ=0.993096,-1.848901,1.220801/
&DEVC ID='TC-L7PR2', QUANTITY='THERMOCOUPLE', XYZ=0.993096,-1.848901,1.333501/

&DEVC ID='FLOW01', QUANTITY='MASS FLOW', XB=0.658902,0.691102,-1.807546,-1.807546,0.63235,0.69031/

&DEVC ID='FLOW02', QUANTITY='MASS FLOW', XB=0.658902,0.691102,-1.807546,-1.807546,0.74505,0.80301/

&DEVC ID='FLOW03', QUANTITY='MASS FLOW', XB=0.658902,0.691102,-1.807546,-1.807546,0.85775,0.91571/

&DEVC ID='FLOW04', QUANTITY='MASS FLOW', XB=0.658902,0.691102,-1.807546,-1.807546,0.97045,1.02841/

&DEVC ID='FLOW05', QUANTITY='MASS FLOW', XB=0.658902,0.691102,-1.807546,-1.807546,1.08315,1.14111/

&DEVC ID='FLOW06', QUANTITY='MASS FLOW', XB=0.658902,0.691102,-1.807546,-1.807546,1.19585,1.25381/

&DEVC ID='FLOW07', QUANTITY='MASS FLOW', XB=0.658902,0.691102,-1.807546,-1.807546,1.30855,1.36651/

&DEVC ID='heat flow', QUANTITY='HEAT FLOW', XB=0.658902,0.658902,-1.839737,-0.294136,0.60498,2.00568/

&DEVC ID='mass flow', QUANTITY='MASS FLOW', XB=0.658902,0.658902,-1.839737,-0.294137,0.60498,2.00568/

&DEVC ID='volume flow', QUANTITY='VOLUME FLOW', XB=0.658902,0.658902,-1.839737,-0.294137,0.60498,2.00568/

&DEVC ID='heat flow plenum', QUANTITY='HEAT FLOW', XB=0.240302,1.109702,-1.807546,-1.807546,1.39388,1.42608/

&DEVC ID='mass flow plenum', QUANTITY='MASS FLOW', XB=0.240302,1.109702,-1.807546,-1.807546,1.39388,1.42608/

&DEVC ID='volume flow plenum', QUANTITY='VOLUME FLOW', XB=0.240302,1.109702,-1.807546,-1.807546,1.39388,1.42608/

&SURF ID='ADIABATIC',
COLOR='GRAY 80',
ADIABATIC=.TRUE./

&SURF ID='fire',
RGB=255,102,0,
HRRPUA=58.33,
TMP_FRONT=300.0/

&OBST ID='Obstruction', XB=0.240302,1.109702,-1.855846,-1.839736,0.60498,0.633155, SURF_ID6='ADIABATIC','ADIABATIC','ADIABATIC','fire','ADIABATIC','ADIABATIC'/

&OBST ID='west wall', XB=0.24,0.24,-1.81,-1.8,0.6,0.72, COLOR='INVISIBLE', SURF_ID='ADIABATIC'/

&OBST ID='west wall', XB=0.24,0.24,-1.81,-1.8,0.72,0.84, COLOR='INVISIBLE', SURF_ID='ADIABATIC'/

&OBST ID='west wall', XB=0.24,0.24,-1.81,-1.8,0.84,0.94, COLOR='INVISIBLE', SURF_ID='ADIABATIC'/

&OBST ID='west wall', XB=0.24,0.24,-1.81,-1.8,0.94,1.06, COLOR='INVISIBLE', SURF_ID='ADIABATIC'/

&OBST ID='west wall', XB=0.24,0.24,-1.81,-1.8,1.06,1.16, COLOR='INVISIBLE', SURF_ID='ADIABATIC'/

&OBST ID='west wall', XB=0.24,0.24,-1.81,-1.8,1.16,1.28, COLOR='INVISIBLE', SURF_ID='ADIABATIC'/

&OBST ID='west wall', XB=0.24,0.24,-1.81,-1.8,1.28,1.395, COLOR='INVISIBLE', SURF_ID='ADIABATIC'/

&OBST ID='west wall', XB=0.24,0.24,-1.8,-0.94,0.6,0.72, COLOR='INVISIBLE', SURF_ID='ADIABATIC'/

&OBST ID='west wall', XB=0.24,0.24,-1.8,-0.94,0.72,0.84, COLOR='INVISIBLE', SURF_ID='ADIABATIC'/

&OBST ID='west wall', XB=0.24,0.24,-1.8,-0.94,0.84,0.94, COLOR='INVISIBLE', SURF_ID='ADIABATIC'/

&OBST ID='west wall', XB=0.24,0.24,-1.8,-0.94,0.94,1.06, COLOR='INVISIBLE', SURF_ID='ADIABATIC'/

&OBST ID='west wall', XB=0.24,0.24,-1.8,-0.94,1.06,1.16, COLOR='INVISIBLE', SURF_ID='ADIABATIC'/

&OBST ID='west wall', XB=0.24,0.24,-1.8,-0.94,1.16,1.28, COLOR='INVISIBLE', SURF_ID='ADIABATIC'/

&OBST ID='west wall', XB=0.24,0.24,-1.8,-0.94,1.28,1.39, COLOR='INVISIBLE', SURF_ID='ADIABATIC'/

&OBST ID='roof', XB=0.24,0.67,-1.81,-1.8,1.395,1.395, COLOR='GRAY 68', SURF_ID='ADIABATIC'/

&OBST ID='roof', XB=0.67,1.11,-1.81,-1.8,1.395,1.395, COLOR='GRAY 68', SURF_ID='ADIABATIC'/

&OBST ID='roof', XB=0.24,0.69,-1.8,-0.94,1.39,1.39, COLOR='GRAY 68', SURF_ID='ADIABATIC'/

&OBST ID='roof', XB=0.69,1.11,-1.8,-0.94,1.39,1.39, COLOR='GRAY 68', SURF_ID='ADIABATIC'/

&OBST ID='east wall', XB=1.11,1.11,-1.81,-1.8,0.6,0.72, COLOR='INVISIBLE', SURF_ID='ADIABATIC'/

&OBST ID='east wall', XB=1.11,1.11,-1.81,-1.8,0.72,0.84, COLOR='INVISIBLE', SURF_ID='ADIABATIC'/

&OBST ID='east wall', XB=1.11,1.11,-1.81,-1.8,0.84,0.94, COLOR='INVISIBLE', SURF_ID='ADIABATIC'/

&OBST ID='east wall', XB=1.11,1.11,-1.81,-1.8,0.94,1.06, COLOR='INVISIBLE', SURF_ID='ADIABATIC'/

&OBST ID='east wall', XB=1.11,1.11,-1.81,-1.8,1.06,1.16, COLOR='INVISIBLE', SURF_ID='ADIABATIC'/

&OBST ID='east wall', XB=1.11,1.11,-1.81,-1.8,1.16,1.28, COLOR='INVISIBLE', SURF_ID='ADIABATIC'/

&OBST ID='east wall', XB=1.11,1.11,-1.81,-1.8,1.28,1.395, COLOR='INVISIBLE', SURF_ID='ADIABATIC'/

&OBST ID='east wall', XB=1.11,1.11,-1.8,-0.94,0.6,0.72, COLOR='INVISIBLE', SURF_ID='ADIABATIC'/

&OBST ID='east wall', XB=1.11,1.11,-1.8,-0.94,0.72,0.84, COLOR='INVISIBLE', SURF_ID='ADIABATIC'/

&OBST ID='east wall', XB=1.11,1.11,-1.8,-0.94,0.84,0.94, COLOR='INVISIBLE', SURF_ID='ADIABATIC'/

&OBST ID='east wall', XB=1.11,1.11,-1.8,-0.94,0.94,1.06, COLOR='INVISIBLE', SURF_ID='ADIABATIC'/

&OBST ID='east wall', XB=1.11,1.11,-1.8,-0.94,1.06,1.16, COLOR='INVISIBLE', SURF_ID='ADIABATIC'/

&OBST ID='east wall', XB=1.11,1.11,-1.8,-0.94,1.16,1.28, COLOR='INVISIBLE', SURF_ID='ADIABATIC'/

&OBST ID='east wall', XB=1.11,1.11,-1.8,-0.94,1.28,1.39, COLOR='INVISIBLE', SURF_ID='ADIABATIC'/

&OBST ID='floor of conference salon', XB=0.24,0.67,-1.81,-1.8,1.28,1.28, COLOR='GRAY 68', SURF_ID='ADIABATIC'/

&OBST ID='floor of conference salon', XB=0.67,1.11,-1.81,-1.8,1.28,1.28, COLOR='GRAY 68', SURF_ID='ADIABATIC'/

&OBST ID='floor of conference salon', XB=0.24,0.69,-1.8,-0.94,1.28,1.28, COLOR='GRAY 68', SURF_ID='ADIABATIC'/

&OBST ID='floor of conference salon', XB=0.69,1.11,-1.8,-0.94,1.28,1.28, COLOR='GRAY 68', SURF_ID='ADIABATIC'/

&OBST ID='floor of 6th level', XB=0.24,0.67,-1.81,-1.8,1.17,1.17, COLOR='GRAY 68', SURF_ID='ADIABATIC'/

&OBST ID='floor of 6th level', XB=0.67,1.11,-1.81,-1.8,1.17,1.17, COLOR='GRAY 68', SURF_ID='ADIABATIC'/

&OBST ID='floor of 6th level', XB=0.24,0.69,-1.8,-0.94,1.17,1.17, COLOR='GRAY 68', SURF_ID='ADIABATIC'/

&OBST ID='floor of 6th level', XB=0.69,1.11,-1.8,-0.94,1.17,1.17, COLOR='GRAY 68', SURF_ID='ADIABATIC'/

&OBST ID='floor of 5th level', XB=0.24,0.67,-1.81,-1.8,1.055,1.055, COLOR='GRAY 68', SURF_ID='ADIABATIC'/

&OBST ID='floor of 5th level', XB=0.67,1.11,-1.81,-1.8,1.055,1.055, COLOR='GRAY 68', SURF_ID='ADIABATIC'/

&OBST ID='floor of 5th level', XB=0.24,0.69,-1.8,-0.94,1.06,1.06, COLOR='GRAY 68', SURF_ID='ADIABATIC'/

&OBST ID='floor of 5th level', XB=0.69,1.11,-1.8,-0.94,1.06,1.06, COLOR='GRAY 68', SURF_ID='ADIABATIC'/

&OBST ID='floor of 4th level', XB=0.24,0.67,-1.81,-1.8,0.945,0.945, COLOR='GRAY 68', SURF_ID='ADIABATIC'/

&OBST ID='floor of 4th level', XB=0.67,1.11,-1.81,-1.8,0.945,0.945, COLOR='GRAY 68', SURF_ID='ADIABATIC'/

&OBST ID='floor of 4th level', XB=0.24,0.69,-1.8,-0.94,0.94,0.94, COLOR='GRAY 68', SURF_ID='ADIABATIC'/

&OBST ID='floor of 4th level', XB=0.69,1.11,-1.8,-0.94,0.94,0.94, COLOR='GRAY 68', SURF_ID='ADIABATIC'/

&OBST ID='floor of 3rd level', XB=0.24,0.67,-1.81,-1.8,0.83,0.83, COLOR='GRAY 68', SURF_ID='ADIABATIC'/

&OBST ID='floor of 3rd level', XB=0.67,1.11,-1.81,-1.8,0.83,0.83, COLOR='GRAY 68', SURF_ID='ADIABATIC'/

&OBST ID='floor of 3rd level', XB=0.24,0.69,-1.8,-0.94,0.83,0.83, COLOR='GRAY 68', SURF_ID='ADIABATIC'/

&OBST ID='floor of 3rd level', XB=0.69,1.11,-1.8,-0.94,0.83,0.83, COLOR='GRAY 68', SURF_ID='ADIABATIC'/

&OBST ID='floor of 2nd level', XB=0.24,0.67,-1.81,-1.8,0.72,0.72, COLOR='GRAY 68', SURF_ID='ADIABATIC'/

&OBST ID='floor of 2nd level', XB=0.67,1.11,-1.81,-1.8,0.72,0.72, COLOR='GRAY 68', SURF_ID='ADIABATIC'/

&OBST ID='floor of 2nd level', XB=0.24,0.69,-1.8,-0.94,0.72,0.72, COLOR='GRAY 68', SURF_ID='ADIABATIC'/

&OBST ID='floor of 2nd level', XB=0.69,1.11,-1.8,-0.94,0.72,0.72, COLOR='GRAY 68', SURF_ID='ADIABATIC'/

&OBST ID='floor of 1st level', XB=0.24,0.67,-1.81,-1.8,0.605,0.605, COLOR='GRAY 68', SURF_ID='ADIABATIC'/

&OBST ID='floor of 1st level', XB=0.67,1.11,-1.81,-1.8,0.605,0.605, COLOR='GRAY 68', SURF_ID='ADIABATIC'/

&OBST ID='floor of 1st level', XB=0.24,0.69,-1.8,-0.94,0.6,0.6, COLOR='GRAY 68', SURF_ID='ADIABATIC'/

&OBST ID='floor of 1st level', XB=0.69,1.11,-1.8,-0.94,0.6,0.6, COLOR='GRAY 68', SURF_ID='ADIABATIC'/

&OBST ID='plenum west', XB=0.24,0.24,-1.855,-1.81,0.605,0.72, COLOR='INVISIBLE', SURF_ID='ADIABATIC'/

&OBST ID='plenum west', XB=0.24,0.24,-1.855,-1.81,0.72,0.84, COLOR='INVISIBLE', SURF_ID='ADIABATIC'/

&OBST ID='plenum west', XB=0.24,0.24,-1.855,-1.81,0.84,0.94, COLOR='INVISIBLE', SURF_ID='ADIABATIC'/

&OBST ID='plenum west', XB=0.24,0.24,-1.855,-1.81,0.94,1.06, COLOR='INVISIBLE', SURF_ID='ADIABATIC'/

&OBST ID='plenum west', XB=0.24,0.24,-1.855,-1.81,1.06,1.16, COLOR='INVISIBLE', SURF_ID='ADIABATIC'/

&OBST ID='plenum west', XB=0.24,0.24,-1.855,-1.81,1.16,1.28, COLOR='INVISIBLE', SURF_ID='ADIABATIC'/

&OBST ID='plenum west', XB=0.24,0.24,-1.855,-1.81,1.28,1.4, COLOR='INVISIBLE', SURF_ID='ADIABATIC'/

&OBST ID='plenum west', XB=0.24,0.24,-1.855,-1.81,1.4,1.425, COLOR='INVISIBLE', SURF_ID='ADIABATIC'/

&OBST ID='plenum top', XB=0.24,1.11,-1.855,-1.81,1.425,1.425, COLOR='CYAN', SURF_ID='ADIABATIC'/

&OBST ID='plenum east', XB=1.11,1.11,-1.855,-1.81,0.605,0.72, COLOR='CYAN', SURF_ID='ADIABATIC'/

&OBST ID='plenum east', XB=1.11,1.11,-1.855,-1.81,0.72,0.84, COLOR='CYAN', SURF_ID='ADIABATIC'/

&OBST ID='plenum east', XB=1.11,1.11,-1.855,-1.81,0.84,0.94, COLOR='CYAN', SURF_ID='ADIABATIC'/

&OBST ID='plenum east', XB=1.11,1.11,-1.855,-1.81,0.94,1.06, COLOR='CYAN', SURF_ID='ADIABATIC'/

&OBST ID='plenum east', XB=1.11,1.11,-1.855,-1.81,1.06,1.16, COLOR='CYAN', SURF_ID='ADIABATIC'/

&OBST ID='plenum east', XB=1.11,1.11,-1.855,-1.81,1.16,1.28, COLOR='CYAN', SURF_ID='ADIABATIC'/

&OBST ID='plenum east', XB=1.11,1.11,-1.855,-1.81,1.28,1.4, COLOR='CYAN', SURF_ID='ADIABATIC'/

&OBST ID='plenum east', XB=1.11,1.11,-1.855,-1.81,1.4,1.425, COLOR='CYAN', SURF_ID='ADIABATIC'/

&OBST ID='plenum south face', XB=0.24,0.67,-1.855,-1.855,0.605,0.72, COLOR='INVISIBLE', SURF_ID='ADIABATIC'/

&OBST ID='plenum south face', XB=0.67,1.11,-1.855,-1.855,0.605,0.72, COLOR='INVISIBLE', SURF_ID='ADIABATIC'/

&OBST ID='plenum south face', XB=0.24,0.67,-1.855,-1.855,0.72,0.84, COLOR='INVISIBLE', SURF_ID='ADIABATIC'/

&OBST ID='plenum south face', XB=0.67,1.11,-1.855,-1.855,0.72,0.84, COLOR='INVISIBLE', SURF_ID='ADIABATIC'/

&OBST ID='plenum south face', XB=0.24,0.67,-1.855,-1.855,0.84,0.94, COLOR='INVISIBLE', SURF_ID='ADIABATIC'/

&OBST ID='plenum south face', XB=0.67,1.11,-1.855,-1.855,0.84,0.94, COLOR='INVISIBLE', SURF_ID='ADIABATIC'/

&OBST ID='plenum south face', XB=0.24,0.67,-1.855,-1.855,0.94,1.06, COLOR='INVISIBLE', SURF_ID='ADIABATIC'/

&OBST ID='plenum south face', XB=0.67,1.11,-1.855,-1.855,0.94,1.06, COLOR='INVISIBLE', SURF_ID='ADIABATIC'/

&OBST ID='plenum south face', XB=0.24,0.67,-1.855,-1.855,1.06,1.16, COLOR='INVISIBLE', SURF_ID='ADIABATIC'/

&OBST ID='plenum south face', XB=0.67,1.11,-1.855,-1.855,1.06,1.16, COLOR='INVISIBLE', SURF_ID='ADIABATIC'/

&OBST ID='plenum south face', XB=0.24,0.67,-1.855,-1.855,1.16,1.28, COLOR='INVISIBLE', SURF_ID='ADIABATIC'/

&OBST ID='plenum south face', XB=0.67,1.11,-1.855,-1.855,1.16,1.28, COLOR='INVISIBLE', SURF_ID='ADIABATIC'/

&OBST ID='plenum south face', XB=0.24,0.67,-1.855,-1.855,1.28,1.4, COLOR='INVISIBLE', SURF_ID='ADIABATIC'/

&OBST ID='plenum south face', XB=0.67,1.11,-1.855,-1.855,1.28,1.4, COLOR='INVISIBLE', SURF_ID='ADIABATIC'/

&OBST ID='plenum south face', XB=0.24,1.11,-1.855,-1.855,1.4,1.425, COLOR='INVISIBLE', SURF_ID='ADIABATIC'/

&OBST ID='plenum buttom', XB=0.24,0.67,-1.855,-1.81,0.605,0.605, COLOR='CYAN', SURF_ID='ADIABATIC'/

&OBST ID='plenum buttom', XB=0.67,1.11,-1.855,-1.81,0.605,0.605, COLOR='CYAN', SURF_ID='ADIABATIC'/

&OBST ID='AcDbRegion - 11B2', XB=0.24,0.275,-1.81,-1.81,0.6,0.72, COLOR='GRAY 80', SURF_ID='ADIABATIC'/

&OBST ID='AcDbRegion - 11B2', XB=0.275,0.305,-1.81,-1.81,0.6,0.63, COLOR='GRAY 80', SURF_ID='ADIABATIC'/

&OBST ID='AcDbRegion - 11B2', XB=0.275,0.305,-1.81,-1.81,0.69,0.72, COLOR='GRAY 80', SURF_ID='ADIABATIC'/

&OBST ID='AcDbRegion - 11B2', XB=0.305,0.335,-1.81,-1.81,0.6,0.72, COLOR='GRAY 80', SURF_ID='ADIABATIC'/

&OBST ID='AcDbRegion - 11B2', XB=0.335,0.37,-1.81,-1.81,0.6,0.63, COLOR='GRAY 80', SURF_ID='ADIABATIC'/

&OBST ID='AcDbRegion - 11B2', XB=0.335,0.37,-1.81,-1.81,0.69,0.72, COLOR='GRAY 80', SURF_ID='ADIABATIC'/

&OBST ID='AcDbRegion - 11B2', XB=0.37,0.4,-1.81,-1.81,0.6,0.72, COLOR='GRAY 80', SURF_ID='ADIABATIC'/

&OBST ID='AcDbRegion - 11B2', XB=0.4,0.435,-1.81,-1.81,0.6,0.63, COLOR='GRAY 80', SURF_ID='ADIABATIC'/

&OBST ID='AcDbRegion - 11B2', XB=0.4,0.435,-1.81,-1.81,0.69,0.72, COLOR='GRAY 80', SURF_ID='ADIABATIC'/

&OBST ID='AcDbRegion - 11B2', XB=0.435,0.465,-1.81,-1.81,0.6,0.72, COLOR='GRAY 80', SURF_ID='ADIABATIC'/

&OBST ID='AcDbRegion - 11B2', XB=0.465,0.5,-1.81,-1.81,0.6,0.63, COLOR='GRAY 80', SURF_ID='ADIABATIC'/

&OBST ID='AcDbRegion - 11B2', XB=0.465,0.5,-1.81,-1.81,0.69,0.72, COLOR='GRAY 80', SURF_ID='ADIABATIC'/

&OBST ID='AcDbRegion - 11B2', XB=0.5,0.53,-1.81,-1.81,0.6,0.72, COLOR='GRAY 80', SURF_ID='ADIABATIC'/

&OBST ID='AcDbRegion - 11B2', XB=0.53,0.56,-1.81,-1.81,0.6,0.63, COLOR='GRAY 80', SURF_ID='ADIABATIC'/

&OBST ID='AcDbRegion - 11B2', XB=0.53,0.56,-1.81,-1.81,0.69,0.72, COLOR='GRAY 80', SURF_ID='ADIABATIC'/

&OBST ID='AcDbRegion - 11B2', XB=0.56,0.595,-1.81,-1.81,0.6,0.72, COLOR='GRAY 80', SURF_ID='ADIABATIC'/

&OBST ID='AcDbRegion - 11B2', XB=0.595,0.625,-1.81,-1.81,0.6,0.63, COLOR='GRAY 80', SURF_ID='ADIABATIC'/

&OBST ID='AcDbRegion - 11B2', XB=0.595,0.625,-1.81,-1.81,0.69,0.72, COLOR='GRAY 80', SURF_ID='ADIABATIC'/

&OBST ID='AcDbRegion - 11B2', XB=0.625,0.66,-1.81,-1.81,0.6,0.72, COLOR='GRAY 80', SURF_ID='ADIABATIC'/

&OBST ID='AcDbRegion - 11B2', XB=0.66,0.67,-1.81,-1.81,0.6,0.63, COLOR='GRAY 80', SURF_ID='ADIABATIC'/

&OBST ID='AcDbRegion - 11B2', XB=0.66,0.67,-1.81,-1.81,0.69,0.72, COLOR='GRAY 80', SURF_ID='ADIABATIC'/

&OBST ID='AcDbRegion - 11B2', XB=0.67,0.69,-1.81,-1.81,0.6,0.63, COLOR='GRAY 80', SURF_ID='ADIABATIC'/

&OBST ID='AcDbRegion - 11B2', XB=0.67,0.69,-1.81,-1.81,0.69,0.72, COLOR='GRAY 80', SURF_ID='ADIABATIC'/

&OBST ID='AcDbRegion - 11B2', XB=0.69,0.725,-1.81,-1.81,0.6,0.72, COLOR='GRAY 80', SURF_ID='ADIABATIC'/

&OBST ID='AcDbRegion - 11B2', XB=0.725,0.755,-1.81,-1.81,0.6,0.63, COLOR='GRAY 80', SURF_ID='ADIABATIC'/

&OBST ID='AcDbRegion - 11B2', XB=0.725,0.755,-1.81,-1.81,0.69,0.72, COLOR='GRAY 80', SURF_ID='ADIABATIC'/

&OBST ID='AcDbRegion - 11B2', XB=0.755,0.79,-1.81,-1.81,0.6,0.72, COLOR='GRAY 80', SURF_ID='ADIABATIC'/

&OBST ID='AcDbRegion - 11B2', XB=0.79,0.82,-1.81,-1.81,0.6,0.63, COLOR='GRAY 80', SURF_ID='ADIABATIC'/

&OBST ID='AcDbRegion - 11B2', XB=0.79,0.82,-1.81,-1.81,0.69,0.72, COLOR='GRAY 80', SURF_ID='ADIABATIC'/

&OBST ID='AcDbRegion - 11B2', XB=0.82,0.85,-1.81,-1.81,0.6,0.72, COLOR='GRAY 80', SURF_ID='ADIABATIC'/

&OBST ID='AcDbRegion - 11B2', XB=0.85,0.885,-1.81,-1.81,0.6,0.63, COLOR='GRAY 80', SURF_ID='ADIABATIC'/

&OBST ID='AcDbRegion - 11B2', XB=0.85,0.885,-1.81,-1.81,0.69,0.72, COLOR='GRAY 80', SURF_ID='ADIABATIC'/

&OBST ID='AcDbRegion - 11B2', XB=0.885,0.915,-1.81,-1.81,0.6,0.72, COLOR='GRAY 80', SURF_ID='ADIABATIC'/

&OBST ID='AcDbRegion - 11B2', XB=0.915,0.95,-1.81,-1.81,0.6,0.63, COLOR='GRAY 80', SURF_ID='ADIABATIC'/

&OBST ID='AcDbRegion - 11B2', XB=0.915,0.95,-1.81,-1.81,0.69,0.72, COLOR='GRAY 80', SURF_ID='ADIABATIC'/

&OBST ID='AcDbRegion - 11B2', XB=0.95,0.98,-1.81,-1.81,0.6,0.72, COLOR='GRAY 80', SURF_ID='ADIABATIC'/

&OBST ID='AcDbRegion - 11B2', XB=0.98,1.015,-1.81,-1.81,0.6,0.63, COLOR='GRAY 80', SURF_ID='ADIABATIC'/

&OBST ID='AcDbRegion - 11B2', XB=0.98,1.015,-1.81,-1.81,0.69,0.72, COLOR='GRAY 80', SURF_ID='ADIABATIC'/

&OBST ID='AcDbRegion - 11B2', XB=1.015,1.045,-1.81,-1.81,0.6,0.72, COLOR='GRAY 80', SURF_ID='ADIABATIC'/

&OBST ID='AcDbRegion - 11B2', XB=1.045,1.08,-1.81,-1.81,0.6,0.63, COLOR='GRAY 80', SURF_ID='ADIABATIC'/

&OBST ID='AcDbRegion - 11B2', XB=1.045,1.08,-1.81,-1.81,0.69,0.72, COLOR='GRAY 80', SURF_ID='ADIABATIC'/

&OBST ID='AcDbRegion - 11B2', XB=1.08,1.11,-1.81,-1.81,0.6,0.72, COLOR='GRAY 80', SURF_ID='ADIABATIC'/

&OBST ID='AcDbRegion - 11B2', XB=0.24,0.275,-1.81,-1.81,0.72,0.84, COLOR='GRAY 80', SURF_ID='ADIABATIC'/

&OBST ID='AcDbRegion - 11B2', XB=0.275,0.305,-1.81,-1.81,0.72,0.745, COLOR='GRAY 80', SURF_ID='ADIABATIC'/

&OBST ID='AcDbRegion - 11B2', XB=0.275,0.305,-1.81,-1.81,0.805,0.84, COLOR='GRAY 80', SURF_ID='ADIABATIC'/

&OBST ID='AcDbRegion - 11B2', XB=0.305,0.335,-1.81,-1.81,0.72,0.84, COLOR='GRAY 80', SURF_ID='ADIABATIC'/

&OBST ID='AcDbRegion - 11B2', XB=0.335,0.37,-1.81,-1.81,0.72,0.745, COLOR='GRAY 80', SURF_ID='ADIABATIC'/

&OBST ID='AcDbRegion - 11B2', XB=0.335,0.37,-1.81,-1.81,0.805,0.84, COLOR='GRAY 80', SURF_ID='ADIABATIC'/

&OBST ID='AcDbRegion - 11B2', XB=0.37,0.4,-1.81,-1.81,0.72,0.84, COLOR='GRAY 80', SURF_ID='ADIABATIC'/

&OBST ID='AcDbRegion - 11B2', XB=0.4,0.435,-1.81,-1.81,0.72,0.745, COLOR='GRAY 80', SURF_ID='ADIABATIC'/

&OBST ID='AcDbRegion - 11B2', XB=0.4,0.435,-1.81,-1.81,0.805,0.84, COLOR='GRAY 80', SURF_ID='ADIABATIC'/

&OBST ID='AcDbRegion - 11B2', XB=0.435,0.465,-1.81,-1.81,0.72,0.84, COLOR='GRAY 80', SURF_ID='ADIABATIC'/

&OBST ID='AcDbRegion - 11B2', XB=0.465,0.5,-1.81,-1.81,0.72,0.745, COLOR='GRAY 80', SURF_ID='ADIABATIC'/

&OBST ID='AcDbRegion - 11B2', XB=0.465,0.5,-1.81,-1.81,0.805,0.84, COLOR='GRAY 80', SURF_ID='ADIABATIC'/

&OBST ID='AcDbRegion - 11B2', XB=0.5,0.53,-1.81,-1.81,0.72,0.84, COLOR='GRAY 80', SURF_ID='ADIABATIC'/

&OBST ID='AcDbRegion - 11B2', XB=0.53,0.56,-1.81,-1.81,0.72,0.745, COLOR='GRAY 80', SURF_ID='ADIABATIC'/

&OBST ID='AcDbRegion - 11B2', XB=0.53,0.56,-1.81,-1.81,0.805,0.84, COLOR='GRAY 80', SURF_ID='ADIABATIC'/

&OBST ID='AcDbRegion - 11B2', XB=0.56,0.595,-1.81,-1.81,0.72,0.84, COLOR='GRAY 80', SURF_ID='ADIABATIC'/

&OBST ID='AcDbRegion - 11B2', XB=0.595,0.625,-1.81,-1.81,0.72,0.745, COLOR='GRAY 80', SURF_ID='ADIABATIC'/

&OBST ID='AcDbRegion - 11B2', XB=0.595,0.625,-1.81,-1.81,0.805,0.84, COLOR='GRAY 80', SURF_ID='ADIABATIC'/

&OBST ID='AcDbRegion - 11B2', XB=0.625,0.66,-1.81,-1.81,0.72,0.84, COLOR='GRAY 80', SURF_ID='ADIABATIC'/

&OBST ID='AcDbRegion - 11B2', XB=0.66,0.67,-1.81,-1.81,0.72,0.745, COLOR='GRAY 80', SURF_ID='ADIABATIC'/

&OBST ID='AcDbRegion - 11B2', XB=0.66,0.67,-1.81,-1.81,0.805,0.84, COLOR='GRAY 80', SURF_ID='ADIABATIC'/

&OBST ID='AcDbRegion - 11B2', XB=0.67,0.69,-1.81,-1.81,0.72,0.745, COLOR='GRAY 80', SURF_ID='ADIABATIC'/

&OBST ID='AcDbRegion - 11B2', XB=0.67,0.69,-1.81,-1.81,0.805,0.84, COLOR='GRAY 80', SURF_ID='ADIABATIC'/

&OBST ID='AcDbRegion - 11B2', XB=0.69,0.725,-1.81,-1.81,0.72,0.84, COLOR='GRAY 80', SURF_ID='ADIABATIC'/

&OBST ID='AcDbRegion - 11B2', XB=0.725,0.755,-1.81,-1.81,0.72,0.745, COLOR='GRAY 80', SURF_ID='ADIABATIC'/

&OBST ID='AcDbRegion - 11B2', XB=0.725,0.755,-1.81,-1.81,0.805,0.84, COLOR='GRAY 80', SURF_ID='ADIABATIC'/

&OBST ID='AcDbRegion - 11B2', XB=0.755,0.79,-1.81,-1.81,0.72,0.84, COLOR='GRAY 80', SURF_ID='ADIABATIC'/

&OBST ID='AcDbRegion - 11B2', XB=0.79,0.82,-1.81,-1.81,0.72,0.745, COLOR='GRAY 80', SURF_ID='ADIABATIC'/

&OBST ID='AcDbRegion - 11B2', XB=0.79,0.82,-1.81,-1.81,0.805,0.84, COLOR='GRAY 80', SURF_ID='ADIABATIC'/

&OBST ID='AcDbRegion - 11B2', XB=0.82,0.85,-1.81,-1.81,0.72,0.84, COLOR='GRAY 80', SURF_ID='ADIABATIC'/

&OBST ID='AcDbRegion - 11B2', XB=0.85,0.885,-1.81,-1.81,0.72,0.745, COLOR='GRAY 80', SURF_ID='ADIABATIC'/

&OBST ID='AcDbRegion - 11B2', XB=0.85,0.885,-1.81,-1.81,0.805,0.84, COLOR='GRAY 80', SURF_ID='ADIABATIC'/

&OBST ID='AcDbRegion - 11B2', XB=0.885,0.915,-1.81,-1.81,0.72,0.84, COLOR='GRAY 80', SURF_ID='ADIABATIC'/

&OBST ID='AcDbRegion - 11B2', XB=0.915,0.95,-1.81,-1.81,0.72,0.745, COLOR='GRAY 80', SURF_ID='ADIABATIC'/

&OBST ID='AcDbRegion - 11B2', XB=0.915,0.95,-1.81,-1.81,0.805,0.84, COLOR='GRAY 80', SURF_ID='ADIABATIC'/

&OBST ID='AcDbRegion - 11B2', XB=0.95,0.98,-1.81,-1.81,0.72,0.84, COLOR='GRAY 80', SURF_ID='ADIABATIC'/

&OBST ID='AcDbRegion - 11B2', XB=0.98,1.015,-1.81,-1.81,0.72,0.745, COLOR='GRAY 80', SURF_ID='ADIABATIC'/

&OBST ID='AcDbRegion - 11B2', XB=0.98,1.015,-1.81,-1.81,0.805,0.84, COLOR='GRAY 80', SURF_ID='ADIABATIC'/

&OBST ID='AcDbRegion - 11B2', XB=1.015,1.045,-1.81,-1.81,0.72,0.84, COLOR='GRAY 80', SURF_ID='ADIABATIC'/

&OBST ID='AcDbRegion - 11B2', XB=1.045,1.08,-1.81,-1.81,0.72,0.745, COLOR='GRAY 80', SURF_ID='ADIABATIC'/

&OBST ID='AcDbRegion - 11B2', XB=1.045,1.08,-1.81,-1.81,0.805,0.84, COLOR='GRAY 80', SURF_ID='ADIABATIC'/

&OBST ID='AcDbRegion - 11B2', XB=1.08,1.11,-1.81,-1.81,0.72,0.84, COLOR='GRAY 80', SURF_ID='ADIABATIC'/

&OBST ID='AcDbRegion - 11B2', XB=0.24,0.275,-1.81,-1.81,0.84,0.94, COLOR='GRAY 80', SURF_ID='ADIABATIC'/

&OBST ID='AcDbRegion - 11B2', XB=0.275,0.305,-1.81,-1.81,0.84,0.86, COLOR='GRAY 80', SURF_ID='ADIABATIC'/

&OBST ID='AcDbRegion - 11B2', XB=0.275,0.305,-1.81,-1.81,0.915,0.94, COLOR='GRAY 80', SURF_ID='ADIABATIC'/

&OBST ID='AcDbRegion - 11B2', XB=0.305,0.335,-1.81,-1.81,0.84,0.94, COLOR='GRAY 80', SURF_ID='ADIABATIC'/

&OBST ID='AcDbRegion - 11B2', XB=0.335,0.37,-1.81,-1.81,0.84,0.86, COLOR='GRAY 80', SURF_ID='ADIABATIC'/

&OBST ID='AcDbRegion - 11B2', XB=0.335,0.37,-1.81,-1.81,0.915,0.94, COLOR='GRAY 80', SURF_ID='ADIABATIC'/

&OBST ID='AcDbRegion - 11B2', XB=0.37,0.4,-1.81,-1.81,0.84,0.94, COLOR='GRAY 80', SURF_ID='ADIABATIC'/

&OBST ID='AcDbRegion - 11B2', XB=0.4,0.435,-1.81,-1.81,0.84,0.86, COLOR='GRAY 80', SURF_ID='ADIABATIC'/

&OBST ID='AcDbRegion - 11B2', XB=0.4,0.435,-1.81,-1.81,0.915,0.94, COLOR='GRAY 80', SURF_ID='ADIABATIC'/

&OBST ID='AcDbRegion - 11B2', XB=0.435,0.465,-1.81,-1.81,0.84,0.94, COLOR='GRAY 80', SURF_ID='ADIABATIC'/

&OBST ID='AcDbRegion - 11B2', XB=0.465,0.5,-1.81,-1.81,0.84,0.86, COLOR='GRAY 80', SURF_ID='ADIABATIC'/

&OBST ID='AcDbRegion - 11B2', XB=0.465,0.5,-1.81,-1.81,0.915,0.94, COLOR='GRAY 80', SURF_ID='ADIABATIC'/

&OBST ID='AcDbRegion - 11B2', XB=0.5,0.53,-1.81,-1.81,0.84,0.94, COLOR='GRAY 80', SURF_ID='ADIABATIC'/

&OBST ID='AcDbRegion - 11B2', XB=0.53,0.56,-1.81,-1.81,0.84,0.86, COLOR='GRAY 80', SURF_ID='ADIABATIC'/

&OBST ID='AcDbRegion - 11B2', XB=0.53,0.56,-1.81,-1.81,0.915,0.94, COLOR='GRAY 80', SURF_ID='ADIABATIC'/

&OBST ID='AcDbRegion - 11B2', XB=0.56,0.595,-1.81,-1.81,0.84,0.94, COLOR='GRAY 80', SURF_ID='ADIABATIC'/

&OBST ID='AcDbRegion - 11B2', XB=0.595,0.625,-1.81,-1.81,0.84,0.86, COLOR='GRAY 80', SURF_ID='ADIABATIC'/

&OBST ID='AcDbRegion - 11B2', XB=0.595,0.625,-1.81,-1.81,0.915,0.94, COLOR='GRAY 80', SURF_ID='ADIABATIC'/

&OBST ID='AcDbRegion - 11B2', XB=0.625,0.66,-1.81,-1.81,0.84,0.94, COLOR='GRAY 80', SURF_ID='ADIABATIC'/

&OBST ID='AcDbRegion - 11B2', XB=0.66,0.67,-1.81,-1.81,0.84,0.86, COLOR='GRAY 80', SURF_ID='ADIABATIC'/

&OBST ID='AcDbRegion - 11B2', XB=0.66,0.67,-1.81,-1.81,0.915,0.94, COLOR='GRAY 80', SURF_ID='ADIABATIC'/

&OBST ID='AcDbRegion - 11B2', XB=0.67,0.69,-1.81,-1.81,0.84,0.86, COLOR='GRAY 80', SURF_ID='ADIABATIC'/

&OBST ID='AcDbRegion - 11B2', XB=0.67,0.69,-1.81,-1.81,0.915,0.94, COLOR='GRAY 80', SURF_ID='ADIABATIC'/

&OBST ID='AcDbRegion - 11B2', XB=0.69,0.725,-1.81,-1.81,0.84,0.94, COLOR='GRAY 80', SURF_ID='ADIABATIC'/

&OBST ID='AcDbRegion - 11B2', XB=0.725,0.755,-1.81,-1.81,0.84,0.86, COLOR='GRAY 80', SURF_ID='ADIABATIC'/

&OBST ID='AcDbRegion - 11B2', XB=0.725,0.755,-1.81,-1.81,0.915,0.94, COLOR='GRAY 80', SURF_ID='ADIABATIC'/

&OBST ID='AcDbRegion - 11B2', XB=0.755,0.79,-1.81,-1.81,0.84,0.94, COLOR='GRAY 80', SURF_ID='ADIABATIC'/

&OBST ID='AcDbRegion - 11B2', XB=0.79,0.82,-1.81,-1.81,0.84,0.86, COLOR='GRAY 80', SURF_ID='ADIABATIC'/

&OBST ID='AcDbRegion - 11B2', XB=0.79,0.82,-1.81,-1.81,0.915,0.94, COLOR='GRAY 80', SURF_ID='ADIABATIC'/

&OBST ID='AcDbRegion - 11B2', XB=0.82,0.85,-1.81,-1.81,0.84,0.94, COLOR='GRAY 80', SURF_ID='ADIABATIC'/

&OBST ID='AcDbRegion - 11B2', XB=0.85,0.885,-1.81,-1.81,0.84,0.86, COLOR='GRAY 80', SURF_ID='ADIABATIC'/

&OBST ID='AcDbRegion - 11B2', XB=0.85,0.885,-1.81,-1.81,0.915,0.94, COLOR='GRAY 80', SURF_ID='ADIABATIC'/

&OBST ID='AcDbRegion - 11B2', XB=0.885,0.915,-1.81,-1.81,0.84,0.94, COLOR='GRAY 80', SURF_ID='ADIABATIC'/

&OBST ID='AcDbRegion - 11B2', XB=0.915,0.95,-1.81,-1.81,0.84,0.86, COLOR='GRAY 80', SURF_ID='ADIABATIC'/

&OBST ID='AcDbRegion - 11B2', XB=0.915,0.95,-1.81,-1.81,0.915,0.94, COLOR='GRAY 80', SURF_ID='ADIABATIC'/

&OBST ID='AcDbRegion - 11B2', XB=0.95,0.98,-1.81,-1.81,0.84,0.94, COLOR='GRAY 80', SURF_ID='ADIABATIC'/

&OBST ID='AcDbRegion - 11B2', XB=0.98,1.015,-1.81,-1.81,0.84,0.86, COLOR='GRAY 80', SURF_ID='ADIABATIC'/

&OBST ID='AcDbRegion - 11B2', XB=0.98,1.015,-1.81,-1.81,0.915,0.94, COLOR='GRAY 80', SURF_ID='ADIABATIC'/

&OBST ID='AcDbRegion - 11B2', XB=1.015,1.045,-1.81,-1.81,0.84,0.94, COLOR='GRAY 80', SURF_ID='ADIABATIC'/

&OBST ID='AcDbRegion - 11B2', XB=1.045,1.08,-1.81,-1.81,0.84,0.86, COLOR='GRAY 80', SURF_ID='ADIABATIC'/

&OBST ID='AcDbRegion - 11B2', XB=1.045,1.08,-1.81,-1.81,0.915,0.94, COLOR='GRAY 80', SURF_ID='ADIABATIC'/

&OBST ID='AcDbRegion - 11B2', XB=1.08,1.11,-1.81,-1.81,0.84,0.94, COLOR='GRAY 80', SURF_ID='ADIABATIC'/

&OBST ID='AcDbRegion - 11B2', XB=0.24,0.275,-1.81,-1.81,0.94,1.06, COLOR='GRAY 80', SURF_ID='ADIABATIC'/

&OBST ID='AcDbRegion - 11B2', XB=0.275,0.305,-1.81,-1.81,0.94,0.97, COLOR='GRAY 80', SURF_ID='ADIABATIC'/

&OBST ID='AcDbRegion - 11B2', XB=0.275,0.305,-1.81,-1.81,1.03,1.06, COLOR='GRAY 80', SURF_ID='ADIABATIC'/

&OBST ID='AcDbRegion - 11B2', XB=0.305,0.335,-1.81,-1.81,0.94,1.06, COLOR='GRAY 80', SURF_ID='ADIABATIC'/

&OBST ID='AcDbRegion - 11B2', XB=0.335,0.37,-1.81,-1.81,0.94,0.97, COLOR='GRAY 80', SURF_ID='ADIABATIC'/

&OBST ID='AcDbRegion - 11B2', XB=0.335,0.37,-1.81,-1.81,1.03,1.06, COLOR='GRAY 80', SURF_ID='ADIABATIC'/

&OBST ID='AcDbRegion - 11B2', XB=0.37,0.4,-1.81,-1.81,0.94,1.06, COLOR='GRAY 80', SURF_ID='ADIABATIC'/

&OBST ID='AcDbRegion - 11B2', XB=0.4,0.435,-1.81,-1.81,0.94,0.97, COLOR='GRAY 80', SURF_ID='ADIABATIC'/

&OBST ID='AcDbRegion - 11B2', XB=0.4,0.435,-1.81,-1.81,1.03,1.06, COLOR='GRAY 80', SURF_ID='ADIABATIC'/

&OBST ID='AcDbRegion - 11B2', XB=0.435,0.465,-1.81,-1.81,0.94,1.06, COLOR='GRAY 80', SURF_ID='ADIABATIC'/

&OBST ID='AcDbRegion - 11B2', XB=0.465,0.5,-1.81,-1.81,0.94,0.97, COLOR='GRAY 80', SURF_ID='ADIABATIC'/

&OBST ID='AcDbRegion - 11B2', XB=0.465,0.5,-1.81,-1.81,1.03,1.06, COLOR='GRAY 80', SURF_ID='ADIABATIC'/

&OBST ID='AcDbRegion - 11B2', XB=0.5,0.53,-1.81,-1.81,0.94,1.06, COLOR='GRAY 80', SURF_ID='ADIABATIC'/

&OBST ID='AcDbRegion - 11B2', XB=0.53,0.56,-1.81,-1.81,0.94,0.97, COLOR='GRAY 80', SURF_ID='ADIABATIC'/

&OBST ID='AcDbRegion - 11B2', XB=0.53,0.56,-1.81,-1.81,1.03,1.06, COLOR='GRAY 80', SURF_ID='ADIABATIC'/

&OBST ID='AcDbRegion - 11B2', XB=0.56,0.595,-1.81,-1.81,0.94,1.06, COLOR='GRAY 80', SURF_ID='ADIABATIC'/

&OBST ID='AcDbRegion - 11B2', XB=0.595,0.625,-1.81,-1.81,0.94,0.97, COLOR='GRAY 80', SURF_ID='ADIABATIC'/

&OBST ID='AcDbRegion - 11B2', XB=0.595,0.625,-1.81,-1.81,1.03,1.06, COLOR='GRAY 80', SURF_ID='ADIABATIC'/

&OBST ID='AcDbRegion - 11B2', XB=0.625,0.66,-1.81,-1.81,0.94,1.06, COLOR='GRAY 80', SURF_ID='ADIABATIC'/

&OBST ID='AcDbRegion - 11B2', XB=0.66,0.67,-1.81,-1.81,0.94,0.97, COLOR='GRAY 80', SURF_ID='ADIABATIC'/

&OBST ID='AcDbRegion - 11B2', XB=0.66,0.67,-1.81,-1.81,1.03,1.06, COLOR='GRAY 80', SURF_ID='ADIABATIC'/

&OBST ID='AcDbRegion - 11B2', XB=0.67,0.69,-1.81,-1.81,0.94,0.97, COLOR='GRAY 80', SURF_ID='ADIABATIC'/

&OBST ID='AcDbRegion - 11B2', XB=0.67,0.69,-1.81,-1.81,1.03,1.06, COLOR='GRAY 80', SURF_ID='ADIABATIC'/

&OBST ID='AcDbRegion - 11B2', XB=0.69,0.725,-1.81,-1.81,0.94,1.06, COLOR='GRAY 80', SURF_ID='ADIABATIC'/

&OBST ID='AcDbRegion - 11B2', XB=0.725,0.755,-1.81,-1.81,0.94,0.97, COLOR='GRAY 80', SURF_ID='ADIABATIC'/

&OBST ID='AcDbRegion - 11B2', XB=0.725,0.755,-1.81,-1.81,1.03,1.06, COLOR='GRAY 80', SURF_ID='ADIABATIC'/

&OBST ID='AcDbRegion - 11B2', XB=0.755,0.79,-1.81,-1.81,0.94,1.06, COLOR='GRAY 80', SURF_ID='ADIABATIC'/

&OBST ID='AcDbRegion - 11B2', XB=0.79,0.82,-1.81,-1.81,0.94,0.97, COLOR='GRAY 80', SURF_ID='ADIABATIC'/

&OBST ID='AcDbRegion - 11B2', XB=0.79,0.82,-1.81,-1.81,1.03,1.06, COLOR='GRAY 80', SURF_ID='ADIABATIC'/

&OBST ID='AcDbRegion - 11B2', XB=0.82,0.85,-1.81,-1.81,0.94,1.06, COLOR='GRAY 80', SURF_ID='ADIABATIC'/

&OBST ID='AcDbRegion - 11B2', XB=0.85,0.885,-1.81,-1.81,0.94,0.97, COLOR='GRAY 80', SURF_ID='ADIABATIC'/

&OBST ID='AcDbRegion - 11B2', XB=0.85,0.885,-1.81,-1.81,1.03,1.06, COLOR='GRAY 80', SURF_ID='ADIABATIC'/

&OBST ID='AcDbRegion - 11B2', XB=0.885,0.915,-1.81,-1.81,0.94,1.06, COLOR='GRAY 80', SURF_ID='ADIABATIC'/

&OBST ID='AcDbRegion - 11B2', XB=0.915,0.95,-1.81,-1.81,0.94,0.97, COLOR='GRAY 80', SURF_ID='ADIABATIC'/

&OBST ID='AcDbRegion - 11B2', XB=0.915,0.95,-1.81,-1.81,1.03,1.06, COLOR='GRAY 80', SURF_ID='ADIABATIC'/

&OBST ID='AcDbRegion - 11B2', XB=0.95,0.98,-1.81,-1.81,0.94,1.06, COLOR='GRAY 80', SURF_ID='ADIABATIC'/

&OBST ID='AcDbRegion - 11B2', XB=0.98,1.015,-1.81,-1.81,0.94,0.97, COLOR='GRAY 80', SURF_ID='ADIABATIC'/

&OBST ID='AcDbRegion - 11B2', XB=0.98,1.015,-1.81,-1.81,1.03,1.06, COLOR='GRAY 80', SURF_ID='ADIABATIC'/

&OBST ID='AcDbRegion - 11B2', XB=1.015,1.045,-1.81,-1.81,0.94,1.06, COLOR='GRAY 80', SURF_ID='ADIABATIC'/

&OBST ID='AcDbRegion - 11B2', XB=1.045,1.08,-1.81,-1.81,0.94,0.97, COLOR='GRAY 80', SURF_ID='ADIABATIC'/

&OBST ID='AcDbRegion - 11B2', XB=1.045,1.08,-1.81,-1.81,1.03,1.06, COLOR='GRAY 80', SURF_ID='ADIABATIC'/

&OBST ID='AcDbRegion - 11B2', XB=1.08,1.11,-1.81,-1.81,0.94,1.06, COLOR='GRAY 80', SURF_ID='ADIABATIC'/

&OBST ID='AcDbRegion - 11B2', XB=0.24,0.275,-1.81,-1.81,1.06,1.16, COLOR='GRAY 80', SURF_ID='ADIABATIC'/

&OBST ID='AcDbRegion - 11B2', XB=0.275,0.305,-1.81,-1.81,1.06,1.085, COLOR='GRAY 80', SURF_ID='ADIABATIC'/

&OBST ID='AcDbRegion - 11B2', XB=0.275,0.305,-1.81,-1.81,1.14,1.16, COLOR='GRAY 80', SURF_ID='ADIABATIC'/

&OBST ID='AcDbRegion - 11B2', XB=0.305,0.335,-1.81,-1.81,1.06,1.16, COLOR='GRAY 80', SURF_ID='ADIABATIC'/

&OBST ID='AcDbRegion - 11B2', XB=0.335,0.37,-1.81,-1.81,1.06,1.085, COLOR='GRAY 80', SURF_ID='ADIABATIC'/

&OBST ID='AcDbRegion - 11B2', XB=0.335,0.37,-1.81,-1.81,1.14,1.16, COLOR='GRAY 80', SURF_ID='ADIABATIC'/

&OBST ID='AcDbRegion - 11B2', XB=0.37,0.4,-1.81,-1.81,1.06,1.16, COLOR='GRAY 80', SURF_ID='ADIABATIC'/

&OBST ID='AcDbRegion - 11B2', XB=0.4,0.435,-1.81,-1.81,1.06,1.085, COLOR='GRAY 80', SURF_ID='ADIABATIC'/

&OBST ID='AcDbRegion - 11B2', XB=0.4,0.435,-1.81,-1.81,1.14,1.16, COLOR='GRAY 80', SURF_ID='ADIABATIC'/

&OBST ID='AcDbRegion - 11B2', XB=0.435,0.465,-1.81,-1.81,1.06,1.16, COLOR='GRAY 80', SURF_ID='ADIABATIC'/

&OBST ID='AcDbRegion - 11B2', XB=0.465,0.5,-1.81,-1.81,1.06,1.085, COLOR='GRAY 80', SURF_ID='ADIABATIC'/

&OBST ID='AcDbRegion - 11B2', XB=0.465,0.5,-1.81,-1.81,1.14,1.16, COLOR='GRAY 80', SURF_ID='ADIABATIC'/

&OBST ID='AcDbRegion - 11B2', XB=0.5,0.53,-1.81,-1.81,1.06,1.16, COLOR='GRAY 80', SURF_ID='ADIABATIC'/

&OBST ID='AcDbRegion - 11B2', XB=0.53,0.56,-1.81,-1.81,1.06,1.085, COLOR='GRAY 80', SURF_ID='ADIABATIC'/

&OBST ID='AcDbRegion - 11B2', XB=0.53,0.56,-1.81,-1.81,1.14,1.16, COLOR='GRAY 80', SURF_ID='ADIABATIC'/

&OBST ID='AcDbRegion - 11B2', XB=0.56,0.595,-1.81,-1.81,1.06,1.16, COLOR='GRAY 80', SURF_ID='ADIABATIC'/

&OBST ID='AcDbRegion - 11B2', XB=0.595,0.625,-1.81,-1.81,1.06,1.085, COLOR='GRAY 80', SURF_ID='ADIABATIC'/

&OBST ID='AcDbRegion - 11B2', XB=0.595,0.625,-1.81,-1.81,1.14,1.16, COLOR='GRAY 80', SURF_ID='ADIABATIC'/

&OBST ID='AcDbRegion - 11B2', XB=0.625,0.66,-1.81,-1.81,1.06,1.16, COLOR='GRAY 80', SURF_ID='ADIABATIC'/

&OBST ID='AcDbRegion - 11B2', XB=0.66,0.67,-1.81,-1.81,1.06,1.085, COLOR='GRAY 80', SURF_ID='ADIABATIC'/

&OBST ID='AcDbRegion - 11B2', XB=0.66,0.67,-1.81,-1.81,1.14,1.16, COLOR='GRAY 80', SURF_ID='ADIABATIC'/

&OBST ID='AcDbRegion - 11B2', XB=0.67,0.69,-1.81,-1.81,1.06,1.085, COLOR='GRAY 80', SURF_ID='ADIABATIC'/

&OBST ID='AcDbRegion - 11B2', XB=0.67,0.69,-1.81,-1.81,1.14,1.16, COLOR='GRAY 80', SURF_ID='ADIABATIC'/

&OBST ID='AcDbRegion - 11B2', XB=0.69,0.725,-1.81,-1.81,1.06,1.16, COLOR='GRAY 80', SURF_ID='ADIABATIC'/

&OBST ID='AcDbRegion - 11B2', XB=0.725,0.755,-1.81,-1.81,1.06,1.085, COLOR='GRAY 80', SURF_ID='ADIABATIC'/

&OBST ID='AcDbRegion - 11B2', XB=0.725,0.755,-1.81,-1.81,1.14,1.16, COLOR='GRAY 80', SURF_ID='ADIABATIC'/

&OBST ID='AcDbRegion - 11B2', XB=0.755,0.79,-1.81,-1.81,1.06,1.16, COLOR='GRAY 80', SURF_ID='ADIABATIC'/

&OBST ID='AcDbRegion - 11B2', XB=0.79,0.82,-1.81,-1.81,1.06,1.085, COLOR='GRAY 80', SURF_ID='ADIABATIC'/

&OBST ID='AcDbRegion - 11B2', XB=0.79,0.82,-1.81,-1.81,1.14,1.16, COLOR='GRAY 80', SURF_ID='ADIABATIC'/

&OBST ID='AcDbRegion - 11B2', XB=0.82,0.85,-1.81,-1.81,1.06,1.16, COLOR='GRAY 80', SURF_ID='ADIABATIC'/

&OBST ID='AcDbRegion - 11B2', XB=0.85,0.885,-1.81,-1.81,1.06,1.085, COLOR='GRAY 80', SURF_ID='ADIABATIC'/

&OBST ID='AcDbRegion - 11B2', XB=0.85,0.885,-1.81,-1.81,1.14,1.16, COLOR='GRAY 80', SURF_ID='ADIABATIC'/

&OBST ID='AcDbRegion - 11B2', XB=0.885,0.915,-1.81,-1.81,1.06,1.16, COLOR='GRAY 80', SURF_ID='ADIABATIC'/

&OBST ID='AcDbRegion - 11B2', XB=0.915,0.95,-1.81,-1.81,1.06,1.085, COLOR='GRAY 80', SURF_ID='ADIABATIC'/

&OBST ID='AcDbRegion - 11B2', XB=0.915,0.95,-1.81,-1.81,1.14,1.16, COLOR='GRAY 80', SURF_ID='ADIABATIC'/

&OBST ID='AcDbRegion - 11B2', XB=0.95,0.98,-1.81,-1.81,1.06,1.16, COLOR='GRAY 80', SURF_ID='ADIABATIC'/

&OBST ID='AcDbRegion - 11B2', XB=0.98,1.015,-1.81,-1.81,1.06,1.085, COLOR='GRAY 80', SURF_ID='ADIABATIC'/

&OBST ID='AcDbRegion - 11B2', XB=0.98,1.015,-1.81,-1.81,1.14,1.16, COLOR='GRAY 80', SURF_ID='ADIABATIC'/

&OBST ID='AcDbRegion - 11B2', XB=1.015,1.045,-1.81,-1.81,1.06,1.16, COLOR='GRAY 80', SURF_ID='ADIABATIC'/

&OBST ID='AcDbRegion - 11B2', XB=1.045,1.08,-1.81,-1.81,1.06,1.085, COLOR='GRAY 80', SURF_ID='ADIABATIC'/

&OBST ID='AcDbRegion - 11B2', XB=1.045,1.08,-1.81,-1.81,1.14,1.16, COLOR='GRAY 80', SURF_ID='ADIABATIC'/

&OBST ID='AcDbRegion - 11B2', XB=1.08,1.11,-1.81,-1.81,1.06,1.16, COLOR='GRAY 80', SURF_ID='ADIABATIC'/

&OBST ID='AcDbRegion - 11B2', XB=0.24,0.275,-1.81,-1.81,1.16,1.28, COLOR='GRAY 80', SURF_ID='ADIABATIC'/

&OBST ID='AcDbRegion - 11B2', XB=0.275,0.305,-1.81,-1.81,1.16,1.195, COLOR='GRAY 80', SURF_ID='ADIABATIC'/

&OBST ID='AcDbRegion - 11B2', XB=0.275,0.305,-1.81,-1.81,1.255,1.28, COLOR='GRAY 80', SURF_ID='ADIABATIC'/

&OBST ID='AcDbRegion - 11B2', XB=0.305,0.335,-1.81,-1.81,1.16,1.28, COLOR='GRAY 80', SURF_ID='ADIABATIC'/

&OBST ID='AcDbRegion - 11B2', XB=0.335,0.37,-1.81,-1.81,1.16,1.195, COLOR='GRAY 80', SURF_ID='ADIABATIC'/

&OBST ID='AcDbRegion - 11B2', XB=0.335,0.37,-1.81,-1.81,1.255,1.28, COLOR='GRAY 80', SURF_ID='ADIABATIC'/

&OBST ID='AcDbRegion - 11B2', XB=0.37,0.4,-1.81,-1.81,1.16,1.28, COLOR='GRAY 80', SURF_ID='ADIABATIC'/

&OBST ID='AcDbRegion - 11B2', XB=0.4,0.435,-1.81,-1.81,1.16,1.195, COLOR='GRAY 80', SURF_ID='ADIABATIC'/

&OBST ID='AcDbRegion - 11B2', XB=0.4,0.435,-1.81,-1.81,1.255,1.28, COLOR='GRAY 80', SURF_ID='ADIABATIC'/

&OBST ID='AcDbRegion - 11B2', XB=0.435,0.465,-1.81,-1.81,1.16,1.28, COLOR='GRAY 80', SURF_ID='ADIABATIC'/

&OBST ID='AcDbRegion - 11B2', XB=0.465,0.5,-1.81,-1.81,1.16,1.195, COLOR='GRAY 80', SURF_ID='ADIABATIC'/

&OBST ID='AcDbRegion - 11B2', XB=0.465,0.5,-1.81,-1.81,1.255,1.28, COLOR='GRAY 80', SURF_ID='ADIABATIC'/

&OBST ID='AcDbRegion - 11B2', XB=0.5,0.53,-1.81,-1.81,1.16,1.28, COLOR='GRAY 80', SURF_ID='ADIABATIC'/

&OBST ID='AcDbRegion - 11B2', XB=0.53,0.56,-1.81,-1.81,1.16,1.195, COLOR='GRAY 80', SURF_ID='ADIABATIC'/

&OBST ID='AcDbRegion - 11B2', XB=0.53,0.56,-1.81,-1.81,1.255,1.28, COLOR='GRAY 80', SURF_ID='ADIABATIC'/

&OBST ID='AcDbRegion - 11B2', XB=0.56,0.595,-1.81,-1.81,1.16,1.28, COLOR='GRAY 80', SURF_ID='ADIABATIC'/

&OBST ID='AcDbRegion - 11B2', XB=0.595,0.625,-1.81,-1.81,1.16,1.195, COLOR='GRAY 80', SURF_ID='ADIABATIC'/

&OBST ID='AcDbRegion - 11B2', XB=0.595,0.625,-1.81,-1.81,1.255,1.28, COLOR='GRAY 80', SURF_ID='ADIABATIC'/

&OBST ID='AcDbRegion - 11B2', XB=0.625,0.66,-1.81,-1.81,1.16,1.28, COLOR='GRAY 80', SURF_ID='ADIABATIC'/

&OBST ID='AcDbRegion - 11B2', XB=0.66,0.67,-1.81,-1.81,1.16,1.195, COLOR='GRAY 80', SURF_ID='ADIABATIC'/

&OBST ID='AcDbRegion - 11B2', XB=0.66,0.67,-1.81,-1.81,1.255,1.28, COLOR='GRAY 80', SURF_ID='ADIABATIC'/

&OBST ID='AcDbRegion - 11B2', XB=0.67,0.69,-1.81,-1.81,1.16,1.195, COLOR='GRAY 80', SURF_ID='ADIABATIC'/

&OBST ID='AcDbRegion - 11B2', XB=0.67,0.69,-1.81,-1.81,1.255,1.28, COLOR='GRAY 80', SURF_ID='ADIABATIC'/

&OBST ID='AcDbRegion - 11B2', XB=0.69,0.725,-1.81,-1.81,1.16,1.28, COLOR='GRAY 80', SURF_ID='ADIABATIC'/

&OBST ID='AcDbRegion - 11B2', XB=0.725,0.755,-1.81,-1.81,1.16,1.195, COLOR='GRAY 80', SURF_ID='ADIABATIC'/

&OBST ID='AcDbRegion - 11B2', XB=0.725,0.755,-1.81,-1.81,1.255,1.28, COLOR='GRAY 80', SURF_ID='ADIABATIC'/

&OBST ID='AcDbRegion - 11B2', XB=0.755,0.79,-1.81,-1.81,1.16,1.28, COLOR='GRAY 80', SURF_ID='ADIABATIC'/

&OBST ID='AcDbRegion - 11B2', XB=0.79,0.82,-1.81,-1.81,1.16,1.195, COLOR='GRAY 80', SURF_ID='ADIABATIC'/

&OBST ID='AcDbRegion - 11B2', XB=0.79,0.82,-1.81,-1.81,1.255,1.28, COLOR='GRAY 80', SURF_ID='ADIABATIC'/

&OBST ID='AcDbRegion - 11B2', XB=0.82,0.85,-1.81,-1.81,1.16,1.28, COLOR='GRAY 80', SURF_ID='ADIABATIC'/

&OBST ID='AcDbRegion - 11B2', XB=0.85,0.885,-1.81,-1.81,1.16,1.195, COLOR='GRAY 80', SURF_ID='ADIABATIC'/

&OBST ID='AcDbRegion - 11B2', XB=0.85,0.885,-1.81,-1.81,1.255,1.28, COLOR='GRAY 80', SURF_ID='ADIABATIC'/

&OBST ID='AcDbRegion - 11B2', XB=0.885,0.915,-1.81,-1.81,1.16,1.28, COLOR='GRAY 80', SURF_ID='ADIABATIC'/

&OBST ID='AcDbRegion - 11B2', XB=0.915,0.95,-1.81,-1.81,1.16,1.195, COLOR='GRAY 80', SURF_ID='ADIABATIC'/

&OBST ID='AcDbRegion - 11B2', XB=0.915,0.95,-1.81,-1.81,1.255,1.28, COLOR='GRAY 80', SURF_ID='ADIABATIC'/

&OBST ID='AcDbRegion - 11B2', XB=0.95,0.98,-1.81,-1.81,1.16,1.28, COLOR='GRAY 80', SURF_ID='ADIABATIC'/

&OBST ID='AcDbRegion - 11B2', XB=0.98,1.015,-1.81,-1.81,1.16,1.195, COLOR='GRAY 80', SURF_ID='ADIABATIC'/

&OBST ID='AcDbRegion - 11B2', XB=0.98,1.015,-1.81,-1.81,1.255,1.28, COLOR='GRAY 80', SURF_ID='ADIABATIC'/

&OBST ID='AcDbRegion - 11B2', XB=1.015,1.045,-1.81,-1.81,1.16,1.28, COLOR='GRAY 80', SURF_ID='ADIABATIC'/

&OBST ID='AcDbRegion - 11B2', XB=1.045,1.08,-1.81,-1.81,1.16,1.195, COLOR='GRAY 80', SURF_ID='ADIABATIC'/

&OBST ID='AcDbRegion - 11B2', XB=1.045,1.08,-1.81,-1.81,1.255,1.28, COLOR='GRAY 80', SURF_ID='ADIABATIC'/

&OBST ID='AcDbRegion - 11B2', XB=1.08,1.11,-1.81,-1.81,1.16,1.28, COLOR='GRAY 80', SURF_ID='ADIABATIC'/

&OBST ID='AcDbRegion - 11B2', XB=0.24,0.275,-1.81,-1.81,1.28,1.395, COLOR='GRAY 80', SURF_ID='ADIABATIC'/

&OBST ID='AcDbRegion - 11B2', XB=0.275,0.305,-1.81,-1.81,1.28,1.31, COLOR='GRAY 80', SURF_ID='ADIABATIC'/

&OBST ID='AcDbRegion - 11B2', XB=0.275,0.305,-1.81,-1.81,1.365,1.395, COLOR='GRAY 80', SURF_ID='ADIABATIC'/

&OBST ID='AcDbRegion - 11B2', XB=0.305,0.335,-1.81,-1.81,1.28,1.395, COLOR='GRAY 80', SURF_ID='ADIABATIC'/

&OBST ID='AcDbRegion - 11B2', XB=0.335,0.37,-1.81,-1.81,1.28,1.31, COLOR='GRAY 80', SURF_ID='ADIABATIC'/

&OBST ID='AcDbRegion - 11B2', XB=0.335,0.37,-1.81,-1.81,1.365,1.395, COLOR='GRAY 80', SURF_ID='ADIABATIC'/

&OBST ID='AcDbRegion - 11B2', XB=0.37,0.4,-1.81,-1.81,1.28,1.395, COLOR='GRAY 80', SURF_ID='ADIABATIC'/

&OBST ID='AcDbRegion - 11B2', XB=0.4,0.435,-1.81,-1.81,1.28,1.31, COLOR='GRAY 80', SURF_ID='ADIABATIC'/

&OBST ID='AcDbRegion - 11B2', XB=0.4,0.435,-1.81,-1.81,1.365,1.395, COLOR='GRAY 80', SURF_ID='ADIABATIC'/

&OBST ID='AcDbRegion - 11B2', XB=0.435,0.465,-1.81,-1.81,1.28,1.395, COLOR='GRAY 80', SURF_ID='ADIABATIC'/

&OBST ID='AcDbRegion - 11B2', XB=0.465,0.5,-1.81,-1.81,1.28,1.31, COLOR='GRAY 80', SURF_ID='ADIABATIC'/

&OBST ID='AcDbRegion - 11B2', XB=0.465,0.5,-1.81,-1.81,1.365,1.395, COLOR='GRAY 80', SURF_ID='ADIABATIC'/

&OBST ID='AcDbRegion - 11B2', XB=0.5,0.53,-1.81,-1.81,1.28,1.395, COLOR='GRAY 80', SURF_ID='ADIABATIC'/

&OBST ID='AcDbRegion - 11B2', XB=0.53,0.56,-1.81,-1.81,1.28,1.31, COLOR='GRAY 80', SURF_ID='ADIABATIC'/

&OBST ID='AcDbRegion - 11B2', XB=0.53,0.56,-1.81,-1.81,1.365,1.395, COLOR='GRAY 80', SURF_ID='ADIABATIC'/

&OBST ID='AcDbRegion - 11B2', XB=0.56,0.595,-1.81,-1.81,1.28,1.395, COLOR='GRAY 80', SURF_ID='ADIABATIC'/

&OBST ID='AcDbRegion - 11B2', XB=0.595,0.625,-1.81,-1.81,1.28,1.31, COLOR='GRAY 80', SURF_ID='ADIABATIC'/

&OBST ID='AcDbRegion - 11B2', XB=0.595,0.625,-1.81,-1.81,1.365,1.395, COLOR='GRAY 80', SURF_ID='ADIABATIC'/

&OBST ID='AcDbRegion - 11B2', XB=0.625,0.66,-1.81,-1.81,1.28,1.395, COLOR='GRAY 80', SURF_ID='ADIABATIC'/

&OBST ID='AcDbRegion - 11B2', XB=0.66,0.67,-1.81,-1.81,1.28,1.31, COLOR='GRAY 80', SURF_ID='ADIABATIC'/

&OBST ID='AcDbRegion - 11B2', XB=0.66,0.67,-1.81,-1.81,1.365,1.395, COLOR='GRAY 80', SURF_ID='ADIABATIC'/

&OBST ID='AcDbRegion - 11B2', XB=0.67,0.69,-1.81,-1.81,1.28,1.31, COLOR='GRAY 80', SURF_ID='ADIABATIC'/

&OBST ID='AcDbRegion - 11B2', XB=0.67,0.69,-1.81,-1.81,1.365,1.395, COLOR='GRAY 80', SURF_ID='ADIABATIC'/

&OBST ID='AcDbRegion - 11B2', XB=0.69,0.725,-1.81,-1.81,1.28,1.395, COLOR='GRAY 80', SURF_ID='ADIABATIC'/

&OBST ID='AcDbRegion - 11B2', XB=0.725,0.755,-1.81,-1.81,1.28,1.31, COLOR='GRAY 80', SURF_ID='ADIABATIC'/

&OBST ID='AcDbRegion - 11B2', XB=0.725,0.755,-1.81,-1.81,1.365,1.395, COLOR='GRAY 80', SURF_ID='ADIABATIC'/

&OBST ID='AcDbRegion - 11B2', XB=0.755,0.79,-1.81,-1.81,1.28,1.395, COLOR='GRAY 80', SURF_ID='ADIABATIC'/

&OBST ID='AcDbRegion - 11B2', XB=0.79,0.82,-1.81,-1.81,1.28,1.31, COLOR='GRAY 80', SURF_ID='ADIABATIC'/

&OBST ID='AcDbRegion - 11B2', XB=0.79,0.82,-1.81,-1.81,1.365,1.395, COLOR='GRAY 80', SURF_ID='ADIABATIC'/

&OBST ID='AcDbRegion - 11B2', XB=0.82,0.85,-1.81,-1.81,1.28,1.395, COLOR='GRAY 80', SURF_ID='ADIABATIC'/

&OBST ID='AcDbRegion - 11B2', XB=0.85,0.885,-1.81,-1.81,1.28,1.31, COLOR='GRAY 80', SURF_ID='ADIABATIC'/

&OBST ID='AcDbRegion - 11B2', XB=0.85,0.885,-1.81,-1.81,1.365,1.395, COLOR='GRAY 80', SURF_ID='ADIABATIC'/

&OBST ID='AcDbRegion - 11B2', XB=0.885,0.915,-1.81,-1.81,1.28,1.395, COLOR='GRAY 80', SURF_ID='ADIABATIC'/

&OBST ID='AcDbRegion - 11B2', XB=0.915,0.95,-1.81,-1.81,1.28,1.31, COLOR='GRAY 80', SURF_ID='ADIABATIC'/

&OBST ID='AcDbRegion - 11B2', XB=0.915,0.95,-1.81,-1.81,1.365,1.395, COLOR='GRAY 80', SURF_ID='ADIABATIC'/

&OBST ID='AcDbRegion - 11B2', XB=0.95,0.98,-1.81,-1.81,1.28,1.395, COLOR='GRAY 80', SURF_ID='ADIABATIC'/

&OBST ID='AcDbRegion - 11B2', XB=0.98,1.015,-1.81,-1.81,1.28,1.31, COLOR='GRAY 80', SURF_ID='ADIABATIC'/

&OBST ID='AcDbRegion - 11B2', XB=0.98,1.015,-1.81,-1.81,1.365,1.395, COLOR='GRAY 80', SURF_ID='ADIABATIC'/

&OBST ID='AcDbRegion - 11B2', XB=1.015,1.045,-1.81,-1.81,1.28,1.395, COLOR='GRAY 80', SURF_ID='ADIABATIC'/

&OBST ID='AcDbRegion - 11B2', XB=1.045,1.08,-1.81,-1.81,1.28,1.31, COLOR='GRAY 80', SURF_ID='ADIABATIC'/

&OBST ID='AcDbRegion - 11B2', XB=1.045,1.08,-1.81,-1.81,1.365,1.395, COLOR='GRAY 80', SURF_ID='ADIABATIC'/

&OBST ID='AcDbRegion - 11B2', XB=1.08,1.11,-1.81,-1.81,1.28,1.395, COLOR='GRAY 80', SURF_ID='ADIABATIC'/

&OBST ID='north wall', XB=0.24,0.65,-0.94,-0.94,0.6,0.72, COLOR='GRAY 68', SURF_ID='ADIABATIC'/

&OBST ID='north wall', XB=0.65,0.68,-0.94,-0.94,0.6,0.63, COLOR='GRAY 68', SURF_ID='ADIABATIC'/

&OBST ID='north wall', XB=0.65,0.68,-0.94,-0.94,0.7,0.72, COLOR='GRAY 68', SURF_ID='ADIABATIC'/

&OBST ID='north wall', XB=0.68,0.69,-0.94,-0.94,0.6,0.72, COLOR='GRAY 68', SURF_ID='ADIABATIC'/

&OBST ID='north wall', XB=0.69,1.11,-0.94,-0.94,0.6,0.72, COLOR='GRAY 68', SURF_ID='ADIABATIC'/

&OBST ID='north wall', XB=0.24,0.65,-0.94,-0.94,0.72,0.84, COLOR='GRAY 68', SURF_ID='ADIABATIC'/

&OBST ID='north wall', XB=0.65,0.68,-0.94,-0.94,0.72,0.74, COLOR='GRAY 68', SURF_ID='ADIABATIC'/

&OBST ID='north wall', XB=0.65,0.68,-0.94,-0.94,0.81,0.84, COLOR='GRAY 68', SURF_ID='ADIABATIC'/

&OBST ID='north wall', XB=0.68,0.69,-0.94,-0.94,0.72,0.84, COLOR='GRAY 68', SURF_ID='ADIABATIC'/

&OBST ID='north wall', XB=0.69,1.11,-0.94,-0.94,0.72,0.84, COLOR='GRAY 68', SURF_ID='ADIABATIC'/

&OBST ID='north wall', XB=0.24,0.65,-0.94,-0.94,0.84,0.94, COLOR='GRAY 68', SURF_ID='ADIABATIC'/

&OBST ID='north wall', XB=0.65,0.68,-0.94,-0.94,0.84,0.85, COLOR='GRAY 68', SURF_ID='ADIABATIC'/

&OBST ID='north wall', XB=0.65,0.68,-0.94,-0.94,0.92,0.94, COLOR='GRAY 68', SURF_ID='ADIABATIC'/

&OBST ID='north wall', XB=0.68,0.69,-0.94,-0.94,0.84,0.94, COLOR='GRAY 68', SURF_ID='ADIABATIC'/

&OBST ID='north wall', XB=0.69,1.11,-0.94,-0.94,0.84,0.94, COLOR='GRAY 68', SURF_ID='ADIABATIC'/

&OBST ID='north wall', XB=0.24,0.65,-0.94,-0.94,0.94,1.06, COLOR='GRAY 68', SURF_ID='ADIABATIC'/

&OBST ID='north wall', XB=0.65,0.68,-0.94,-0.94,0.94,0.97, COLOR='GRAY 68', SURF_ID='ADIABATIC'/

&OBST ID='north wall', XB=0.65,0.68,-0.94,-0.94,1.04,1.06, COLOR='GRAY 68', SURF_ID='ADIABATIC'/

&OBST ID='north wall', XB=0.68,0.69,-0.94,-0.94,0.94,1.06, COLOR='GRAY 68', SURF_ID='ADIABATIC'/

&OBST ID='north wall', XB=0.69,1.11,-0.94,-0.94,0.94,1.06, COLOR='GRAY 68', SURF_ID='ADIABATIC'/

&OBST ID='north wall', XB=0.24,0.65,-0.94,-0.94,1.06,1.16, COLOR='GRAY 68', SURF_ID='ADIABATIC'/

&OBST ID='north wall', XB=0.65,0.68,-0.94,-0.94,1.06,1.08, COLOR='GRAY 68', SURF_ID='ADIABATIC'/

&OBST ID='north wall', XB=0.65,0.68,-0.94,-0.94,1.15,1.16, COLOR='GRAY 68', SURF_ID='ADIABATIC'/

&OBST ID='north wall', XB=0.68,0.69,-0.94,-0.94,1.06,1.16, COLOR='GRAY 68', SURF_ID='ADIABATIC'/

&OBST ID='north wall', XB=0.69,1.11,-0.94,-0.94,1.06,1.16, COLOR='GRAY 68', SURF_ID='ADIABATIC'/

&OBST ID='north wall', XB=0.24,0.65,-0.94,-0.94,1.16,1.28, COLOR='GRAY 68', SURF_ID='ADIABATIC'/

&OBST ID='north wall', XB=0.65,0.68,-0.94,-0.94,1.16,1.19, COLOR='GRAY 68', SURF_ID='ADIABATIC'/

&OBST ID='north wall', XB=0.65,0.68,-0.94,-0.94,1.26,1.28, COLOR='GRAY 68', SURF_ID='ADIABATIC'/

&OBST ID='north wall', XB=0.68,0.69,-0.94,-0.94,1.16,1.28, COLOR='GRAY 68', SURF_ID='ADIABATIC'/

&OBST ID='north wall', XB=0.69,1.11,-0.94,-0.94,1.16,1.28, COLOR='GRAY 68', SURF_ID='ADIABATIC'/

&OBST ID='north wall', XB=0.24,0.65,-0.94,-0.94,1.28,1.39, COLOR='GRAY 68', SURF_ID='ADIABATIC'/

&OBST ID='north wall', XB=0.65,0.68,-0.94,-0.94,1.28,1.3, COLOR='GRAY 68', SURF_ID='ADIABATIC'/

&OBST ID='north wall', XB=0.65,0.68,-0.94,-0.94,1.37,1.39, COLOR='GRAY 68', SURF_ID='ADIABATIC'/

&OBST ID='north wall', XB=0.68,0.69,-0.94,-0.94,1.28,1.39, COLOR='GRAY 68', SURF_ID='ADIABATIC'/

&OBST ID='north wall', XB=0.69,1.11,-0.94,-0.94,1.28,1.39, COLOR='GRAY 68', SURF_ID='ADIABATIC'/

&VENT ID='Mesh Vent: Meshnew-a-a-a [XMIN]', SURF_ID='ADIABATIC', XB=0.24,0.24,-1.86,-1.8,0.6,0.72, COLOR='INVISIBLE'/

&VENT ID='Mesh Vent: Meshnew-a-a-a [YMIN]', SURF_ID='ADIABATIC', XB=0.24,0.67,-1.86,-1.86,0.6,0.72, COLOR='INVISIBLE'/

&VENT ID='Mesh Vent: Meshnew-a-a-a [ZMIN]', SURF_ID='ADIABATIC', XB=0.24,0.67,-1.86,-1.8,0.6,0.6, COLOR='INVISIBLE'/

&VENT ID='Mesh Vent: Meshnew-a-a-b [XMAX]', SURF_ID='ADIABATIC', XB=1.12,1.12,-1.86,-1.8,0.6,0.72, COLOR='INVISIBLE'/

&VENT ID='Mesh Vent: Meshnew-a-a-b [YMIN]', SURF_ID='ADIABATIC', XB=0.67,1.12,-1.86,-1.86,0.6,0.72, COLOR='INVISIBLE'/

&VENT ID='Mesh Vent: Meshnew-a-a-b [ZMIN]', SURF_ID='ADIABATIC', XB=0.67,1.12,-1.86,-1.8,0.6,0.6, COLOR='INVISIBLE'/

&VENT ID='Mesh Vent: Meshnew-a-b-a [XMIN]', SURF_ID='ADIABATIC', XB=0.24,0.24,-1.86,-1.8,0.72,0.84, COLOR='INVISIBLE'/

&VENT ID='Mesh Vent: Meshnew-a-b-a [YMIN]', SURF_ID='ADIABATIC', XB=0.24,0.67,-1.86,-1.86,0.72,0.84, COLOR='INVISIBLE'/

&VENT ID='Mesh Vent: Meshnew-a-b-b [XMAX]', SURF_ID='ADIABATIC', XB=1.12,1.12,-1.86,-1.8,0.72,0.84, COLOR='INVISIBLE'/

&VENT ID='Mesh Vent: Meshnew-a-b-b [YMIN]', SURF_ID='ADIABATIC', XB=0.67,1.12,-1.86,-1.86,0.72,0.84, COLOR='INVISIBLE'/

&VENT ID='Mesh Vent: Meshnew-a-c-a [XMIN]', SURF_ID='ADIABATIC', XB=0.24,0.24,-1.86,-1.8,0.84,0.94, COLOR='INVISIBLE'/

&VENT ID='Mesh Vent: Meshnew-a-c-a [YMIN]', SURF_ID='ADIABATIC', XB=0.24,0.67,-1.86,-1.86,0.84,0.94, COLOR='INVISIBLE'/

&VENT ID='Mesh Vent: Meshnew-a-c-b [XMAX]', SURF_ID='ADIABATIC', XB=1.12,1.12,-1.86,-1.8,0.84,0.94, COLOR='INVISIBLE'/

&VENT ID='Mesh Vent: Meshnew-a-c-b [YMIN]', SURF_ID='ADIABATIC', XB=0.67,1.12,-1.86,-1.86,0.84,0.94, COLOR='INVISIBLE'/

&VENT ID='Mesh Vent: Meshnew-a-d-a [XMIN]', SURF_ID='ADIABATIC', XB=0.24,0.24,-1.86,-1.8,0.94,1.06, COLOR='INVISIBLE'/

&VENT ID='Mesh Vent: Meshnew-a-d-a [YMIN]', SURF_ID='ADIABATIC', XB=0.24,0.67,-1.86,-1.86,0.94,1.06, COLOR='INVISIBLE'/

&VENT ID='Mesh Vent: Meshnew-a-d-b [XMAX]', SURF_ID='ADIABATIC', XB=1.12,1.12,-1.86,-1.8,0.94,1.06, COLOR='INVISIBLE'/

&VENT ID='Mesh Vent: Meshnew-a-d-b [YMIN]', SURF_ID='ADIABATIC', XB=0.67,1.12,-1.86,-1.86,0.94,1.06, COLOR='INVISIBLE'/

&VENT ID='Mesh Vent: Meshnew-a-e-a [XMIN]', SURF_ID='ADIABATIC', XB=0.24,0.24,-1.86,-1.8,1.06,1.16, COLOR='INVISIBLE'/

&VENT ID='Mesh Vent: Meshnew-a-e-a [YMIN]', SURF_ID='ADIABATIC', XB=0.24,0.67,-1.86,-1.86,1.06,1.16, COLOR='INVISIBLE'/

&VENT ID='Mesh Vent: Meshnew-a-e-b [XMAX]', SURF_ID='ADIABATIC', XB=1.12,1.12,-1.86,-1.8,1.06,1.16, COLOR='INVISIBLE'/

&VENT ID='Mesh Vent: Meshnew-a-e-b [YMIN]', SURF_ID='ADIABATIC', XB=0.67,1.12,-1.86,-1.86,1.06,1.16, COLOR='INVISIBLE'/

&VENT ID='Mesh Vent: Meshnew-a-f-a [XMIN]', SURF_ID='ADIABATIC', XB=0.24,0.24,-1.86,-1.8,1.16,1.28, COLOR='INVISIBLE'/

&VENT ID='Mesh Vent: Meshnew-a-f-a [YMIN]', SURF_ID='ADIABATIC', XB=0.24,0.67,-1.86,-1.86,1.16,1.28, COLOR='INVISIBLE'/

&VENT ID='Mesh Vent: Meshnew-a-f-b [XMAX]', SURF_ID='ADIABATIC', XB=1.12,1.12,-1.86,-1.8,1.16,1.28, COLOR='INVISIBLE'/

&VENT ID='Mesh Vent: Meshnew-a-f-b [YMIN]', SURF_ID='ADIABATIC', XB=0.67,1.12,-1.86,-1.86,1.16,1.28, COLOR='INVISIBLE'/

&VENT ID='Mesh Vent: Meshnew-a-g-a [XMIN]', SURF_ID='ADIABATIC', XB=0.24,0.24,-1.86,-1.8,1.28,1.4, COLOR='INVISIBLE'/

&VENT ID='Mesh Vent: Meshnew-a-g-a [YMIN]', SURF_ID='ADIABATIC', XB=0.24,0.67,-1.86,-1.86,1.28,1.4, COLOR='INVISIBLE'/

&VENT ID='Mesh Vent: Meshnew-a-g-b [XMAX]', SURF_ID='ADIABATIC', XB=1.12,1.12,-1.86,-1.8,1.28,1.4, COLOR='INVISIBLE'/

&VENT ID='Mesh Vent: Meshnew-a-g-b [YMIN]', SURF_ID='ADIABATIC', XB=0.67,1.12,-1.86,-1.86,1.28,1.4, COLOR='INVISIBLE'/

&VENT ID='Mesh Vent: Meshnew-a-h [XMAX]', SURF_ID='ADIABATIC', XB=1.12,1.12,-1.86,-1.8,1.4,1.5, COLOR='INVISIBLE'/

&VENT ID='Mesh Vent: Meshnew-a-h [XMIN]', SURF_ID='ADIABATIC', XB=0.24,0.24,-1.86,-1.8,1.4,1.5, COLOR='INVISIBLE'/

&VENT ID='Mesh Vent: Meshnew-a-h [YMIN]', SURF_ID='ADIABATIC', XB=0.24,1.12,-1.86,-1.86,1.4,1.5, COLOR='INVISIBLE'/

&VENT ID='Mesh Vent: Meshnew-a-i-a [XMIN]', SURF_ID='ADIABATIC', XB=0.24,0.24,-1.8,-0.84,0.6,0.72, COLOR='INVISIBLE'/

&VENT ID='Mesh Vent: Meshnew-a-i-a [ZMIN]', SURF_ID='ADIABATIC', XB=0.24,0.69,-1.8,-0.84,0.6,0.6, COLOR='INVISIBLE'/

&VENT ID='Mesh Vent: Meshnew-a-i-b [XMAX]', SURF_ID='ADIABATIC', XB=1.12,1.12,-1.8,-0.84,0.6,0.72, COLOR='INVISIBLE'/

&VENT ID='Mesh Vent: Meshnew-a-i-b [ZMIN]', SURF_ID='ADIABATIC', XB=0.69,1.12,-1.8,-0.84,0.6,0.6, COLOR='INVISIBLE'/

&VENT ID='Mesh Vent: Meshnew-a-j-a [XMIN]', SURF_ID='ADIABATIC', XB=0.24,0.24,-1.8,-0.84,0.72,0.84, COLOR='INVISIBLE'/

&VENT ID='Mesh Vent: Meshnew-a-j-b [XMAX]', SURF_ID='ADIABATIC', XB=1.12,1.12,-1.8,-0.84,0.72,0.84, COLOR='INVISIBLE'/

&VENT ID='Mesh Vent: Meshnew-a-k-a [XMIN]', SURF_ID='ADIABATIC', XB=0.24,0.24,-1.8,-0.84,0.84,0.94, COLOR='INVISIBLE'/

&VENT ID='Mesh Vent: Meshnew-a-k-b [XMAX]', SURF_ID='ADIABATIC', XB=1.12,1.12,-1.8,-0.84,0.84,0.94, COLOR='INVISIBLE'/

&VENT ID='Mesh Vent: Meshnew-a-l-a [XMIN]', SURF_ID='ADIABATIC', XB=0.24,0.24,-1.8,-0.84,0.94,1.06, COLOR='INVISIBLE'/

&VENT ID='Mesh Vent: Meshnew-a-l-b [XMAX]', SURF_ID='ADIABATIC', XB=1.12,1.12,-1.8,-0.84,0.94,1.06, COLOR='INVISIBLE'/

&VENT ID='Mesh Vent: Meshnew-a-m-a [XMIN]', SURF_ID='ADIABATIC', XB=0.24,0.24,-1.8,-0.84,1.06,1.16, COLOR='INVISIBLE'/

&VENT ID='Mesh Vent: Meshnew-a-m-b [XMAX]', SURF_ID='ADIABATIC', XB=1.12,1.12,-1.8,-0.84,1.06,1.16, COLOR='INVISIBLE'/

&VENT ID='Mesh Vent: Meshnew-a-n-a [XMIN]', SURF_ID='ADIABATIC', XB=0.24,0.24,-1.8,-0.84,1.16,1.28, COLOR='INVISIBLE'/

&VENT ID='Mesh Vent: Meshnew-a-n-b [XMAX]', SURF_ID='ADIABATIC', XB=1.12,1.12,-1.8,-0.84,1.16,1.28, COLOR='INVISIBLE'/

&VENT ID='Mesh Vent: Meshnew-a-o-a [XMIN]', SURF_ID='ADIABATIC', XB=0.24,0.24,-1.8,-0.84,1.28,1.4, COLOR='INVISIBLE'/

&VENT ID='Mesh Vent: Meshnew-a-o-b [XMAX]', SURF_ID='ADIABATIC', XB=1.12,1.12,-1.8,-0.84,1.28,1.4, COLOR='INVISIBLE'/

&VENT ID='Mesh Vent: Meshnew-a-p-a [XMIN]', SURF_ID='ADIABATIC', XB=0.24,0.24,-1.8,-0.84,1.4,1.5, COLOR='INVISIBLE'/

&VENT ID='Mesh Vent: Meshnew-a-p-b [XMAX]', SURF_ID='ADIABATIC', XB=1.12,1.12,-1.8,-0.84,1.4,1.5, COLOR='INVISIBLE'/

&VENT ID='Mesh Vent: Meshnew-b-a-a [XMIN]', SURF_ID='ADIABATIC', XB=0.24,0.24,-1.86,-0.84,1.5,1.61, COLOR='INVISIBLE'/

&VENT ID='Mesh Vent: Meshnew-b-a-a [YMIN]', SURF_ID='ADIABATIC', XB=0.24,0.68,-1.86,-1.86,1.5,1.61, COLOR='INVISIBLE'/

&VENT ID='Mesh Vent: Meshnew-b-a-b [XMIN]', SURF_ID='ADIABATIC', XB=0.24,0.24,-1.86,-0.84,1.61,1.72, COLOR='INVISIBLE'/

&VENT ID='Mesh Vent: Meshnew-b-a-b [YMIN]', SURF_ID='ADIABATIC', XB=0.24,0.68,-1.86,-1.86,1.61,1.72, COLOR='INVISIBLE'/

&VENT ID='Mesh Vent: Meshnew-b-b-a [XMAX]', SURF_ID='ADIABATIC', XB=1.12,1.12,-1.86,-0.84,1.5,1.61, COLOR='INVISIBLE'/

&VENT ID='Mesh Vent: Meshnew-b-b-a [YMIN]', SURF_ID='ADIABATIC', XB=0.68,1.12,-1.86,-1.86,1.5,1.61, COLOR='INVISIBLE'/

&VENT ID='Mesh Vent: Meshnew-b-b-b [XMAX]', SURF_ID='ADIABATIC', XB=1.12,1.12,-1.86,-0.84,1.61,1.72, COLOR='INVISIBLE'/

&VENT ID='Mesh Vent: Meshnew-b-b-b [YMIN]', SURF_ID='ADIABATIC', XB=0.68,1.12,-1.86,-1.86,1.61,1.72, COLOR='INVISIBLE'/

&VENT ID='Mesh Vent: Meshnew-c-a [XMIN]', SURF_ID='ADIABATIC', XB=0.24,0.24,-1.86,-0.84,1.72,2.0, COLOR='INVISIBLE'/

&VENT ID='Mesh Vent: Meshnew-c-a [YMIN]', SURF_ID='ADIABATIC', XB=0.24,0.7,-1.86,-1.86,1.72,2.0, COLOR='INVISIBLE'/

&VENT ID='Mesh Vent: Meshnew-c-a [ZMAX]', SURF_ID='OPEN', XB=0.24,0.7,-1.86,-0.84,2.0,2.0, COLOR='INVISIBLE'/

&VENT ID='Mesh Vent: Meshnew-c-b [XMAX]', SURF_ID='ADIABATIC', XB=1.12,1.12,-1.86,-0.84,1.72,2.0, COLOR='INVISIBLE'/

&VENT ID='Mesh Vent: Meshnew-c-b [YMIN]', SURF_ID='ADIABATIC', XB=0.7,1.12,-1.86,-1.86,1.72,2.0, COLOR='INVISIBLE'/

&VENT ID='Mesh Vent: Meshnew-c-b [ZMAX]', SURF_ID='OPEN', XB=0.7,1.12,-1.86,-0.84,2.0,2.0, COLOR='INVISIBLE'/

&VENT ID='Mesh Vent: Meshnew-d-a-a [XMAX]', SURF_ID='ADIABATIC', XB=1.12,1.12,-0.84,-0.58,0.6,0.84, COLOR='INVISIBLE'/

&VENT ID='Mesh Vent: Meshnew-d-a-a [XMIN]', SURF_ID='ADIABATIC', XB=0.24,0.24,-0.84,-0.58,0.6,0.84, COLOR='INVISIBLE'/

&VENT ID='Mesh Vent: Meshnew-d-a-a [ZMIN]', SURF_ID='ADIABATIC', XB=0.24,1.12,-0.84,-0.58,0.6,0.6, COLOR='INVISIBLE'/

&VENT ID='Mesh Vent: Meshnew-d-a-b [XMAX]', SURF_ID='ADIABATIC', XB=1.12,1.12,-0.84,-0.58,0.84,1.06, COLOR='INVISIBLE'/

&VENT ID='Mesh Vent: Meshnew-d-a-b [XMIN]', SURF_ID='ADIABATIC', XB=0.24,0.24,-0.84,-0.58,0.84,1.06, COLOR='INVISIBLE'/

&VENT ID='Mesh Vent: Meshnew-d-b-a [XMAX]', SURF_ID='ADIABATIC', XB=1.12,1.12,-0.84,-0.58,1.06,1.28, COLOR='INVISIBLE'/

&VENT ID='Mesh Vent: Meshnew-d-b-a [XMIN]', SURF_ID='ADIABATIC', XB=0.24,0.24,-0.84,-0.58,1.06,1.28, COLOR='INVISIBLE'/

&VENT ID='Mesh Vent: Meshnew-d-b-b [XMAX]', SURF_ID='ADIABATIC', XB=1.12,1.12,-0.84,-0.58,1.28,1.5, COLOR='INVISIBLE'/

&VENT ID='Mesh Vent: Meshnew-d-b-b [XMIN]', SURF_ID='ADIABATIC', XB=0.24,0.24,-0.84,-0.58,1.28,1.5, COLOR='INVISIBLE'/

&VENT ID='Mesh Vent: Meshnew-e [XMAX]', SURF_ID='ADIABATIC', XB=1.12,1.12,-0.84,-0.58,1.5,1.72, COLOR='INVISIBLE'/

&VENT ID='Mesh Vent: Meshnew-e [XMIN]', SURF_ID='ADIABATIC', XB=0.24,0.24,-0.84,-0.58,1.5,1.72, COLOR='INVISIBLE'/

&VENT ID='Mesh Vent: Meshnew-f [XMAX]', SURF_ID='ADIABATIC', XB=1.12,1.12,-0.84,-0.58,1.72,2.0, COLOR='INVISIBLE'/

&VENT ID='Mesh Vent: Meshnew-f [XMIN]', SURF_ID='ADIABATIC', XB=0.24,0.24,-0.84,-0.58,1.72,2.0, COLOR='INVISIBLE'/

&VENT ID='Mesh Vent: Meshnew-f [ZMAX]', SURF_ID='OPEN', XB=0.24,1.12,-0.84,-0.58,2.0,2.0, COLOR='INVISIBLE'/

&VENT ID='Mesh Vent: Meshnew-g-a-a [XMAX]', SURF_ID='ADIABATIC', XB=1.12,1.12,-0.58,-0.28,0.6,0.84, COLOR='INVISIBLE'/

&VENT ID='Mesh Vent: Meshnew-g-a-a [XMIN]', SURF_ID='ADIABATIC', XB=0.24,0.24,-0.58,-0.28,0.6,0.84, COLOR='INVISIBLE'/

&VENT ID='Mesh Vent: Meshnew-g-a-a [YMAX]', SURF_ID='OPEN', XB=0.24,1.12,-0.28,-0.28,0.6,0.84, COLOR='INVISIBLE'/

&VENT ID='Mesh Vent: Meshnew-g-a-a [ZMIN]', SURF_ID='ADIABATIC', XB=0.24,1.12,-0.58,-0.28,0.6,0.6, COLOR='INVISIBLE'/

&VENT ID='Mesh Vent: Meshnew-g-a-b [XMAX]', SURF_ID='ADIABATIC', XB=1.12,1.12,-0.58,-0.28,0.84,1.06, COLOR='INVISIBLE'/

&VENT ID='Mesh Vent: Meshnew-g-a-b [XMIN]', SURF_ID='ADIABATIC', XB=0.24,0.24,-0.58,-0.28,0.84,1.06, COLOR='INVISIBLE'/

&VENT ID='Mesh Vent: Meshnew-g-a-b [YMAX]', SURF_ID='OPEN', XB=0.24,1.12,-0.28,-0.28,0.84,1.06, COLOR='INVISIBLE'/

&VENT ID='Mesh Vent: Meshnew-g-b [XMAX]', SURF_ID='ADIABATIC', XB=1.12,1.12,-0.58,-0.28,1.06,1.5, COLOR='INVISIBLE'/

&VENT ID='Mesh Vent: Meshnew-g-b [XMIN]', SURF_ID='ADIABATIC', XB=0.24,0.24,-0.58,-0.28,1.06,1.5, COLOR='INVISIBLE'/

&VENT ID='Mesh Vent: Meshnew-g-b [YMAX]', SURF_ID='OPEN', XB=0.24,1.12,-0.28,-0.28,1.06,1.5, COLOR='INVISIBLE'/

&VENT ID='Mesh Vent: Meshnew-h-merged-a [XMAX]', SURF_ID='ADIABATIC', XB=1.12,1.12,-0.58,-0.28,1.5,1.72, COLOR='INVISIBLE'/

&VENT ID='Mesh Vent: Meshnew-h-merged-a [XMIN]', SURF_ID='ADIABATIC', XB=0.24,0.24,-0.58,-0.28,1.5,1.72, COLOR='INVISIBLE'/

&VENT ID='Mesh Vent: Meshnew-h-merged-a [YMAX]', SURF_ID='OPEN', XB=0.24,1.12,-0.28,-0.28,1.5,1.72, COLOR='INVISIBLE'/

&VENT ID='Mesh Vent: Meshnew-h-merged-b [XMAX]', SURF_ID='ADIABATIC', XB=1.12,1.12,-0.58,-0.28,1.72,2.0, COLOR='INVISIBLE'/

&VENT ID='Mesh Vent: Meshnew-h-merged-b [XMIN]', SURF_ID='ADIABATIC', XB=0.24,0.24,-0.58,-0.28,1.72,2.0, COLOR='INVISIBLE'/

&VENT ID='Mesh Vent: Meshnew-h-merged-b [YMAX]', SURF_ID='OPEN', XB=0.24,1.12,-0.28,-0.28,1.72,2.0, COLOR='INVISIBLE'/

&VENT ID='Mesh Vent: Meshnew-h-merged-b [ZMAX]', SURF_ID='OPEN', XB=0.24,1.12,-0.58,-0.28,2.0,2.0, COLOR='INVISIBLE'/

&SLCF QUANTITY='VELOCITY', VECTOR=.TRUE., PBY=-1.340646/

&SLCF QUANTITY='TEMPERATURE', PBY=-1.340646/

&SLCF QUANTITY='VELOCITY', VECTOR=.TRUE., PBY=-0.954246/

&SLCF QUANTITY='TEMPERATURE', PBY=-0.954246/

&SLCF QUANTITY='VELOCITY', VECTOR=.TRUE., PBY=-1.823646/

&SLCF QUANTITY='TEMPERATURE', PBY=-1.823646/

&SLCF QUANTITY='VELOCITY', VECTOR=.TRUE., PBX=0.658902/

&SLCF QUANTITY='TEMPERATURE', PBX=0.658902/

&DEVC ID='Velocity P L_STEADY STATE', QUANTITY='VELOCITY', XB=0.62,0.62,-1.82,-1.82,0.63,1.41, POINTS=15/

&DEVC ID='Velocity In Mid_STEADY STATE', QUANTITY='VELOCITY', XB=0.67,0.67,-1.39,-1.39,0.63,1.36, POINTS=14/

&DEVC ID='Velocity P Mid_STEADY STATE', QUANTITY='VELOCITY', XB=0.67,0.67,-1.82,-1.82,0.63,1.41, POINTS=15/

&DEVC ID='Velocity P R_STEADY STATE', QUANTITY='VELOCITY', XB=0.72,0.72,-1.82,-1.82,0.63,1.41, POINTS=15/

&DEVC ID='Velocity In B_STEADY STATE', QUANTITY='VELOCITY', XB=0.67,0.67,-1.29,-1.29,0.63,1.36, POINTS=14/

&DEVC ID='Viscosity P L_STEADY STATE', QUANTITY='VISCOSITY', XB=0.62,0.62,-1.82,-1.82,0.63,1.41, POINTS=15/

&DEVC ID='Velocity In F_STEADY STATE', QUANTITY='VELOCITY', XB=0.67,0.67,-1.49,-1.49,0.63,1.36, POINTS=14/

&DEVC ID='Viscosity P Mid_STEADY STATE', QUANTITY='VISCOSITY', XB=0.67,0.67,-1.82,-1.82,0.63,1.41, POINTS=15/

&DEVC ID='Viscosity In F_STEADY STATE', QUANTITY='VISCOSITY', XB=0.67,0.67,-1.49,-1.49,0.63,1.36, POINTS=14/

&DEVC ID='Viscosity P R_STEADY STATE', QUANTITY='VISCOSITY', XB=0.72,0.72,-1.82,-1.82,0.63,1.41, POINTS=15/

&DEVC ID='Viscosity In Mid_STEADY STATE', QUANTITY='VISCOSITY', XB=0.67,0.67,-1.39,-1.39,0.63,1.36, POINTS=14/

&DEVC ID='Viscosity In B_STEADY STATE', QUANTITY='VISCOSITY', XB=0.67,0.67,-1.29,-1.29,0.63,1.36, POINTS=14/

&DEVC ID='Density In B_STEADY STATE', QUANTITY='DENSITY', XB=0.67,0.67,-1.29,-1.29,0.63,1.36, POINTS=14/

&DEVC ID='Density In Mid_STEADY STATE', QUANTITY='DENSITY', XB=0.67,0.67,-1.39,-1.39,0.63,1.36, POINTS=14/

&DEVC ID='Density In F_STEADY STATE', QUANTITY='DENSITY', XB=0.67,0.67,-1.49,-1.49,0.63,1.36, POINTS=14/

&DEVC ID='Density P R_STEADY STATE', QUANTITY='DENSITY', XB=0.72,0.72,-1.82,-1.82,0.63,1.41, POINTS=15/

&DEVC ID='Density P Mid_STEADY STATE', QUANTITY='DENSITY', XB=0.67,0.67,-1.82,-1.82,0.63,1.41, POINTS=15/

&DEVC ID='Density P L_STEADY STATE', QUANTITY='DENSITY', XB=0.62,0.62,-1.82,-1.82,0.63,1.41, POINTS=15/

&DEVC ID='Temp P R_STEADY STATE', QUANTITY='TEMPERATURE', XB=0.72,0.72,-1.82,-1.82,0.63,1.41, POINTS=15/

&DEVC ID='Temp P Mid_STEADY STATE', QUANTITY='TEMPERATURE', XB=0.67,0.67,-1.82,-1.82,0.63,1.41, POINTS=15/

&DEVC ID='Temp P L_STEADY STATE', QUANTITY='TEMPERATURE', XB=0.62,0.62,-1.82,-1.82,0.63,1.41, POINTS=15/

&DEVC ID='Temp In Mid_STEADY STATE', QUANTITY='TEMPERATURE', XB=0.67,0.67,-1.29,-1.29,0.63,1.36, POINTS=14/

&DEVC ID='Temp In B_STEADY STATE', QUANTITY='TEMPERATURE', XB=0.67,0.67,-1.39,-1.39,0.63,1.36, POINTS=14/

&DEVC ID='Temp In F_STEADY STATE', QUANTITY='TEMPERATURE', XB=0.67,0.67,-1.49,-1.49,0.63,1.36, POINTS=14/

&TAIL /

Appendix C (FDS input code for case 2 with helium in full-scale)

scaledupcase2.fds
Generated by PyroSim - Version 2021.2.0512
17-Jun-2022 9:50:27 AM

&HEAD CHID='scaledupcase2'/
&TIME T_END=1000.0/
&DUMP DT_RESTART=300.0, DT_SL3D=0.25/
&RADI RADIATION=.FALSE./

&MESH ID='Meshnew-a-a-a', IJK=86,12,24, XB=-12.96,0.37,-25.56,-23.7,-18.0,-14.28/
&MESH ID='Meshnew-a-a-b', IJK=90,12,24, XB=0.37,14.32,-25.56,-23.7,-18.0,-14.28/
&MESH ID='Meshnew-a-b-a', IJK=86,12,24, XB=-12.96,0.37,-25.56,-23.7,-14.28,-10.56/
&MESH ID='Meshnew-a-b-b', IJK=90,12,24, XB=0.37,14.32,-25.56,-23.7,-14.28,-10.56/
&MESH ID='Meshnew-a-c-a', IJK=86,12,20, XB=-12.96,0.37,-25.56,-23.7,-10.56,-7.46/
&MESH ID='Meshnew-a-c-b', IJK=90,12,20, XB=0.37,14.32,-25.56,-23.7,-10.56,-7.46/
&MESH ID='Meshnew-a-d-a', IJK=86,12,24, XB=-12.96,0.37,-25.56,-23.7,-7.46,-3.74/
&MESH ID='Meshnew-a-d-b', IJK=90,12,24, XB=0.37,14.32,-25.56,-23.7,-7.46,-3.74/
&MESH ID='Meshnew-a-e-a', IJK=86,12,20, XB=-12.96,0.37,-25.56,-23.7,-3.74,-0.64/
&MESH ID='Meshnew-a-e-b', IJK=90,12,20, XB=0.37,14.32,-25.56,-23.7,-3.74,-0.64/
&MESH ID='Meshnew-a-f-a', IJK=86,12,24, XB=-12.96,0.37,-25.56,-23.7,-0.64,3.08/
&MESH ID='Meshnew-a-f-b', IJK=90,12,24, XB=0.37,14.32,-25.56,-23.7,-0.64,3.08/
&MESH ID='Meshnew-a-g-a', IJK=86,12,24, XB=-12.96,0.37,-25.56,-23.7,3.08,6.8/
&MESH ID='Meshnew-a-g-b', IJK=90,12,24, XB=0.37,14.32,-25.56,-23.7,3.08,6.8/
&MESH ID='Meshnew-a-h', IJK=176,12,20, XB=-12.96,14.32,-25.56,-23.7,6.8,9.9/
&MESH ID='Meshnew-a-i-a', IJK=45,96,12, XB=-12.96,0.99,-23.7,6.06,-18.0,-14.28/
&MESH ID='Meshnew-a-i-b', IJK=43,96,12, XB=0.99,14.32,-23.7,6.06,-18.0,-14.28/
&MESH ID='Meshnew-a-j-a', IJK=45,96,12, XB=-12.96,0.99,-23.7,6.06,-14.28,-10.56/
&MESH ID='Meshnew-a-j-b', IJK=43,96,12, XB=0.99,14.32,-23.7,6.06,-14.28,-10.56/
&MESH ID='Meshnew-a-k-a', IJK=45,96,10, XB=-12.96,0.99,-23.7,6.06,-10.56,-7.46/
&MESH ID='Meshnew-a-k-b', IJK=43,96,10, XB=0.99,14.32,-23.7,6.06,-10.56,-7.46/
&MESH ID='Meshnew-a-l-a', IJK=45,96,12, XB=-12.96,0.99,-23.7,6.06,-7.46,-3.74/

```
&MESH ID='Meshnew-a-l-b', IJK=43,96,12, XB=0.99,14.32,-23.7,6.06,-7.46,-3.74/
&MESH ID='Meshnew-a-m-a', IJK=45,96,10, XB=-12.96,0.99,-23.7,6.06,-3.74,-0.64/
&MESH ID='Meshnew-a-m-b', IJK=43,96,10, XB=0.99,14.32,-23.7,6.06,-3.74,-0.64/
&MESH ID='Meshnew-a-n-a', IJK=45,96,12, XB=-12.96,0.99,-23.7,6.06,-0.64,3.08/
&MESH ID='Meshnew-a-n-b', IJK=43,96,12, XB=0.99,14.32,-23.7,6.06,-0.64,3.08/
&MESH ID='Meshnew-a-o-a', IJK=45,96,12, XB=-12.96,0.99,-23.7,6.06,3.08,6.8/
&MESH ID='Meshnew-a-o-b', IJK=43,96,12, XB=0.99,14.32,-23.7,6.06,3.08,6.8/
&MESH ID='Meshnew-a-p-a', IJK=45,96,10, XB=-12.96,0.99,-23.7,6.06,6.8,9.9/
&MESH ID='Meshnew-a-p-b', IJK=43,96,10, XB=0.99,14.32,-23.7,6.06,6.8,9.9/
&MESH ID='Meshnew-b-a-a', IJK=44,102,11, XB=-12.96,0.68,-25.56,6.06,9.9,13.31/
&MESH ID='Meshnew-b-a-b', IJK=44,102,11, XB=-12.96,0.68,-25.56,6.06,13.31,16.72/
&MESH ID='Meshnew-b-b-a', IJK=44,102,11, XB=0.68,14.32,-25.56,6.06,9.9,13.31/
&MESH ID='Meshnew-b-b-b', IJK=44,102,11, XB=0.68,14.32,-25.56,6.06,13.31,16.72/
&MESH ID='Meshnew-c-a', IJK=23,51,14, XB=-12.96,1.3,-25.56,6.06,16.72,25.4/
&MESH ID='Meshnew-c-b', IJK=21,51,14, XB=1.3,14.32,-25.56,6.06,16.72,25.4/
&MESH ID='Meshnew-d-a-a', IJK=88,26,24, XB=-12.96,14.32,6.06,14.12,-18.0,-10.56/
&MESH ID='Meshnew-d-a-b', IJK=88,26,22, XB=-12.96,14.32,6.06,14.12,-10.56,-3.74/
&MESH ID='Meshnew-d-b-a', IJK=88,26,22, XB=-12.96,14.32,6.06,14.12,-3.74,3.08/
&MESH ID='Meshnew-d-b-b', IJK=88,26,22, XB=-12.96,14.32,6.06,14.12,3.08,9.9/
&MESH ID='Meshnew-e', IJK=88,26,22, XB=-12.96,14.32,6.06,14.12,9.9,16.72/
&MESH ID='Meshnew-f', IJK=44,13,14, XB=-12.96,14.32,6.06,14.12,16.72,25.4/
&MESH ID='Meshnew-g-a-a', IJK=44,15,12, XB=-12.96,14.32,14.12,23.42,-18.0,-10.56/
&MESH ID='Meshnew-g-a-b', IJK=44,15,11, XB=-12.96,14.32,14.12,23.42,-10.56,-3.74/
&MESH ID='Meshnew-g-b', IJK=44,15,22, XB=-12.96,14.32,14.12,23.42,-3.74,9.9/
&MESH ID='Meshnew-h-merged-a', IJK=44,15,11, XB=-12.96,14.32,14.12,23.42,9.9,16.72/
&MESH ID='Meshnew-h-merged-b', IJK=44,15,14, XB=-12.96,14.32,14.12,23.42,16.72,25.4/


&REAC ID='PMMA',
    FYI='SFPE Handbook, 3rd Edition',
    FUEL='REAC_FUEL',
    C=1.0,
    H=1.6,
    O=0.4,
    CO_YIELD=0.01,
    SOOT_YIELD=0.022,
    RADIATIVE_FRACTION=0.35/
```

&DEVC ID='TC-L1-M1', QUANTITY='THERMOCOUPLE', XYZ=0.465976,-21.919763,-16.223669/
&DEVC ID='TC-L2-M1', QUANTITY='THERMOCOUPLE', XYZ=0.465976,-21.919763,-12.729969/
&DEVC ID='TC-L3-M1', QUANTITY='THERMOCOUPLE', XYZ=0.465971,-21.91976,-9.236257/
&DEVC ID='TC-L4-M1', QUANTITY='THERMOCOUPLE', XYZ=0.465971,-21.91976,-5.742557/
&DEVC ID='TC-L5-M1', QUANTITY='THERMOCOUPLE', XYZ=0.465971,-21.91976,-2.248857/
&DEVC ID='TC-L6-M1', QUANTITY='THERMOCOUPLE', XYZ=0.465971,-21.91976,1.045203/
&DEVC ID='TC-L7-M1', QUANTITY='THERMOCOUPLE', XYZ=0.465971,-21.91976,4.838363/
&DEVC ID='TC-L1-M2', QUANTITY='THERMOCOUPLE', XYZ=0.465976,-17.269763,-16.223669/
&DEVC ID='TC-L2-M2', QUANTITY='THERMOCOUPLE', XYZ=0.465976,-17.269763,-12.729969/
&DEVC ID='TC-L3-M2', QUANTITY='THERMOCOUPLE', XYZ=0.465971,-17.26976,-9.236257/
&DEVC ID='TC-L4-M2', QUANTITY='THERMOCOUPLE', XYZ=0.465971,-17.26976,-5.742557/
&DEVC ID='TC-L5-M2', QUANTITY='THERMOCOUPLE', XYZ=0.465971,-17.26976,-2.248857/
&DEVC ID='TC-L6-M2', QUANTITY='THERMOCOUPLE', XYZ=0.465971,-17.26976,1.045203/
&DEVC ID='TC-L7-M2', QUANTITY='THERMOCOUPLE', XYZ=0.465971,-17.26976,4.838363/
&DEVC ID='TC-L1-M3', QUANTITY='THERMOCOUPLE', XYZ=0.465976,-11.069763,-16.223669/
&DEVC ID='TC-L2-M3', QUANTITY='THERMOCOUPLE', XYZ=0.465976,-11.069763,-12.729969/
&DEVC ID='TC-L3-M3', QUANTITY='THERMOCOUPLE', XYZ=0.465971,-11.06976,-9.236257/
&DEVC ID='TC-L4-M3', QUANTITY='THERMOCOUPLE', XYZ=0.465971,-11.06976,-5.742557/
&DEVC ID='TC-L5-M3', QUANTITY='THERMOCOUPLE', XYZ=0.465971,-11.06976,-2.248857/
&DEVC ID='TC-L6-M3', QUANTITY='THERMOCOUPLE', XYZ=0.465971,-11.06976,1.045203/
&DEVC ID='TC-L7-M3', QUANTITY='THERMOCOUPLE', XYZ=0.465971,-11.06976,4.838363/
&DEVC ID='TC-L1-M4', QUANTITY='THERMOCOUPLE', XYZ=0.465976,-4.869763,-16.223669/
&DEVC ID='TC-L2-M4', QUANTITY='THERMOCOUPLE', XYZ=0.465976,-4.869763,-12.729969/
&DEVC ID='TC-L3-M4', QUANTITY='THERMOCOUPLE', XYZ=0.465971,-4.86976,-9.236257/
&DEVC ID='TC-L4-M4', QUANTITY='THERMOCOUPLE', XYZ=0.465971,-4.86976,-5.742557/
&DEVC ID='TC-L5-M4', QUANTITY='THERMOCOUPLE', XYZ=0.465971,-4.86976,-2.248857/
&DEVC ID='TC-L6-M4', QUANTITY='THERMOCOUPLE', XYZ=0.465971,-4.86976,1.045203/
&DEVC ID='TC-L7-M4', QUANTITY='THERMOCOUPLE', XYZ=0.465971,-4.86976,4.838363/
&DEVC ID='TC-L1-M5', QUANTITY='THERMOCOUPLE', XYZ=0.465976,1.330237,-16.223669/
&DEVC ID='TC-L2-M5', QUANTITY='THERMOCOUPLE', XYZ=0.465976,1.330237,-12.729969/
&DEVC ID='TC-L3-M5', QUANTITY='THERMOCOUPLE', XYZ=0.465971,1.33024,-9.236257/
&DEVC ID='TC-L4-M5', QUANTITY='THERMOCOUPLE', XYZ=0.465971,1.33024,-5.742557/
&DEVC ID='TC-L5-M5', QUANTITY='THERMOCOUPLE', XYZ=0.465971,1.33024,-2.248857/
&DEVC ID='TC-L6-M5', QUANTITY='THERMOCOUPLE', XYZ=0.465971,1.33024,1.045203/
&DEVC ID='TC-L7-M5', QUANTITY='THERMOCOUPLE', XYZ=0.465971,1.33024,4.838363/
&DEVC ID='TC-L1-L1', QUANTITY='THERMOCOUPLE', XYZ=-9.454024,-21.919763,-16.223669/

&DEVC ID='TC-L2-L1', QUANTITY='THERMOCOUPLE', XYZ=-9.454024,-21.919763,-12.729969/
&DEVC ID='TC-L3-L1', QUANTITY='THERMOCOUPLE', XYZ=-9.454029,-21.91976,-9.236257/
&DEVC ID='TC-L4-L1', QUANTITY='THERMOCOUPLE', XYZ=-9.454029,-21.91976,-5.742557/
&DEVC ID='TC-L5-L1', QUANTITY='THERMOCOUPLE', XYZ=-9.454029,-21.91976,-2.248857/
&DEVC ID='TC-L6-L1', QUANTITY='THERMOCOUPLE', XYZ=-9.454029,-21.91976,1.045203/
&DEVC ID='TC-L7-L1', QUANTITY='THERMOCOUPLE', XYZ=-9.454029,-21.91976,4.838363/
&DEVC ID='TC-L1-L2', QUANTITY='THERMOCOUPLE', XYZ=-9.454024,-17.269763,-16.223669/
&DEVC ID='TC-L2-L2', QUANTITY='THERMOCOUPLE', XYZ=-9.454024,-17.269763,-12.729969/
&DEVC ID='TC-L3-L2', QUANTITY='THERMOCOUPLE', XYZ=-9.454029,-17.26976,-9.236257/
&DEVC ID='TC-L4-L2', QUANTITY='THERMOCOUPLE', XYZ=-9.454029,-17.26976,-5.742557/
&DEVC ID='TC-L5-L2', QUANTITY='THERMOCOUPLE', XYZ=-9.454029,-17.26976,-2.248857/
&DEVC ID='TC-L6-L2', QUANTITY='THERMOCOUPLE', XYZ=-9.454029,-17.26976,1.045203/
&DEVC ID='TC-L7-L2', QUANTITY='THERMOCOUPLE', XYZ=-9.454029,-17.26976,4.838363/
&DEVC ID='TC-L1-L3', QUANTITY='THERMOCOUPLE', XYZ=-9.454024,-11.069763,-16.223669/
&DEVC ID='TC-L2-L3', QUANTITY='THERMOCOUPLE', XYZ=-9.454024,-11.069763,-12.729969/
&DEVC ID='TC-L3-L3', QUANTITY='THERMOCOUPLE', XYZ=-9.454029,-11.06976,-9.236257/
&DEVC ID='TC-L4-L3', QUANTITY='THERMOCOUPLE', XYZ=-9.454029,-11.06976,-5.742557/
&DEVC ID='TC-L5-L3', QUANTITY='THERMOCOUPLE', XYZ=-9.454029,-11.06976,-2.248857/
&DEVC ID='TC-L6-L3', QUANTITY='THERMOCOUPLE', XYZ=-9.454029,-11.06976,1.045203/
&DEVC ID='TC-L7-L3', QUANTITY='THERMOCOUPLE', XYZ=-9.454029,-11.06976,4.838363/
&DEVC ID='TC-L1-L4', QUANTITY='THERMOCOUPLE', XYZ=-9.454024,-4.869763,-16.223669/
&DEVC ID='TC-L2-L4', QUANTITY='THERMOCOUPLE', XYZ=-9.454024,-4.869763,-12.729969/
&DEVC ID='TC-L3-L4', QUANTITY='THERMOCOUPLE', XYZ=-9.454029,-4.86976,-9.236257/
&DEVC ID='TC-L4-L4', QUANTITY='THERMOCOUPLE', XYZ=-9.454029,-4.86976,-5.742557/
&DEVC ID='TC-L5-L4', QUANTITY='THERMOCOUPLE', XYZ=-9.454029,-4.86976,-2.248857/
&DEVC ID='TC-L6-L4', QUANTITY='THERMOCOUPLE', XYZ=-9.454029,-4.86976,1.045203/
&DEVC ID='TC-L7-L4', QUANTITY='THERMOCOUPLE', XYZ=-9.454029,-4.86976,4.838363/
&DEVC ID='TC-L1-L5', QUANTITY='THERMOCOUPLE', XYZ=-9.454024,1.330237,-16.223669/
&DEVC ID='TC-L2-L5', QUANTITY='THERMOCOUPLE', XYZ=-9.454024,1.330237,-12.729969/
&DEVC ID='TC-L3-L5', QUANTITY='THERMOCOUPLE', XYZ=-9.454029,1.33024,-9.236257/
&DEVC ID='TC-L4-L5', QUANTITY='THERMOCOUPLE', XYZ=-9.454029,1.33024,-5.742557/
&DEVC ID='TC-L5-L5', QUANTITY='THERMOCOUPLE', XYZ=-9.454029,1.33024,-2.248857/
&DEVC ID='TC-L6-L5', QUANTITY='THERMOCOUPLE', XYZ=-9.454029,1.33024,1.045203/
&DEVC ID='TC-L7-L5', QUANTITY='THERMOCOUPLE', XYZ=-9.454029,1.33024,4.838363/
&DEVC ID='TC-L1-R1', QUANTITY='THERMOCOUPLE', XYZ=10.385976,-21.919763,-16.223669/
&DEVC ID='TC-L2-R1', QUANTITY='THERMOCOUPLE', XYZ=10.385976,-21.919763,-12.729969/
&DEVC ID='TC-L3-R1', QUANTITY='THERMOCOUPLE', XYZ=10.385971,-21.91976,-9.236257/

&DEVC ID='TC-L4-R1', QUANTITY='THERMOCOUPLE', XYZ=10.385971,-21.91976,-5.742557/
&DEVC ID='TC-L5-R1', QUANTITY='THERMOCOUPLE', XYZ=10.385971,-21.91976,-2.248857/
&DEVC ID='TC-L6-R1', QUANTITY='THERMOCOUPLE', XYZ=10.385971,-21.91976,1.045203/
&DEVC ID='TC-L7-R1', QUANTITY='THERMOCOUPLE', XYZ=10.385971,-21.91976,4.838363/
&DEVC ID='TC-L1-R2', QUANTITY='THERMOCOUPLE', XYZ=10.385976,-17.269763,-16.223669/
&DEVC ID='TC-L2-R2', QUANTITY='THERMOCOUPLE', XYZ=10.385976,-17.269763,-12.729969/
&DEVC ID='TC-L3-R2', QUANTITY='THERMOCOUPLE', XYZ=10.385971,-17.26976,-9.236257/
&DEVC ID='TC-L4-R2', QUANTITY='THERMOCOUPLE', XYZ=10.385971,-17.26976,-5.742557/
&DEVC ID='TC-L5-R2', QUANTITY='THERMOCOUPLE', XYZ=10.385971,-17.26976,-2.248857/
&DEVC ID='TC-L6-R2', QUANTITY='THERMOCOUPLE', XYZ=10.385971,-17.26976,1.045203/
&DEVC ID='TC-L7-R2', QUANTITY='THERMOCOUPLE', XYZ=10.385971,-17.26976,4.838363/
&DEVC ID='TC-L1-R3', QUANTITY='THERMOCOUPLE', XYZ=10.385976,-11.069763,-16.223669/
&DEVC ID='TC-L2-R3', QUANTITY='THERMOCOUPLE', XYZ=10.385976,-11.069763,-12.729969/
&DEVC ID='TC-L3-R3', QUANTITY='THERMOCOUPLE', XYZ=10.385971,-11.06976,-9.236257/
&DEVC ID='TC-L4-R3', QUANTITY='THERMOCOUPLE', XYZ=10.385971,-11.06976,-5.742557/
&DEVC ID='TC-L5-R3', QUANTITY='THERMOCOUPLE', XYZ=10.385971,-11.06976,-2.248857/
&DEVC ID='TC-L6-R3', QUANTITY='THERMOCOUPLE', XYZ=10.385971,-11.06976,1.045203/
&DEVC ID='TC-L7-R3', QUANTITY='THERMOCOUPLE', XYZ=10.385971,-11.06976,4.838363/
&DEVC ID='TC-L1-R4', QUANTITY='THERMOCOUPLE', XYZ=10.385976,-4.869763,-16.223669/
&DEVC ID='TC-L2-R4', QUANTITY='THERMOCOUPLE', XYZ=10.385976,-4.869763,-12.729969/
&DEVC ID='TC-L3-R4', QUANTITY='THERMOCOUPLE', XYZ=10.385971,-4.86976,-9.236257/
&DEVC ID='TC-L4-R4', QUANTITY='THERMOCOUPLE', XYZ=10.385971,-4.86976,-5.742557/
&DEVC ID='TC-L5-R4', QUANTITY='THERMOCOUPLE', XYZ=10.385971,-4.86976,-2.248857/
&DEVC ID='TC-L6-R4', QUANTITY='THERMOCOUPLE', XYZ=10.385971,-4.86976,1.045203/
&DEVC ID='TC-L7-R4', QUANTITY='THERMOCOUPLE', XYZ=10.385971,-4.86976,4.838363/
&DEVC ID='TC-L1-R5', QUANTITY='THERMOCOUPLE', XYZ=10.385976,1.330237,-16.223669/
&DEVC ID='TC-L2-R5', QUANTITY='THERMOCOUPLE', XYZ=10.385976,1.330237,-12.729969/
&DEVC ID='TC-L3-R5', QUANTITY='THERMOCOUPLE', XYZ=10.385971,1.33024,-9.236257/
&DEVC ID='TC-L4-R5', QUANTITY='THERMOCOUPLE', XYZ=10.385971,1.33024,-5.742557/
&DEVC ID='TC-L5-R5', QUANTITY='THERMOCOUPLE', XYZ=10.385971,1.33024,-2.248857/
&DEVC ID='TC-L6-R5', QUANTITY='THERMOCOUPLE', XYZ=10.385971,1.33024,1.045203/
&DEVC ID='TC-L7-R5', QUANTITY='THERMOCOUPLE', XYZ=10.385971,1.33024,4.838363/
&DEVC ID='TC-L1PM1', QUANTITY='THERMOCOUPLE', XYZ=0.465976,-24.285931,-16.223669/
&DEVC ID='TC-L2PM1', QUANTITY='THERMOCOUPLE', XYZ=0.465976,-24.285931,-12.729969/
&DEVC ID='TC-L3PM1', QUANTITY='THERMOCOUPLE', XYZ=0.465976,-24.285931,-9.236269/
&DEVC ID='TC-L4PM1', QUANTITY='THERMOCOUPLE', XYZ=0.465976,-24.285931,-5.742569/
&DEVC ID='TC-L5PM1', QUANTITY='THERMOCOUPLE', XYZ=0.465976,-24.285931,-2.248869/

&DEVC ID='TC-L6PM1', QUANTITY='THERMOCOUPLE', XYZ=0.465976,-24.285931,1.244831/
&DEVC ID='TC-L7PM1', QUANTITY='THERMOCOUPLE', XYZ=0.465976,-24.285931,4.738531/
&DEVC ID='TC-L1PM2', QUANTITY='THERMOCOUPLE', XYZ=0.465976,-25.215931,-16.223669/
&DEVC ID='TC-L2PM2', QUANTITY='THERMOCOUPLE', XYZ=0.465976,-25.215931,-12.729969/
&DEVC ID='TC-L3PM2', QUANTITY='THERMOCOUPLE', XYZ=0.465976,-25.215931,-9.236269/
&DEVC ID='TC-L4PM2', QUANTITY='THERMOCOUPLE', XYZ=0.465976,-25.215931,-5.742569/
&DEVC ID='TC-L5PM2', QUANTITY='THERMOCOUPLE', XYZ=0.465976,-25.215931,-2.248869/
&DEVC ID='TC-L6PM2', QUANTITY='THERMOCOUPLE', XYZ=0.465976,-25.215931,1.244831/
&DEVC ID='TC-L7PM2', QUANTITY='THERMOCOUPLE', XYZ=0.465976,-25.215931,4.738531/
&DEVC ID='TC-L1PL1', QUANTITY='THERMOCOUPLE', XYZ=-9.454024,-24.285931,-16.223669/
&DEVC ID='TC-L2PL1', QUANTITY='THERMOCOUPLE', XYZ=-9.454024,-24.285931,-12.729969/
&DEVC ID='TC-L3PL1', QUANTITY='THERMOCOUPLE', XYZ=-9.454024,-24.285931,-9.236269/
&DEVC ID='TC-L4PL1', QUANTITY='THERMOCOUPLE', XYZ=-9.454024,-24.285931,-5.742569/
&DEVC ID='TC-L5PL1', QUANTITY='THERMOCOUPLE', XYZ=-9.454024,-24.285931,-2.248869/
&DEVC ID='TC-L6PL1', QUANTITY='THERMOCOUPLE', XYZ=-9.454024,-24.285931,1.244831/
&DEVC ID='TC-L7PL1', QUANTITY='THERMOCOUPLE', XYZ=-9.454024,-24.285931,4.738531/
&DEVC ID='TC-L1PL2', QUANTITY='THERMOCOUPLE', XYZ=-9.454024,-25.215931,-16.223669/
&DEVC ID='TC-L2PL2', QUANTITY='THERMOCOUPLE', XYZ=-9.454024,-25.215931,-12.729969/
&DEVC ID='TC-L3PL2', QUANTITY='THERMOCOUPLE', XYZ=-9.454024,-25.215931,-9.236269/
&DEVC ID='TC-L4PL2', QUANTITY='THERMOCOUPLE', XYZ=-9.454024,-25.215931,-5.742569/
&DEVC ID='TC-L5PL2', QUANTITY='THERMOCOUPLE', XYZ=-9.454024,-25.215931,-2.248869/
&DEVC ID='TC-L6PL2', QUANTITY='THERMOCOUPLE', XYZ=-9.454024,-25.215931,1.244831/
&DEVC ID='TC-L7PL2', QUANTITY='THERMOCOUPLE', XYZ=-9.454024,-25.215931,4.738531/
&DEVC ID='TC-L1PR1', QUANTITY='THERMOCOUPLE', XYZ=10.385976,-24.285931,-16.223669/
&DEVC ID='TC-L2PR1', QUANTITY='THERMOCOUPLE', XYZ=10.385976,-24.285931,-12.729969/
&DEVC ID='TC-L3PR1', QUANTITY='THERMOCOUPLE', XYZ=10.385976,-24.285931,-9.236269/
&DEVC ID='TC-L4PR1', QUANTITY='THERMOCOUPLE', XYZ=10.385976,-24.285931,-5.742569/
&DEVC ID='TC-L5PR1', QUANTITY='THERMOCOUPLE', XYZ=10.385976,-24.285931,-2.248869/
&DEVC ID='TC-L6PR1', QUANTITY='THERMOCOUPLE', XYZ=10.385976,-24.285931,1.244831/
&DEVC ID='TC-L7PR1', QUANTITY='THERMOCOUPLE', XYZ=10.385976,-24.285931,4.738531/
&DEVC ID='TC-L1PR2', QUANTITY='THERMOCOUPLE', XYZ=10.385976,-25.215931,-16.223669/
&DEVC ID='TC-L2PR2', QUANTITY='THERMOCOUPLE', XYZ=10.385976,-25.215931,-12.729969/
&DEVC ID='TC-L3PR2', QUANTITY='THERMOCOUPLE', XYZ=10.385976,-25.215931,-9.236269/
&DEVC ID='TC-L4PR2', QUANTITY='THERMOCOUPLE', XYZ=10.385976,-25.215931,-5.742569/
&DEVC ID='TC-L5PR2', QUANTITY='THERMOCOUPLE', XYZ=10.385976,-25.215931,-2.248869/
&DEVC ID='TC-L6PR2', QUANTITY='THERMOCOUPLE', XYZ=10.385976,-25.215931,1.244831/
&DEVC ID='TC-L7PR2', QUANTITY='THERMOCOUPLE', XYZ=10.385976,-25.215931,4.738531/

&DEVC ID='FLOW01', QUANTITY='MASS FLOW', XB=0.025962,1.024162,-23.933926,-23.933926,-16.99715,-15.20039/

&DEVC ID='FLOW02', QUANTITY='MASS FLOW', XB=0.025962,1.024162,-23.933926,-23.933926,-13.50345,-11.70669/

&DEVC ID='FLOW03', QUANTITY='MASS FLOW', XB=0.025962,1.024162,-23.933926,-23.933926,-10.00975,-8.21299/

&DEVC ID='FLOW04', QUANTITY='MASS FLOW', XB=0.025962,1.024162,-23.933926,-23.933926,-6.51605,-4.71929/

&DEVC ID='FLOW05', QUANTITY='MASS FLOW', XB=0.025962,1.024162,-23.933926,-23.933926,-3.02235,-1.22559/

&DEVC ID='FLOW06', QUANTITY='MASS FLOW', XB=0.025962,1.024162,-23.933926,-23.933926,0.47135,2.26811/

&DEVC ID='FLOW07', QUANTITY='MASS FLOW', XB=0.025962,1.024162,-23.933926,-23.933926,3.96505,5.76181/

&DEVC ID='heat flow', QUANTITY='HEAT FLOW', XB=0.025949,0.025949,-24.931833,22.981771,-17.84562,25.57608/

&DEVC ID='mass flow', QUANTITY='MASS FLOW', XB=0.025949,0.025949,-24.931833,22.981767,-17.84562,25.57608/

&DEVC ID='volume flow', QUANTITY='VOLUME FLOW', XB=0.025949,0.025949,-24.931833,22.981767,-17.84562,25.57608/

&DEVC ID='heat flow plenum', QUANTITY='HEAT FLOW', XB=-12.950651,14.000749,-23.933913,-23.933913,6.61028,7.60848/

&DEVC ID='mass flow plenum', QUANTITY='MASS FLOW', XB=-12.950651,14.000749,-23.933913,-23.933913,6.61028,7.60848/

&DEVC ID='volume flow plenum', QUANTITY='VOLUME FLOW', XB=-12.950651,14.000749,-23.933913,-23.933913,6.61028,7.60848/

&SURF ID='ADIABATIC',

COLOR='GRAY 80',

ADIABATIC=.TRUE./

&SURF ID='fire',

RGB=255,102,0,

HRRPUA=951.0,

TMP_FRONT=300.0/

&OBST ID='Obstruction', XB=-12.950638,14.000749,-25.431213,-24.931816,-7.36452,-6.491095, SURF_ID6='ADIABATIC','ADIABATIC','ADIABATIC','fire','ADIABATIC','ADIABATIC'/

&OBST ID='west wall', XB=-12.96,-12.96,-24.01,-23.7,-18.0,-14.28, COLOR='INVISIBLE', SURF_ID='ADIABATIC'/

&OBST ID='west wall', XB=-12.96,-12.96,-24.01,-23.7,-14.28,-10.56, COLOR='INVISIBLE', SURF_ID='ADIABATIC'/

&OBST ID='west wall', XB=-12.96,-12.96,-24.01,-23.7,-10.56,-7.46, COLOR='INVISIBLE', SURF_ID='ADIABATIC'/

&OBST ID='west wall', XB=-12.96,-12.96,-24.01,-23.7,-7.46,-3.74, COLOR='INVISIBLE', SURF_ID='ADIABATIC'/

&OBST ID='west wall', XB=-12.96,-12.96,-24.01,-23.7,-3.74,-0.64, COLOR='INVISIBLE', SURF_ID='ADIABATIC'/

&OBST ID='west wall', XB=-12.96,-12.96,-24.01,-23.7,-0.64,3.08, COLOR='INVISIBLE', SURF_ID='ADIABATIC'/

&OBST ID='west wall', XB=-12.96,-12.96,-24.01,-23.7,3.08,6.645, COLOR='INVISIBLE', SURF_ID='ADIABATIC'/

&OBST ID='west wall', XB=-12.96,-12.96,-23.7,2.96,-18.0,-14.28, COLOR='INVISIBLE', SURF_ID='ADIABATIC'/

&OBST ID='west wall', XB=-12.96,-12.96,-23.7,2.96,-14.28,-10.56, COLOR='INVISIBLE', SURF_ID='ADIABATIC'/

&OBST ID='west wall', XB=-12.96,-12.96,-23.7,2.96,-10.56,-7.46, COLOR='INVISIBLE', SURF_ID='ADIABATIC'/

&OBST ID='west wall', XB=-12.96,-12.96,-23.7,2.96,-7.46,-3.74, COLOR='INVISIBLE', SURF_ID='ADIABATIC'/

&OBST ID='west wall', XB=-12.96,-12.96,-23.7,2.96,-3.74,-0.64, COLOR='INVISIBLE', SURF_ID='ADIABATIC'/

&OBST ID='west wall', XB=-12.96,-12.96,-23.7,2.96,-0.64,3.08, COLOR='INVISIBLE', SURF_ID='ADIABATIC'/

&OBST ID='west wall', XB=-12.96,-12.96,-23.7,2.96,3.08,6.49, COLOR='INVISIBLE', SURF_ID='ADIABATIC'/

&OBST ID='roof', XB=-12.96,0.37,-24.01,-23.7,6.645,6.645, COLOR='GRAY 68', SURF_ID='ADIABATIC'/

&OBST ID='roof', XB=0.37,14.01,-24.01,-23.7,6.645,6.645, COLOR='GRAY 68', SURF_ID='ADIABATIC'/

&OBST ID='roof', XB=-12.96,0.99,-23.7,2.96,6.49,6.49, COLOR='GRAY 68', SURF_ID='ADIABATIC'/

&OBST ID='roof', XB=0.99,14.01,-23.7,2.96,6.49,6.49, COLOR='GRAY 68', SURF_ID='ADIABATIC'/

&OBST ID='east wall', XB=14.01,14.01,-24.01,-23.7,-18.0,-14.28, COLOR='GRAY 68', SURF_ID='ADIABATIC'/

&OBST ID='east wall', XB=14.01,14.01,-24.01,-23.7,-14.28,-10.56, COLOR='GRAY 68', SURF_ID='ADIABATIC'/

&OBST ID='east wall', XB=14.01,14.01,-24.01,-23.7,-10.56,-7.46, COLOR='GRAY 68', SURF_ID='ADIABATIC'/

&OBST ID='east wall', XB=14.01,14.01,-24.01,-23.7,-7.46,-3.74, COLOR='GRAY 68', SURF_ID='ADIABATIC'/

&OBST ID='east wall', XB=14.01,14.01,-24.01,-23.7,-3.74,-0.64, COLOR='GRAY 68', SURF_ID='ADIABATIC'/

&OBST ID='east wall', XB=14.01,14.01,-24.01,-23.7,-0.64,3.08, COLOR='GRAY 68', SURF_ID='ADIABATIC'/

&OBST ID='east wall', XB=14.01,14.01,-24.01,-23.7,3.08,6.645, COLOR='GRAY 68', SURF_ID='ADIABATIC'/

&OBST ID='east wall', XB=14.01,14.01,-23.7,2.96,-18.0,-14.28, COLOR='GRAY 68', SURF_ID='ADIABATIC'/

&OBST ID='east wall', XB=14.01,14.01,-23.7,2.96,-14.28,-10.56, COLOR='GRAY 68', SURF_ID='ADIABATIC'/

&OBST ID='east wall', XB=14.01,14.01,-23.7,2.96,-10.56,-7.46, COLOR='GRAY 68', SURF_ID='ADIABATIC'/

&OBST ID='east wall', XB=14.01,14.01,-23.7,2.96,-7.46,-3.74, COLOR='GRAY 68', SURF_ID='ADIABATIC'/

&OBST ID='east wall', XB=14.01,14.01,-23.7,2.96,-3.74,-0.64, COLOR='GRAY 68', SURF_ID='ADIABATIC'/

&OBST ID='east wall', XB=14.01,14.01,-23.7,2.96,-0.64,3.08, COLOR='GRAY 68', SURF_ID='ADIABATIC'/

&OBST ID='east wall', XB=14.01,14.01,-23.7,2.96,3.08,6.49, COLOR='GRAY 68', SURF_ID='ADIABATIC'/

&OBST ID='floor of conference salon', XB=-12.96,0.37,-24.01,-23.7,3.08,3.08, COLOR='GRAY 68', SURF_ID='ADIABATIC'/

&OBST ID='floor of conference salon', XB=0.37,14.01,-24.01,-23.7,3.08,3.08, COLOR='GRAY 68', SURF_ID='ADIABATIC'/

&OBST ID='floor of conference salon', XB=-12.96,0.99,-23.7,2.96,3.08,3.08, COLOR='GRAY 68', SURF_ID='ADIABATIC'/

&OBST ID='floor of conference salon', XB=0.99,14.01,-23.7,2.96,3.08,3.08, COLOR='GRAY 68', SURF_ID='ADIABATIC'/

&OBST ID='floor of 6th level', XB=-12.96,0.37,-24.01,-23.7,-0.33,-0.33, COLOR='GRAY 68', SURF_ID='ADIABATIC'/

&OBST ID='floor of 6th level', XB=0.37,14.01,-24.01,-23.7,-0.33,-0.33, COLOR='GRAY 68', SURF_ID='ADIABATIC'/

&OBST ID='floor of 6th level', XB=-12.96,0.99,-23.7,2.96,-0.33,-0.33, COLOR='GRAY 68', SURF_ID='ADIABATIC'/

&OBST ID='floor of 6th level', XB=0.99,14.01,-23.7,2.96,-0.33,-0.33, COLOR='GRAY 68', SURF_ID='ADIABATIC'/

&OBST ID='floor of 5th level', XB=-12.96,0.37,-24.01,-23.7,-3.895,-3.895, COLOR='GRAY 68', SURF_ID='ADIABATIC'/

&OBST ID='floor of 5th level', XB=0.37,14.01,-24.01,-23.7,-3.895,-3.895, COLOR='GRAY 68', SURF_ID='ADIABATIC'/

&OBST ID='floor of 5th level', XB=-12.96,0.99,-23.7,2.96,-3.74,-3.74, COLOR='GRAY 68', SURF_ID='ADIABATIC'/

&OBST ID='floor of 5th level', XB=0.99,14.01,-23.7,2.96,-3.74,-3.74, COLOR='GRAY 68', SURF_ID='ADIABATIC'/

&OBST ID='floor of 4th level', XB=-12.96,0.37,-24.01,-23.7,-7.305,-7.305, COLOR='GRAY 68', SURF_ID='ADIABATIC'/

&OBST ID='floor of 4th level', XB=0.37,14.01,-24.01,-23.7,-7.305,-7.305, COLOR='GRAY 68', SURF_ID='ADIABATIC'/

&OBST ID='floor of 4th level', XB=-12.96,0.99,-23.7,2.96,-7.46,-7.46, COLOR='GRAY 68', SURF_ID='ADIABATIC'/

&OBST ID='floor of 4th level', XB=0.99,14.01,-23.7,2.96,-7.46,-7.46, COLOR='GRAY 68', SURF_ID='ADIABATIC'/

&OBST ID='floor of 3rd level', XB=-12.96,0.37,-24.01,-23.7,-10.87,-10.87, COLOR='GRAY 68', SURF_ID='ADIABATIC'/

&OBST ID='floor of 3rd level', XB=0.37,14.01,-24.01,-23.7,-10.87,-10.87, COLOR='GRAY 68', SURF_ID='ADIABATIC'/

&OBST ID='floor of 3rd level', XB=-12.96,0.99,-23.7,2.96,-10.87,-10.87, COLOR='GRAY 68', SURF_ID='ADIABATIC'/

&OBST ID='floor of 3rd level', XB=0.99,14.01,-23.7,2.96,-10.87,-10.87, COLOR='GRAY 68', SURF_ID='ADIABATIC'/

&OBST ID='floor of 2nd level', XB=-12.96,0.37,-24.01,-23.7,-14.28,-14.28, COLOR='GRAY 68', SURF_ID='ADIABATIC'/

&OBST ID='floor of 2nd level', XB=0.37,14.01,-24.01,-23.7,-14.28,-14.28, COLOR='GRAY 68', SURF_ID='ADIABATIC'/

&OBST ID='floor of 2nd level', XB=-12.96,0.99,-23.7,2.96,-14.28,-14.28, COLOR='GRAY 68', SURF_ID='ADIABATIC'/

&OBST ID='floor of 2nd level', XB=0.99,14.01,-23.7,2.96,-14.28,-14.28, COLOR='GRAY 68', SURF_ID='ADIABATIC'/

&OBST ID='floor of 1st level', XB=-12.96,0.37,-24.01,-23.7,-17.845,-17.845, COLOR='GRAY 68', SURF_ID='ADIABATIC'/

&OBST ID='floor of 1st level', XB=0.37,14.01,-24.01,-23.7,-17.845,-17.845, COLOR='GRAY 68', SURF_ID='ADIABATIC'/

&OBST ID='floor of 1st level', XB=-12.96,0.99,-23.7,2.96,-18.0,-18.0, COLOR='GRAY 68', SURF_ID='ADIABATIC'/

&OBST ID='floor of 1st level', XB=0.99,14.01,-23.7,2.96,-18.0,-18.0, COLOR='GRAY 68', SURF_ID='ADIABATIC'/

&OBST ID='plenum west', XB=-12.96,-12.96,-25.405,-24.01,-17.845,-14.28, COLOR='INVISIBLE', SURF_ID='ADIABATIC'/

&OBST ID='plenum west', XB=-12.96,-12.96,-25.405,-24.01,-14.28,-10.56, COLOR='INVISIBLE', SURF_ID='ADIABATIC'/

&OBST ID='plenum west', XB=-12.96,-12.96,-25.405,-24.01,-10.56,-7.46, COLOR='INVISIBLE', SURF_ID='ADIABATIC'/

&OBST ID='plenum west', XB=-12.96,-12.96,-25.405,-24.01,-7.46,-3.74, COLOR='INVISIBLE', SURF_ID='ADIABATIC'/

&OBST ID='plenum west', XB=-12.96,-12.96,-25.405,-24.01,-3.74,-0.64, COLOR='INVISIBLE', SURF_ID='ADIABATIC'/

&OBST ID='plenum west', XB=-12.96,-12.96,-25.405,-24.01,-0.64,3.08, COLOR='INVISIBLE', SURF_ID='ADIABATIC'/

&OBST ID='plenum west', XB=-12.96,-12.96,-25.405,-24.01,3.08,6.8, COLOR='INVISIBLE', SURF_ID='ADIABATIC'/

&OBST ID='plenum west', XB=-12.96,-12.96,-25.405,-24.01,6.8,7.575, COLOR='INVISIBLE', SURF_ID='ADIABATIC'/

&OBST ID='plenum top', XB=-12.96,14.01,-25.405,-24.01,7.575,7.575, COLOR='CYAN', SURF_ID='ADIABATIC'/

&OBST ID='plenum east', XB=14.01,14.01,-25.405,-24.01,-17.845,-14.28, COLOR='CYAN', SURF_ID='ADIABATIC'/

&OBST ID='plenum east', XB=14.01,14.01,-25.405,-24.01,-14.28,-10.56, COLOR='CYAN', SURF_ID='ADIABATIC'/

&OBST ID='plenum east', XB=14.01,14.01,-25.405,-24.01,-10.56,-7.46, COLOR='CYAN', SURF_ID='ADIABATIC'/

&OBST ID='plenum east', XB=14.01,14.01,-25.405,-24.01,-7.46,-3.74, COLOR='CYAN', SURF_ID='ADIABATIC'/

&OBST ID='plenum east', XB=14.01,14.01,-25.405,-24.01,-3.74,-0.64, COLOR='CYAN', SURF_ID='ADIABATIC'/

&OBST ID='plenum east', XB=14.01,14.01,-25.405,-24.01,-0.64,3.08, COLOR='CYAN', SURF_ID='ADIABATIC'/

&OBST ID='plenum east', XB=14.01,14.01,-25.405,-24.01,3.08,6.8, COLOR='CYAN', SURF_ID='ADIABATIC'/

&OBST ID='plenum east', XB=14.01,14.01,-25.405,-24.01,6.8,7.575, COLOR='CYAN', SURF_ID='ADIABATIC'/

&OBST ID='plenum south face', XB=-12.96,0.37,-25.405,-25.405,-17.845,-14.28, COLOR='INVISIBLE', SURF_ID='ADIABATIC'/

&OBST ID='plenum south face', XB=0.37,14.01,-25.405,-25.405,-17.845,-14.28, COLOR='INVISIBLE', SURF_ID='ADIABATIC'/

&OBST ID='plenum south face', XB=-12.96,0.37,-25.405,-25.405,-14.28,-10.56, COLOR='INVISIBLE', SURF_ID='ADIABATIC'/

&OBST ID='plenum south face', XB=0.37,14.01,-25.405,-25.405,-14.28,-10.56, COLOR='INVISIBLE', SURF_ID='ADIABATIC'/

&OBST ID='plenum south face', XB=-12.96,0.37,-25.405,-25.405,-10.56,-7.46, COLOR='INVISIBLE', SURF_ID='ADIABATIC'/

&OBST ID='plenum south face', XB=0.37,14.01,-25.405,-25.405,-10.56,-7.46, COLOR='INVISIBLE', SURF_ID='ADIABATIC'/

&OBST ID='plenum south face', XB=-12.96,0.37,-25.405,-25.405,-7.46,-3.74, COLOR='INVISIBLE', SURF_ID='ADIABATIC'/

&OBST ID='plenum south face', XB=0.37,14.01,-25.405,-25.405,-7.46,-3.74, COLOR='INVISIBLE', SURF_ID='ADIABATIC'/

&OBST ID='plenum south face', XB=-12.96,0.37,-25.405,-25.405,-3.74,-0.64, COLOR='INVISIBLE', SURF_ID='ADIABATIC'/

&OBST ID='plenum south face', XB=0.37,14.01,-25.405,-25.405,-3.74,-0.64, COLOR='INVISIBLE', SURF_ID='ADIABATIC'/

&OBST ID='plenum south face', XB=-12.96,0.37,-25.405,-25.405,-0.64,3.08, COLOR='INVISIBLE', SURF_ID='ADIABATIC'/

&OBST ID='plenum south face', XB=0.37,14.01,-25.405,-25.405,-0.64,3.08, COLOR='INVISIBLE', SURF_ID='ADIABATIC'/

&OBST ID='plenum south face', XB=-12.96,0.37,-25.405,-25.405,3.08,6.8, COLOR='INVISIBLE', SURF_ID='ADIABATIC'/

&OBST ID='plenum south face', XB=0.37,14.01,-25.405,-25.405,3.08,6.8, COLOR='INVISIBLE', SURF_ID='ADIABATIC'/

&OBST ID='plenum south face', XB=-12.96,14.01,-25.405,-25.405,6.8,7.575, COLOR='INVISIBLE', SURF_ID='ADIABATIC'/

&OBST ID='plenum buttom', XB=-12.96,0.37,-25.405,-24.01,-17.845,-17.845, COLOR='CYAN', SURF_ID='ADIABATIC'/

&OBST ID='plenum buttom', XB=0.37,14.01,-25.405,-24.01,-17.845,-17.845, COLOR='CYAN', SURF_ID='ADIABATIC'/

&OBST ID='AcDbRegion - 11B2', XB=-12.96,-11.875,-24.01,-24.01,-18.0,-14.28, COLOR='GRAY 80', SURF_ID='ADIABATIC'/

&OBST ID='AcDbRegion - 11B2', XB=-11.875,-10.945,-24.01,-24.01,-18.0,-17.07, COLOR='GRAY 80', SURF_ID='ADIABATIC'/

&OBST ID='AcDbRegion - 11B2', XB=-11.875,-10.945,-24.01,-24.01,-15.21,-14.28, COLOR='GRAY 80', SURF_ID='ADIABATIC'/

&OBST ID='AcDbRegion - 11B2', XB=-10.945,-10.015,-24.01,-24.01,-18.0,-14.28, COLOR='GRAY 80', SURF_ID='ADIABATIC'/

&OBST ID='AcDbRegion - 11B2', XB=-10.015,-8.93,-24.01,-24.01,-18.0,-17.07, COLOR='GRAY 80', SURF_ID='ADIABATIC'/

&OBST ID='AcDbRegion - 11B2', XB=-10.015,-8.93,-24.01,-24.01,-15.21,-14.28, COLOR='GRAY 80', SURF_ID='ADIABATIC'/

&OBST ID='AcDbRegion - 11B2', XB=-8.93,-8.0,-24.01,-24.01,-18.0,-14.28, COLOR='GRAY 80', SURF_ID='ADIABATIC'/

&OBST ID='AcDbRegion - 11B2', XB=-8.0,-6.915,-24.01,-24.01,-18.0,-17.07, COLOR='GRAY 80', SURF_ID='ADIABATIC'/

&OBST ID='AcDbRegion - 11B2', XB=-8.0,-6.915,-24.01,-24.01,-15.21,-14.28, COLOR='GRAY 80', SURF_ID='ADIABATIC'/

&OBST ID='AcDbRegion - 11B2', XB=-6.915,-5.985,-24.01,-24.01,-18.0,-14.28, COLOR='GRAY 80', SURF_ID='ADIABATIC'/

&OBST ID='AcDbRegion - 11B2', XB=-5.985,-4.9,-24.01,-24.01,-18.0,-17.07, COLOR='GRAY 80', SURF_ID='ADIABATIC'/

&OBST ID='AcDbRegion - 11B2', XB=-5.985,-4.9,-24.01,-24.01,-15.21,-14.28, COLOR='GRAY 80', SURF_ID='ADIABATIC'/

&OBST ID='AcDbRegion - 11B2', XB=-4.9,-3.97,-24.01,-24.01,-18.0,-14.28, COLOR='GRAY 80', SURF_ID='ADIABATIC'/

&OBST ID='AcDbRegion - 11B2', XB=-3.97,-3.04,-24.01,-24.01,-18.0,-17.07, COLOR='GRAY 80', SURF_ID='ADIABATIC'/

&OBST ID='AcDbRegion - 11B2', XB=-3.97,-3.04,-24.01,-24.01,-15.21,-14.28, COLOR='GRAY 80', SURF_ID='ADIABATIC'/

&OBST ID='AcDbRegion - 11B2', XB=-3.04,-1.955,-24.01,-24.01,-18.0,-14.28, COLOR='GRAY 80', SURF_ID='ADIABATIC'/

&OBST ID='AcDbRegion - 11B2', XB=-1.955,-1.025,-24.01,-24.01,-18.0,-17.07, COLOR='GRAY 80', SURF_ID='ADIABATIC'/

&OBST ID='AcDbRegion - 11B2', XB=-1.955,-1.025,-24.01,-24.01,-15.21,-14.28, COLOR='GRAY 80', SURF_ID='ADIABATIC'/

&OBST ID='AcDbRegion - 11B2', XB=-1.025,0.06,-24.01,-24.01,-18.0,-14.28, COLOR='GRAY 80', SURF_ID='ADIABATIC'/

&OBST ID='AcDbRegion - 11B2', XB=0.06,0.37,-24.01,-24.01,-18.0,-17.07, COLOR='GRAY 80', SURF_ID='ADIABATIC'/

&OBST ID='AcDbRegion - 11B2', XB=0.06,0.37,-24.01,-24.01,-15.21,-14.28, COLOR='GRAY 80', SURF_ID='ADIABATIC'/

&OBST ID='AcDbRegion - 11B2', XB=0.37,0.99,-24.01,-24.01,-18.0,-17.07, COLOR='GRAY 80', SURF_ID='ADIABATIC'/

&OBST ID='AcDbRegion - 11B2', XB=0.37,0.99,-24.01,-24.01,-15.21,-14.28, COLOR='GRAY 80', SURF_ID='ADIABATIC'/

&OBST ID='AcDbRegion - 11B2', XB=0.99,2.075,-24.01,-24.01,-18.0,-14.28, COLOR='GRAY 80', SURF_ID='ADIABATIC'/

&OBST ID='AcDbRegion - 11B2', XB=2.075,3.005,-24.01,-24.01,-18.0,-17.07, COLOR='GRAY 80', SURF_ID='ADIABATIC'/

&OBST ID='AcDbRegion - 11B2', XB=2.075,3.005,-24.01,-24.01,-15.21,-14.28, COLOR='GRAY 80', SURF_ID='ADIABATIC'/

&OBST ID='AcDbRegion - 11B2', XB=3.005,4.09,-24.01,-24.01,-18.0,-14.28, COLOR='GRAY 80', SURF_ID='ADIABATIC'/

&OBST ID='AcDbRegion - 11B2', XB=4.09,5.02,-24.01,-24.01,-18.0,-17.07, COLOR='GRAY 80', SURF_ID='ADIABATIC'/

&OBST ID='AcDbRegion - 11B2', XB=4.09,5.02,-24.01,-24.01,-15.21,-14.28, COLOR='GRAY 80', SURF_ID='ADIABATIC'/

&OBST ID='AcDbRegion - 11B2', XB=5.02,5.95,-24.01,-24.01,-18.0,-14.28, COLOR='GRAY 80', SURF_ID='ADIABATIC'/

&OBST ID='AcDbRegion - 11B2', XB=5.95,7.035,-24.01,-24.01,-18.0,-17.07, COLOR='GRAY 80', SURF_ID='ADIABATIC'/

&OBST ID='AcDbRegion - 11B2', XB=5.95,7.035,-24.01,-24.01,-15.21,-14.28, COLOR='GRAY 80', SURF_ID='ADIABATIC'/

&OBST ID='AcDbRegion - 11B2', XB=7.035,7.965,-24.01,-24.01,-18.0,-14.28, COLOR='GRAY 80', SURF_ID='ADIABATIC'/

&OBST ID='AcDbRegion - 11B2', XB=7.965,9.05,-24.01,-24.01,-18.0,-17.07, COLOR='GRAY 80', SURF_ID='ADIABATIC'/

&OBST ID='AcDbRegion - 11B2', XB=7.965,9.05,-24.01,-24.01,-15.21,-14.28, COLOR='GRAY 80', SURF_ID='ADIABATIC'/

&OBST ID='AcDbRegion - 11B2', XB=9.05,9.98,-24.01,-24.01,-18.0,-14.28, COLOR='GRAY 80', SURF_ID='ADIABATIC'/

&OBST ID='AcDbRegion - 11B2', XB=9.98,11.065,-24.01,-24.01,-18.0,-17.07, COLOR='GRAY 80', SURF_ID='ADIABATIC'/

&OBST ID='AcDbRegion - 11B2', XB=9.98,11.065,-24.01,-24.01,-15.21,-14.28, COLOR='GRAY 80', SURF_ID='ADIABATIC'/

&OBST ID='AcDbRegion - 11B2', XB=11.065,11.995,-24.01,-24.01,-18.0,-14.28, COLOR='GRAY 80', SURF_ID='ADIABATIC'/

&OBST ID='AcDbRegion - 11B2', XB=11.995,13.08,-24.01,-24.01,-18.0,-17.07, COLOR='GRAY 80', SURF_ID='ADIABATIC'/

&OBST ID='AcDbRegion - 11B2', XB=11.995,13.08,-24.01,-24.01,-15.21,-14.28, COLOR='GRAY 80', SURF_ID='ADIABATIC'/

&OBST ID='AcDbRegion - 11B2', XB=13.08,14.01,-24.01,-24.01,-18.0,-14.28, COLOR='GRAY 80', SURF_ID='ADIABATIC'/

&OBST ID='AcDbRegion - 11B2', XB=-12.96,-11.875,-24.01,-24.01,-14.28,-10.56, COLOR='GRAY 80', SURF_ID='ADIABATIC'/

&OBST ID='AcDbRegion - 11B2', XB=-11.875,-10.945,-24.01,-24.01,-14.28,-13.505, COLOR='GRAY 80', SURF_ID='ADIABATIC'/

&OBST ID='AcDbRegion - 11B2', XB=-11.875,-10.945,-24.01,-24.01,-11.645,-10.56, COLOR='GRAY 80', SURF_ID='ADIABATIC'/

&OBST ID='AcDbRegion - 11B2', XB=-10.945,-10.015,-24.01,-24.01,-14.28,-10.56, COLOR='GRAY 80', SURF_ID='ADIABATIC'/

&OBST ID='AcDbRegion - 11B2', XB=-10.015,-8.93,-24.01,-24.01,-14.28,-13.505, COLOR='GRAY 80', SURF_ID='ADIABATIC'/

&OBST ID='AcDbRegion - 11B2', XB=-10.015,-8.93,-24.01,-24.01,-11.645,-10.56, COLOR='GRAY 80', SURF_ID='ADIABATIC'/

&OBST ID='AcDbRegion - 11B2', XB=-8.93,-8.0,-24.01,-24.01,-14.28,-10.56, COLOR='GRAY 80', SURF_ID='ADIABATIC'/

&OBST ID='AcDbRegion - 11B2', XB=-8.0,-6.915,-24.01,-24.01,-14.28,-13.505, COLOR='GRAY 80', SURF_ID='ADIABATIC'/

&OBST ID='AcDbRegion - 11B2', XB=-8.0,-6.915,-24.01,-24.01,-11.645,-10.56, COLOR='GRAY 80', SURF_ID='ADIABATIC'/

&OBST ID='AcDbRegion - 11B2', XB=-6.915,-5.985,-24.01,-24.01,-14.28,-10.56, COLOR='GRAY 80', SURF_ID='ADIABATIC'/

&OBST ID='AcDbRegion - 11B2', XB=-5.985,-4.9,-24.01,-24.01,-14.28,-13.505, COLOR='GRAY 80', SURF_ID='ADIABATIC'/

&OBST ID='AcDbRegion - 11B2', XB=-5.985,-4.9,-24.01,-24.01,-11.645,-10.56, COLOR='GRAY 80', SURF_ID='ADIABATIC'/

&OBST ID='AcDbRegion - 11B2', XB=-4.9,-3.97,-24.01,-24.01,-14.28,-10.56, COLOR='GRAY 80', SURF_ID='ADIABATIC'/

&OBST ID='AcDbRegion - 11B2', XB=-3.97,-3.04,-24.01,-24.01,-14.28,-13.505, COLOR='GRAY 80', SURF_ID='ADIABATIC'/

&OBST ID='AcDbRegion - 11B2', XB=-3.97,-3.04,-24.01,-24.01,-11.645,-10.56, COLOR='GRAY 80', SURF_ID='ADIABATIC'/

&OBST ID='AcDbRegion - 11B2', XB=-3.04,-1.955,-24.01,-24.01,-14.28,-10.56, COLOR='GRAY 80', SURF_ID='ADIABATIC'/

&OBST ID='AcDbRegion - 11B2', XB=-1.955,-1.025,-24.01,-24.01,-14.28,-13.505, COLOR='GRAY 80', SURF_ID='ADIABATIC'/

&OBST ID='AcDbRegion - 11B2', XB=-1.955,-1.025,-24.01,-24.01,-11.645,-10.56, COLOR='GRAY 80', SURF_ID='ADIABATIC'/

&OBST ID='AcDbRegion - 11B2', XB=-1.025,0.06,-24.01,-24.01,-14.28,-10.56, COLOR='GRAY 80', SURF_ID='ADIABATIC'/

&OBST ID='AcDbRegion - 11B2', XB=0.06,0.37,-24.01,-24.01,-14.28,-13.505, COLOR='GRAY 80', SURF_ID='ADIABATIC'/

&OBST ID='AcDbRegion - 11B2', XB=0.06,0.37,-24.01,-24.01,-11.645,-10.56, COLOR='GRAY 80', SURF_ID='ADIABATIC'/

&OBST ID='AcDbRegion - 11B2', XB=0.37,0.99,-24.01,-24.01,-14.28,-13.505, COLOR='GRAY 80', SURF_ID='ADIABATIC'/

&OBST ID='AcDbRegion - 11B2', XB=0.37,0.99,-24.01,-24.01,-11.645,-10.56, COLOR='GRAY 80', SURF_ID='ADIABATIC'/

&OBST ID='AcDbRegion - 11B2', XB=0.99,2.075,-24.01,-24.01,-14.28,-10.56, COLOR='GRAY 80', SURF_ID='ADIABATIC'/

&OBST ID='AcDbRegion - 11B2', XB=2.075,3.005,-24.01,-24.01,-14.28,-13.505, COLOR='GRAY 80', SURF_ID='ADIABATIC'/

&OBST ID='AcDbRegion - 11B2', XB=2.075,3.005,-24.01,-24.01,-11.645,-10.56, COLOR='GRAY 80', SURF_ID='ADIABATIC'/

&OBST ID='AcDbRegion - 11B2', XB=3.005,4.09,-24.01,-24.01,-14.28,-10.56, COLOR='GRAY 80', SURF_ID='ADIABATIC'/

&OBST ID='AcDbRegion - 11B2', XB=4.09,5.02,-24.01,-24.01,-14.28,-13.505, COLOR='GRAY 80', SURF_ID='ADIABATIC'/

&OBST ID='AcDbRegion - 11B2', XB=4.09,5.02,-24.01,-24.01,-11.645,-10.56, COLOR='GRAY 80', SURF_ID='ADIABATIC'/

&OBST ID='AcDbRegion - 11B2', XB=5.02,5.95,-24.01,-24.01,-14.28,-10.56, COLOR='GRAY 80', SURF_ID='ADIABATIC'/

&OBST ID='AcDbRegion - 11B2', XB=5.95,7.035,-24.01,-24.01,-14.28,-13.505, COLOR='GRAY 80', SURF_ID='ADIABATIC'/

&OBST ID='AcDbRegion - 11B2', XB=5.95,7.035,-24.01,-24.01,-11.645,-10.56, COLOR='GRAY 80', SURF_ID='ADIABATIC'/

&OBST ID='AcDbRegion - 11B2', XB=7.035,7.965,-24.01,-24.01,-14.28,-10.56, COLOR='GRAY 80', SURF_ID='ADIABATIC'/

&OBST ID='AcDbRegion - 11B2', XB=7.965,9.05,-24.01,-24.01,-14.28,-13.505, COLOR='GRAY 80', SURF_ID='ADIABATIC'/

&OBST ID='AcDbRegion - 11B2', XB=7.965,9.05,-24.01,-24.01,-11.645,-10.56, COLOR='GRAY 80', SURF_ID='ADIABATIC'/

&OBST ID='AcDbRegion - 11B2', XB=9.05,9.98,-24.01,-24.01,-14.28,-10.56, COLOR='GRAY 80', SURF_ID='ADIABATIC'/

&OBST ID='AcDbRegion - 11B2', XB=9.98,11.065,-24.01,-24.01,-14.28,-13.505, COLOR='GRAY 80', SURF_ID='ADIABATIC'/

&OBST ID='AcDbRegion - 11B2', XB=9.98,11.065,-24.01,-24.01,-11.645,-10.56, COLOR='GRAY 80', SURF_ID='ADIABATIC'/

&OBST ID='AcDbRegion - 11B2', XB=11.065,11.995,-24.01,-24.01,-14.28,-10.56, COLOR='GRAY 80', SURF_ID='ADIABATIC'/

&OBST ID='AcDbRegion - 11B2', XB=11.995,13.08,-24.01,-24.01,-14.28,-13.505, COLOR='GRAY 80', SURF_ID='ADIABATIC'/

&OBST ID='AcDbRegion - 11B2', XB=11.995,13.08,-24.01,-24.01,-11.645,-10.56, COLOR='GRAY 80', SURF_ID='ADIABATIC'/

&OBST ID='AcDbRegion - 11B2', XB=13.08,14.01,-24.01,-24.01,-14.28,-10.56, COLOR='GRAY 80', SURF_ID='ADIABATIC'/

&OBST ID='AcDbRegion - 11B2', XB=-12.96,-11.875,-24.01,-24.01,-10.56,-7.46, COLOR='GRAY 80', SURF_ID='ADIABATIC'/

&OBST ID='AcDbRegion - 11B2', XB=-11.875,-10.945,-24.01,-24.01,-10.56,-9.94, COLOR='GRAY 80', SURF_ID='ADIABATIC'/

&OBST ID='AcDbRegion - 11B2', XB=-11.875,-10.945,-24.01,-24.01,-8.235,-7.46, COLOR='GRAY 80', SURF_ID='ADIABATIC'/

&OBST ID='AcDbRegion - 11B2', XB=-10.945,-10.015,-24.01,-24.01,-10.56,-7.46, COLOR='GRAY 80', SURF_ID='ADIABATIC'/

&OBST ID='AcDbRegion - 11B2', XB=-10.015,-8.93,-24.01,-24.01,-10.56,-9.94, COLOR='GRAY 80', SURF_ID='ADIABATIC'/

&OBST ID='AcDbRegion - 11B2', XB=-10.015,-8.93,-24.01,-24.01,-8.235,-7.46, COLOR='GRAY 80', SURF_ID='ADIABATIC'/

&OBST ID='AcDbRegion - 11B2', XB=-8.93,-8.0,-24.01,-24.01,-10.56,-7.46, COLOR='GRAY 80', SURF_ID='ADIABATIC'/

&OBST ID='AcDbRegion - 11B2', XB=-8.0,-6.915,-24.01,-24.01,-10.56,-9.94, COLOR='GRAY 80', SURF_ID='ADIABATIC'/

&OBST ID='AcDbRegion - 11B2', XB=-8.0,-6.915,-24.01,-24.01,-8.235,-7.46, COLOR='GRAY 80', SURF_ID='ADIABATIC'/

&OBST ID='AcDbRegion - 11B2', XB=-6.915,-5.985,-24.01,-24.01,-10.56,-7.46, COLOR='GRAY 80', SURF_ID='ADIABATIC'/

&OBST ID='AcDbRegion - 11B2', XB=-5.985,-4.9,-24.01,-24.01,-10.56,-9.94, COLOR='GRAY 80', SURF_ID='ADIABATIC'/

&OBST ID='AcDbRegion - 11B2', XB=-5.985,-4.9,-24.01,-24.01,-8.235,-7.46, COLOR='GRAY 80', SURF_ID='ADIABATIC'/

&OBST ID='AcDbRegion - 11B2', XB=-4.9,-3.97,-24.01,-24.01,-10.56,-7.46, COLOR='GRAY 80', SURF_ID='ADIABATIC'/

&OBST ID='AcDbRegion - 11B2', XB=-3.97,-3.04,-24.01,-24.01,-10.56,-9.94, COLOR='GRAY 80', SURF_ID='ADIABATIC'/

&OBST ID='AcDbRegion - 11B2', XB=-3.97,-3.04,-24.01,-24.01,-8.235,-7.46, COLOR='GRAY 80', SURF_ID='ADIABATIC'/

&OBST ID='AcDbRegion - 11B2', XB=-3.04,-1.955,-24.01,-24.01,-10.56,-7.46, COLOR='GRAY 80', SURF_ID='ADIABATIC'/

&OBST ID='AcDbRegion - 11B2', XB=-1.955,-1.025,-24.01,-24.01,-10.56,-9.94, COLOR='GRAY 80', SURF_ID='ADIABATIC'/

&OBST ID='AcDbRegion - 11B2', XB=-1.955,-1.025,-24.01,-24.01,-8.235,-7.46, COLOR='GRAY 80', SURF_ID='ADIABATIC'/

&OBST ID='AcDbRegion - 11B2', XB=-1.025,0.06,-24.01,-24.01,-10.56,-7.46, COLOR='GRAY 80', SURF_ID='ADIABATIC'/

&OBST ID='AcDbRegion - 11B2', XB=0.06,0.37,-24.01,-24.01,-10.56,-9.94, COLOR='GRAY 80', SURF_ID='ADIABATIC'/

&OBST ID='AcDbRegion - 11B2', XB=0.06,0.37,-24.01,-24.01,-8.235,-7.46, COLOR='GRAY 80', SURF_ID='ADIABATIC'/

&OBST ID='AcDbRegion - 11B2', XB=0.37,0.99,-24.01,-24.01,-10.56,-9.94, COLOR='GRAY 80', SURF_ID='ADIABATIC'/

&OBST ID='AcDbRegion - 11B2', XB=0.37,0.99,-24.01,-24.01,-8.235,-7.46, COLOR='GRAY 80', SURF_ID='ADIABATIC'/

&OBST ID='AcDbRegion - 11B2', XB=0.99,2.075,-24.01,-24.01,-10.56,-7.46, COLOR='GRAY 80', SURF_ID='ADIABATIC'/

&OBST ID='AcDbRegion - 11B2', XB=2.075,3.005,-24.01,-24.01,-10.56,-9.94, COLOR='GRAY 80', SURF_ID='ADIABATIC'/

&OBST ID='AcDbRegion - 11B2', XB=2.075,3.005,-24.01,-24.01,-8.235,-7.46, COLOR='GRAY 80', SURF_ID='ADIABATIC'/

&OBST ID='AcDbRegion - 11B2', XB=3.005,4.09,-24.01,-24.01,-10.56,-7.46, COLOR='GRAY 80', SURF_ID='ADIABATIC'/

&OBST ID='AcDbRegion - 11B2', XB=4.09,5.02,-24.01,-24.01,-10.56,-9.94, COLOR='GRAY 80', SURF_ID='ADIABATIC'/

&OBST ID='AcDbRegion - 11B2', XB=4.09,5.02,-24.01,-24.01,-8.235,-7.46, COLOR='GRAY 80', SURF_ID='ADIABATIC'/

&OBST ID='AcDbRegion - 11B2', XB=5.02,5.95,-24.01,-24.01,-10.56,-7.46, COLOR='GRAY 80', SURF_ID='ADIABATIC'/

&OBST ID='AcDbRegion - 11B2', XB=5.95,7.035,-24.01,-24.01,-10.56,-9.94, COLOR='GRAY 80', SURF_ID='ADIABATIC'/

&OBST ID='AcDbRegion - 11B2', XB=5.95,7.035,-24.01,-24.01,-8.235,-7.46, COLOR='GRAY 80', SURF_ID='ADIABATIC'/

&OBST ID='AcDbRegion - 11B2', XB=7.035,7.965,-24.01,-24.01,-10.56,-7.46, COLOR='GRAY 80', SURF_ID='ADIABATIC'/

&OBST ID='AcDbRegion - 11B2', XB=7.965,9.05,-24.01,-24.01,-10.56,-9.94, COLOR='GRAY 80', SURF_ID='ADIABATIC'/

&OBST ID='AcDbRegion - 11B2', XB=7.965,9.05,-24.01,-24.01,-8.235,-7.46, COLOR='GRAY 80', SURF_ID='ADIABATIC'/

&OBST ID='AcDbRegion - 11B2', XB=9.05,9.98,-24.01,-24.01,-10.56,-7.46, COLOR='GRAY 80', SURF_ID='ADIABATIC'/

&OBST ID='AcDbRegion - 11B2', XB=9.98,11.065,-24.01,-24.01,-10.56,-9.94, COLOR='GRAY 80', SURF_ID='ADIABATIC'/

&OBST ID='AcDbRegion - 11B2', XB=9.98,11.065,-24.01,-24.01,-8.235,-7.46, COLOR='GRAY 80', SURF_ID='ADIABATIC'/

&OBST ID='AcDbRegion - 11B2', XB=11.065,11.995,-24.01,-24.01,-10.56,-7.46, COLOR='GRAY 80', SURF_ID='ADIABATIC'/

&OBST ID='AcDbRegion - 11B2', XB=11.995,13.08,-24.01,-24.01,-10.56,-9.94, COLOR='GRAY 80', SURF_ID='ADIABATIC'/

&OBST ID='AcDbRegion - 11B2', XB=11.995,13.08,-24.01,-24.01,-8.235,-7.46, COLOR='GRAY 80', SURF_ID='ADIABATIC'/

&OBST ID='AcDbRegion - 11B2', XB=13.08,14.01,-24.01,-24.01,-10.56,-7.46, COLOR='GRAY 80', SURF_ID='ADIABATIC'/

&OBST ID='AcDbRegion - 11B2', XB=-12.96,-11.875,-24.01,-24.01,-7.46,-3.74, COLOR='GRAY 80', SURF_ID='ADIABATIC'/

&OBST ID='AcDbRegion - 11B2', XB=-11.875,-10.945,-24.01,-24.01,-7.46,-6.53, COLOR='GRAY 80', SURF_ID='ADIABATIC'/

&OBST ID='AcDbRegion - 11B2', XB=-11.875,-10.945,-24.01,-24.01,-4.67,-3.74, COLOR='GRAY 80', SURF_ID='ADIABATIC'/

&OBST ID='AcDbRegion - 11B2', XB=-10.945,-10.015,-24.01,-24.01,-7.46,-3.74, COLOR='GRAY 80', SURF_ID='ADIABATIC'/

&OBST ID='AcDbRegion - 11B2', XB=-10.015,-8.93,-24.01,-24.01,-7.46,-6.53, COLOR='GRAY 80', SURF_ID='ADIABATIC'/

&OBST ID='AcDbRegion - 11B2', XB=-10.015,-8.93,-24.01,-24.01,-4.67,-3.74, COLOR='GRAY 80', SURF_ID='ADIABATIC'/

&OBST ID='AcDbRegion - 11B2', XB=-8.93,-8.0,-24.01,-24.01,-7.46,-3.74, COLOR='GRAY 80', SURF_ID='ADIABATIC'/

&OBST ID='AcDbRegion - 11B2', XB=-8.0,-6.915,-24.01,-24.01,-7.46,-6.53, COLOR='GRAY 80', SURF_ID='ADIABATIC'/

&OBST ID='AcDbRegion - 11B2', XB=-8.0,-6.915,-24.01,-24.01,-4.67,-3.74, COLOR='GRAY 80', SURF_ID='ADIABATIC'/

&OBST ID='AcDbRegion - 11B2', XB=-6.915,-5.985,-24.01,-24.01,-7.46,-3.74, COLOR='GRAY 80', SURF_ID='ADIABATIC'/

&OBST ID='AcDbRegion - 11B2', XB=-5.985,-4.9,-24.01,-24.01,-7.46,-6.53, COLOR='GRAY 80', SURF_ID='ADIABATIC'/

&OBST ID='AcDbRegion - 11B2', XB=-5.985,-4.9,-24.01,-24.01,-4.67,-3.74, COLOR='GRAY 80', SURF_ID='ADIABATIC'/

&OBST ID='AcDbRegion - 11B2', XB=-4.9,-3.97,-24.01,-24.01,-7.46,-3.74, COLOR='GRAY 80', SURF_ID='ADIABATIC'/

&OBST ID='AcDbRegion - 11B2', XB=-3.97,-3.04,-24.01,-24.01,-7.46,-6.53, COLOR='GRAY 80', SURF_ID='ADIABATIC'/

&OBST ID='AcDbRegion - 11B2', XB=-3.97,-3.04,-24.01,-24.01,-4.67,-3.74, COLOR='GRAY 80', SURF_ID='ADIABATIC'/

&OBST ID='AcDbRegion - 11B2', XB=-3.04,-1.955,-24.01,-24.01,-7.46,-3.74, COLOR='GRAY 80', SURF_ID='ADIABATIC'/

&OBST ID='AcDbRegion - 11B2', XB=-1.955,-1.025,-24.01,-24.01,-7.46,-6.53, COLOR='GRAY 80', SURF_ID='ADIABATIC'/

&OBST ID='AcDbRegion - 11B2', XB=-1.955,-1.025,-24.01,-24.01,-4.67,-3.74, COLOR='GRAY 80', SURF_ID='ADIABATIC'/

&OBST ID='AcDbRegion - 11B2', XB=-1.025,0.06,-24.01,-24.01,-7.46,-3.74, COLOR='GRAY 80', SURF_ID='ADIABATIC'/

&OBST ID='AcDbRegion - 11B2', XB=0.06,0.37,-24.01,-24.01,-7.46,-6.53, COLOR='GRAY 80', SURF_ID='ADIABATIC'/

&OBST ID='AcDbRegion - 11B2', XB=0.06,0.37,-24.01,-24.01,-4.67,-3.74, COLOR='GRAY 80', SURF_ID='ADIABATIC'/

&OBST ID='AcDbRegion - 11B2', XB=0.37,0.99,-24.01,-24.01,-7.46,-6.53, COLOR='GRAY 80', SURF_ID='ADIABATIC'/

&OBST ID='AcDbRegion - 11B2', XB=0.37,0.99,-24.01,-24.01,-4.67,-3.74, COLOR='GRAY 80', SURF_ID='ADIABATIC'/

&OBST ID='AcDbRegion - 11B2', XB=0.99,2.075,-24.01,-24.01,-7.46,-3.74, COLOR='GRAY 80', SURF_ID='ADIABATIC'/

&OBST ID='AcDbRegion - 11B2', XB=2.075,3.005,-24.01,-24.01,-7.46,-6.53, COLOR='GRAY 80', SURF_ID='ADIABATIC'/

&OBST ID='AcDbRegion - 11B2', XB=2.075,3.005,-24.01,-24.01,-4.67,-3.74, COLOR='GRAY 80', SURF_ID='ADIABATIC'/

&OBST ID='AcDbRegion - 11B2', XB=3.005,4.09,-24.01,-24.01,-7.46,-3.74, COLOR='GRAY 80', SURF_ID='ADIABATIC'/

&OBST ID='AcDbRegion - 11B2', XB=4.09,5.02,-24.01,-24.01,-7.46,-6.53, COLOR='GRAY 80', SURF_ID='ADIABATIC'/

&OBST ID='AcDbRegion - 11B2', XB=4.09,5.02,-24.01,-24.01,-4.67,-3.74, COLOR='GRAY 80', SURF_ID='ADIABATIC'/

&OBST ID='AcDbRegion - 11B2', XB=5.02,5.95,-24.01,-24.01,-7.46,-3.74, COLOR='GRAY 80', SURF_ID='ADIABATIC'/

&OBST ID='AcDbRegion - 11B2', XB=5.95,7.035,-24.01,-24.01,-7.46,-6.53, COLOR='GRAY 80', SURF_ID='ADIABATIC'/

&OBST ID='AcDbRegion - 11B2', XB=5.95,7.035,-24.01,-24.01,-4.67,-3.74, COLOR='GRAY 80', SURF_ID='ADIABATIC'/

&OBST ID='AcDbRegion - 11B2', XB=7.035,7.965,-24.01,-24.01,-7.46,-3.74, COLOR='GRAY 80', SURF_ID='ADIABATIC'/

&OBST ID='AcDbRegion - 11B2', XB=7.965,9.05,-24.01,-24.01,-7.46,-6.53, COLOR='GRAY 80', SURF_ID='ADIABATIC'/

&OBST ID='AcDbRegion - 11B2', XB=7.965,9.05,-24.01,-24.01,-4.67,-3.74, COLOR='GRAY 80', SURF_ID='ADIABATIC'/

&OBST ID='AcDbRegion - 11B2', XB=9.05,9.98,-24.01,-24.01,-7.46,-3.74, COLOR='GRAY 80', SURF_ID='ADIABATIC'/

&OBST ID='AcDbRegion - 11B2', XB=9.98,11.065,-24.01,-24.01,-7.46,-6.53, COLOR='GRAY 80', SURF_ID='ADIABATIC'/

&OBST ID='AcDbRegion - 11B2', XB=9.98,11.065,-24.01,-24.01,-4.67,-3.74, COLOR='GRAY 80', SURF_ID='ADIABATIC'/

&OBST ID='AcDbRegion - 11B2', XB=11.065,11.995,-24.01,-24.01,-7.46,-3.74, COLOR='GRAY 80', SURF_ID='ADIABATIC'/

&OBST ID='AcDbRegion - 11B2', XB=11.995,13.08,-24.01,-24.01,-7.46,-6.53, COLOR='GRAY 80', SURF_ID='ADIABATIC'/

&OBST ID='AcDbRegion - 11B2', XB=11.995,13.08,-24.01,-24.01,-4.67,-3.74, COLOR='GRAY 80', SURF_ID='ADIABATIC'/

&OBST ID='AcDbRegion - 11B2', XB=13.08,14.01,-24.01,-24.01,-7.46,-3.74, COLOR='GRAY 80', SURF_ID='ADIABATIC'/

&OBST ID='AcDbRegion - 11B2', XB=-12.96,-11.875,-24.01,-24.01,-3.74,-0.64, COLOR='GRAY 80', SURF_ID='ADIABATIC'/

&OBST ID='AcDbRegion - 11B2', XB=-11.875,-10.945,-24.01,-24.01,-3.74,-2.965, COLOR='GRAY 80', SURF_ID='ADIABATIC'/

&OBST ID='AcDbRegion - 11B2', XB=-11.875,-10.945,-24.01,-24.01,-1.26,-0.64, COLOR='GRAY 80', SURF_ID='ADIABATIC'/

&OBST ID='AcDbRegion - 11B2', XB=-10.945,-10.015,-24.01,-24.01,-3.74,-0.64, COLOR='GRAY 80', SURF_ID='ADIABATIC'/

&OBST ID='AcDbRegion - 11B2', XB=-10.015,-8.93,-24.01,-24.01,-3.74,-2.965, COLOR='GRAY 80', SURF_ID='ADIABATIC'/

&OBST ID='AcDbRegion - 11B2', XB=-10.015,-8.93,-24.01,-24.01,-1.26,-0.64, COLOR='GRAY 80', SURF_ID='ADIABATIC'/

&OBST ID='AcDbRegion - 11B2', XB=-8.93,-8.0,-24.01,-24.01,-3.74,-0.64, COLOR='GRAY 80', SURF_ID='ADIABATIC'/

&OBST ID='AcDbRegion - 11B2', XB=-8.0,-6.915,-24.01,-24.01,-3.74,-2.965, COLOR='GRAY 80', SURF_ID='ADIABATIC'/

&OBST ID='AcDbRegion - 11B2', XB=-8.0,-6.915,-24.01,-24.01,-1.26,-0.64, COLOR='GRAY 80', SURF_ID='ADIABATIC'/

&OBST ID='AcDbRegion - 11B2', XB=-6.915,-5.985,-24.01,-24.01,-3.74,-0.64, COLOR='GRAY 80', SURF_ID='ADIABATIC'/

&OBST ID='AcDbRegion - 11B2', XB=-5.985,-4.9,-24.01,-24.01,-3.74,-2.965, COLOR='GRAY 80', SURF_ID='ADIABATIC'/

&OBST ID='AcDbRegion - 11B2', XB=-5.985,-4.9,-24.01,-24.01,-1.26,-0.64, COLOR='GRAY 80', SURF_ID='ADIABATIC'/

&OBST ID='AcDbRegion - 11B2', XB=-4.9,-3.97,-24.01,-24.01,-3.74,-0.64, COLOR='GRAY 80', SURF_ID='ADIABATIC'/

&OBST ID='AcDbRegion - 11B2', XB=-3.97,-3.04,-24.01,-24.01,-3.74,-2.965, COLOR='GRAY 80', SURF_ID='ADIABATIC'/

&OBST ID='AcDbRegion - 11B2', XB=-3.97,-3.04,-24.01,-24.01,-1.26,-0.64, COLOR='GRAY 80', SURF_ID='ADIABATIC'/

&OBST ID='AcDbRegion - 11B2', XB=-3.04,-1.955,-24.01,-24.01,-3.74,-0.64, COLOR='GRAY 80', SURF_ID='ADIABATIC'/

&OBST ID='AcDbRegion - 11B2', XB=-1.955,-1.025,-24.01,-24.01,-3.74,-2.965, COLOR='GRAY 80', SURF_ID='ADIABATIC'/

&OBST ID='AcDbRegion - 11B2', XB=-1.955,-1.025,-24.01,-24.01,-1.26,-0.64, COLOR='GRAY 80', SURF_ID='ADIABATIC'/

&OBST ID='AcDbRegion - 11B2', XB=-1.025,0.06,-24.01,-24.01,-3.74,-0.64, COLOR='GRAY 80', SURF_ID='ADIABATIC'/

&OBST ID='AcDbRegion - 11B2', XB=0.06,0.37,-24.01,-24.01,-3.74,-2.965, COLOR='GRAY 80', SURF_ID='ADIABATIC'/

&OBST ID='AcDbRegion - 11B2', XB=0.06,0.37,-24.01,-24.01,-1.26,-0.64, COLOR='GRAY 80', SURF_ID='ADIABATIC'/

&OBST ID='AcDbRegion - 11B2', XB=0.37,0.99,-24.01,-24.01,-3.74,-2.965, COLOR='GRAY 80', SURF_ID='ADIABATIC'/

&OBST ID='AcDbRegion - 11B2', XB=0.37,0.99,-24.01,-24.01,-1.26,-0.64, COLOR='GRAY 80', SURF_ID='ADIABATIC'/

&OBST ID='AcDbRegion - 11B2', XB=0.99,2.075,-24.01,-24.01,-3.74,-0.64, COLOR='GRAY 80', SURF_ID='ADIABATIC'/

&OBST ID='AcDbRegion - 11B2', XB=2.075,3.005,-24.01,-24.01,-3.74,-2.965, COLOR='GRAY 80', SURF_ID='ADIABATIC'/

&OBST ID='AcDbRegion - 11B2', XB=2.075,3.005,-24.01,-24.01,-1.26,-0.64, COLOR='GRAY 80', SURF_ID='ADIABATIC'/

&OBST ID='AcDbRegion - 11B2', XB=3.005,4.09,-24.01,-24.01,-3.74,-0.64, COLOR='GRAY 80', SURF_ID='ADIABATIC'/

&OBST ID='AcDbRegion - 11B2', XB=4.09,5.02,-24.01,-24.01,-3.74,-2.965, COLOR='GRAY 80', SURF_ID='ADIABATIC'/

&OBST ID='AcDbRegion - 11B2', XB=4.09,5.02,-24.01,-24.01,-1.26,-0.64, COLOR='GRAY 80', SURF_ID='ADIABATIC'/

&OBST ID='AcDbRegion - 11B2', XB=5.02,5.95,-24.01,-24.01,-3.74,-0.64, COLOR='GRAY 80', SURF_ID='ADIABATIC'/

&OBST ID='AcDbRegion - 11B2', XB=5.95,7.035,-24.01,-24.01,-3.74,-2.965, COLOR='GRAY 80', SURF_ID='ADIABATIC'/

&OBST ID='AcDbRegion - 11B2', XB=5.95,7.035,-24.01,-24.01,-1.26,-0.64, COLOR='GRAY 80', SURF_ID='ADIABATIC'/

&OBST ID='AcDbRegion - 11B2', XB=7.035,7.965,-24.01,-24.01,-3.74,-0.64, COLOR='GRAY 80', SURF_ID='ADIABATIC'/

&OBST ID='AcDbRegion - 11B2', XB=7.965,9.05,-24.01,-24.01,-3.74,-2.965, COLOR='GRAY 80', SURF_ID='ADIABATIC'/

&OBST ID='AcDbRegion - 11B2', XB=7.965,9.05,-24.01,-24.01,-1.26,-0.64, COLOR='GRAY 80', SURF_ID='ADIABATIC'/

&OBST ID='AcDbRegion - 11B2', XB=9.05,9.98,-24.01,-24.01,-3.74,-0.64, COLOR='GRAY 80', SURF_ID='ADIABATIC'/

&OBST ID='AcDbRegion - 11B2', XB=9.98,11.065,-24.01,-24.01,-3.74,-2.965, COLOR='GRAY 80', SURF_ID='ADIABATIC'/

&OBST ID='AcDbRegion - 11B2', XB=9.98,11.065,-24.01,-24.01,-1.26,-0.64, COLOR='GRAY 80', SURF_ID='ADIABATIC'/

&OBST ID='AcDbRegion - 11B2', XB=11.065,11.995,-24.01,-24.01,-3.74,-0.64, COLOR='GRAY 80', SURF_ID='ADIABATIC'/

&OBST ID='AcDbRegion - 11B2', XB=11.995,13.08,-24.01,-24.01,-3.74,-2.965, COLOR='GRAY 80', SURF_ID='ADIABATIC'/

&OBST ID='AcDbRegion - 11B2', XB=11.995,13.08,-24.01,-24.01,-1.26,-0.64, COLOR='GRAY 80', SURF_ID='ADIABATIC'/

&OBST ID='AcDbRegion - 11B2', XB=13.08,14.01,-24.01,-24.01,-3.74,-0.64, COLOR='GRAY 80', SURF_ID='ADIABATIC'/

&OBST ID='AcDbRegion - 11B2', XB=-12.96,-11.875,-24.01,-24.01,-0.64,3.08, COLOR='GRAY 80', SURF_ID='ADIABATIC'/

&OBST ID='AcDbRegion - 11B2', XB=-11.875,-10.945,-24.01,-24.01,-0.64,0.445, COLOR='GRAY 80', SURF_ID='ADIABATIC'/

&OBST ID='AcDbRegion - 11B2', XB=-11.875,-10.945,-24.01,-24.01,2.305,3.08, COLOR='GRAY 80', SURF_ID='ADIABATIC'/

&OBST ID='AcDbRegion - 11B2', XB=-10.945,-10.015,-24.01,-24.01,-0.64,3.08, COLOR='GRAY 80', SURF_ID='ADIABATIC'/

&OBST ID='AcDbRegion - 11B2', XB=-10.015,-8.93,-24.01,-24.01,-0.64,0.445, COLOR='GRAY 80', SURF_ID='ADIABATIC'/

&OBST ID='AcDbRegion - 11B2', XB=-10.015,-8.93,-24.01,-24.01,2.305,3.08, COLOR='GRAY 80', SURF_ID='ADIABATIC'/

&OBST ID='AcDbRegion - 11B2', XB=-8.93,-8.0,-24.01,-24.01,-0.64,3.08, COLOR='GRAY 80', SURF_ID='ADIABATIC'/

&OBST ID='AcDbRegion - 11B2', XB=-8.0,-6.915,-24.01,-24.01,-0.64,0.445, COLOR='GRAY 80', SURF_ID='ADIABATIC'/

&OBST ID='AcDbRegion - 11B2', XB=-8.0,-6.915,-24.01,-24.01,2.305,3.08, COLOR='GRAY 80', SURF_ID='ADIABATIC'/

&OBST ID='AcDbRegion - 11B2', XB=-6.915,-5.985,-24.01,-24.01,-0.64,3.08, COLOR='GRAY 80', SURF_ID='ADIABATIC'/

&OBST ID='AcDbRegion - 11B2', XB=-5.985,-4.9,-24.01,-24.01,-0.64,0.445, COLOR='GRAY 80', SURF_ID='ADIABATIC'/

&OBST ID='AcDbRegion - 11B2', XB=-5.985,-4.9,-24.01,-24.01,2.305,3.08, COLOR='GRAY 80', SURF_ID='ADIABATIC'/

&OBST ID='AcDbRegion - 11B2', XB=-4.9,-3.97,-24.01,-24.01,-0.64,3.08, COLOR='GRAY 80', SURF_ID='ADIABATIC'/

&OBST ID='AcDbRegion - 11B2', XB=-3.97,-3.04,-24.01,-24.01,-0.64,0.445, COLOR='GRAY 80', SURF_ID='ADIABATIC'/

&OBST ID='AcDbRegion - 11B2', XB=-3.97,-3.04,-24.01,-24.01,2.305,3.08, COLOR='GRAY 80', SURF_ID='ADIABATIC'/

&OBST ID='AcDbRegion - 11B2', XB=-3.04,-1.955,-24.01,-24.01,-0.64,3.08, COLOR='GRAY 80', SURF_ID='ADIABATIC'/

&OBST ID='AcDbRegion - 11B2', XB=-1.955,-1.025,-24.01,-24.01,-0.64,0.445, COLOR='GRAY 80', SURF_ID='ADIABATIC'/

&OBST ID='AcDbRegion - 11B2', XB=-1.955,-1.025,-24.01,-24.01,2.305,3.08, COLOR='GRAY 80', SURF_ID='ADIABATIC'/

&OBST ID='AcDbRegion - 11B2', XB=-1.025,0.06,-24.01,-24.01,-0.64,3.08, COLOR='GRAY 80', SURF_ID='ADIABATIC'/

&OBST ID='AcDbRegion - 11B2', XB=0.06,0.37,-24.01,-24.01,-0.64,0.445, COLOR='GRAY 80', SURF_ID='ADIABATIC'/

&OBST ID='AcDbRegion - 11B2', XB=0.06,0.37,-24.01,-24.01,2.305,3.08, COLOR='GRAY 80', SURF_ID='ADIABATIC'/

&OBST ID='AcDbRegion - 11B2', XB=0.37,0.99,-24.01,-24.01,-0.64,0.445, COLOR='GRAY 80', SURF_ID='ADIABATIC'/

&OBST ID='AcDbRegion - 11B2', XB=0.37,0.99,-24.01,-24.01,2.305,3.08, COLOR='GRAY 80', SURF_ID='ADIABATIC'/

&OBST ID='AcDbRegion - 11B2', XB=0.99,2.075,-24.01,-24.01,-0.64,3.08, COLOR='GRAY 80', SURF_ID='ADIABATIC'/

&OBST ID='AcDbRegion - 11B2', XB=2.075,3.005,-24.01,-24.01,-0.64,0.445, COLOR='GRAY 80', SURF_ID='ADIABATIC'/

&OBST ID='AcDbRegion - 11B2', XB=2.075,3.005,-24.01,-24.01,2.305,3.08, COLOR='GRAY 80', SURF_ID='ADIABATIC'/

&OBST ID='AcDbRegion - 11B2', XB=3.005,4.09,-24.01,-24.01,-0.64,3.08, COLOR='GRAY 80', SURF_ID='ADIABATIC'/

&OBST ID='AcDbRegion - 11B2', XB=4.09,5.02,-24.01,-24.01,-0.64,0.445, COLOR='GRAY 80', SURF_ID='ADIABATIC'/

&OBST ID='AcDbRegion - 11B2', XB=4.09,5.02,-24.01,-24.01,2.305,3.08, COLOR='GRAY 80', SURF_ID='ADIABATIC'/

&OBST ID='AcDbRegion - 11B2', XB=5.02,5.95,-24.01,-24.01,-0.64,3.08, COLOR='GRAY 80', SURF_ID='ADIABATIC'/

&OBST ID='AcDbRegion - 11B2', XB=5.95,7.035,-24.01,-24.01,-0.64,0.445, COLOR='GRAY 80', SURF_ID='ADIABATIC'/

&OBST ID='AcDbRegion - 11B2', XB=5.95,7.035,-24.01,-24.01,2.305,3.08, COLOR='GRAY 80', SURF_ID='ADIABATIC'/

&OBST ID='AcDbRegion - 11B2', XB=7.035,7.965,-24.01,-24.01,-0.64,3.08, COLOR='GRAY 80', SURF_ID='ADIABATIC'/

&OBST ID='AcDbRegion - 11B2', XB=7.965,9.05,-24.01,-24.01,-0.64,0.445, COLOR='GRAY 80', SURF_ID='ADIABATIC'/

&OBST ID='AcDbRegion - 11B2', XB=7.965,9.05,-24.01,-24.01,2.305,3.08, COLOR='GRAY 80', SURF_ID='ADIABATIC'/

&OBST ID='AcDbRegion - 11B2', XB=9.05,9.98,-24.01,-24.01,-0.64,3.08, COLOR='GRAY 80', SURF_ID='ADIABATIC'/

&OBST ID='AcDbRegion - 11B2', XB=9.98,11.065,-24.01,-24.01,-0.64,0.445, COLOR='GRAY 80', SURF_ID='ADIABATIC'/

&OBST ID='AcDbRegion - 11B2', XB=9.98,11.065,-24.01,-24.01,2.305,3.08, COLOR='GRAY 80', SURF_ID='ADIABATIC'/

&OBST ID='AcDbRegion - 11B2', XB=11.065,11.995,-24.01,-24.01,-0.64,3.08, COLOR='GRAY 80', SURF_ID='ADIABATIC'/

&OBST ID='AcDbRegion - 11B2', XB=11.995,13.08,-24.01,-24.01,-0.64,0.445, COLOR='GRAY 80', SURF_ID='ADIABATIC'/

&OBST ID='AcDbRegion - 11B2', XB=11.995,13.08,-24.01,-24.01,2.305,3.08, COLOR='GRAY 80', SURF_ID='ADIABATIC'/

&OBST ID='AcDbRegion - 11B2', XB=13.08,14.01,-24.01,-24.01,-0.64,3.08, COLOR='GRAY 80', SURF_ID='ADIABATIC'/

&OBST ID='AcDbRegion - 11B2', XB=-12.96,-11.875,-24.01,-24.01,3.08,6.645, COLOR='GRAY 80', SURF_ID='ADIABATIC'/

&OBST ID='AcDbRegion - 11B2', XB=-11.875,-10.945,-24.01,-24.01,3.08,4.01, COLOR='GRAY 80', SURF_ID='ADIABATIC'/

&OBST ID='AcDbRegion - 11B2', XB=-11.875,-10.945,-24.01,-24.01,5.715,6.645, COLOR='GRAY 80', SURF_ID='ADIABATIC'/

&OBST ID='AcDbRegion - 11B2', XB=-10.945,-10.015,-24.01,-24.01,3.08,6.645, COLOR='GRAY 80', SURF_ID='ADIABATIC'/

&OBST ID='AcDbRegion - 11B2', XB=-10.015,-8.93,-24.01,-24.01,3.08,4.01, COLOR='GRAY 80', SURF_ID='ADIABATIC'/

&OBST ID='AcDbRegion - 11B2', XB=-10.015,-8.93,-24.01,-24.01,5.715,6.645, COLOR='GRAY 80', SURF_ID='ADIABATIC'/

&OBST ID='AcDbRegion - 11B2', XB=-8.93,-8.0,-24.01,-24.01,3.08,6.645, COLOR='GRAY 80', SURF_ID='ADIABATIC'/

&OBST ID='AcDbRegion - 11B2', XB=-8.0,-6.915,-24.01,-24.01,3.08,4.01, COLOR='GRAY 80', SURF_ID='ADIABATIC'/

&OBST ID='AcDbRegion - 11B2', XB=-8.0,-6.915,-24.01,-24.01,5.715,6.645, COLOR='GRAY 80', SURF_ID='ADIABATIC'/

&OBST ID='AcDbRegion - 11B2', XB=-6.915,-5.985,-24.01,-24.01,3.08,6.645, COLOR='GRAY 80', SURF_ID='ADIABATIC'/

&OBST ID='AcDbRegion - 11B2', XB=-5.985,-4.9,-24.01,-24.01,3.08,4.01, COLOR='GRAY 80', SURF_ID='ADIABATIC'/

&OBST ID='AcDbRegion - 11B2', XB=-5.985,-4.9,-24.01,-24.01,5.715,6.645, COLOR='GRAY 80', SURF_ID='ADIABATIC'/

&OBST ID='AcDbRegion - 11B2', XB=-4.9,-3.97,-24.01,-24.01,3.08,6.645, COLOR='GRAY 80', SURF_ID='ADIABATIC'/

&OBST ID='AcDbRegion - 11B2', XB=-3.97,-3.04,-24.01,-24.01,3.08,4.01, COLOR='GRAY 80', SURF_ID='ADIABATIC'/

&OBST ID='AcDbRegion - 11B2', XB=-3.97,-3.04,-24.01,-24.01,5.715,6.645, COLOR='GRAY 80', SURF_ID='ADIABATIC'/

&OBST ID='AcDbRegion - 11B2', XB=-3.04,-1.955,-24.01,-24.01,3.08,6.645, COLOR='GRAY 80', SURF_ID='ADIABATIC'/

&OBST ID='AcDbRegion - 11B2', XB=-1.955,-1.025,-24.01,-24.01,3.08,4.01, COLOR='GRAY 80', SURF_ID='ADIABATIC'/

&OBST ID='AcDbRegion - 11B2', XB=-1.955,-1.025,-24.01,-24.01,5.715,6.645, COLOR='GRAY 80', SURF_ID='ADIABATIC'/

&OBST ID='AcDbRegion - 11B2', XB=-1.025,0.06,-24.01,-24.01,3.08,6.645, COLOR='GRAY 80', SURF_ID='ADIABATIC'/

&OBST ID='AcDbRegion - 11B2', XB=0.06,0.37,-24.01,-24.01,3.08,4.01, COLOR='GRAY 80', SURF_ID='ADIABATIC'/

&OBST ID='AcDbRegion - 11B2', XB=0.06,0.37,-24.01,-24.01,5.715,6.645, COLOR='GRAY 80', SURF_ID='ADIABATIC'/

&OBST ID='AcDbRegion - 11B2', XB=0.37,0.99,-24.01,-24.01,3.08,4.01, COLOR='GRAY 80', SURF_ID='ADIABATIC'/

&OBST ID='AcDbRegion - 11B2', XB=0.37,0.99,-24.01,-24.01,5.715,6.645, COLOR='GRAY 80', SURF_ID='ADIABATIC'/

&OBST ID='AcDbRegion - 11B2', XB=0.99,2.075,-24.01,-24.01,3.08,6.645, COLOR='GRAY 80', SURF_ID='ADIABATIC'/

&OBST ID='AcDbRegion - 11B2', XB=2.075,3.005,-24.01,-24.01,3.08,4.01, COLOR='GRAY 80', SURF_ID='ADIABATIC'/

&OBST ID='AcDbRegion - 11B2', XB=2.075,3.005,-24.01,-24.01,5.715,6.645, COLOR='GRAY 80', SURF_ID='ADIABATIC'/

&OBST ID='AcDbRegion - 11B2', XB=3.005,4.09,-24.01,-24.01,3.08,6.645, COLOR='GRAY 80', SURF_ID='ADIABATIC'/

&OBST ID='AcDbRegion - 11B2', XB=4.09,5.02,-24.01,-24.01,3.08,4.01, COLOR='GRAY 80', SURF_ID='ADIABATIC'/

&OBST ID='AcDbRegion - 11B2', XB=4.09,5.02,-24.01,-24.01,5.715,6.645, COLOR='GRAY 80', SURF_ID='ADIABATIC'/

&OBST ID='AcDbRegion - 11B2', XB=5.02,5.95,-24.01,-24.01,3.08,6.645, COLOR='GRAY 80', SURF_ID='ADIABATIC'/

&OBST ID='AcDbRegion - 11B2', XB=5.95,7.035,-24.01,-24.01,3.08,4.01, COLOR='GRAY 80', SURF_ID='ADIABATIC'/

&OBST ID='AcDbRegion - 11B2', XB=5.95,7.035,-24.01,-24.01,5.715,6.645, COLOR='GRAY 80', SURF_ID='ADIABATIC'/

&OBST ID='AcDbRegion - 11B2', XB=7.035,7.965,-24.01,-24.01,3.08,6.645, COLOR='GRAY 80', SURF_ID='ADIABATIC'/

&OBST ID='AcDbRegion - 11B2', XB=7.965,9.05,-24.01,-24.01,3.08,4.01, COLOR='GRAY 80', SURF_ID='ADIABATIC'/

&OBST ID='AcDbRegion - 11B2', XB=7.965,9.05,-24.01,-24.01,5.715,6.645, COLOR='GRAY 80', SURF_ID='ADIABATIC'/

&OBST ID='AcDbRegion - 11B2', XB=9.05,9.98,-24.01,-24.01,3.08,6.645, COLOR='GRAY 80', SURF_ID='ADIABATIC'/

&OBST ID='AcDbRegion - 11B2', XB=9.98,11.065,-24.01,-24.01,3.08,4.01, COLOR='GRAY 80', SURF_ID='ADIABATIC'/

&OBST ID='AcDbRegion - 11B2', XB=9.98,11.065,-24.01,-24.01,5.715,6.645, COLOR='GRAY 80', SURF_ID='ADIABATIC'/

&OBST ID='AcDbRegion - 11B2', XB=11.065,11.995,-24.01,-24.01,3.08,6.645, COLOR='GRAY 80', SURF_ID='ADIABATIC'/

&OBST ID='AcDbRegion - 11B2', XB=11.995,13.08,-24.01,-24.01,3.08,4.01, COLOR='GRAY 80', SURF_ID='ADIABATIC'/

&OBST ID='AcDbRegion - 11B2', XB=11.995,13.08,-24.01,-24.01,5.715,6.645, COLOR='GRAY 80', SURF_ID='ADIABATIC'/

&OBST ID='AcDbRegion - 11B2', XB=13.08,14.01,-24.01,-24.01,3.08,6.645, COLOR='GRAY 80', SURF_ID='ADIABATIC'/

&OBST ID='north wall', XB=-12.96,-0.25,2.96,2.96,-18.0,-14.28, COLOR='GRAY 68', SURF_ID='ADIABATIC'/

&OBST ID='north wall', XB=-0.25,0.68,2.96,2.96,-18.0,-17.07, COLOR='GRAY 68', SURF_ID='ADIABATIC'/

&OBST ID='north wall', XB=-0.25,0.68,2.96,2.96,-14.9,-14.28, COLOR='GRAY 68', SURF_ID='ADIABATIC'/

&OBST ID='north wall', XB=0.68,0.99,2.96,2.96,-18.0,-14.28, COLOR='GRAY 68', SURF_ID='ADIABATIC'/

&OBST ID='north wall', XB=0.99,14.01,2.96,2.96,-18.0,-14.28, COLOR='GRAY 68', SURF_ID='ADIABATIC'/

&OBST ID='north wall', XB=-12.96,-0.25,2.96,2.96,-14.28,-10.56, COLOR='GRAY 68', SURF_ID='ADIABATIC'/

&OBST ID='north wall', XB=-0.25,0.68,2.96,2.96,-14.28,-13.66, COLOR='GRAY 68', SURF_ID='ADIABATIC'/

&OBST ID='north wall', XB=-0.25,0.68,2.96,2.96,-11.49,-10.56, COLOR='GRAY 68', SURF_ID='ADIABATIC'/

&OBST ID='north wall', XB=0.68,0.99,2.96,2.96,-14.28,-10.56, COLOR='GRAY 68', SURF_ID='ADIABATIC'/

&OBST ID='north wall', XB=0.99,14.01,2.96,2.96,-14.28,-10.56, COLOR='GRAY 68', SURF_ID='ADIABATIC'/

&OBST ID='north wall', XB=-12.96,-0.25,2.96,2.96,-10.56,-7.46, COLOR='GRAY 68', SURF_ID='ADIABATIC'/

&OBST ID='north wall', XB=-0.25,0.68,2.96,2.96,-10.56,-10.25, COLOR='GRAY 68', SURF_ID='ADIABATIC'/

&OBST ID='north wall', XB=-0.25,0.68,2.96,2.96,-8.08,-7.46, COLOR='GRAY 68', SURF_ID='ADIABATIC'/

&OBST ID='north wall', XB=0.68,0.99,2.96,2.96,-10.56,-7.46, COLOR='GRAY 68', SURF_ID='ADIABATIC'/

&OBST ID='north wall', XB=0.99,14.01,2.96,2.96,-10.56,-7.46, COLOR='GRAY 68', SURF_ID='ADIABATIC'/

&OBST ID='north wall', XB=-12.96,-0.25,2.96,2.96,-7.46,-3.74, COLOR='GRAY 68', SURF_ID='ADIABATIC'/

&OBST ID='north wall', XB=-0.25,0.68,2.96,2.96,-7.46,-6.53, COLOR='GRAY 68', SURF_ID='ADIABATIC'/

&OBST ID='north wall', XB=-0.25,0.68,2.96,2.96,-4.36,-3.74, COLOR='GRAY 68', SURF_ID='ADIABATIC'/

&OBST ID='north wall', XB=0.68,0.99,2.96,2.96,-7.46,-3.74, COLOR='GRAY 68', SURF_ID='ADIABATIC'/

&OBST ID='north wall', XB=0.99,14.01,2.96,2.96,-7.46,-3.74, COLOR='GRAY 68', SURF_ID='ADIABATIC'/

&OBST ID='north wall', XB=-12.96,-0.25,2.96,2.96,-3.74,-0.64, COLOR='GRAY 68', SURF_ID='ADIABATIC'/

&OBST ID='north wall', XB=-0.25,0.68,2.96,2.96,-3.74,-3.12, COLOR='GRAY 68', SURF_ID='ADIABATIC'/

&OBST ID='north wall', XB=-0.25,0.68,2.96,2.96,-0.95,-0.64, COLOR='GRAY 68', SURF_ID='ADIABATIC'/

&OBST ID='north wall', XB=0.68,0.99,2.96,2.96,-3.74,-0.64, COLOR='GRAY 68', SURF_ID='ADIABATIC'/

&OBST ID='north wall', XB=0.99,14.01,2.96,2.96,-3.74,-0.64, COLOR='GRAY 68', SURF_ID='ADIABATIC'/

&OBST ID='north wall', XB=-12.96,-0.25,2.96,2.96,-0.64,3.08, COLOR='GRAY 68', SURF_ID='ADIABATIC'/

&OBST ID='north wall', XB=-0.25,0.68,2.96,2.96,-0.64,0.29, COLOR='GRAY 68', SURF_ID='ADIABATIC'/

&OBST ID='north wall', XB=-0.25,0.68,2.96,2.96,2.46,3.08, COLOR='GRAY 68', SURF_ID='ADIABATIC'/

&OBST ID='north wall', XB=0.68,0.99,2.96,2.96,-0.64,3.08, COLOR='GRAY 68', SURF_ID='ADIABATIC'/

&OBST ID='north wall', XB=0.99,14.01,2.96,2.96,-0.64,3.08, COLOR='GRAY 68', SURF_ID='ADIABATIC'/

&OBST ID='north wall', XB=-12.96,-0.25,2.96,2.96,3.08,6.49, COLOR='GRAY 68', SURF_ID='ADIABATIC'/

&OBST ID='north wall', XB=-0.25,0.68,2.96,2.96,3.08,3.7, COLOR='GRAY 68', SURF_ID='ADIABATIC'/

&OBST ID='north wall', XB=-0.25,0.68,2.96,2.96,5.87,6.49, COLOR='GRAY 68', SURF_ID='ADIABATIC'/

&OBST ID='north wall', XB=0.68,0.99,2.96,2.96,3.08,6.49, COLOR='GRAY 68', SURF_ID='ADIABATIC'/

&OBST ID='north wall', XB=0.99,14.01,2.96,2.96,3.08,6.49, COLOR='GRAY 68', SURF_ID='ADIABATIC'/

&VENT ID='Mesh Vent: Meshnew-a-a-a [XMIN]', SURF_ID='ADIABATIC', XB=-12.96,-12.96,-25.56,-23.7,-18.0,-14.28/

&VENT ID='Mesh Vent: Meshnew-a-a-a [YMIN]', SURF_ID='ADIABATIC', XB=-12.96,0.37,-25.56,-25.56,-18.0,-14.28/

&VENT ID='Mesh Vent: Meshnew-a-a-a [ZMIN]', SURF_ID='ADIABATIC', XB=-12.96,0.37,-25.56,-23.7,-18.0,-18.0/

&VENT ID='Mesh Vent: Meshnew-a-a-b [XMAX]', SURF_ID='ADIABATIC', XB=14.32,14.32,-25.56,-23.7,-18.0,-14.28/

&VENT ID='Mesh Vent: Meshnew-a-a-b [YMIN]', SURF_ID='ADIABATIC', XB=0.37,14.32,-25.56,-25.56,-18.0,-14.28/

&VENT ID='Mesh Vent: Meshnew-a-a-b [ZMIN]', SURF_ID='ADIABATIC', XB=0.37,14.32,-25.56,-23.7,-18.0,-18.0/

&VENT ID='Mesh Vent: Meshnew-a-b-a [XMIN]', SURF_ID='ADIABATIC', XB=-12.96,-12.96,-25.56,-23.7,-14.28,-10.56/

&VENT ID='Mesh Vent: Meshnew-a-b-a [YMIN]', SURF_ID='ADIABATIC', XB=-12.96,0.37,-25.56,-25.56,-14.28,-10.56/

&VENT ID='Mesh Vent: Meshnew-a-b-b [XMAX]', SURF_ID='ADIABATIC', XB=14.32,14.32,-25.56,-23.7,-14.28,-10.56/

&VENT ID='Mesh Vent: Meshnew-a-b-b [YMIN]', SURF_ID='ADIABATIC', XB=0.37,14.32,-25.56,-25.56,-14.28,-10.56/

&VENT ID='Mesh Vent: Meshnew-a-c-a [XMIN]', SURF_ID='ADIABATIC', XB=-12.96,-12.96,-25.56,-23.7,-10.56,-7.46/

&VENT ID='Mesh Vent: Meshnew-a-c-a [YMIN]', SURF_ID='ADIABATIC', XB=-12.96,0.37,-25.56,-25.56,-10.56,-7.46/

&VENT ID='Mesh Vent: Meshnew-a-c-b [XMAX]', SURF_ID='ADIABATIC', XB=14.32,14.32,-25.56,-23.7,-10.56,-7.46/

&VENT ID='Mesh Vent: Meshnew-a-c-b [YMIN]', SURF_ID='ADIABATIC', XB=0.37,14.32,-25.56,-25.56,-10.56,-7.46/

&VENT ID='Mesh Vent: Meshnew-a-d-a [XMIN]', SURF_ID='ADIABATIC', XB=-12.96,-12.96,-25.56,-23.7,-7.46,-3.74/

&VENT ID='Mesh Vent: Meshnew-a-d-a [YMIN]', SURF_ID='ADIABATIC', XB=-12.96,0.37,-25.56,-25.56,-7.46,-3.74/

&VENT ID='Mesh Vent: Meshnew-a-d-b [XMAX]', SURF_ID='ADIABATIC', XB=14.32,14.32,-25.56,-23.7,-7.46,-3.74/

&VENT ID='Mesh Vent: Meshnew-a-d-b [YMIN]', SURF_ID='ADIABATIC', XB=0.37,14.32,-25.56,-25.56,-7.46,-3.74/

&VENT ID='Mesh Vent: Meshnew-a-e-a [XMIN]', SURF_ID='ADIABATIC', XB=-12.96,-12.96,-25.56,-23.7,-3.74,-0.64/

&VENT ID='Mesh Vent: Meshnew-a-e-a [YMIN]', SURF_ID='ADIABATIC', XB=-12.96,0.37,-25.56,-25.56,-3.74,-0.64/

&VENT ID='Mesh Vent: Meshnew-a-e-b [XMAX]', SURF_ID='ADIABATIC', XB=14.32,14.32,-25.56,-23.7,-3.74,-0.64/

&VENT ID='Mesh Vent: Meshnew-a-e-b [YMIN]', SURF_ID='ADIABATIC', XB=0.37,14.32,-25.56,-25.56,-3.74,-0.64/

&VENT ID='Mesh Vent: Meshnew-a-f-a [XMIN]', SURF_ID='ADIABATIC', XB=-12.96,-12.96,-25.56,-23.7,-0.64,3.08/

&VENT ID='Mesh Vent: Meshnew-a-f-a [YMIN]', SURF_ID='ADIABATIC', XB=-12.96,0.37,-25.56,-25.56,-0.64,3.08/

&VENT ID='Mesh Vent: Meshnew-a-f-b [XMAX]', SURF_ID='ADIABATIC', XB=14.32,14.32,-25.56,-23.7,-0.64,3.08/

&VENT ID='Mesh Vent: Meshnew-a-f-b [YMIN]', SURF_ID='ADIABATIC', XB=0.37,14.32,-25.56,-25.56,-0.64,3.08/

&VENT ID='Mesh Vent: Meshnew-a-g-a [XMIN]', SURF_ID='ADIABATIC', XB=-12.96,-12.96,-25.56,-23.7,3.08,6.8/

&VENT ID='Mesh Vent: Meshnew-a-g-a [YMIN]', SURF_ID='ADIABATIC', XB=-12.96,0.37,-25.56,-25.56,3.08,6.8/

&VENT ID='Mesh Vent: Meshnew-a-g-b [XMAX]', SURF_ID='ADIABATIC', XB=14.32,14.32,-25.56,-23.7,3.08,6.8/

&VENT ID='Mesh Vent: Meshnew-a-g-b [YMIN]', SURF_ID='ADIABATIC', XB=0.37,14.32,-25.56,-25.56,3.08,6.8/

&VENT ID='Mesh Vent: Meshnew-a-h [XMAX]', SURF_ID='ADIABATIC', XB=14.32,14.32,-25.56,-23.7,6.8,9.9/

&VENT ID='Mesh Vent: Meshnew-a-h [XMIN]', SURF_ID='ADIABATIC', XB=-12.96,-12.96,-25.56,-23.7,6.8,9.9/

&VENT ID='Mesh Vent: Meshnew-a-h [YMIN]', SURF_ID='ADIABATIC', XB=-12.96,14.32,-25.56,-25.56,6.8,9.9/

&VENT ID='Mesh Vent: Meshnew-a-i-a [XMIN]', SURF_ID='ADIABATIC', XB=-12.96,-12.96,-23.7,6.06,-18.0,-14.28/

&VENT ID='Mesh Vent: Meshnew-a-i-a [ZMIN]', SURF_ID='ADIABATIC', XB=-12.96,0.99,-23.7,6.06,-18.0,-18.0/

&VENT ID='Mesh Vent: Meshnew-a-i-b [XMAX]', SURF_ID='ADIABATIC', XB=14.32,14.32,-23.7,6.06,-18.0,-14.28/

&VENT ID='Mesh Vent: Meshnew-a-i-b [ZMIN]', SURF_ID='ADIABATIC', XB=0.99,14.32,-23.7,6.06,-18.0,-18.0/

&VENT ID='Mesh Vent: Meshnew-a-j-a [XMIN]', SURF_ID='ADIABATIC', XB=-12.96,-12.96,-23.7,6.06,-14.28,-10.56/

&VENT ID='Mesh Vent: Meshnew-a-j-b [XMAX]', SURF_ID='ADIABATIC', XB=14.32,14.32,-23.7,6.06,-14.28,-10.56/

&VENT ID='Mesh Vent: Meshnew-a-k-a [XMIN]', SURF_ID='ADIABATIC', XB=-12.96,-12.96,-23.7,6.06,-10.56,-7.46/

&VENT ID='Mesh Vent: Meshnew-a-k-b [XMAX]', SURF_ID='ADIABATIC', XB=14.32,14.32,-23.7,6.06,-10.56,-7.46/

&VENT ID='Mesh Vent: Meshnew-a-l-a [XMIN]', SURF_ID='ADIABATIC', XB=-12.96,-12.96,-23.7,6.06,-7.46,-3.74/

&VENT ID='Mesh Vent: Meshnew-a-l-b [XMAX]', SURF_ID='ADIABATIC', XB=14.32,14.32,-23.7,6.06,-7.46,-3.74/

&VENT ID='Mesh Vent: Meshnew-a-m-a [XMIN]', SURF_ID='ADIABATIC', XB=-12.96,-12.96,-23.7,6.06,-3.74,-0.64/

&VENT ID='Mesh Vent: Meshnew-a-m-b [XMAX]', SURF_ID='ADIABATIC', XB=14.32,14.32,-23.7,6.06,-3.74,-0.64/

&VENT ID='Mesh Vent: Meshnew-a-n-a [XMIN]', SURF_ID='ADIABATIC', XB=-12.96,-12.96,-23.7,6.06,-0.64,3.08/

&VENT ID='Mesh Vent: Meshnew-a-n-b [XMAX]', SURF_ID='ADIABATIC', XB=14.32,14.32,-23.7,6.06,-0.64,3.08/

&VENT ID='Mesh Vent: Meshnew-a-o-a [XMIN]', SURF_ID='ADIABATIC', XB=-12.96,-12.96,-23.7,6.06,3.08,6.8/

&VENT ID='Mesh Vent: Meshnew-a-o-b [XMAX]', SURF_ID='ADIABATIC', XB=14.32,14.32,-23.7,6.06,3.08,6.8/

&VENT ID='Mesh Vent: Meshnew-a-p-a [XMIN]', SURF_ID='ADIABATIC', XB=-12.96,-12.96,-23.7,6.06,6.8,9.9/

&VENT ID='Mesh Vent: Meshnew-a-p-b [XMAX]', SURF_ID='ADIABATIC', XB=14.32,14.32,-23.7,6.06,6.8,9.9/

&VENT ID='Mesh Vent: Meshnew-b-a-a [XMIN]', SURF_ID='ADIABATIC', XB=-12.96,-12.96,-25.56,6.06,9.9,13.31/

&VENT ID='Mesh Vent: Meshnew-b-a-a [YMIN]', SURF_ID='ADIABATIC', XB=-12.96,0.68,-25.56,-25.56,9.9,13.31/

&VENT ID='Mesh Vent: Meshnew-b-a-b [XMIN]', SURF_ID='ADIABATIC', XB=-12.96,-12.96,-25.56,6.06,13.31,16.72/

&VENT ID='Mesh Vent: Meshnew-b-a-b [YMIN]', SURF_ID='ADIABATIC', XB=-12.96,0.68,-25.56,-25.56,13.31,16.72/

&VENT ID='Mesh Vent: Meshnew-b-b-a [XMAX]', SURF_ID='ADIABATIC', XB=14.32,14.32,-25.56,6.06,9.9,13.31/

&VENT ID='Mesh Vent: Meshnew-b-b-a [YMIN]', SURF_ID='ADIABATIC', XB=0.68,14.32,-25.56,-25.56,9.9,13.31/

&VENT ID='Mesh Vent: Meshnew-b-b-b [XMAX]', SURF_ID='ADIABATIC', XB=14.32,14.32,-25.56,6.06,13.31,16.72/

&VENT ID='Mesh Vent: Meshnew-b-b-b [YMIN]', SURF_ID='ADIABATIC', XB=0.68,14.32,-25.56,-25.56,13.31,16.72/

&VENT ID='Mesh Vent: Meshnew-c-a [XMIN]', SURF_ID='ADIABATIC', XB=-12.96,-12.96,-25.56,6.06,16.72,25.4/

&VENT ID='Mesh Vent: Meshnew-c-a [YMIN]', SURF_ID='ADIABATIC', XB=-12.96,1.3,-25.56,-25.56,16.72,25.4/

&VENT ID='Mesh Vent: Meshnew-c-a [ZMAX]', SURF_ID='OPEN', XB=-12.96,1.3,-25.56,6.06,25.4,25.4/

&VENT ID='Mesh Vent: Meshnew-c-b [XMAX]', SURF_ID='ADIABATIC', XB=14.32,14.32,-25.56,6.06,16.72,25.4/

&VENT ID='Mesh Vent: Meshnew-c-b [YMIN]', SURF_ID='ADIABATIC', XB=1.3,14.32,-25.56,-25.56,16.72,25.4/

&VENT ID='Mesh Vent: Meshnew-c-b [ZMAX]', SURF_ID='OPEN', XB=1.3,14.32,-25.56,6.06,25.4,25.4/

&VENT ID='Mesh Vent: Meshnew-d-a-a [XMAX]', SURF_ID='ADIABATIC', XB=14.32,14.32,6.06,14.12,-18.0,-10.56/

&VENT ID='Mesh Vent: Meshnew-d-a-a [XMIN]', SURF_ID='ADIABATIC', XB=-12.96,-12.96,6.06,14.12,-18.0,-10.56/

&VENT ID='Mesh Vent: Meshnew-d-a-a [ZMIN]', SURF_ID='ADIABATIC', XB=-12.96,14.32,6.06,14.12,-18.0,-18.0/

&VENT ID='Mesh Vent: Meshnew-d-a-b [XMAX]', SURF_ID='ADIABATIC', XB=14.32,14.32,6.06,14.12,-10.56,-3.74/

&VENT ID='Mesh Vent: Meshnew-d-a-b [XMIN]', SURF_ID='ADIABATIC', XB=-12.96,-12.96,6.06,14.12,-10.56,-3.74/

&VENT ID='Mesh Vent: Meshnew-d-b-a [XMAX]', SURF_ID='ADIABATIC', XB=14.32,14.32,6.06,14.12,-3.74,3.08/

&VENT ID='Mesh Vent: Meshnew-d-b-a [XMIN]', SURF_ID='ADIABATIC', XB=-12.96,-12.96,6.06,14.12,-3.74,3.08/

&VENT ID='Mesh Vent: Meshnew-d-b-b [XMAX]', SURF_ID='ADIABATIC', XB=14.32,14.32,6.06,14.12,3.08,9.9/

&VENT ID='Mesh Vent: Meshnew-d-b-b [XMIN]', SURF_ID='ADIABATIC', XB=-12.96,-12.96,6.06,14.12,3.08,9.9/

&VENT ID='Mesh Vent: Meshnew-e [XMAX]', SURF_ID='ADIABATIC', XB=14.32,14.32,6.06,14.12,9.9,16.72/

&VENT ID='Mesh Vent: Meshnew-e [XMIN]', SURF_ID='ADIABATIC', XB=-12.96,-12.96,6.06,14.12,9.9,16.72/

&VENT ID='Mesh Vent: Meshnew-f [XMAX]', SURF_ID='ADIABATIC', XB=14.32,14.32,6.06,14.12,16.72,25.4/

&VENT ID='Mesh Vent: Meshnew-f [XMIN]', SURF_ID='ADIABATIC', XB=-12.96,-12.96,6.06,14.12,16.72,25.4/

&VENT ID='Mesh Vent: Meshnew-f [ZMAX]', SURF_ID='OPEN', XB=-12.96,14.32,6.06,14.12,25.4,25.4/

&VENT ID='Mesh Vent: Meshnew-g-a-a [XMAX]', SURF_ID='ADIABATIC', XB=14.32,14.32,14.12,23.42,-18.0,-10.56/

&VENT ID='Mesh Vent: Meshnew-g-a-a [XMIN]', SURF_ID='ADIABATIC', XB=-12.96,-12.96,14.12,23.42,-18.0,-10.56/

&VENT ID='Mesh Vent: Meshnew-g-a-a [YMAX]', SURF_ID='OPEN', XB=-12.96,14.32,23.42,23.42,-18.0,-10.56/

&VENT ID='Mesh Vent: Meshnew-g-a-a [ZMIN]', SURF_ID='ADIABATIC', XB=-12.96,14.32,14.12,23.42,-18.0,-18.0/

&VENT ID='Mesh Vent: Meshnew-g-a-b [XMAX]', SURF_ID='ADIABATIC', XB=14.32,14.32,14.12,23.42,-10.56,-3.74/

&VENT ID='Mesh Vent: Meshnew-g-a-b [XMIN]', SURF_ID='ADIABATIC', XB=-12.96,-12.96,14.12,23.42,-10.56,-3.74/

&VENT ID='Mesh Vent: Meshnew-g-a-b [YMAX]', SURF_ID='OPEN', XB=-12.96,14.32,23.42,23.42,-10.56,-3.74/

&VENT ID='Mesh Vent: Meshnew-g-b [XMAX]', SURF_ID='ADIABATIC', XB=14.32,14.32,14.12,23.42,-3.74,9.9/

&VENT ID='Mesh Vent: Meshnew-g-b [XMIN]', SURF_ID='ADIABATIC', XB=-12.96,-12.96,14.12,23.42,-3.74,9.9/

&VENT ID='Mesh Vent: Meshnew-g-b [YMAX]', SURF_ID='OPEN', XB=-12.96,14.32,23.42,23.42,-3.74,9.9/

&VENT ID='Mesh Vent: Meshnew-h-merged-a [XMAX]', SURF_ID='ADIABATIC', XB=14.32,14.32,14.12,23.42,9.9,16.72/

&VENT ID='Mesh Vent: Meshnew-h-merged-a [XMIN]', SURF_ID='ADIABATIC', XB=-12.96,-12.96,14.12,23.42,9.9,16.72/

&VENT ID='Mesh Vent: Meshnew-h-merged-a [YMAX]', SURF_ID='OPEN', XB=-12.96,14.32,23.42,23.42,9.9,16.72/

&VENT ID='Mesh Vent: Meshnew-h-merged-b [XMAX]', SURF_ID='ADIABATIC', XB=14.32,14.32,14.12,23.42,16.72,25.4/

&VENT ID='Mesh Vent: Meshnew-h-merged-b [XMIN]', SURF_ID='ADIABATIC', XB=-12.96,-12.96,14.12,23.42,16.72,25.4/

&VENT ID='Mesh Vent: Meshnew-h-merged-b [YMAX]', SURF_ID='OPEN', XB=-12.96,14.32,23.42,23.42,16.72,25.4/

&VENT ID='Mesh Vent: Meshnew-h-merged-b [ZMAX]', SURF_ID='OPEN', XB=-12.96,14.32,14.12,23.42,25.4,25.4/

&SLCF QUANTITY='VELOCITY', VECTOR=.TRUE., PBY=-9.460013/

&SLCF QUANTITY='TEMPERATURE', PBY=-9.460013/

&SLCF QUANTITY='VELOCITY', VECTOR=.TRUE., PBY=2.518387/

&SLCF QUANTITY='TEMPERATURE', PBY=2.518387/

&SLCF QUANTITY='VELOCITY', VECTOR=.TRUE., PBY=-24.433013/

&SLCF QUANTITY='TEMPERATURE', PBY=-24.433013/

&SLCF QUANTITY='VELOCITY', VECTOR=.TRUE., PBX=0.025949/

&SLCF QUANTITY='TEMPERATURE', PBX=0.025949/

&DEVC ID='Temp plenum_STEADY STATE', QUANTITY='TEMPERATURE', XB=0.615812,0.615812,-24.5,-24.5,-16.263168,4.746498, POINTS=21/

&DEVC ID='Velocity plenum_STEADY STATE', QUANTITY='VELOCITY', XB=0.615812,0.615812,-24.5,-24.5,-16.263168,4.746498, POINTS=21/

&DEVC ID='Temp indoor_STEADY STATE', QUANTITY='TEMPERATURE', XB=0.615812,0.615812,-10.942326,-10.942326,-16.263168,4.746498, POINTS=21/

&DEVC ID='Velocity indoor_STEADY STATE', QUANTITY='VELOCITY', XB=0.615812,0.615812,-10.942326,-10.942326,-16.263168,4.746498, POINTS=21/

&TAIL /